From electromagnetic engineering to wireless power transmission and energy harvesting

Alexandru Takacs

Paul Sabatier University of Toulouse

Université Toulouse III Paul Sabatier

From electromagnetic engineering to wireless power transmission and energy harvesting

Mémoire présenté

en vue de l'obtention d'une qualification HDR (Habilitation à Diriger des Recherches)

par

Alexandru Takacs

Maître de Conférences, Université Toulouse III Paul Sabatier

Jury :

Professeur Ke Wu, Ecole Polytechnique de Montréal, Canada, Rapporteur

Professeur Henri Happy, Université de Lille, Rapporteur

Professeur Robert Staraj, Université de Nice, Rapporteur

Professeur Tan-Phu Vuong, INP Grenoble, Examinateur

Professeur Hervé Aubert, INP Toulouse, Garant HDR, Examinateur

Professeur Corinne Alonso, Université Toulouse III Paul Sabatier, Examinateur

Professeur Daniela Dragomirescu, INSA Toulouse, Examinateur

Eric Cariou, Directeur Général, Uwinloc Toulouse, Examinateur

Patrick Chan, Directeur Produit, Uwinloc, Toulouse, Invité

École doctorale et spécialité : GEET / Électromagnétisme et Systèmes Haute Fréquence

Unité de Recherche : Laboratoire d'Analyse et d'Architecture des Systèmes du CNRS (UPR8001)

Novembre 2018

Table of contents

List of figures

List of abbreviations

EH. : Energy Harvesting

WPT : Wireless Power Transmission/Wireless Power Transfer

RF : Radio Frequency

UHF : Ultra High Frequency

VHF: Very High Frequency

CMOS: Complementary Metal Oxide Semiconductor

PMU: Power Management Unit

SHM: Structural Health Monitoring

TTC: Telemetry, Tracking and Control

LCP: Liquid Cristal Polymer

Tx: Transmitter

Rx: Receiver

MEMS: MicroElectroMechanical Systems

ERAMUS: EuRopean Action Scheme for the Mobility of University Students

CNRS: National Center for Scientific Research

CNES: Centre National d'Etudes Spatiale (French Space Agency)

LAAS: Laboratory for Analysis and Architecture of Systems

ENSEEIHT: École Nationale Supérieure d'Electrotechnique, d'Electronique, d'Informatique, d'Hydraulique et des Télécommunications

MTA: Military Technical Academy of Bucharest

IMT: Institute of MicroTechnology of Bucharest

FF: Far Field

Nf: Near Field

IoT: Internet of Things

2CDAA: two Cross Dipole Antennas

4CDAA: four Cross Dipole Antennas

PCB : Printed Circuit Board

Introduction

This manuscript highlights my past and current research activities, and details my future plans. First, I present my past and present research activities. I focus on research works (Ph. D. thesis, research projects, master internship, etc.) that I directed or co-directed. My professional 'trajectory' is described in the section '*My trajectory through the Research Galaxy*'.

The most valuable results are presented in a condensed form and comprise of:

(i) my early research work in the field of electromagnetic engineering. This covers a period after my Ph. D. thesis, from 2004 to 2007, when I was Researcher at the Institute of Microtechnology of Bucharest and Lecturer at the Military Technical Academy of Bucharest, Romania. This research concerning mainly the RF MEMS circuits and systems and was performed as part of several European Romanian research projects. One of these projects was the FP7 European Network of Excellence AMICOM - Advanced MEMS for RF and MIllimeterwave COMmunications. This research is presented in the section '*Early research works: low loss circuits for microwave and millimeter wave applications*'.

(ii) the research concerning WPT (far-field and near-field) and EH techniques, that is the core of my research in the last eight years. The results I obtained are highlighted in the section '*Wireless power transmission and energy harvesting*'.

(iii) other research activities related to electromagnetic engineering. The most important results, obtained during the last decade (2008-2018), are detailed in the sections '*Compact antennas and antenna miniaturization techniques*', '*Flexible substrate technologies for millimeter wave applications*', and '*Design of passive and active RF and microwave circuits*'.

I don't want here to write a new and extended Ph. D. thesis or to expand papers that I already published. Nevertheless, several research papers detailing the my best research results are annexed in order to give a right picture of my research. In this manuscript I highlight my past and on-going research. My vision of research in the field of WPT and EH and my research project for the next decade are presented in the section '*My research project: the next decade*' I take some risks to define a research project for one decade and the future will validate (or invalidate) my approach. I'm convinced that as Publilius Syrus wrote 'it is a bad plan that

admits of no modification' but in the research, as in navigation, you need to have a *North Star* to follow it for keeping the right direction.

At the end of this manuscript I append the following: a complete list of my publications, a list of Ph. D. students that I supervised or co-supervised, and my CV, including a list of my main research projects, past and ongoing. Several of my articles are also annexed. These articles, published in international journals, elaborate further on the research highlighted in this manuscript.

My trajectory through the Research Galaxy

I had my first research experience during internship started in 1999 at ENSEEIHT Toulouse. As part of the ERASMUS[1,22] program, I travelled from the Military Technical Academy of Bucharest to Toulouse in January of 1999 to do my diploma thesis work. With minimal background in electromagnetism and electromagnetic engineering, I started my work in the field of the electromagnetic modeling under the guidance of Professor Hervé Aubert of ENSEEIHT (at that time an Associate Professor) and Professor Horia Sima of the Military Technical Academy of Bucharest. I collaborated also with two well-known Professors from ENSEEIHT: Prof. Henry Baudrand and Prof. Raymond Crampagne. During this internship I learned numerical methods developed at ENSEEIHT. My second research experience started in 2000 was part of my master's dissertation. The subject of my master's research project was focused to the design and characterization of some low loss microwave circuits (i.e. filters for space applications) manufactured on silicon membrane. During this period I had my first interactions with researchers from LAAS (Dr. Patrick Pons, Prof. Robert Plana, Prof. Jacques Graffeuil, Prof. Thierry Parra, etc.) and with several Ph. D. students of LAAS who have since become well known researchers and colleagues in LAAS (Dr. Anthony Coustou, Dr. Katia Grenier, Prof. David Dubuc, Dr. Laurent Bary, etc.). Later in my professional life I had fructuous scientific collaboration with the aforementioned persons. From a scientific point of view, my work focused on the design of low loss diplexer filters for space (Ka band) applications using a technology developed at LAAS around that time (the micromachined silicon membrane). The results were very promising and during my master's internship I published my first paper at JNM'2000 (Journées Nationales Micro-ondes). The master's internship was also a springboard for my Ph. D thesis that I started in the fall of 2000 under the co-direction of Prof. Hervé Aubert of ENSEEIHT, Toulouse and Prof. Alexandru Serbanescu of the Military Technical Academy of Bucharest. My Ph.D. thesis entitled ' Contribution à la conception de circuits passifs à faibles pertes d'insertion en ondes millimétriques '[3] focused on the design of low loss millimeter wave passive circuits manufactured on silicon membrane substrate. In order to design a very low loss diplexer filter, I proposed an original resonant coupling irises topology[4]. Two optimization methods

---

[1] https://fr.wikipedia.org/wiki/Erasmus

[2] https://info.erasmusplus.fr/

[3] *Contribution to the design of low insertion loss passif circuits for millimeter wave applications*

[4] A. Takacs, H. Aubert, P. Pons, T. Parra, R. Plana, "Miniature coplanar bandstop filters for Ka-band applications based on an original Resonant Coupling Irises topology", *IET Electronics Letters* (IET- former IEE periodical), Issue 20, Vol. 40, pp. 1274–1275, 30 Sept. 2004

(by successive approximations and by genetic algorithm) were also implemented. Using two tapered transitions (waveguide-to-ridged waveguide and microstrip-to-coplanar waveguide) and a microstrip-to-ridged waveguide discontinuity, a low loss and large bandwidth waveguide-to-coplanar waveguide transition was designed and manufactured. A power divider designed for an antenna array demonstrated the reliability of a compact circularly polarized radiating element on silicon membrane substrate. The results obtained during my Ph. D. thesis, defended at Toulouse on June 11 2004, have been published in 4 journals papers[5,6,7,8] and 11 conference papers.

Upon earning my Ph.D., I returned to Romania and became an assistant lecturer at the Military Technical Academy of Bucharest. I had great expectations coming back to MTA but I experienced great disillusions. My assigned teaching duties for 2014-2015 comprised of informatics and programming languages (50%) and military tactics (25%), while only 25% directly related to electrical engineering (signal processing classes assigned by my former Ph. D. advisor, Prof. Alexandru Serbanescu). After spending significant time and energy in appealing the original course subject assignments, I successfully managed to get all the military tactics classes exchanged with more informatics and electronics classes. In terms of research activities, I was able to continue my work thanks to my appointment at the Institute of Microtechnology of Bucharest. In August 2004 I joined, as associate researcher, the Microwave research group of IMT led by Dr. Alexandru Muller. He had been one the examiners during the defense of my Ph. D. thesis. At IMT I found a favorable environment to perform the research. At the beginning of 2005 I also joined the FP7 AMICOM (Advanced MEMS for RF and Millimeter Wave Communications) project (http://www.nano-link.net/amicom.htm), as member of the IMT research team. Thus, my research from 2005 to 2007 was mainly devoted to RF and microwave MEMS circuits and systems. The main results obtained in the frame of several FP7 or Romanian research project concerned mainly the reconfigurable

---

[5] A. Takacs, H. Aubert, P. Pons, T. Parra, R. Plana, "Miniature coplanar bandstop filters for Ka-band applications based on an original Resonant Coupling Irises topology", *IET Electronics Letters* (IET- former IEE periodical), Issue 20, Vol. 40, pp. 1274–1275, 30 Sept. 2004

[6] A. Takacs, D. Lillonga, H. Aubert, J.W. Tao, P. Pons, R. Crampagne, R. Plana, J.Ch. Cayrou, "Design of a Broadband WR-to-CPWG Millimeterwave Transition", *Microwave and Optical Technology Letters* (John Wiley&Sons periodical), vol 43, pp: 11-14, 5 Oct. 2004

[7] D. Dubuc, M. Saadaoui, S. Melle, F. Flourens, L. Rabbia, B. Ducarouge, K. Grenier, P. Pons, A. Boukabache, L. Bary, A. Takacs, H. Aubert, O. Vendier, J.L. Roux, R. Plana, "Smart MEMS concept for high secure RF and millimeterwave communications", *Microelectronics Reliability* (Elsevier journal), Issue 6, Vol. 44, pp.899-907, June 2004

[8] A. Takacs, A. Serbanescu, G. Leu, H. Aubert, P. Pons, T. Parra, R. Plana, "Microwave Passive Circuits Optimization Using Genetic Algorithms", *Romanian Journal of Information Science and Technology*, vol. 7, Number 3-4, pp: 309-316, 2004

MEMS-based millimeter wave filters[9,10]. I performed those research activities in parallel with the didactic activities at MTA where I taught electronics courses at bachelor's and master's levels (around 400 class hours/year). At the end of the 2007 I decided to try another international experience and, in January 2008, I rejoined LAAS as postdoctoral researcher and changed the main axis of my research activity. My research was performed in the frame of a collaborative project (partnership between Continental Automotive, Renault and LAAS) focused on the electromagnetic simulations of LF (coils) and RF antennas used in cars. The goal was to implement several control and access functions: RKE (Remote Keyless Entry), TPMS (Tyre Pressure Monitoring System) and PASE (Passive Start and Entry). The goal of the project, related to applied engineering, was very ambitious: to provide accurate and reliable models and methodologies of electromagnetic simulation in order to predict with a minimum error (less than 10%) the performance of LF and RF antennas produced by the automotive electronics manufacturer (Continental Automotive). This occurred in the early design phase of a new car when only the CAD models were provided by the car manufacturer (Renault). Despite some NDA and confidentiality restrictions, I received permission to publish some results obtained during this period in one international paper[11] and to present 2 papers at international conferences (IEEE indexed). The methodologies developed at this time were introduced in the design flow of Continental and still remain in use today (with some improvements). This one year post-doctoral partnership was very instructive. I learned how the automotive industry works and the inherent requirements, challenges, and restrictions of an industrial research project. I had also very useful interactions with engineers from Continental Toulouse (Sebastien Kesller, Alexandre Morin, Rachid Benbouhout, Fréderic Lathiere, Gregory Siguier, Mohamed Cheikh, François Marou, etc.), Continental Regensburg (Dr. Guy Chakam, Christian Schneider, Peter Turban, etc.) and Renault (Michael Huard, Eric Lardjane). During this year of internship I became aware that, in industry, scientific research must always further/promote economic and marketing goals. In July 2008 I participated in a technical workshop organized in Toulouse with the participation of Renault, Continental Regensburg, and Continental Toulouse. There, on a Friday, it was unanimously decided to implement the newly developed simulation models and methodologies to a new big car ('Grand Espace') under development at Renault. Due to the

---

[9] A.Takacs, D. Neculoiu, D. Vasilache, A. Muller, P. Pons, L. Bary, P. Calmon, H. Aubert, R. Plana, "Tunable bandstop MEMS filter for millimeter wave applications", *IET Electronics Letters*, Issue 12, Vol. 43, pp. 676-677, 7 June 2007

[10] A.Takacs, D. Neculoiu, D. Vasilache, A. Muller, P. Pons, L. Bary, R. Plana, "Design of tunable bandpass MEMS filter for millimeter wave systems", *Revue Roumaine des Sciences Techniques*, tome 51, 4, pp: 471-477, 2006. (ISSN: 0035-4066)

[11] A. Takacs, M. Huard, S. Kessler, G.A. Chakam, E. Lardjane, "Estimation of low frequency coverage inside car for passive access system entry", *IET Electronics Letters*, Issue 12, Vol. 45, No. 12, pp. 596-597, 4 June 2009

urgency (we had only two weeks to work on the project because the 'Grand Espace' project was very advanced), I negotiated with my German, French, Mexican, and Romanian colleagues that used the same 64-core simulation cluster for various ongoing Continental projects to free up 56 cores for the weekend for me and my project. I launched intensive simulations during the weekend and the next Monday morning I analyzed the results of more than 48 hours of intensive computations. The results were very promising butthe same morning my colleague Hervé Foligne of Continental, chief of the project 'access systems' for Renault cars, announced to me that the project 'Grand Espace' was aborted despite of its advanced development phase because the automotive market was entering a recession phase. The decision was taken during the weekend, at the highest management level, at the Renault headquarters. The automotive industry was in crisis in 2008 and 2009. As a result, my research project, collaboration between Continental, Renault, and LAAS, was also aborted in 2009. Once again, I changed the focus of my research, while remaining in the field of the electromagnetic engineering. I joined Prof. Aubert and the LAAS team and the ANR project NANOTERA. Alongside the Nanotera project, I also worked on the miniaturization of the VHF quadrifilar helix antennas for TTC space applications as part of several Research and Technology grants funded by CNES. The NANOTERA project was very interesting, consisting of the experimental validation of the Ratchet effect and its potential applications in the fields of detectors, current generators, and other microwave devices. I worked in collaboration with physicists (specialized in theoretical and experimental physics) and I also started to co-advise, with Prof. Aubert, the master thesis and, subsequently, the Ph. D. thesis of Dina Medhat Mohamed Abdel Maksoud. Dina defended her Ph.D. thesis in October 2012, and his results have been published in one international journal paper[12] and 5 papers published in the proceedings of international conferences. The main challenges of the ANR project were both technological and experimental. The Ratchet effect was experimentally proved by the team of Prof. J-C Portal at cryogenic temperatures by using samples of 2D electronic gases specially manufactured in Japan. At LAAS, we developed an experimental setup working at ambient temperature by using graphene samples manufactured by Dr. Georges Deligeorgis at Forth Heraklion in Greece. The samples were very sensitive and had a very complicated manufacturing process. We obtained promising results just before Dina's defense. Some results were presented in his Ph. D. manuscript[13], but, because of the end of the ANR NANOTERA project, this research axis was abandoned. Nevertheless, another line of research focused on

---

[12] D. Medhat, A. Takacs, H. Aubert, "A methodology to study the electromagnetic behavior of a cryogenic metallic system used to control the ratchet effect", *Progress In Electromagnetics Research M*, Vol. 23, 123-137, 2012

[13] https://tel.archives-ouvertes.fr/tel-00766791

the miniaturization of antenna, which started in parallel with my work on NANOTERA project, was very productive. My first international brevet on antennas[14] was related to an original method to miniaturize VHF quadrifilar helix antennas. The research concerning QHA miniaturization also represented an opportunity for having fruitful scientific interaction with several CNES researchers, notably Dr. Nelson Fonseca (today at ESA), Hubert Diez and Daniel Belot. Also, I mention the work performed with enthusiasm by two master's students that I co-directed during this time: Mingtian Wang and Mohamed Fodil. Mingtiam obtained his Ph. D. diploma from ENAC and University Paul Sabatier of Toulouse in 2014. At the end of 2010, I was hired by Continental Automotive Toulouse as design engineer in charge of antenna design and electromagnetic simulations for automotive applications. I was involved in many ongoing automotive projects concerning mainly the development of various VHF antennas for RKE applications and of LF coils and associated circuits for wireless charging platform for smartphones. It was a very instructive and fruitful professional experience because I gained an understanding of the inherent complexity, challenges, and the strong competition within the automotive industry. I also had professional satisfactions. The VHF antennas that I designed were finally included, with few modifications, in the Continental products (key entry system and badges) and are deployed now at large scale on Renault cars. The research started at Continental in the frame of 'wireless charging platform' concerning the inductive WPT later became one of my research axes, as detailed in the '*Inductive and near-field wireless power transmission*' section of this manuscript. I was also granted several patents that I co-authored with my Continental colleagues: Dr. Mohamed Cheick, Sebastien Kessler and Youri Vassilieff.

At the end of 2011 I joined the Paul Sabatier University of Toulouse and LAAS CNRS where I performed most of my scientific research. The research fields that I explored during my last seven years at LAAS concerns mainly:

(i) WPT and EH research for various applications including, but not limited to: microwave energy harvesting for space application, WPT for battery-less tags and indoor localization and tracking systems, WPT for 'communicating concrete', 'communicating materials', and intelligent building. This is my main research topic and it is highlighted in section '*Wireless power transmission and energy harvesting*'.

---

[14] Hubert Diez, Herve Aubert, Daniel Bellot, Alexandru Takacs, 'Antenne hélice compacte à profil sinusoïdal modulant un motif fractal, brevet CNES', France patent FR2988524 (A1)/FR2988524 (B1). The patent was extended in Europe/international with the title "Compact helical antenna with a sinusoidal profile modulating a fractal pattern", WO2013139935 (A1). Publication date : September 27, 2013

(ii) Compact antenna and miniaturization techniques. The associated research is presented in section *'Compact antennas and antenna miniaturization techniques'*.

(iii) Flexible substrate technologies for millimeter wave applications (section *'Flexible substrate technologies for millimeter wave applications'*)

(iv) Design of RF and microwave circuits and systems (some of my results are presented in the section *'Design of passive and active RF and microwave circuits'*)

My early research works, between 2004 (when I obtained my Ph. D.) and 2011 (when I become Associate Professor – Maître de conferences at thePaul Sabatier University of Toulouse and I joint LAAS-CNRS) are presented in the section *'Early research works: low loss circuits for microwave and millimeter wave applications'*. At LAAS I performed my research as part of several research projects as listed in *'Research projects and responsibilities'*). Among them, several projects represent the core of my scientific evolution :

(i) ICT COST Action IC1301 Wireless Power Transmission for Sustainable Electronics (WiPE)[15]. This COST action, started in 2013, allowed me to network with the most representative European laboratories performing active WPT research. As France's representative in the management committee, I was involved in many key meetings, workshops, and summer schools. Also, I had interesting and fruitful discussions and collaborations with professors, researchers and industry representatives from all of Europe and even from the all the world.

(ii) the project OPTENLOC[16], funded by Occitanie Région and Uwinloc company. This ongoing project allows me to perform research and transfer my research results to industry in the field of far-field WPT. Also, this project incorporates today's trends in the WPT research and helped define my vision of the far-field WPT research (namely, the migration of the research focus from device to systems level, as described in the section *'My research project: the next decade'*).

(iii) the project Material Communicating with the BIM - McBIM[17], funded by ANR (French National Research Agency). The challenging goals of this multidisciplinary research project started in October 2017 involve the use of the WPT techniques and interfaces in order to wirelessly supply power to

---

[15] http://www.cost-ic1301.org/

[16] Intégration **Op**timale d'un système de **T**élé-alimentation en **EN**ergie dans les tags intelligents de **LOC**alisation pour applications industrielles

[17] http://www.agence-nationale-recherche.fr/en/anr-funded-project/?tx_lwmsuivibilan_pi2%5BCODE%5D=ANR-17-CE10-0014

so-named 'sensitive nodes' (see section '*Wireless power transmission for 'communicating materials'*') embedded in concrete and used for SHM applications. To my best knowledge, this innovative and challenging approach has not yet been addressed by the scientific community.

Early research works: low loss circuits for microwave and millimeter wave applications

Some results of my early research work in the field of electromagnetic engineering are highlighted in this section. This research was performed just after my Ph. D. thesis, from 2004 to 2007, when I was Researcher at Institute of Microtechnology of Bucharest and Lecturer at the Military Technical Academy of Bucharest. The research focused mainly on the RF MEMS circuits and systems was performed in the frame of several European (notably, the FP7 European Network of Excellence AMICOM - Advanced MEMS for RF and MIllimeterwave COMmunications-) and Romanian research projects. It was a very interesting period when I interacted with most of the European research community working in the field of RF MEMS. By far, the most valuable results that I obtained are related to the design and characterization of microwaves and millimeter wave MEMS-based reconfigurable filters. The topology of a proposed Tunable BandPass Filter (TBPF) is represented in Figure 1. This topology is based on the use of quarter wavelength stubs in combination with RF MEMS switches (named Two Cantilever Shunt Switches, or TCSS), acting as variable capacitive load for achieving the desired bandpass behavior. The filters were implemented using Finite Ground CoPlanar Waveguide (FGCPW) technology in order to facilitate the integration with other components and the DC actuation of the TCSS.
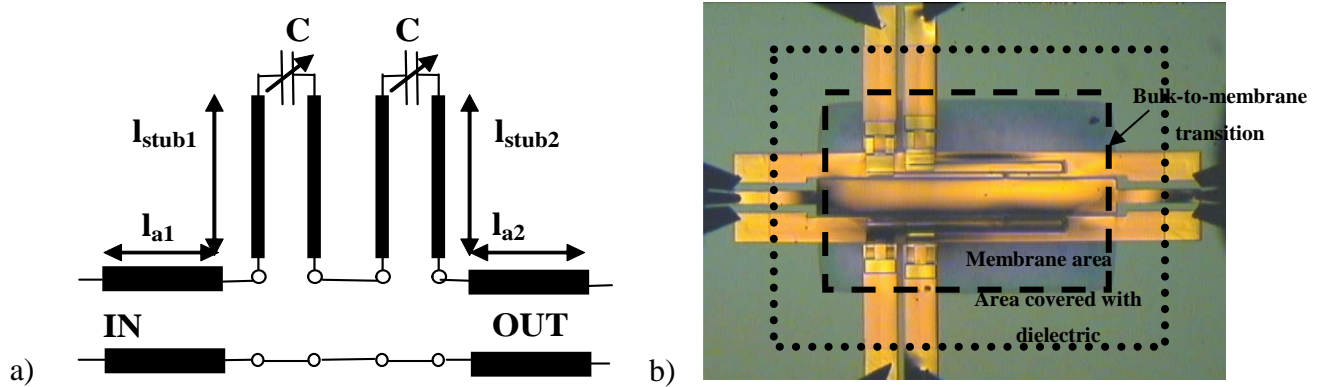
Figure 1. a) Generalized transmission line model for the TBSF topology. The CPW access lines have the geometrical lengths l_{a1} and l_{a2} while l_{stub1} and l_{stub2} represent the geometrical lengths of the stubs; b) photo of the manufactured TBPF.

The experimental results obtained for the V-band TBSF filter are depicted in Figure 2 and more details can be found in the paper *'Tunable bandpass MEMS Filters for Millimeter Wave Applications: design and results'* listed at the end of this manuscript.
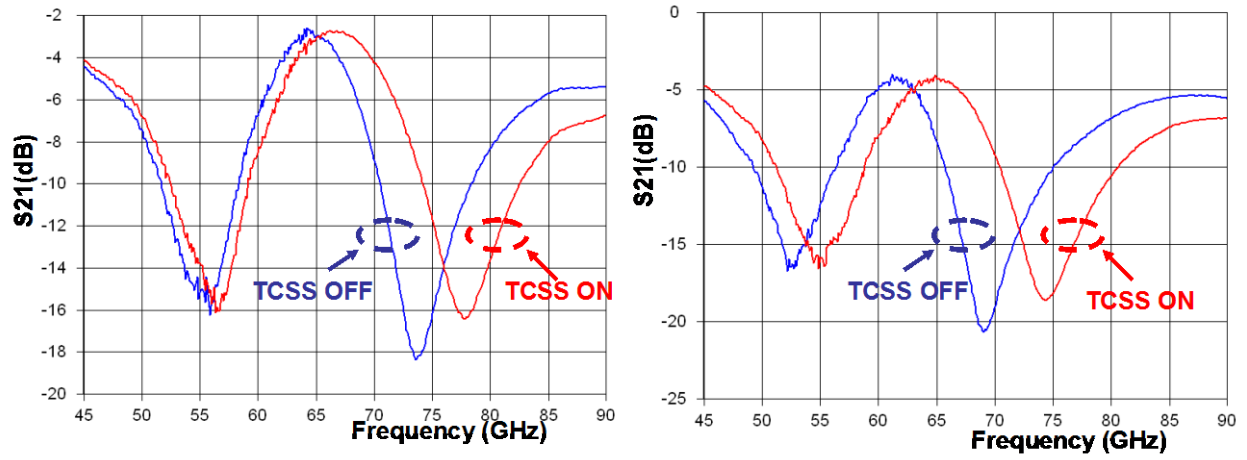
Figure 2. Experimental results for TBPF-Type I (left) and TBPF-type II filters (right)

Compact antennas and antenna miniaturization techniques

Compact antennas and antenna miniaturization techniques[18] are important research topics that were recently boosted by the rising popularity of IoT applications. As explained previously, I started my research on these topics in 2008 and my best results are related to the compact VHF QHA for satellite applications and compact antennas for EH/WPT applications.

VHF quadrifilar helix antennas have been used since the 1950s for the implementation of TTC link in many satellite missions, but they have become too bulky for modern satellites. Based on an original optimization method combined with intensive electromagnetic simulations, we developed an original miniaturization technique consisting of the inductive loading of the QHA helical wires by shaping them into a sinusoidal modulated in fractal manner. This technique was patented and our results were published in 3 journal papers[19,20,21] and several communications presented at international symposia and conferences. The paper *'Miniaturization of Compact Quadrifilar Helix Antennas for Telemetry, Tracking, and Command Applications'* annexed at the end of this manuscript gives an exhaustive picture of the results obtained in the field of QHA miniaturization for space applications. Two master's students, Mingtian Wang and Mohamed Fodil, worked on this topic under my supervision during their master's internships.

When I started my research on far-field WPT, I realized that a compact antenna having a best trade-off between its electromagnetic performance and size is a key element for any successful rectenna design. Several compact antennas designed for rectenna were proposed and are represented in Figure 3. The 2CDAA (Two Cross Dipole Antenna Array), represented in Figure 3.a) and Figure 3.b), is a compact array composed by two cross dipoles[22]. Each cross dipole is composed by two dipoles printed on PCB and placed in a crossed configuration. A metallic plate properly positioned behind the 2CDAA can be used as reflector

---

[18] M. Fallahpour, R. Zoughi, "Antenna Miniaturization Techniques: A Review of Topology- and Material-Based Methods", *IEEE Antennas and Propagation Magazine*, Vol. 60, Issue 1, Feb. 2018

[19] A. Takacs, N. J.G. Fonseca, H. Aubert, "Height Reduction of the Axial-Mode Open-Ended Quadrifilar Helical Antenna", *IEEE Antenna and Wireless Propagation Letters*, vol. 9, pp. 942-945, 2010

[20] A. Takacs, H. Aubert, H. Diez, D. Belot, "Miniaturization of Quadrifilar Helical Antenna: Impact on Efficiency and Phase Center Position", *IET Microwaves, Antennas & Propagation*, Volume 7, Issue 3, 19 February 2013, pp. 202 – 207

[21] A. Takacs, H. Aubert, D. Belot, H. Diez, "Miniaturization of Compact Quadrifilar Helix Antennas for Telemetry, Tracking and Command Applications", *Progress In Electromagnetics Research C*, Vol. 60, 125-136, 2015

[22] A. Takacs, H. Aubert, S. Fredon, L. Despoisse, "Design and Characterization of Effective Antennas for K-band Rectennas", in *Proc. of IEEE EUCAP'2015*, Lisbon, Portugal, April'2015

to improve the antenna gain. This antenna array has a surface of 2.5 cm^2 that is only 0.6 λ^2 at 14.7 GHz, the targeted operating frequency. It uses an original feeding network composed of only one stripline, which is also an appropriate solution for the associated rectenna design[23]. The 2CDAA exhibits a high gain (10 dB) radiation pattern with a quite wide 3dB beamwidth at least 52°, which fulfills the technical requirements for a high-efficiency K-band rectenna for satellite applications.

a)   b)   c)

d)   f)
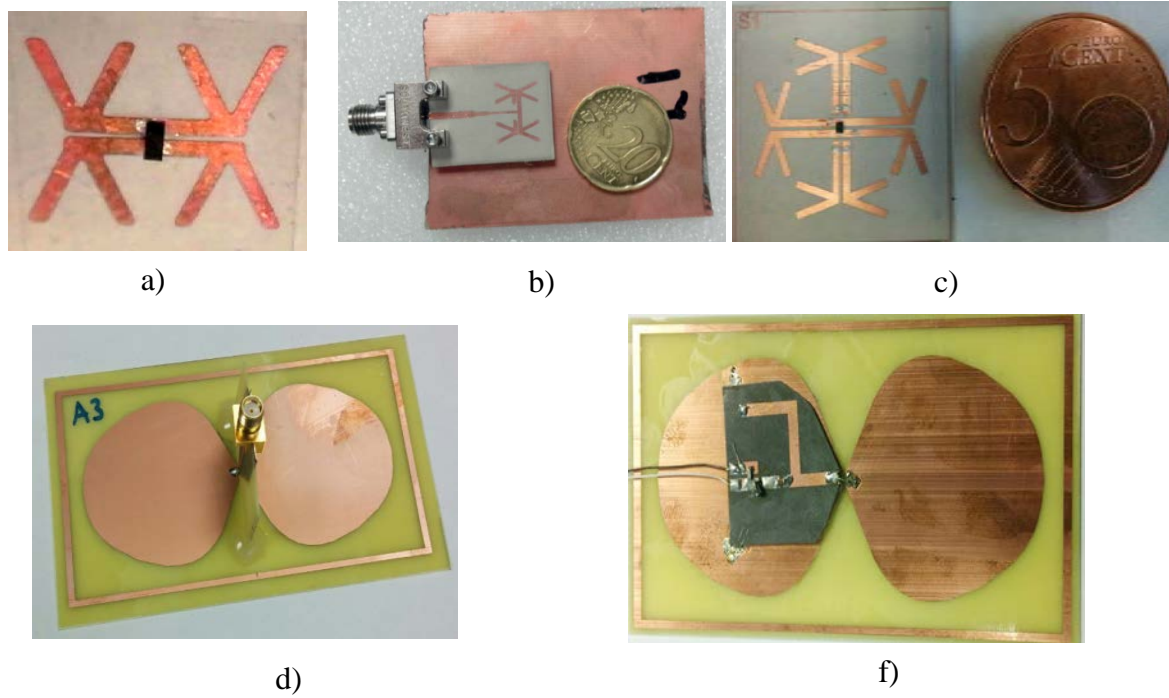
Figure 3. Photo of several compact antennas and rectennas: a) a compact rectenna using a two cross dipole antenna array (2CDAA) for K band applications; b) the 2CDAA with its stripline to microstrip transition implemented for antenna characterization; c) a rectenna for Ku/K band applications using a compact multiband 4CDAA (four cross dipole antenna array); d) compact wideband flat dipole antenna, with its rectangular ring, for a low profile rectenna operating in ISM 868 MHz/915 MHz band.

The topology of the 2CDAA was extended to an array formed by four cross dipole antennas (4CDAA, represented in Figure 3.c). This antenna also exhibits multiband behavior and was successfully integrated in a Ku/K band rectenna[24]. The topology of this antenna as well as the associated results are presented in the paper "*Multiband rectenna for microwave applications*" annexed at the end of this manuscript. For the rectennas designed for WPT applications in the ISM 868 MHz/ ISM 915 MHz, a new

---

[23] A. Takacs, H. Aubert, S. Charlot, "Ultra-Compact Ku band Rectenna", in *Proc. of IEEE IMS'2015*, Phoenix, USA, 17-22 May, 2015

[24] A. Okba, A. Takacs, H. Aubert, S. Charlot, P-F. Calmon, "Multiband rectenna for microwave applications", *Comptes Rendus Physique, Elsevier*, Vol. 18, Issue 2, pp 107-117, Feb. 2017

and compact topology was proposed here. It consists of a Flat Dipole Antenna (FDA) enclosed by a rectangular ring as represented in Figure 3.d). The FDA is a modified version of the standard half-wavelength dipole antenna and was obtained by changing the geometry of the two constitutive quarter-wavelength monopoles. The monopole shape could be triangular, quasi-triangular or quasi-circular. In our case, the quasi-circular shape was chosen, as shown in Figure 3.d). As expected, the most interesting result arising from this geometrical modification is the increase of the frequency bandwidth. For the standard straight half-wavelength dipole, the current flows only along the physical length of the two constitutive monopoles (or arms) and, consequently, the operating/resonant frequency is mainly driven by this length. When the shape of the monopoles is rounded off, the current takes multiple paths causing the wideband behavior of such an antenna[25]. The wideband FDA is then miniaturized by adding a rectangular ring as illustrated in Figure 3.d). This rectangular ring, acting as a one wavelength loop, is electromagnetically coupled to the FDA and the obtained antenna is then miniaturized without deteriorating its performance. This compact antenna was integrated in planar rectennas designed for IoT applications. The paper *'Compact Flat Dipole Rectenna for IoT Applications',* listed at the end of the manuscript, details more the FDA topology and presents more results concerning both the FDA and the associated flat dipole rectennas. More research is ongoing and aims to obtain more compact antennas (i.e., by using a quarter-wave FDA coupled with a half-wave loop).

---

[25] A. Okba, A. Takacs, and H. Aubert, "Compact Flat Dipole Rectenna for IoT Applications," *Progress In Electromagnetics Research C*, Vol. 87, 39-49, 2018

Wireless power transmission and energy harvesting

In 1864, J.C. Maxwell unified the electromagnetic theory by introducing a set of differential equations known as 'Maxwell equations'. Maxwell's work was groundbreaking and represents a milestone in the development of electromagnetic physics. His results have been made possible as a result of 200 years of research performed by talented Scientists including, but not limited to, Coulomb, Ampère, Faraday, Lenz, Œrsted, Gauss, and Huygens. Maxwell's equations explained most of the known electromagnetic phenomena and introduced the idea that electromagnetic waves should exist. Some years later, in 1887, Heinrich Hertz experimentally proved the existence of electromagnetic waves. The Hertz experiment opened the way for the use of such waves to transfer/transmit 'something' from one point to other without the use of wires. Two talented scientists and inspired inventors explored two different and apparently opposite research directions: (i) the use of the electromagnetic waves to transmit information (Marconi's approach, which opened the way for radio communications, a better alternative to the telegraph); and (ii) the use of electromagnetic waves to transmit energy (Tesla's approach, which opened the way for wireless power transmission/transfer, or WPT, as an alternative to the wired grid used for electricity distribution). Marconi's approach was easier to implement and important advances were rapidly obtained in the field. The 20th century confirmed the 'supremacy' of the Marconi approach (wireless communications) over Tesla's approach (WPT), with several notable exceptions: (i) the technology of induction cooking, based on power transmission in the near-field region by using the magnetic field, was first introduced in a World Fair at Chicago in 1933 and was then developed at large scale starting from 1970; (ii) the birth of the RFID technology in 1950 as a consequence of an espionage affair (Russians spied on the American embassy in Moscow by using a rudimentary RFID technology), and (iii) the Brown experiments (1960-1980) that demonstrated that is possible to transmit energy at a distance, in the far-field region, by using RF and microwave waves. At the beginning of the 21st century, WPT research once again raised interest through a focus on new fields of applications: wireless charging of various electronics devices (smartphones, laptops, electronic bio-implants, etc), wireless charging of electric cars, implementation of battery-less systems (including, but not limited to: wireless sensors, active

tags, cyber-physical systems, etc.). Figure 4 shown the photos of several WPT demonstrators and products illustrating the historical evolution of WPT concepts and research.
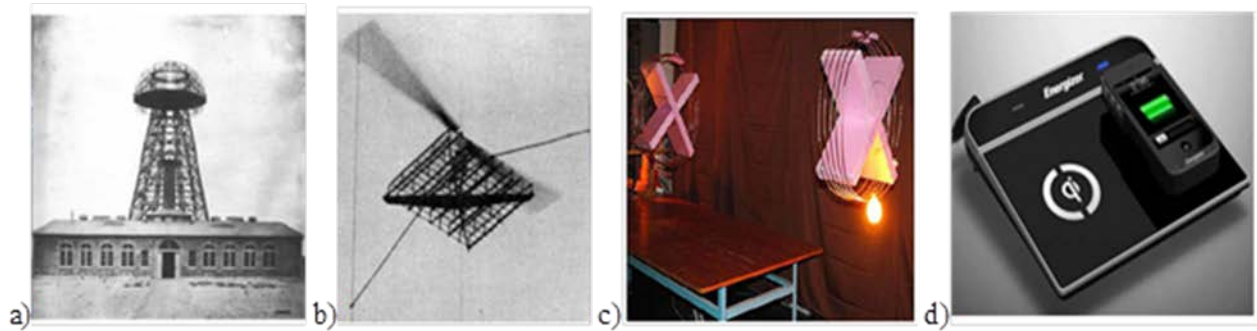
Figure 4. Examples of WPT demonstrators and product: a) Wardenclyffe tower build by Nicolas Tesla for his WPT experiments (near-field WPT); b) the 'drone' of W. C. Brown powered by a microwave link (far-field WPT); c) Witricity systems (near-field WPT); d) a charging platform for smartphone (near-field WPT, Qi standard), manufactured by Energizer.

Inductive and near-field wireless power transmission

My first contact with WPT technology and the related research was more or less hazardous. At the end of 2010, with ten years of experience in the field of RF and microwave circuit design, I was hired by Continental Automotive Toulouse (former Siemens VDO) as design engineer in charge with antenna design and electromagnetic simulations for automotive applications. In May 2011 I was ask by Dr. Mohamed Cheick and Youri Vassilieff to become involved in the design of LF coils and associated systems intended to be used by the automotive wireless charging platform for smartphones, a new 'automotive product/system' under development at Continental. I accepted enthusiastically and I shifted my research from RF to LF, from far-field to near-field, and from electric field to magnetic field. I make the right choice in terms of research and my work was granted with several French and international patents[26][27][28]. As presented later in this section, I continued to work in the field of inductive WPT even after my departure from Continental and inductive WPT remains an important aspect of my research. The WPT techniques can be classified as illustrated in Figure 5. In 2012, Continental Automotive funded a direct research grant, in collaboration with LAAS-CNRS, concerning the development of accurate simulation models and design methodologies for the LF coil designs and associated systems integrated in the automotive wireless charging platform for smartphones that were under development at that time at Continental.

---

[26] Cheikh Mohamed; Kessler Sebastien; Takacs Alexandru, "Dispositif et procède de configuration d'antenne", French patent FR2984020 (A1), FR2984020 (B1) and international patent WO2013087198 (A1). Publication date June 14, 2013

[27] Takacs Alexandru, Vassilieff Youri, Cheikh Mohamed "Dispositif de chargement inductif d'un appareil portable intégrant une antenne de communication en champ proche" Patent (France) : FR2981519 (A1). US patent - US2013093387 (A1)- Chinese patent CN103051067 (A)- with the title "Inductive charging device for a portable apparatus incorporating a near-field communication antenna". Publication date : April 19, 2013

[28] Takacs Alexandru, Cheikh Mohamed, Kessler Sébastien, "Procédé de caractérisation d'un dispositif portable par une antenne embarquée dans un véhicule automobile", Patent (France) 2983808-A1 and international patent "Method for characterizing a portable device by way of an antenna on board a motor vehicle" Publication Number 2013/087197. Publication Date : June 20, 2013
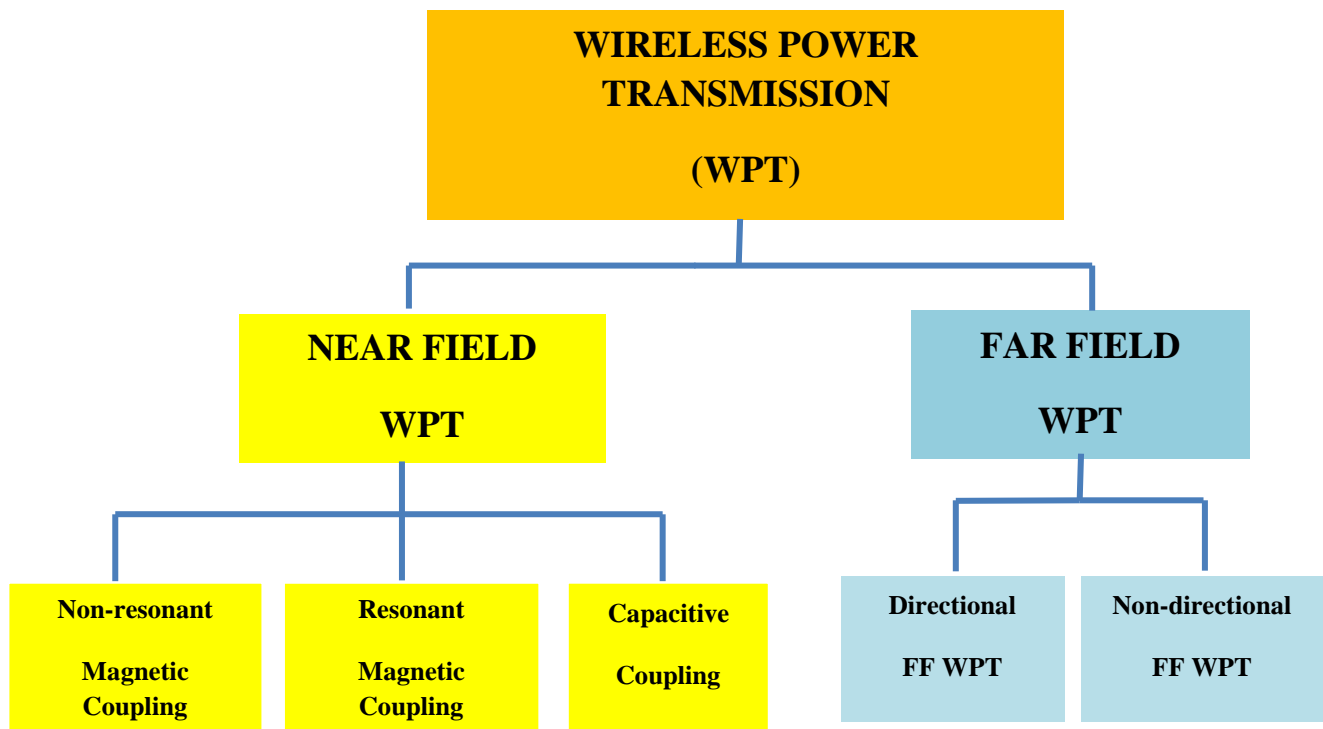
Figure 5. Classification of WPT techniques.

In fact, this work was a continuation of the research that I performed in 2011 as engineer at Continental. It was the subject of the postdoctoral internship of Dr. David Jugieu that I directed from 01.04.2012 to 31.03.2013. His thesis was entitled: *'Etude et modélisation électromagnétique du transfert d'énergie pour le chargeur inductif'*. David's work was continued by Guillaume Vigneau in the framework of CIFRE thesis (collaboration Continental – LAAS) started in February 2013. I co-directed Guillaume's Ph. D. thesis alongside Dr. Mohamed Cheikh from Continental. Despite some restrictive NDA clauses, the results obtained by David and Guillaume were published in one international (journal) paper[29] and 3 communications presented at international symposia.

---

[29] G. Vigneau, M. Cheikh, R. Benbouhout, A. Takacs, "Design and Modeling of PCB Coils for Inductive Power Charging", *Wireless Power Transfer, (Cambridge University Press)*, Vol. 2, Special Issue 02, Sept. 2015, pp 143 – 152.

Energy harvesting for space applications

In October 2011 I came back to LAAS CNRS and I joined the University of Toulouse III Paul Sabatier as Associate Professor (Maître de Conferences). Professor Aubert proposed that I join the LAAS team as part of a Research & Technology research grant (R&T)[30] funded by the French Space Agency (CNES). I accepted enthusiastically. My choice proved to be the right one, as harvesting of the electromagnetic energy and the far-field WPT have become major aspect of my research for at least a decade. For this grant, the goal of the research performed by a consortium composed by CNES, Thales Alenia Space, and LAAS was to identify and quantify the various 'environmental' sources of energy that may exist on-board broadcasting geostationary satellites and that could be harvested and used as energy (micro-) sources for wireless sensors. Two sources of energy were identified: (i) the electromagnetic energy generated by the spill-over losses of broadcasting microwave antennas and (ii) the thermal gradient between the internal and the external body of the satellite. I designed several rectifiers and rectennas and we proved that we can harvest electromagnetic energy in order to power a wireless sensor (e.g., a temperature sensor and a low-power transmitter) that can be used for SHM (Structure health monitoring) application on satellite antenna panels. This proof-of-concept, based on results obtained in 2011-2013, was published for the first time in 2013[31,32]. It is fair to recognize that rectennas are not novelties in the field of the scientific research. The first rectennas were designed by Brown's team fifty years ago for WPT applications (e.g., to power wirelessly a small electric helicopter – in fact a small drone – but the term was not yet used in the 1960s). The rectennas developed by Brown's team and later

---

[30] R&T CNES n° 115052 « Evaluation de diverses micro-sources de génération et stockage d'énergie », 2011-2012

[31] A. Takacs, H. Aubert, L. Despoisse, S. Fredon, "Broadcast energy", *IET Electronics Letters*, Issue 11, Vol. 49, 23 May 2013, p. 682

[32] A. Takacs, H. Aubert, L. Despoisse, S. Fredon, "Microwave energy harvesting for satellite applications", *IET Electronics Letters*, Issue 11, Vol. 49, pp. 722-723, 23 May 2013

by other researchers (Chang's team[33]) were designed for WPT applications[34], where DC power in the range of thousands of μW/mW had to be delivered at the output of the rectenna/rectennas array. Later, several pilot experiments were conducted in Grand Bassin, La Reunion, France, and in Hawaii, USA, in order to supply electricity to a remote location by beaming the electrical power (WPT, far-field technique). In the Grand Bassin experiment[35], a power of 65 W (targeted 10kW in the case study but finally not implemented for demonstration due to high costs) was delivered over a distance of 700 m by a microwave link operating at 2.45 GHz with an overall efficiency (Tx to Rx) of 6%. In 2008, a long-range WPT experiment was conducted on one of the islands of Hawaii. A DC power around 20 W was collected (by WPT) over a distance of 148 kilometers.

In the 21st century, the interest for rectennas rose again because of emerging applications such as: (i) the harvesting of the RF energy generated by various sources (TV broadcasting transmitters, GSM base stations, GSM smartphones, WiFI routers, etc.); (ii) the implementation of energy-autonomous low-power devices and systems (e.g. wireless sensors, battery-less active tags, cyber-physical devices and systems, etc.). In these scenarios the rectennas must operate at very low values of the illuminating/incident electromagnetic power densities (typically less than 1μW/cm^2) with an efficiency as high as possible. The DC output power of such rectennas is in the range of hundreds of μW and does not exceed, in optimistic scenarios, thousands of μW. Additional restrictions may also apply and mainly concern the compactness, the back-scattering of harmonics, or the manufacturing cost. For such

---

[33] T.-W. Yoo and K. Chang, "Theoretical and experimental development of 10 and 35 GHz rectennas," *IEEE Trans. Microw. Theory Techn.*, vol.40, no. 6, pp. 1259–1266, Jun. 1992.

[34] W. C. Brown, "The history of power transmission by radio waves," *IEEE Trans. Microw. Theory Techn.*, vol. 32, no. 9, pp. 1230-1242, 1984.

[35] A. Douyere et al., 'Grand Bassin Case Study: An Original Proof-of-Concept Prototype for Wireless Power Transportation', in *Proc. of WPTC'2018*, available online at: https://www.researchgate.net/profile/Alexandre_Douyere/publication/325788950_Grand_Bassin_Case_Study_An_Original_Proof-Of-Concept_Prototype_for_Wireless_Power_Transportation/links/5b23ce45aca272277fb25d10/Grand-Bassin-Case-Study-An-Original-Proof-Of-Concept-Prototype-for-Wireless-Power-Transportation.pdf?origin=publication_detail

applications, the design, the technology of fabrication, and even the characterization method of a rectenna are related to: (i) the estimated values of the incident/illuminating power densities; (ii) the amount of the expected (to be delivered) DC power; (iii) the operating frequency/bandwidth; and (iv) the particularity of the application.

After proving the feasibility of microwave energy harvesting for space application, we also obtained two other research grants from CNES in order improve the efficiency and the compactness of the rectennas operating in K, Ku, and C-bands. We published new papers and I focused my research on compact, efficient, and multi-band rectenna designs operating in K, Ku, and C bands. Only few research works, including experimental results[36,37,38,39], have been reported on rectenna design at frequencies higher than 10 GHz. The reason for this relative lack of published designs at such frequencies is the inherent limitations for obtaining an effective high-frequency rectenna design: (i) the non-linear devices (e.g. Schottky diodes) have intrinsic limitations[40] and the associated simulations models are not very accurate; (ii) for compact design, the electromagnetic coupling between the antenna and the rectifier can be very strong and its impact should be taken into account in the design; (iii) the impact of any connector used for characterization can be carefully quantified (the end-launch connectors may have important losses, as their dimensions are in the same size range as the rectenna and a parasitic electromagnetic coupling can occur between the structure under test and its end-launch connector). The published designs also primarily address WPT applications because of

[36] T.-W. Yoo and K. Chang, "Theoretical and experimental development of 10 and 35 GHz rectennas," *IEEE Trans. Microw. Theory Techn.*, vol.40, no. 6, pp. 1259–1266, Jun. 1992

[37] Y.-J. Ren, M.-Y. Li, K. Chang, "35 GHz rectifying antenna for wireless power transmission," *IET Electronics Letters*, vol.43, no.11, pp.602-603, May 24 2007

[38] S. Ladan, A. B. Guntupalli, K. Wu, "A High-Efficiency 24 GHz Rectenna Development Towards Millimeter-Wave Energy Harvesting and Wireless Power Transmission", *IEEE Transactions on Circuits and Systems*, Vol. 61, Issue 12, pp. 3358-3366, December 2014

[39] A. Collado, A. Georgiadis, "24GHz Substrate Integrated Waveguide (SIW) Rectenna for Energy Harvesting and Wireless Power Transmission", *IEEE MTT-S International Conference*, Seattle, WA, 2-7 June 2013

[40] C. H. P. Lorenz, S. Hemour and K. Wu, "Physical Mechanism and Theoretical Foundation of Ambient RF Power Harvesting Using Zero-Bias Diodes," in *IEEE Trans. on Microwave Theory and Techniques*, vol. 64, no. 7, pp. 2146-2158, July 2016

the lack of terrestrial environmental electromagnetic energy at such high frequencies. Thus my field of research was relatively open and somewhat exploratory.

For any rectenna design there are several choices to do concerning:

(i) antenna topology. Depending on application and design requirements, the antennas need to fit some restrictions in terms of operating bandwidth, polarization, size, efficiency, gain, and radiation pattern/beamwidth.

(ii) the choice of the non-linear device used by the rectifier. By far, the most popular non-linear devices in use are the Schottky diodes and the CMOS transistors (for integrated rectifiers). The technology of the Schottky diodes is by far the most matured, but it is intrinsically limited in terms of thermionic emission-based rectification, thermal voltage, and maximum responsivity. There are also other non-linear devices[41,42,43] that can be used in rectifiers such as: tunnel diodes, MIM diodes, and spindiodes. These diodes can partially overcome the intrinsic limitations of the Schotkky diodes but are 'fragile' and not yet produced at industrial scale.

(iii) the rectifier topology. Classical rectifier topologies, such as single diode (series or shunt), voltage multiplier, or bridge rectifier, were intensively used in rectenna design. The rectifier topology should be selected based on: (a) the non-linear element used for the rectification, (b) the available RF power at the input of the rectifier, and (c) the required DC voltage at the output of the rectifier.

(iv) the adopted matching technique between the antenna and the rectifier. In order to maximize the power transfer between the antenna and the rectifier, a complex conjugate matching has to be accomplished at the targeted operating frequency (i.e., the impedance of the antenna must equal the complex conjugate of the input impedance of the rectifier,

[41] S. Hemour and K. Wu, "Radio-Frequency Rectifier for Electromagnetic Energy Harvesting: Development Path and Future Outlook," in *Proceedings of the IEEE*, vol. 102, no. 11, pp. 1667-1691, Nov. 2014

[42] S. Hemour *et al*., "Towards Low-Power High-Efficiency RF and Microwave Energy Harvesting," in *IEEE Transactions on Microwave Theory and Techniques*, vol. 62, no. 4, pp. 965-976, April 2014

[43]C. H. P. Lorenz et al., "Breaking the Efficiency Barrier for Ambient Microwave Power Harvesting With Heterojunction Backward Tunnel Diodes," in *IEEE Transactions on Microwave Theory and Techniques*, vol. 63, no. 12, pp. 4544-4555, Dec. 2015

including its matching circuit, if any). Typically two approaches can be used: (a) the antenna and the rectifier are both matched to 50 Ω; (b) the antenna and rectifier impedances (including that of the matching circuit, if any) are properly controlled in order to verify the complex conjugate (impedance) matching condition.

(v) the DC and RF filtering. Typically, a low-pass filter is intercalated between the rectifier and the load and an RF filtering function should be implemented between antenna and the rectifier to prevent the backscattering, by the antenna, of the energy at harmonic frequencies. Usually, the matching circuit between the rectifier and antenna exhibits a band-pass behavior but sometimes a dedicated RF filter should be intercalated between antenna and rectifier or a special design should be implemented on the antenna side in order to prevent the backscattering phenomenon.

When I started my research on RF and microwave energy harvesting for space applications, I took into account the electromagnetic maps provided by Thales Alenia Space and CNES[44] concerning the available electric field on satellite panels as well as other restrictions imposed by CNES concerning the design and the implementation of the rectennas. As suggested by CNES, the adopted topology of the rectenna should be as simple as possible, as compact as possible, and manufactured using materials and devices (COTS) qualified, or at least pre-qualified, for space applications. For these reasons, I exclusively used Schotkky diodes (many already used in mixer or detectors for space applications) and prime quality RF substrate (e.g., Rogers RT6002, which is a substrate certified for military applications). Based on these inputs and requirements, we proposed two types of rectenna designs: one using patch antenna and the microstrip technology and one using printed dipole antennas and coplanar striplines for interconnections. Several fabricated rectennas (using patch and printed dipole antennas) are represented in Figure 6. We started with an in-line design (microstrip technology) as illustrated in Figure 6.a) but the rectenna surface was quite large (as compared to the wavelength). We also decided to try another approach: we replaced the patch antenna with a printed dipole antenna and we implemented the complex conjugate matching by

---

[44] A. Takacs, H. Aubert, S. Fredon, L. Despoisse, H. Blondeaux, "Microwave power harvesting for satellite health monitoring," *IEEE Trans. on Microwave Theory Tech*, Vol.: 62, Issue: 4 , pp. 1090 - 1098, April 2014

properly controlling the input impedance of the rectifier and of the antenna[45]. Using cross-dipole topologies we proposed:

(i) rectenna topologies using a cross dipole (Figure 6.b1)

(ii) rectenna topologies using an antenna array composed by two cross dipole antennas, as illustrated in Figure 6.b2)

(iii) rectenna topologies using an antenna array composed by four cross dipole antennas, as illustrated in Figure 6.b3).
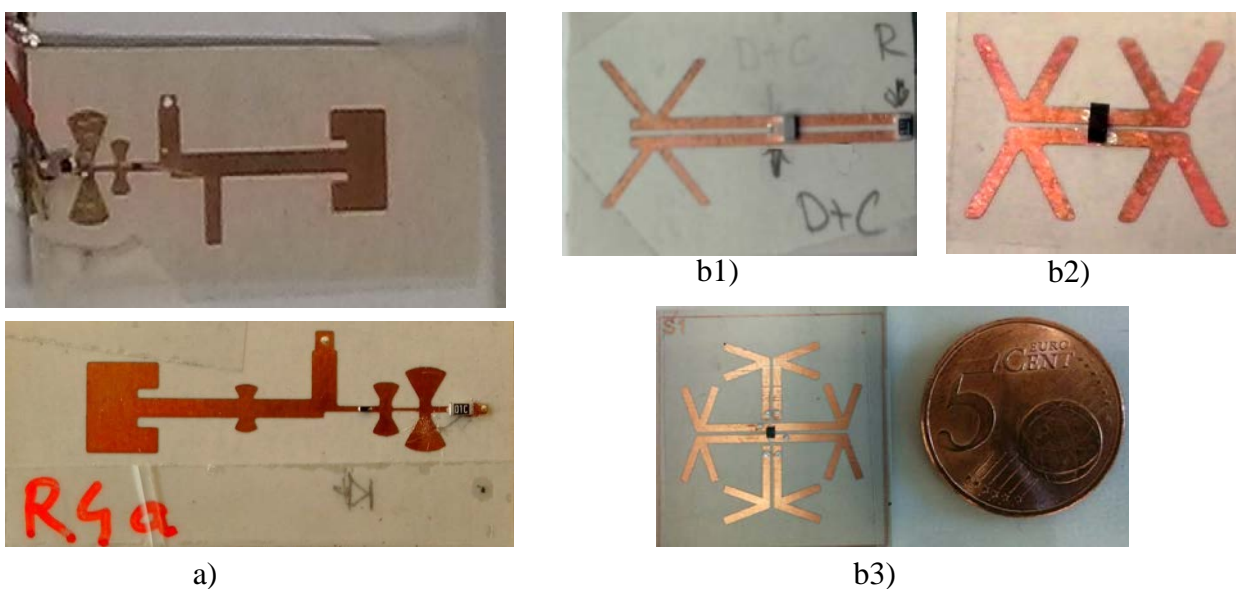
Figure 6. Photos of rectennas manufactured as part of the R&T CNES grants: a) rectennas using patch antenna and the microstrip technology, and, b1) rectenna using printed dipole antenna and coplanar stripline for interconnections, b2) rectenna using two cross dipole antenna array (2CDAA) and coplanar stripline for interconnections[46], b3) rectenna using four cross dipole antenna array (4CDAA) and coplanar stripline for interconnections.

By far, the most innovative topology is implemented in the rectenna shown in Figure 6.b3). The proposed topology is composed of an array of four cross dipole antennas (4CDAA) and a

---

[45] A. Takacs, H. Aubert, S. Charlot, "Ultra-Compact Ku band Rectenna", in *Proc. of IEEE IMS'2015*, Phoenix, USA, 17-22 May, 2015.

[46] A. Takacs, H. Aubert, A. Luca, S. Charlot, S. Fredon, L. Despoisse, "Rectenna Design for K Band Application", in *Proc. of 2014 European Microwave Conference*, Rome, Italy, 5-10 October 2014

silicon Schottky diode, Skyworks SMS7630[47], mounted in shunt configuration. The PCB layout and a photo of the manufactured rectenna are shown in Figure 6.b3). The antenna array and the diode are implemented on top of the PCB while the RF shunt capacitor is mounted on the bottom side of the PCB (not shown in Figure 6.b3). This compact rectenna exhibits a multi-band behavior at frequencies that correspond to the available multiple resonant frequencies of the cross dipole antenna array. The experimental results demonstrate that a DC power greater than 1 mW can be harvested in the Ku band (12 GHz, the main operating frequency) for electric field amplitudes higher than 38 V/m. This DC power is sufficient to power a wireless sensor (including the sensor, the sensing device, the power management unit and the wireless transceiver) for satellite health monitoring applications. The design and characterization of this 4CDAA rectenna is detailed in the paper '*Multiband rectenna for microwave applications*' annexed at the end of this manuscript.

---

[47] http://www.skyworksinc.com/Product/511/SMS7630_Series

Wireless power transmission for batteryless applications

Wireless power transmission for batteryless tags, wireless sensing devices, and indoor localization and tracking systems

In the last decade, RF power transmission has regained particular interest thanks to the large-scale deployment of wireless electronic systems used in Internet of Things scenarios (IoTs), where wireless sensors and tags are used in many applications, such as patient in-home health monitoring[48], structural health monitoring[49], automobile/aircraft health monitoring[50], etc. In order to increase the energy autonomy of such wireless sensors and tags, two scenarios are usually considered:

i. Wireless Power Transmission (WPT), where the wireless powering is carried out using dedicated RF sources. This scenario is useful for the 3D indoor localization of objects with passive (or batteryless) Radio-Frequency IDentification (RFID) tags [6]. Indeed, WPT can be used to supply power to low-cost, maintenance-free, autonomous tags. The main advantage of WPT is the control of the whole transmission chain. As the user sets the frequency and the amount of the transmitted power, the system's efficiency can be accurately estimated for such a scenario;

ii. Energy Harvesting (EH), where the ambient RF energy is harvested. In this scenario, the frequency and the power generated by RF sources (from, e.g., Television, GSM, or Wi-Fi networks) are not under the users' control. Furthermore, the low ambient RF power densities make energy harvesting very difficult to exploit in practice.

In these two scenarios, rectennas are usually designed for harvesting the available electromagnetic energy and to supply power to DC-to-DC boost converters and power

---

[48] S. Junnila *et al.*, "Wireless, Multipurpose In-Home Health Monitoring Platform: Two Case Trials," *IEEE Trans. Inf. Technol. Biomed.*, vol. 14, no. 2, pp. 447–455, Mar. 2010

[49] Harms, S. Sedigh, and F. Bastianini, "Structural Health Monitoring of Bridges Using Wireless Sensor Networks," *IEEE Instrum. Meas. Mag.*, vol. 13, no. 6, pp. 14–18, Dec. 2010

[50] A. Mishra, F. Gondal, A. Afrashteh, and R. Wilson, "Embedded wireless sensors for aircraft/automobile tire structural health monitoring," VA, USA, 25-28 Sept. 2006, pp. 163–165

management units of passive (batteryless) and wireless sensors. The block diagram of standard rectennas is shown in Figure 7. It is composed of two main passive devices: the antenna and the rectifier.

The antenna captures the ambient electromagnetic energy and converts it into a guided RF signal. The antenna radiation efficiency drives the RF-to-DC efficiency of the rectenna and, consequently, it must be maximized. Furthermore, the size of the antenna must be as small as possible in order to be embedded in most systems in use nowadays. For a given bandwidth, the best trade-off has to be found between size and radiation efficiency of the antenna.

The rectifier converts the guided RF signal into the DC power for supplying DC-to-DC boost converters and electronic devices, such as sensors. The key component is the non-linear device (e.g., Schottky diode or transistor) used to convert the RF signal into a DC voltage. This device is carefully selected in this study in order to rectify low-power signals. Moreover, the rectifying process generates undesirable harmonics at the input and output ports of the non-linear device. At the input port, a matching circuit/band-pass filter is usually placed to prevent these harmonics from being re-radiated by the antenna and to maximize the energy transfer. In addition, the harmonics generated at the output port are low-pass filtered along with the fundamental harmonic. The load (that is, the DC-to-DC boost converter and sensing device) is then supplied with the required DC power to operate.
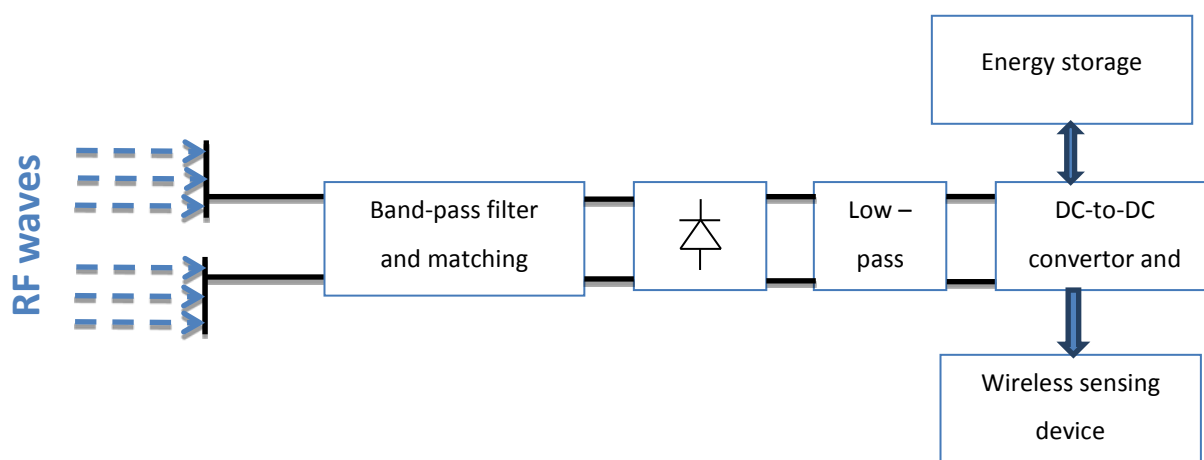
Figure 7. Block diagram of a standard rectenna loaded by the DC-to-DC boost converter and the passive (batteryless) and wireless sensing device.

In December 2015 we were contacted by a Toulouse start-up, Uwinloc[51], that began developing an innovative system for indoor localization. The Uwinloc system was revolutionary because they proposed the first battery-less tag for tracking a large volume of assets. The basic principle of such a system, shown in Figure 8, is to use a minimized number of synchronized UWB beacons to precisely localize UWB baterryless tags powered wirelessly by a WPT far-field technique. A system of synchronous UWB beacons assures the precise localization of battery-less UWB tags. The tags are equipped with rectennas and receive the energy wirelessly from the beacons that also transmit a RF energy/power in an ISM frequency band.
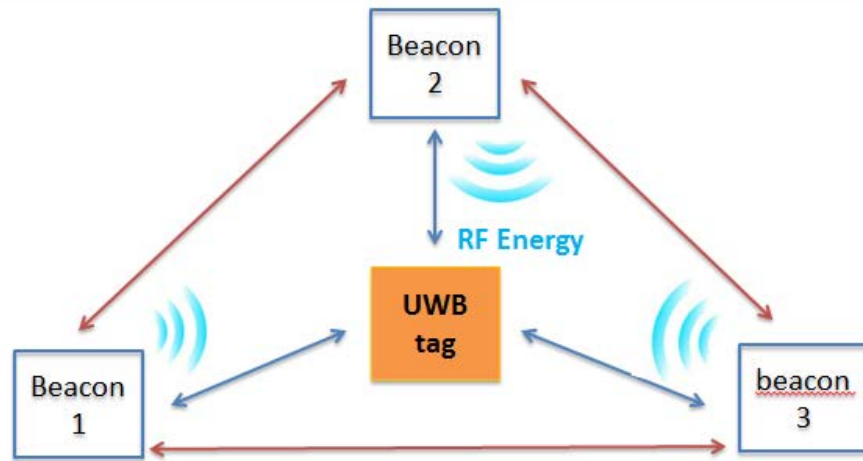
Figure 8. RF energy harvesting and 3D indoor localization scenario using battery-less UWB tags and a system of synchronous beacons

After signing an NDA (Non-Disclosure Agreement), we started to work together with Uwinloc as part of a collaboration project[52] funded by Uwinloc (from June 2016 to April 2017). Following the design requirements provided by Uwinloc, we proposed innovative rectenna and rectifier topologies and we quantified the main limitation of such WPT systems. We still collaborate with Uwinloc beyond the end of this first research project. At the end of

---

[51] http://uwinloc.com/

[52] Research grant (référence CNRS n° 147165) «La transmission sans fils d'énergie par ondes RF, disposant d'une puissance rayonnée supérieure ou égale à 1W (EIRP), dans le spectre UHF (860-960 MHz) pour télé-alimentation de tags »,.

2017, we were awarded a research grant (OPTENLOC[53]) co-funded by Région Occitanie (in the frame of GRAINE call) and by Uwinloc. As part of this ongoing OPTENLOC project (started in January 2018) the research focus shifted from the optimization of the WPT receiver side (i.e., the design and the optimization of the rectenna and its optimal integration with the electronics of the UWB tag) to the optimization of the overall WPT system, including both the Tx (RF sources) and Rx (the rectennas integrated into the battery-less tag) parts of the system. Thus, our ongoing research is focused on:

(i) the optimal integration of the UHF rectenna into the UWB batteryless tag. The tag should be as compact as possible, low profile, and insensitive to its environment. The size of the UHF antenna has to be further miniaturized and integrated on the same PCB as the UWB antenna. There are very few published results[54,55,56] concerning the integration of the UWB and UHF antennas and basically two solutions can be envisaged : (1) two separate antennas (one for UHF and one for UWB) or (2) a single multiband antenna covering both the UHF and UWB frequency bands. The first solution is less compact while the second one can be more compact but requires the use of diplexer systems. The final choice should be a best trade-off between antagonist criteria concerning the compactness, the losses, and the intrinsic antenna/antennas performances (gain, efficiency, input impedances, etc.).

(ii) the characterization and the modeling of a propagation channel for at least several typical indoor locations.

---

[53] Research grant OPTENLOC : 'Intégration Optimale d'un système de Télé-alimentation en ENergie dans les tags intelligents de LOCalisation pour applications industrielles', 2018-2020

[54] Fantuzzi, D. Massoti, A. Constanzo "Simultaneous UHF energy harvesting and UWB-RFID communication", In *Proc. of IEEE MTT-Symp.*, May 2015, pp. 1-4

[55] X. Gao, Z. Shen, "UHF/UWB tag antenna of circular polarization", IEEE Trans on Antennas and Propagation, vol. 64, no. 9, Sept. 2016

[56] C. Cruz, J.R. Costa, C.A. Fernandes, "Hybrid UHF/UWB antenna for passive indoor identification and localization systems", *IEEE Trans on Antennas and Propagation*, vol. 61, no. 1, January 2013

(iii) the development of methodologies and strategies to find : (1) the minimum number of RF sources for a given indoor location and (ii) the best-site implantation of the UHF RF sources, at least for typical indoor locations.

(iv) the development of a phasing/time delay command system for the RF sources in order to increase, on demand, the amount of RF energy available in some particular location where the UWB don't have enough energy to communicate with the beacon. Basically, the RF power radiated by the RF sources is regulated, but it is possible to control the relative phase or the time delay (if waveform pulses are used) between the RF sources in order to improve the power density of the electromagnetic waves in targeted location.

An overview of the state of the art in the field of the far-field WPT[57] demonstrates that this topic is intensively addressed by the scientific community. Progress has been made in the development of innovative solutions for implementing the basic parts of such a system. To the best of my knowledge, there are no published results concerning a complete far-field WPT system for tags localization. This full-system approach forms the core of the ongoing research performed together with our industrial partner (Uwinloc) as part of the OPTENLOC project.

---

[57] A. Costanzo, D. Masotti, "Smart Solutions in Smart Spaces: Getting the Most from Far-Field Wireless Power Transfer", *IEEE Microwave Magazine*, May 2016

Wireless power transmission for 'communicating materials'

The terms *'communicating materials'* and *'communicating concrete'* are related to materials (and concrete structures) that are able to communicate with their environment, process and exchange information, and store data in their own structure. In particular,*'communicating concrete'* is an interesting and challenging concept that forms the focus of the ANR-McBIM ('Material Communicating with the BIM')[58] research project. I started to work on the proposal of this project at the end of 2016 together with Prof. Daniela Dragomirescu (leader of the LAAS team involved in this project) and Dr. William Derigent from University of Lorraine and CRAN laboratory (the coordinator of the McBIM project). The project was selected by ANR and the research start effectively in 2018

To implement this *'communicating concrete'* concept, several scientific challenges should be overcome: a) robust wireless communications, not impacted by the concrete environment, must be achieved; b) innovative RF harvesting techniques that maximize the lifetime of the embedded sensor nodes must be developed; c) new data management strategies, controlling how data, either generated by sensor nodes, or sent by users, are spread into the WSN for a fast and reliable data storage and retrieval, must be implemented; d) the definition of a native BIM interoperability of the concrete material, based on IFC standard, to ensure a correct communication with BIM platforms. Together with the LAAS team made of Prof. Daniela Dragomirescu and Gael Loubet, a very enthusiastic Ph. D student that I co-advise with Daniela, we searched for an optimized solution to overcome the aforementioned challenges and to design a robust wireless communications system, adapted to the concrete environment and equipped with RF harvesting and WPT techniques to maximize the lifetime of the embedded sensors.

The *'communicating concrete'* will exchange information with its environment by using embedded WSN. The WSN architecture is composed of two types of wireless entities:

---

[58] ANR-McBIM ('Material Communicating with the BIM'/ Matière Communicante au service du BIM), research project 2018-2020 : https://mcbim.cran.univ-lorraine.fr/

"sensing node", whose mission will be to capture data on the concrete's properties (i.e., temperature, humidity, cracks, or corrosion) and "communicating node", able to aggregate data coming from different sensing nodes, to store product information, to communicate with their environment or other communicating nodes and to actively monitor the concrete state. The development of robust, energy-efficient WSNs is then key to developing communicating materials. This requires designing low-energy wireless communication architectures that are resilient to electromagnetic perturbations induced by the water and steel in the concrete. In this context, some original energy harvesting technologies (e.g. RF EH) or wireless power transmission could be envisaged to be used to generate nearly autonomous (from a DC energy point of view) sensing nodes. The communicating nodes will be powered via wired connections placed on the surface of the concrete material. The number of sensing and communicating nodes will vary from a type of communicating concrete to another, as function of industrial and functional technical specifications. Two network architectures (NA1 and NA2) are envisaged, as represented in Figure 9 and Figure 10. There is only one Internet gateway for the communication nodes in NA1 (i.e. there is only one main communication node, or CN, connected to the internet, while all other CNs communicate with the Internet via the main communication node). In NA2, each CN is connected to the Internet. From a specification point of view, the sensing node, or SN, uses a minimalist architecture (a low-power sensor equipped with an ultra-low power transmitter) in order to reduce its DC consumption. The SN will be equipped with a WPT/EH interface and should use a low-power communication technology (e.g. Bluetooth 5, RFID, UWB LoRaWAN, etc.) operating at low bit-rate. A possible implementation/architecture of such an SN is represented in Figure 11. The EH/WPT interface is the key element and the originality of this ambitious architecture. This interface will avoid any maintenance and will increase the lifetime of the SN. The available electromagnetic power density is usually very low in both EH or WPT scenarios and, consequently, the use of a DC-to-DC converter and a storage element is mandatory. The targeted lifetime (at least 50 years) is very ambitious. Certainly, the lifetime of such SN architecture will be limited by the lifetime of the storage element (e.g. a supercapacitor). In most of the envisaged scenarios, the periodicity of the measurements is not critical (i.e., temperature and humidity measurements every hour, corrosion measurement every week, etc.) and the estimated bit-rate required to send the data is quite low. Consequently, a long time for

storage element charging and between two consecutive data slot transmissions can be authorized.
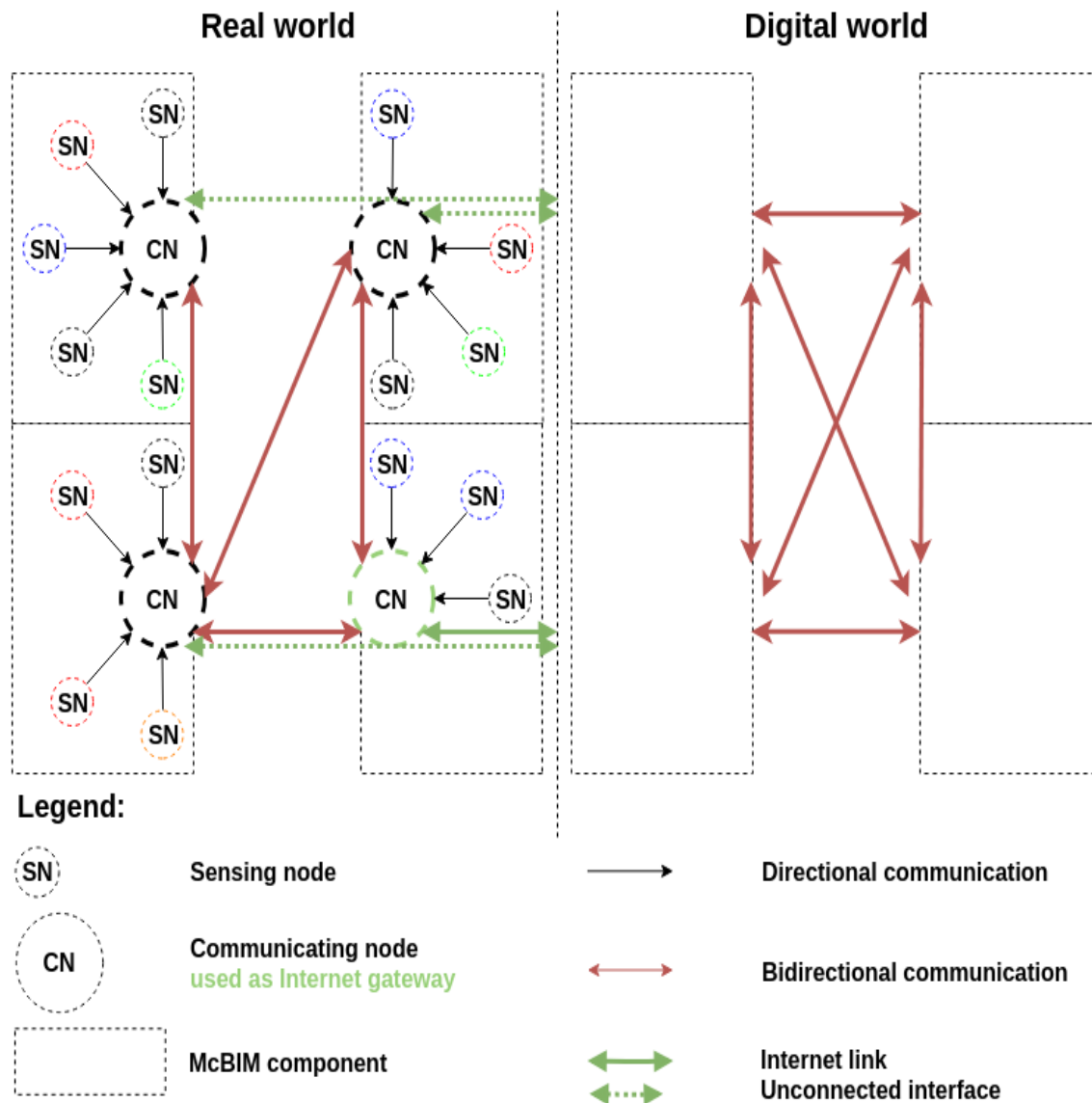
Figure 9. Network architecture (NA1) for the 'communicating concrete' and McBIM application. Only one communicating node is used as Internet gateway between the physical/real and digital world.
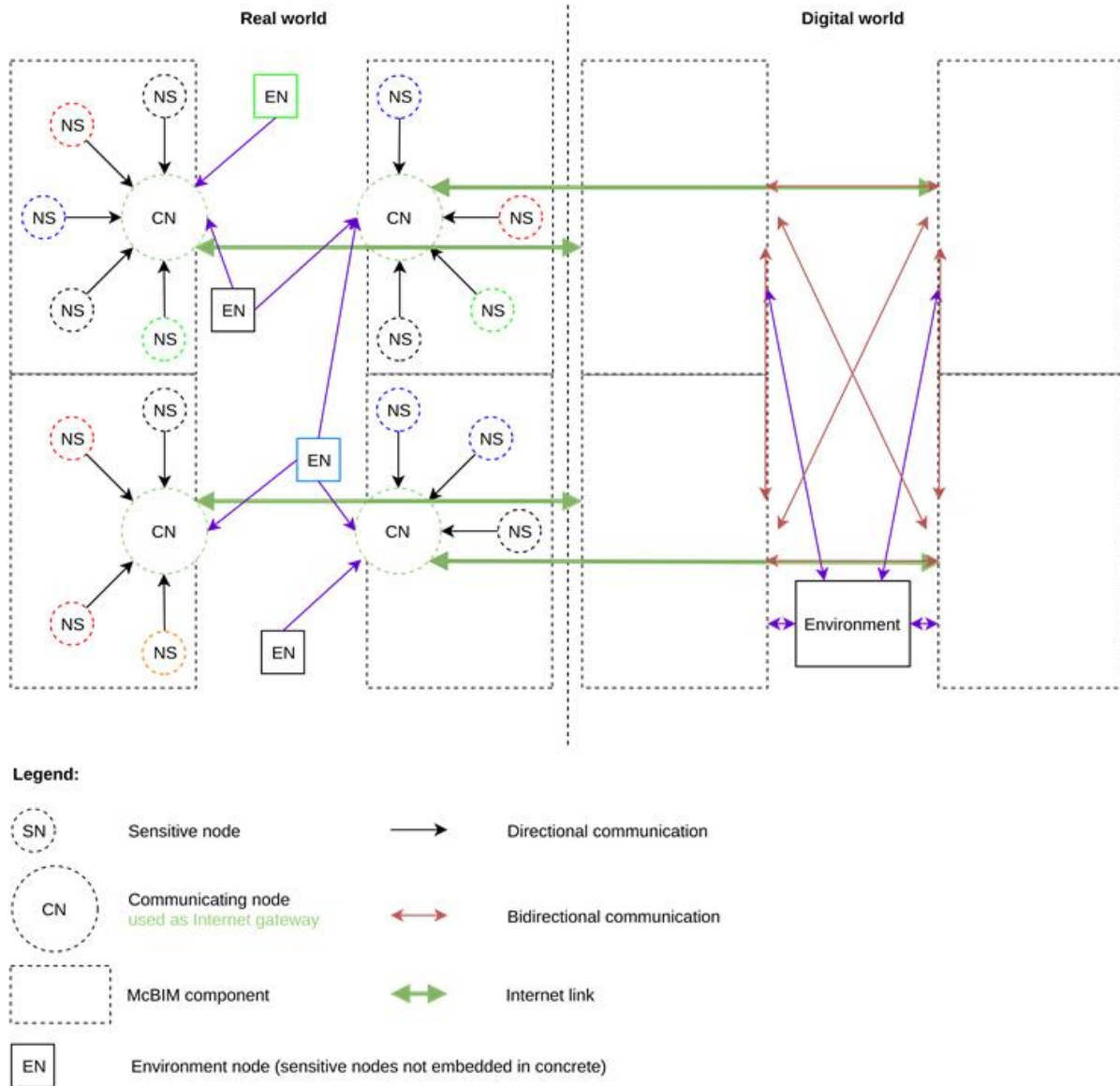
Figure 10. Network architecture (NA2) for the 'communicating concrete' and McBIM application. All communicating nodes are equipped with Internet gateways.

The main challenges of the WPT interface are related to:

(i) the design of an effective antenna, embedded in concrete, with gain and efficiency as high as possible. Also, this antenna operating in an ISM band should be as compact as possible and insensitive to various concrete compositions. The WPT antenna is collocating with the Tx antenna (used by the low-power transmitter). Two solutions can be envisaged: (1) one (multiband) antenna covering both Tx and WPT frequency bands equipped with a diplexer or (2) two different antennas (one for WPT and another one for Tx).

34

(ii) the optimization of the WPT interface (rectenna) in terms of the harvested DC voltage and power efficiency. Also, the rectenna should able to operate efficiently with very low electromagnetic power densities and having as load fluctuating complex impedances (corresponding to the input impedance of the DC unit).

(iii) the optimal integration between the WPT interface and the DC power unit (including a DC-to-DC boost convertor and a PMU unit).
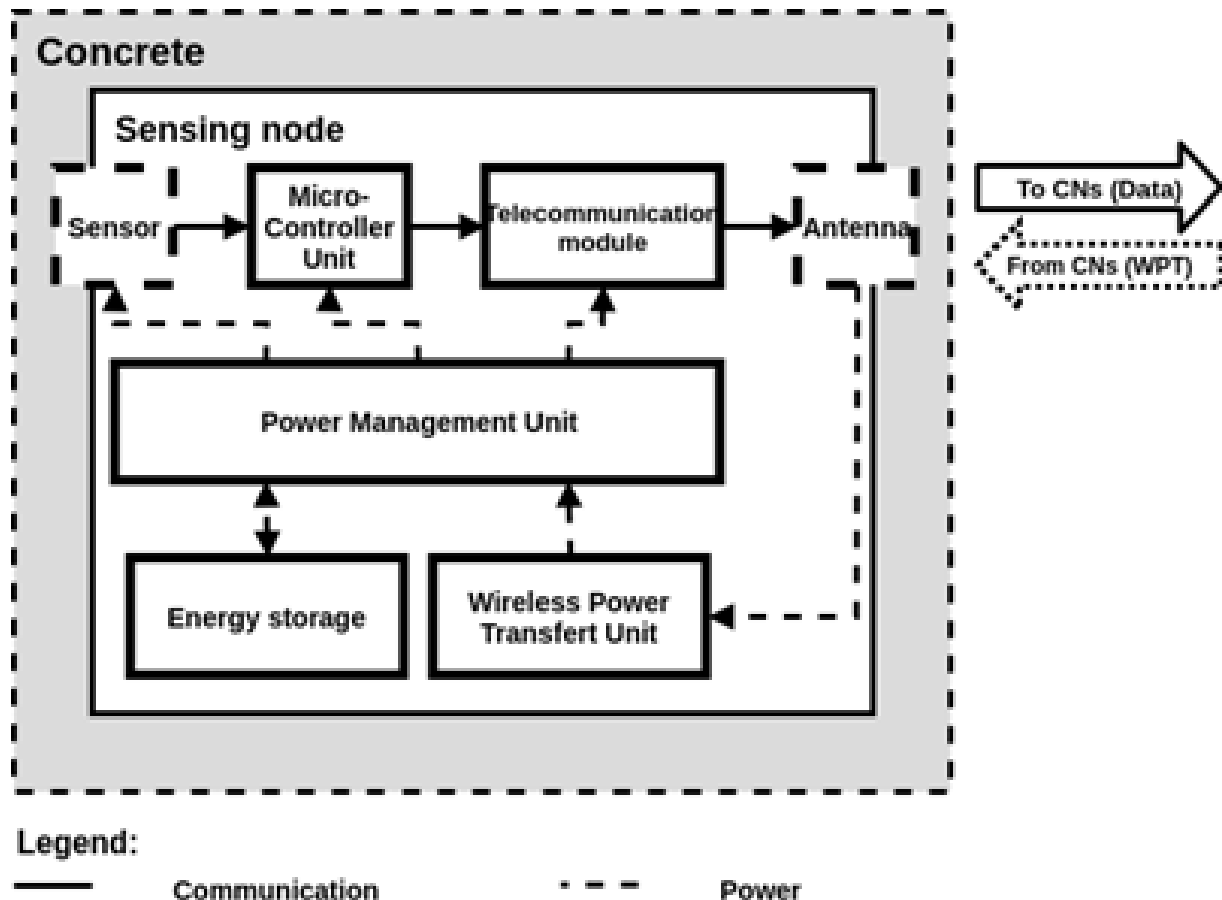
Figure 11. Architecture of a/the sensing node.

Work is currently being performed on the McBIM project and the ongoing research should open the way for new concepts in the field of structural health monitoring of smart buildings

35

and civil infrastructures. A paper on these topics[59] was recently accepted and published on *IEEE ACCESS* (in special issue on *Wirelessly Powered Networks: Algorithms, Applications and Technologies*, Nov. 2018)

---

[59] G. Loubet, A. Takacs, D. Dragomirescu, "Towards the Design of Wireless Communicating Reinforced Concrete", *IEEE Access*, *Special Issue on Wirelessly Powered Networks: Algorithms, Applications and Technologies*, preprint version available on *https://ieeexplore.ieee.org/document/8546738,* accessed online on Nov. 29, 2018

Flexible substrate technologies for millimeter wave applications

In the past decade, interest from both academia and industry in the field of flexible electronics has risen enormously due to the uniquely valuable properties of being bendable, conformably shaped, elastic, lightweight, and non-breakable. This research topic is also a research priority of many national and international agencies. The flexible substrate technology is the basic building block for any flexible electronics implementation. Especially, the implementation at large scale of IoT applications requires smart objects, smart hardware, and conformal implementation[60]. This conformal implementation can be fulfilled using flexible or wearable substrates[61]. Most of today's applications of flexible electronics cover/utilize the spectrum of RF and microwave frequencies, but the rising of millimeter wave applications (radar, 5G communications, millimeter wave radar and sensing for autonomous applications, millimeter wave imaging, etc.) also boosted the interest for millimeter wave flexible substrates.

As part of several past research projects, LAAS initiated the development of a new flexible technology appropriate for millimeter wave applications. The research was piloted by Prof. Daniela Dragomirescu and involved the technical team the Micro and Nanotechnology platforms of LAAS[62] and the TEAM[63] service of LAAS. The choice of kapton as material substrate for this technology was motivated mainly by its good trade-off in terms of mechanical, chemical, and electrical proprieties. As shown in Table 1, only LCP overcame kapton in terms of its dielectric loss properties. The millimeter wave applications require both high patterning accuracy (in the range of microns), and low losses for the metallization layers.

---

[60] F. Alimenti et al., "Smart Hardware for Smart Objects: Microwave Electronic Circuits to Make Objects Smart," in *IEEE Microwave Magazine*, vol. 19, no. 6, pp. 48-68, Sept.-Oct. 2018

[61] S. Lemey, S. Agneessens and H. Rogier, "Wearable Smart Objects: Microwaves Propelling Smart Textiles: A Review of Holistic Designs for Wireless Textile Nodes," in *IEEE Microwave Magazine*, vol. 19, no. 6, pp. 83-100, Sept.-Oct. 2018

[62] https://www.laas.fr/public/en/micro-and-nanotechnologies-platform

[63] https://www.laas.fr/public/en/team

For these reasons, the selected approach was to use a conventional technological process where photolithography, chemical etching, and the physical vapor deposition (PVD) coating process are combined to fabricate the metallic patterns. This process is more expensive that the inkjet printing technology but offers a better quality of the metallization layer in term of patterning accuracy and metal losses.

Table 1. Comparative properties of organic substrates

Material	PET	PEN	Kapton	LCP	Paper
Dielectric constant	3.3~3.4	~2.9	3.2~3.4	~3.1	~3.2
Loss Tangent	~0.01	~0.025	~0.002	0.002~0.005	~0.007
Melting Point	~260 °C	~265 °C	NA	285 °C~315 °C	NA
Glass-transition temperature	78 °C	121°C	410°C	NA	NA
Chemical resistance	Good	Good	Good	Excellent	NA
Mechanical properties	Good	Good	Excellent	Good	NA

In 2013, I started to work with Prof. Dragomirescu on this topic by co-directing the Ph. D. thesis of Zhening Yang. The main goals of Zhening's Ph. D. thesis were:

(i) to improve the technological process of the Kapton flexible substrate,

(ii) to characterize the electrical performances of the kapton-based flexible technology form DC to W-band,

(iii) to implement passive devices on kapton substrate (i.e. transmission lines, antenna, filters, etc.),

(iv) to develop the heterogeneous integration process on Kapton flexible substrate.

Two technological methods were developed during Zhening's thesis :(i) one using the lift-off process and the other one using a wet etching process. The main technological steps of the lift-off process are represented in Figure 12. Main technological steps of the lift-off process, while the wet etching process is detailed in Figure 13.
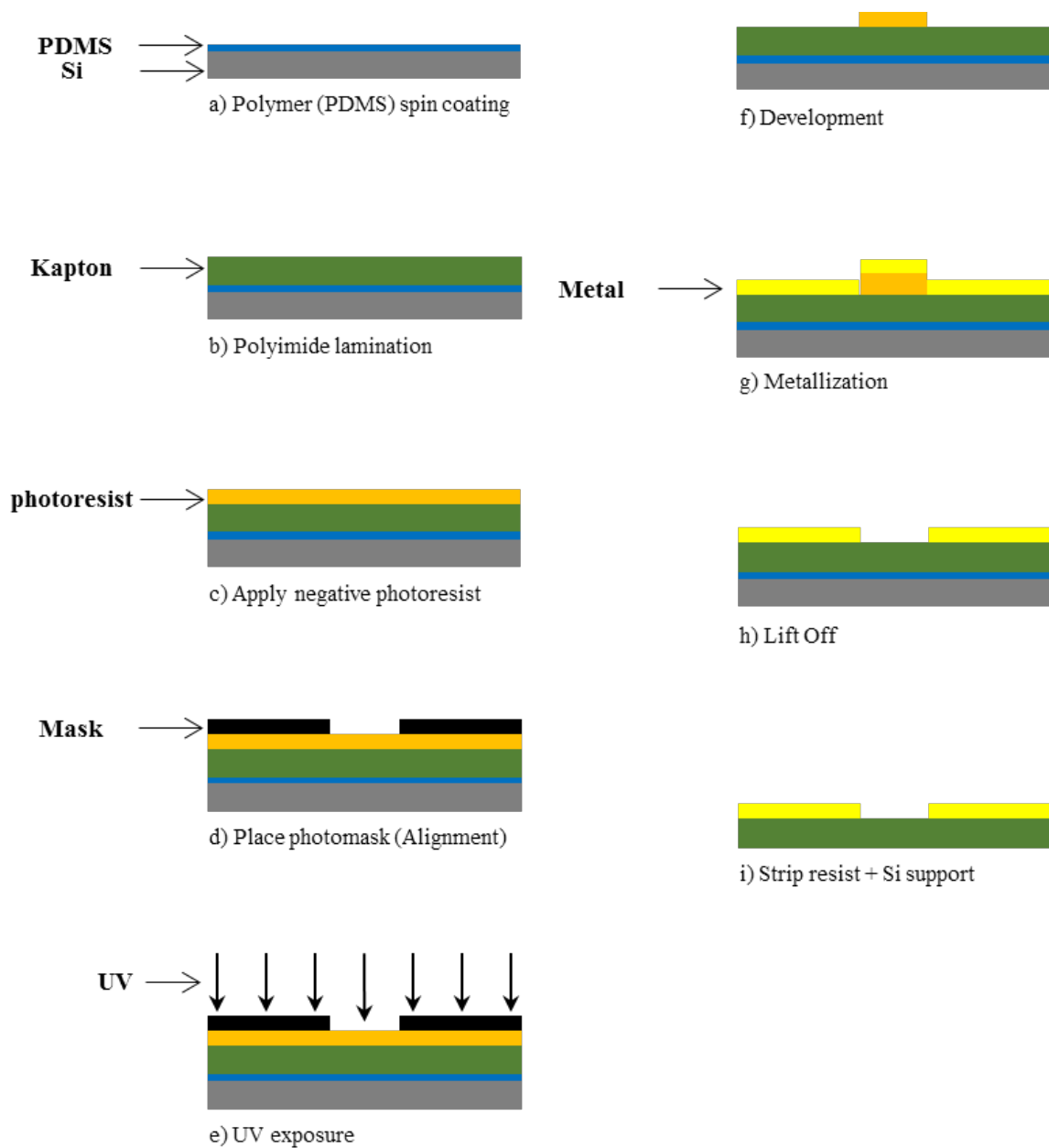
Figure 12. Main technological steps of the lift-off process

Another key issue for any flexible technology is the technological solution/process to heterogeneously integrate active circuits on such flexible passive structures (e.g., to integrate a CMOS transceiver with an antenna and sensors in order to implement a wireless sensor node

for SHM applications). A 3D heterogeneous approach based on a flip-chip process was adopted in our laboratory[64].

PDMS →
Si →
a) Polymer (PDMS) spin coating

Kapton →
b) Polyimide lamination;

Metal →
c) Metallization

photoresist →
d) Apply positive photoresist

Mask →
e) Place photomask (Alignment)

UV →
f) UV exposure

g) Development

h) Wet etching

i) Strip resist + Si support
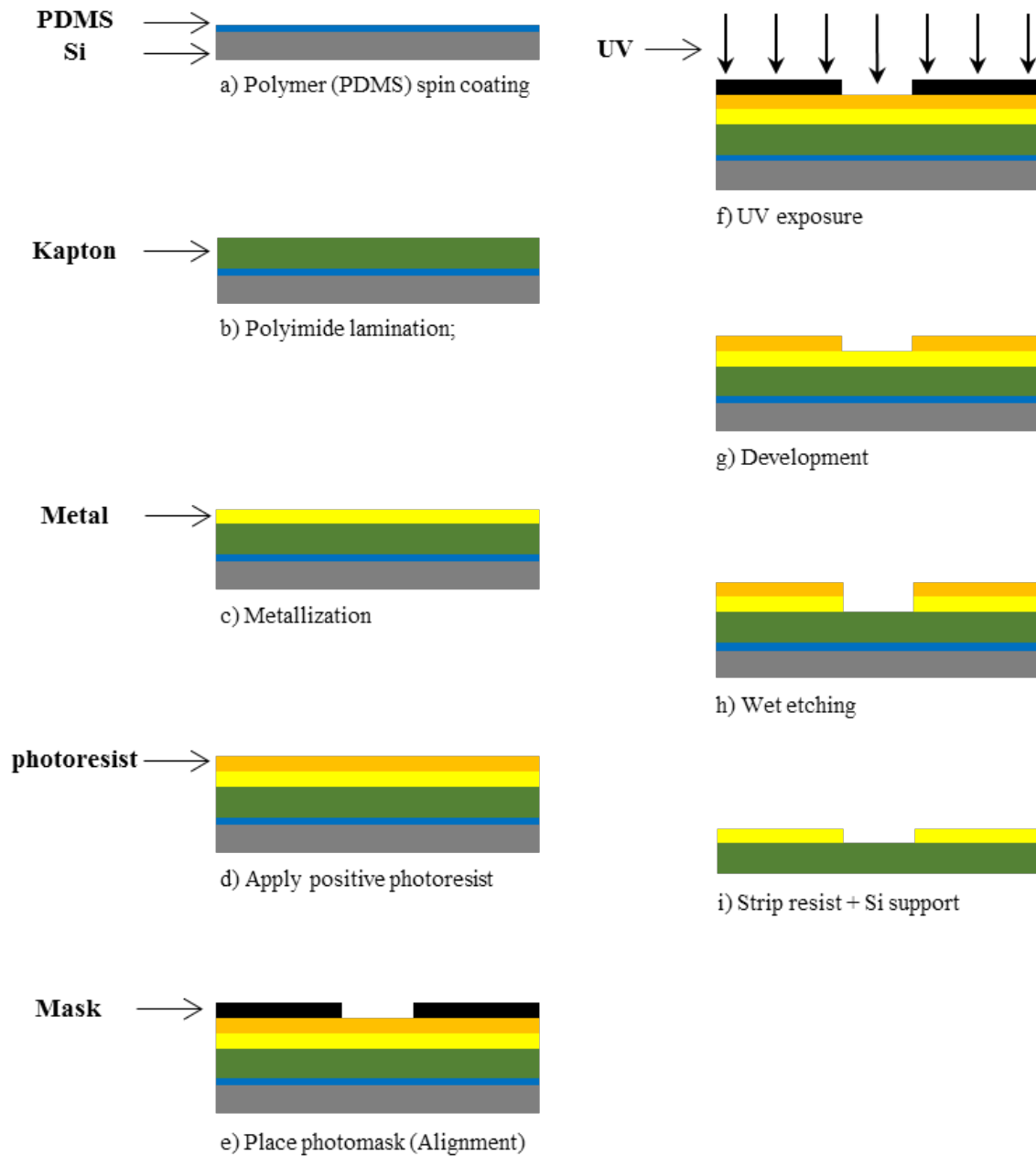
[64] M. M. Jatlaoui, D. Dragomirescu, S. Charlot, P. Pons, H. Aubert, and R. Plana, "3D Heterogeneous Integration of Wireless Communicating Nano-Sensors on Flexible Substrate," *SPIE Adv. Top. Optoelectron. Microelectron. Nanotechnologies*, p. 78211E–78211E–7, 2010

Figure 13. Main technological steps of the wet-etching method

In order to implement the flip-chip process, two approaches are possible: (i) a flip-chip with Au stud bumps implemented on the pads of the integrated circuit (chip), or (ii) a flip-chip process with Au electroplated bumps implemented on the kapton surface. The first approach, using Au stud bumps, was initially developed in our laboratory but has a major drawback: the gold stud bumping is a semi-manual process that lacks reproducibility and reliability mainly when a large number of gold stud bumps/chip is required. The second method, with Au bumps developed on the Kapton surface, leads to a more reliable result. Au bumps are created using a technological process developed during Zhening's Ph. D. thesis. As shown in Figure 14, we can assure a very good quality and alignment for the gold bumps directly fabricated and patterned on the Kapton with the main steps presented in

Figure 15.

a)   b)
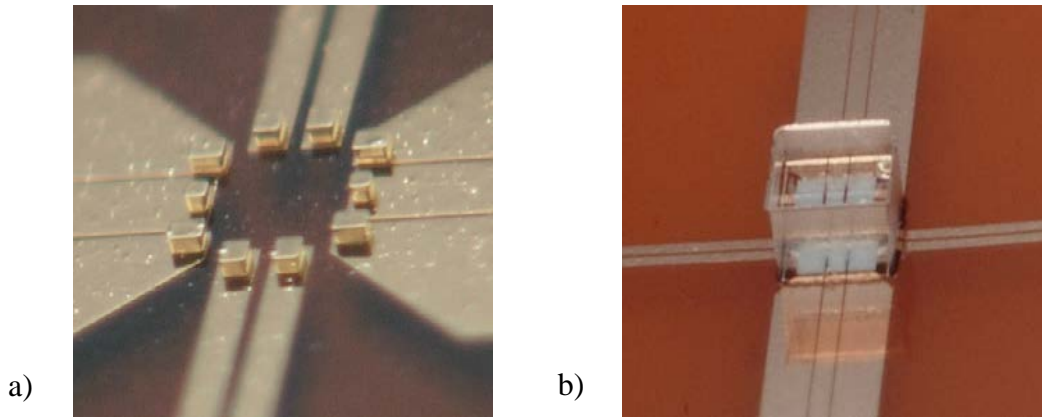
Figure 14. a) Photo of the gold bumps patterned on the kapton surface; b) photo of the glass dummy chip mounted by a flip-chip process on the kapton surface

The Kapton structure represented in Figure 14.a) was designed in order to accommodate a CMOS V-band low noise amplifier (LNA) designed in our laboratory and fabricated using the 65 nm CMOS process from ST Microelectronics. Many tests were performed using dummy chips fabricated on glass substrate. The dummy chips have a size (400 µm x 400 µm) and a pad configuration identical with those of the 'real' LNA. A non-conductive adhesive polymer is deposited on the inner surface delimited by the Au bumps and the chip is stuck by thermo-compression onto the Kapton surface.

41
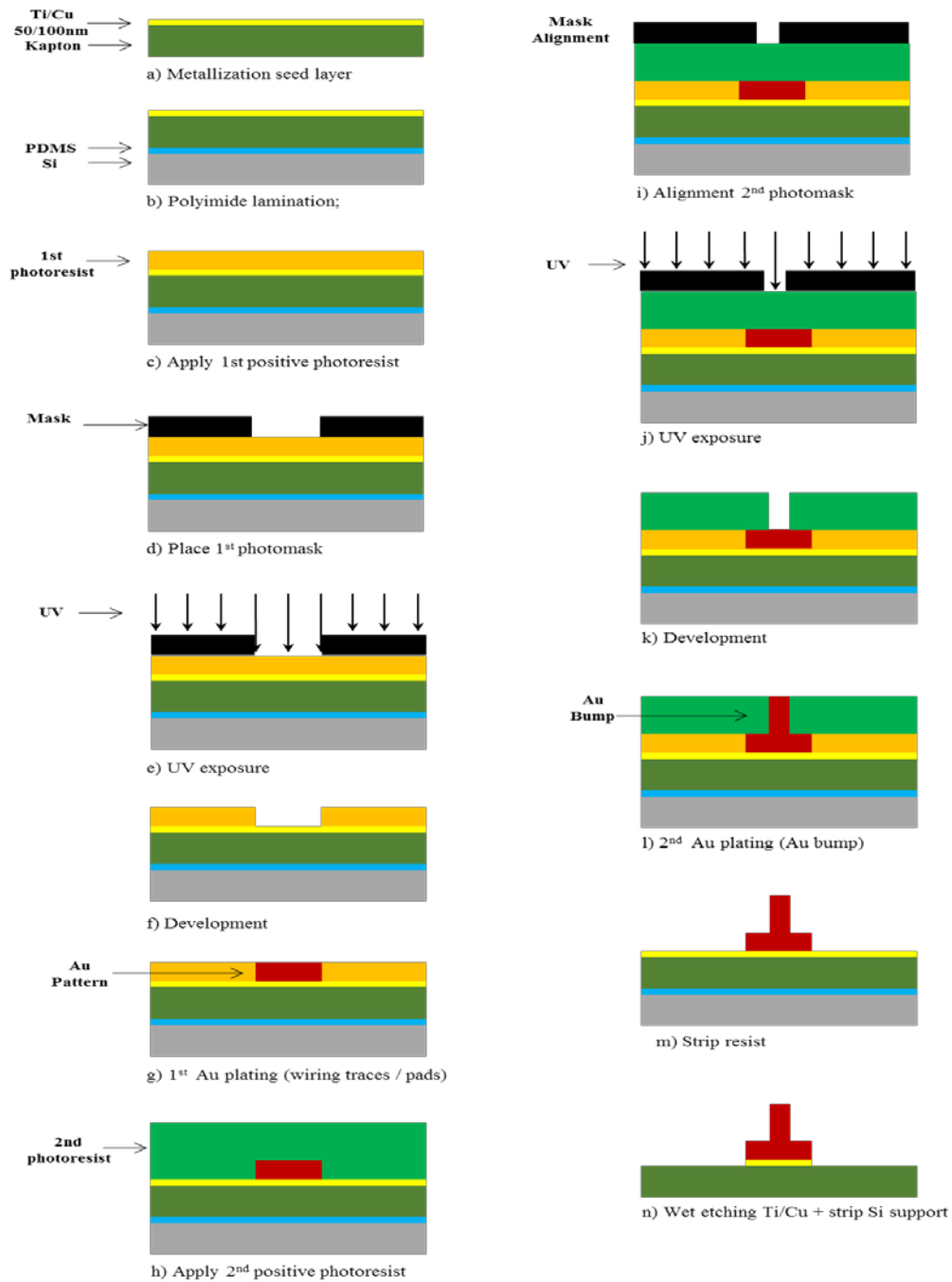
Figure 15. Technological steps when the gold bumps are fabricated directly on the Kapton surface

The main challenge is how to deposit a non-conductive adhesive polymer on a surface as small as 240 µm × 250 µm on Kapton. Unfortunately, this method does not lead to a fully

reliable results. During many tests performed by Zhening, at least one contact (between the gold bump and the pads of the dummy chip) was negatively impacted by the presence of the non-conductive polymer. An alternative method to overcome the adhesive issue can be the use of a raised-die under-fill configuration for the flip-chip[65]. Unfortunately, LAAS is not equipped with assembling machines compatible with the raised-die under-fill configuration for the flip-chip. Also, many passive structures were fabricated during Zhening's Ph. D. thesis[66]. They are represented in

Figure 16.

a)

b)

c)
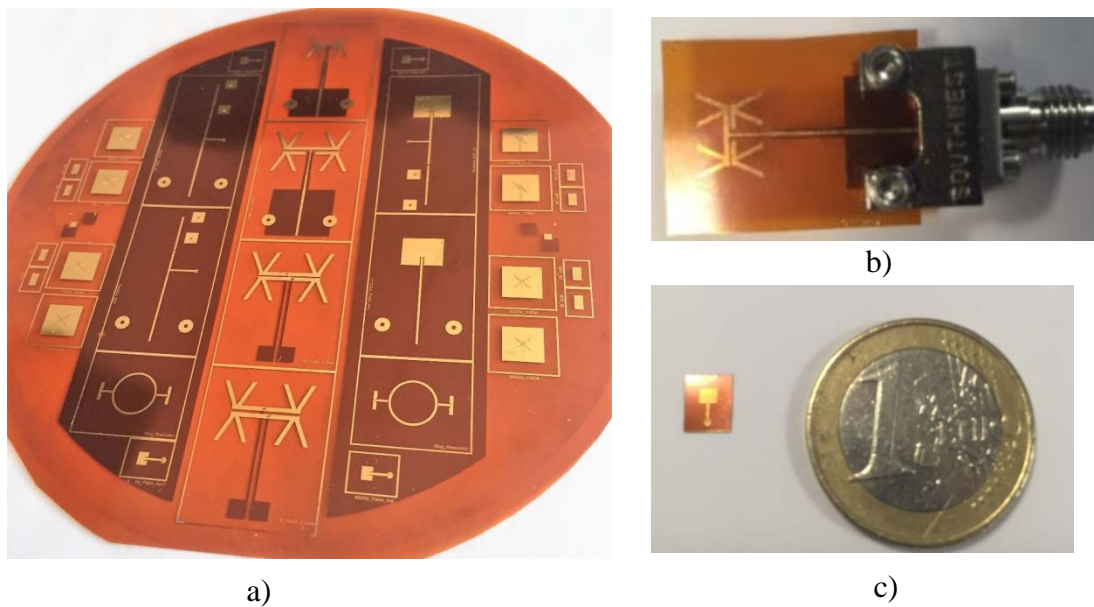
Figure 16. Photos of: a) Kapton wafer manufactured during Zhening Yang's Ph. D. thesis, b) 2CDAA designed for Ku band applications with its transition microstrip-to-stripline assembled with an end-launch connector, c) V-band microstrip patch antenna.

Figure 16. a) shows a manufactured Kapton wafer including:

---

[65] Z. Zhang, S. Luo, and C. P. Wong, "Recent Advances in Flip-Chip Underfill: Materials Process and Reliability," *Adv. Flip Chip Packag.*, vol. 27, no. 3, pp. 155–199, 2013

[66] Z. Yang, "Flexible Substrate Technology for Millimeter Wave Applications", Ph. D thesis of University of Toulouse, France, defended on Dec. 20, 2016

(i) circular ring resonator structures[67] used in order to determine dielectric characteristics (i.e., relative electric permittivity/dielectric constant and the dielectric loss tangent).

(ii) an antenna array formed by two cross dipoles (abbreviated 2CDAA: two cross dipole antenna array). Theses antennas were designed for K/Ku band energy harvesting and WPT applications. The Ku band CDAA assembled with an end-launch connector is also represented in

Figure 16 b).

(iii) V-band microstrip patch antennas, also represented in

Figure 16 b).

(iv) V-band and W-band cross slot dipole antennas.

More results and discussions concerning these structures are presented in the paper *'Flexible Substrate Technology for Millimeter Wave Wireless Power Transmission'*, annexed to this manuscript.

---

[67] Z. Yang, A. Takacs, S. Charlot, D. Dragomirescu, "Flexible Substrate Technology for Millimeter Wave Wireless Power Transmission", *Wireless Power Transfer (Cambridge University Press)*, Vol.3, N°1, pp.24-33, March 2016

Design of passive and active RF and microwave circuits

Since the 2000s, I was involved in many projects requiring the design, the fabrication, and the characterization of various circuits for RF and microwave applications. There is no room in this manuscript to fully describe all these research activities. For this reason, I chose to focus this section on the work concerning the design and the implementation of a MMIC core-chip solution for the satellite Beamforming Antenna Control Systems (BACS). The research concerning this topic was performed during the Ph. D. thesis of Matthieu Gastaldi that I co-advised with Prof. Daniela Dragomirescu. This work was funded by CNES and Thales Alenia Space and consisted of an exploratory project. Matthieu's main goal was to explore the potential of the CMOS technology for the implementation of a CMOS core-chip solution for beamforming antenna control systems that are currently implemented by using GaAs technologies. For sure, the CMOS technology has not yet been developed extensively enough to overcome the RF performances of GaAs technology in terms of linearity, power handling, cut-off frequency, etc. Nevertheless, because of the multilayer approach of the CMOS technology, the CMOS MMIC offers other incontestable advantages such us high integration, footprint reduction, and low consumption capabilities. Also, the integration on the same chip of RF and digital functions can be easily implemented on CMOS technology, opening the way for the mass/volume reduction of satellite payload. For this reason, the use of CMOS technology is now explored as a possible candidate for the next generation of RF MMIC for space applications. The selected technology by CNES and Thales Alenia was the 0.25µm SiGe (SGB25V) CMOS technology from IHP, Germany[68]. During Matthieu's Ph. D., he explored the possibility of implementing some electronic functions required in BACS (e.g. attenuation, phase shifting, etc.). As requested by CNES and Thales Alenia Space, Matthieu's manuscript and most of his results are confidential until January 2019. A patent pending was registered by TAS in December 2016. Notwithstanding confidentiality requirements, together

---

[68] https://www.ihp-microelectronics.com/en/departments/technology/overview.html

with Matthieu we published some of the results (one journal paper[69] and one communication[70] that was presented at an international conference). The most important results obtained during Matthieu's Ph. D. thesis concern the design and the characterization of CMOS based attenuators, phase shifters, and compact slow-wave line structures. One of the original phase-shifting topologies proposed during Matthieu's Ph.D. thesis is shown in Figure 17.
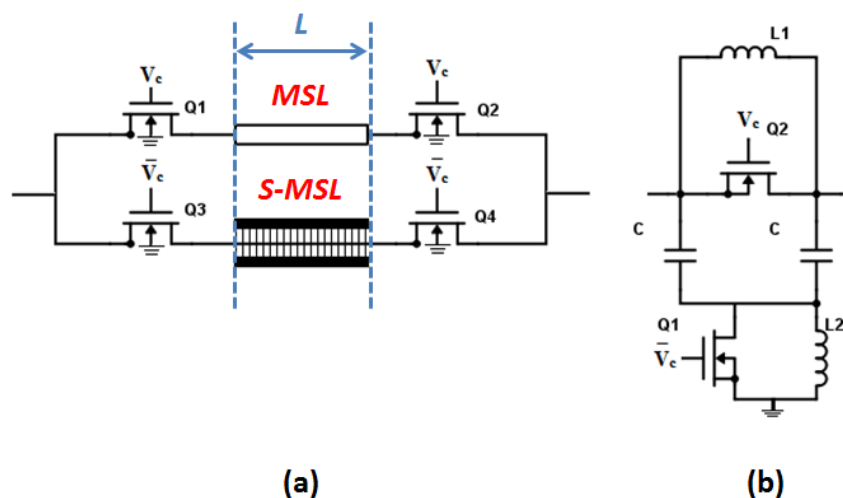
Figure 17. Proposed phase shifting cell based on Slow wave lines (SWL) (a) proposed phase shifting topology using microstrip lines (Shielded Micro-Strip Line) (b) example of the classical topology.

This phase shifter uses SiGe cold FETs, which have no bias current, as switches and Slow-wave lines (SWL). The phase shift is obtained as a delay between the two signal paths (Figure 17 a). The first transmission line is a classical Micro-Strip Line (MSL) and the other transmission is a slow-wave line named Shielded Micro-Strip Line (S-MSL). For comparison, a classic topology is represented in Figure 17 b. This classic topology[71,72] is valid for phase

---

[69] M. Gastaldi, D. Dragomirescu, A. Takacs, V. Armengaud, S. Rochette, "Micro-strip slow wave line for phase shifting cells", IET Electronics Letters, Vol. 51, No. 20, pp. 1589–1591, 1st October 2015

[70] M. Gastaldi, D. Dragomirescu, A. Takacs, V. Armengaud, "Compact Phase Shifting Cell Based on Micro-Strip Slow Wave Lines", 17th edition of the International Symposium on RF-MEMS and RF-MICROSYSTEMS (MEMSWAVE 2016), July 2016, Bucharest, Romania

[71] B-W. Min; G.M. Rebeiz, , "Single-Ended and Differential Ka-Band BiCMOS Phased Array Front-Ends," IEEE Journal of Solid-State Circuits, vol.43, no.10, pp.2239-2250, Oct. 2008

shifters between 90° and 11.25°. The manufactured phase shifting cells (the proposed SWL topology using MSL/S-MSL and the 'classic' topology) are represented in Figure 18. The experimental results depicted in Figure 19 confirm the performance of the proposed topology (phase shift behavior) in the targeted Ku frequency band.
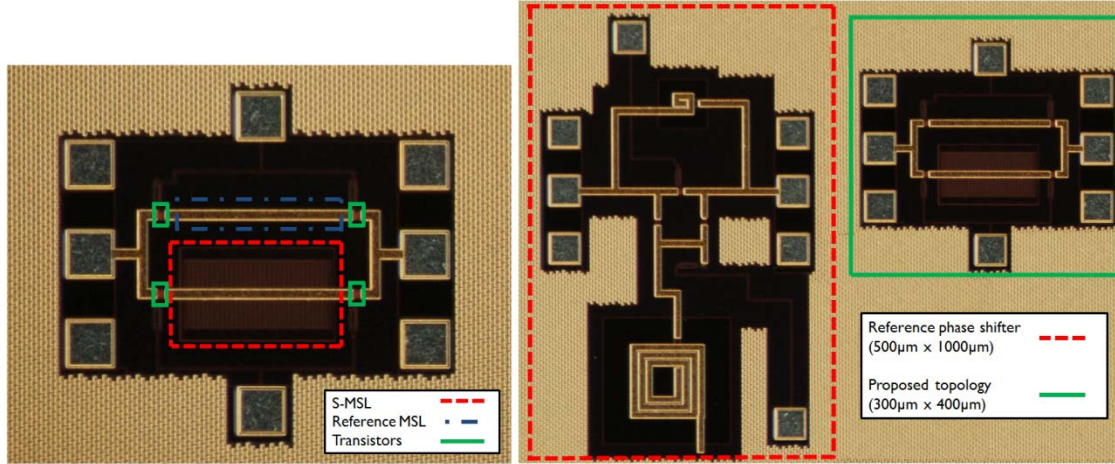
Figure 18. Photo of the manufactured CMOS phase shifting cell using MSL/S-MSL lines (left) and size comparison between hybrid topology and SWL based solution (right)

More results and discussions can be found in the paper '*Compact Phase Shifting Cell Based on Micro-Strip Slow Wave Lines*' annexed to the end of this manuscript.
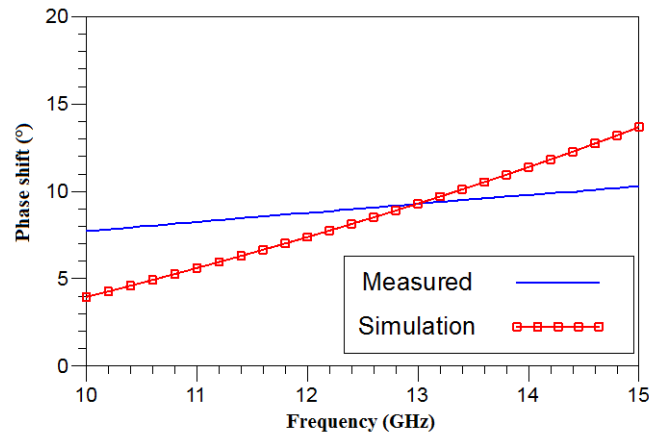
Figure 19. Phase shift of the SWL PS.

---

[72] I. Kalyoncu; E. Ozeren, M. Kaynak; Y. Gurbuz, "A 4-bit SiGe passive phase shifter for X-band phased arrays," in Proc. of *2013 IEEE Radio and Wireless Symposium (RWS),* pp.310-312, 20-23 Jan. 2013

My research project: the next decade

For the next decade, I expect to continue my ongoing research activities, while also generating new avenues of research that take into account my scientific background, my current interests, the opportunities that may appear in term of scientific collaborations and funding, and the global evolution of the electromagnetic engineering research at national and international level. While open to pursuing novel research avenues, my proposed research project guide my short and intermediate term goals, and channel my funding acquisition activities and the types of collaborations I may participate into.

Certainly, I will still be working in the field of electromagnetic engineering and I will devote most of my efforts in the fields of WPT and EH research. These fields have grown very fast during the last five years. The WPT research reached a certain degree of maturity and new industrial applications are implemented by innovative companies. But there still is plenty of room for research because of new concepts, topologies, and designs that need to be implemented to address the many emerging applications. During the last few years I worked more in the field of the far-field WPT and certainly I will continue to work for at least the next three years on the far-field WPT because of very interesting ongoing research projects that I have (OPTENLOC and ANR-McBIM). Certainly, the project OPTENLOC and the collaboration with Uwinloc company are very promising and I view these projects as a springboard towards new research projects:

(i) a Ph. D. thesis project (collaboration LAAS-Uwinloc) was already submitted and we are awaiting for the decision of ANRT[73],

(ii) together with Uwinloc, we intend to create a common research laboratory focused on wireless power transmission for IoT applications and we will submit a common proposal to the next ANR[74] (LabCom).

---

[73] http://www.anrt.asso.fr/fr/cifre-7843

[74] http://www.agence-nationale-recherche.fr/financer-votre-projet/plan-d-action-2019/

The most promising research axis seems is, to me, the far-field WPT and its emerging applications in the field of wireless sensors networks, cyber-physical systems, and IoT systems. In the last five years, the research concerning the far-field WPT was focused mainly at device level and performed separately on Tx side (RF power sources)[75] or Rx side (e.g. rectennas). Many state-of-the-art recently proposed rectenna designs claim, among others: (i) a higher efficiency[76], (ii) a broadband[77] or multiband behavior[78,79], (iii) the ability to harvest energy coming from various directions, and (iv) a good trade-off between size (compactness) and performances[80]. The 'hybridization' of the RF energy harvesting with other EH techniques was also addressed by combining: (i) RF EH with solar energy harvesting[81], (ii) RF EH with the vibrational/mechanic[82] or kinetic[83] energy harvesting, (iii) RF EH with thermal energy

[75] M. Thian A. Barakat V. Fusco "High-efficiency harmonic-peaking class-EF power amplifiers with enhanced maximum operating frequency" *IEEE Trans. Microwave Theory Tech.* vol. 63 no. 2 pp. 659-671 Feb. 2015

[76] V. Kuhn, C. Lahuec, F. Seguin, and C. Person, "A Multi-Band Stacked RF Energy Harvester With RF-to-DC Efficiency Up to 84%", *IEEE Trans. Microw. Theory Tech.*, vol. 63, no. 5, pp. 1768–1778, May 2015

[77] C. Song, Y. Huang, J. Zhou, J. Zhang, S. Yuan, P. Carter, "A High-Efficiency Broadband Rectenna for Ambient Wireless Energy Harvesting", *IEEE Trans. on Antennas and Propagation*, Vol. 101, Issue 8, pp. 3486 - 3495, August 2015

[78] K. Niotaki, S. Kim, S. Jeong, A. Collado, A. Georgiadis, and M. M. Tentzeris, "A Compact Dual-Band Rectenna Using Slot-Loaded Dual Band Folded Dipole Antenna," *IEEE Antennas Wirel. Propag. Lett.*, vol. 12, pp. 1634–1637, December 2013

[79] C. Song et al., ''A novel six-band dual CP rectenna using improved impedance matching technique for ambient RF energy harvesting,'' *IEEE Trans. Antennas Propag.*, vol. 64, no. 7, pp. 3160–3171, Jul. 2016

[80] Q. Awais, Y. Jin, H. T. Chattha, M. Jamil, H. Qiang and B. A. Khawaja, "A Compact Rectenna System With High Conversion Efficiency for Wireless Energy Harvesting," in *IEEE Access*, vol. 6, pp. 35857-35866, 2018

[81] K. Niotaki, A. Collado, A. Georgiadis, K. Sangkil, M. M. Tentzeris, "Solar/electromagnetic energy harvesting and wireless power transmission", *Proc. IEEE*, vol. 102, no. 11, pp. 1712-1722, Nov. 2014

[82] C. H. P. Lorenz, S. Hemour, W. Liu, A. Badel, F. Formosa and K. Wu, "Hybrid Power Harvesting for Increased Power Conversion Efficiency," in *IEEE Microwave and Wireless Components Letters*, vol. 25, no. 10, pp. 687-689, Oct. 2015

[83] X. Gu, S. Hemour, L. Guo and K. Wu, "Integrated Cooperative Ambient Power Harvester Collecting Ubiquitous Radio Frequency and Kinetic Energy," in *IEEE Transactions on Microwave Theory and Techniques*, vol. 66, no. 9, pp. 4178-4190, Sept. 2018

harvesting[84]. The impact of the waveform signal optimization in WPT systems[85] was also addressed in the literature but only at the rectifier level. It was proved that the waveform presenting a high Peak-to-Average Power Ratio (PAPR) improves the rectifier's efficiency. A global approach, concerning the real impacts of various complex signal waveforms on the Tx-to-Rx WPT link, needs to be developed.

My conviction is that the far-field WPT will shift *from the device level to the system level*. More precisely the WPT will be an added value for communication or sensing systems and new concepts, topologies, and design methodologies will have to be implemented. To be honest, the integration of far-field WPT with communication techniques[86], announced in state-of-the-art complete systems, was not yet reported in the literature. For example, the majority of state-of-the-art rectennas designed for WSN, SHM, and IoT applications are characterized as standalone device connected to a resistive load. This is a very restrictive approach (*mea culpa*…for simplicity reason I also adopted this method for many of my rectenna designs). Only few 'rectenna' papers[87,88,89] present experimental results obtained in a most realist scenario (e.g., a rectenna connected with a DC-to-DC boost convertor). As part of ongoing OPTENLOC and ANR-McBIM projects, we are now facing a 'complete' design paradigm on

---

[84] S. Lemey, F. Declercq, H. Rogier, "Textile antennas as hybrid energy-harvesting platforms", *Proc. IEEE*, vol. 102, no. 11, pp. 1833-1857, Nov. 2014

[85] A. Boaventura D. Belo R. Fernandes A. Collado A. Georgiadis N. B. Carvalho "Boosting the efficiency: Unconventional waveform design for efficient wireless power transfer" *IEEE Microwave Mag.* vol. 16 no. 3 pp. 87-96 Apr. 2015.

[86] A. Costanzo and D. Masotti, "Smart Solutions in Smart Spaces: Getting the Most from Far-Field Wireless Power Transfer," in *IEEE Microwave Magazine*, vol. 17, no. 5, pp. 30-45, May 2016.

[87] J. Bito, R. Bahr, J. G. Hester, S. A. Nauroze, A. Georgiadis, and M. M. Tentzeris, "A Novel Solar and Electromagnetic Energy Harvesting System With a 3-D Printed Package for Energy Efficient Internet-of-Things Wireless Sensors," *IEEE Trans. Microw. Theory Tech.*, vol. 65, no. 5, pp. 1831–1842, May 2017.

[88] J. Kimionis et al., "Zero-Power Sensors for Smart Objects: Novel Zero-Power Additively Manufactured Wireless Sensor Modules for IoT Applications," *IEEE Microw. Mag.*, vol. 19, no. 6, pp. 32–47, Sep. 2018.

[89] S. D. Assimonis, S-N. Daskalakis, A. Bletsas, "Sensitive and Efficient RF Harvesting Supply for Batteryless Backscatter Sensor Networks", *IEEE Transactions on Microwave Theory and Techniques*, Vol. 64, No. 4, pp. 1327-1338, April 2016

the Rx side integrating: (i) a UHF rectenna, a power management unit, and a UWB transmitter, (ii) a UHF rectenna, a DC-to-DC boost convertor, and a PMU with an ultra-low power transmitter (the choice has not yet been made among Bluetooth 5, UWB or LoRaWan technologies). We are convinced that even an optimized 'complete' design on the Rx side will not fulfill the technical requirements of the targeted applications and a complete systems optimization on both the Tx and Rx side, including the propagation channel as well, will be mandatory. On the Tx side, it will be mandatory to find the best-site position for the Tx transmitter,as function of the implementation scenario, and to propose a phasing/timing technique in order to increase dynamically and 'on demand' the power densitiy levels at the required locations.

One very challenging idea that I had (in fact it arose during many brainstorming that we had together with Nuno Carvallo, Luca Roselli Alessandra Costanzo and Apostolis Georgiadis during the meetings of the EU COST action IC1301 WiPE) was to power (by WPT) space probes, small cubesats, or other space flying objects and space assets in order to increase their energy autonomy. As known, space probes suffer from a severe problem, which is the limited energy available for their operation. Energy supply is fundamental for continuous operation and, ultimately, the most important sub-system for its sustainable functioning. Consider, for instance, the last space probe put on Comet 67P/Churyumov–Gerasimenko, called "Philae", which was sent by Rosetta to operate and to monitor comet activity. Its operation was jeopardized due to the fact that it landed on a shadowed zone, and therefore was not exposed to direct sunlight. Since its operational energy is only based on solar harvesters, the energy available for its work was very limited and many of the expected scientific experimental data were thus eventually lost. One alternative for energizing such a probe is to find other energy sources or to provide energy wirelessly by WPT techniques from a mothership (e.g., a Rosetta spacecraft, since Rosetta can have much higher and more predictable sun exposuse than the Philae probe itself) to a space probe (e.g., Philae). This idea was developed as part of the project proposal *ERASTUS* submitted as an answer to the European Commission call H2020-LEIT-SPACE – COMPET-03-2015 by a consortium made

of: LAAS CNRS France, EVO[90] Portugal, IT[91] Portugal, UNIPG[92] Italy, SES SPA[93] Italy, CTTC[94] Spain, UNIBO[95] Italy. The main goal of the ERASTUS project was to validate a *"Wireless Power Transmission Solution for Powering Up Space Assets"* and it was quite futurist at the time of submission and even today because it proposed a 'complete far-field WPT system evaluation'. The project was submitted to the funding agency in April 2015. It scored well, but not enough to be selected for funding. We note that all the technology required for such a complete system is already available. The main drawbacks of such a system are the complexity and the end-to-end energy efficiency that is quite low. But the space exploration was not limited (either in the past, or today) and certainly will not be limited in the future by complexity and low efficiency issues. For this reason, I believe that this idea that can be extended to another futurist concept: ***the flying constellation of a shared space laboratory***, illustrated in Figure 20. As known, the CubeSats are limited in terms of energy and communication range capabilities because of their small size. Cubesats embarks small payloads, used for scientific experiments, but they are typically launched on LEO or MEO orbit. Consequently, the lifetime of such Cubesats is quite limited.

---

[90] EVOLEO Technologies LDA, Portugal

[91] Instituto de Telecomunicações, Portugal

[92] Universita Degli Studi di Perugia, Italy

[93] SELEX ES SPA, Italy

[94] Centre Tecnologic de Telecomunicacions de Catalunya, Spain

[95] Alma Mater Studiorum – Universita di Bologna, Italy
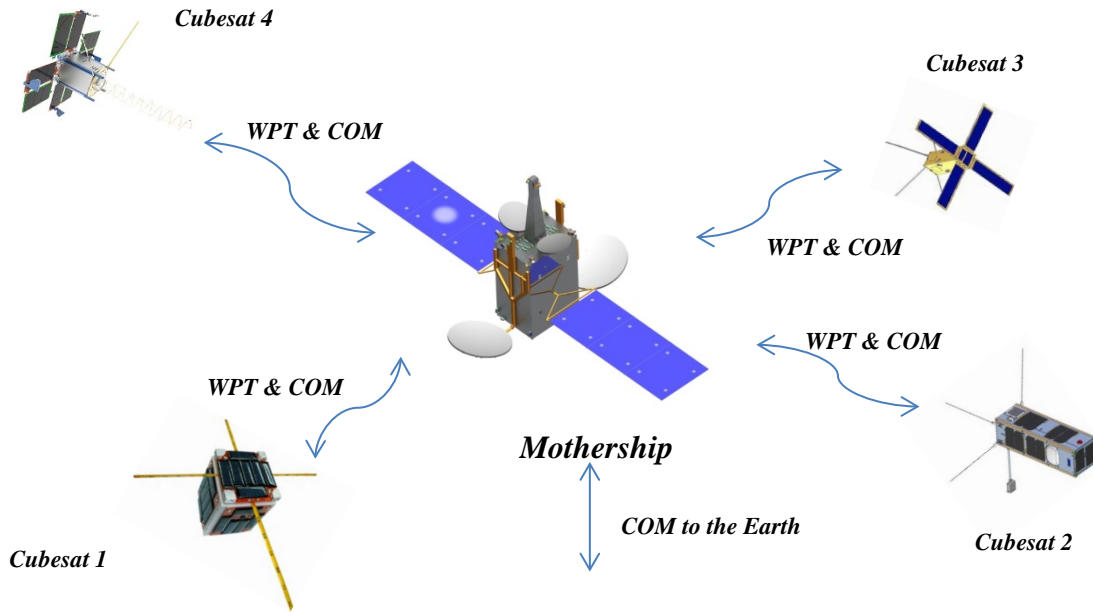
Figure 20. Concept of the flying constellation for a shared space laboratory.

As shown in Figure 20, the flying constellation is composed by one big 'mothership' spacecraft (satellite) that can be positioned on a selected orbit (far from Earth if required, i.e., on a geostationary orbit - GEO). This 'mothership' satellite is well equipped in terms of energy and communication ability: it can communicate over long distances, it is reliable, and has an increased lifetime. It can embark and launch on orbit a constellation of cubesats belonging to different entities (e.g., universities, companies, public, or private agencies) performing scientific experiments independently. Due to their size and fabrication costs, the cubesats have limited capabilities in term of energy and communications. A bidirectional communication (COM) is established at relatively short range with the mothership, which then relays the data to Earth by using its long range communications system. On demand, the mothership can provide energy to the cubesat in order to (i) overcome peaks of DC consumption required by some of the scientific experiments/tasks performed by the cubesats, (ii) collect data from the Cubesats when available in large quantity, (iii) for any other unexpected need of energy that cannot be fulfilled by the limited energy sources embarked on the cubesats (low weight battery and low size solar panels). Thus, a mixed WPT and COM (communication) link should be established between the mothership and the cubesats. Cubesats can also communicate with each other by using direct radio links, if available, or by

53

TUNABLE BANDPASS MEMS FILTERS FOR MILLIMETER WAVE APPLICATIONS: DESIGN AND RESULTS

ALEXANDRU TAKACS[1,3]
DAN NECULOIU[2]
DAN VASILACHE[2]
ALEXANDRU MULLER[2]
PATRICK PONS[3]
LAURENT BARY[3]
PIERRE-FRANÇOIS CALMON[3]
HERVE AUBERT[3]
ROBERT PLANA[3]

Abstract: This paper addresses the design and modeling of millimeter wave tunable filters using CoPlanar Waveguide (CPW) quarter wavelength stubs and MEMS (Micro-Electro-Mechanical-Systems) switches. In order to design bandpass tunable MEMS filters an accurate design methodology based on the transmission line theory is presented. The tunable behavior is achieved using original MEMS switches: Two Cantilever Shunt Switch (TCSS). The overall structures, including TCSS, have been manufactured using dielectric membrane, in order to minimize the insertion losses. The obtained simulation and experimental results confirm the proposed design methodology and indicate very good performances in millimeter wave band.

Keywords: MEMS, bandpass filter, tunable filter, millimeter wave, coplanar waveguide.

1. Introduction

The filters still remain key elements in the modern receiver design. In order to achieve important receiver parameters such as selectivity, sensitivity

---

[1] Military Technical Academy, 81-83 George Cosbuc Ave., Sector 5, 050141, Bucharest, Romania, e-mail: takacs@mta.ro

[2] IMT-Bucharest, 126A Erou Iancu Nicolae Str., 077190, Bucharest, Romania, e-mails: neculoiu@imt.ro, danv@imt.ro, alexm@imt.ro

[3] CNRS; LAAS; Université de Toulouse, 7 Avenue du Colonel Roche, 31077 Toulouse Cedex 4, France, e-mails: atakacs@laas.fr, ppons@laas.fr, bary@laas.fr, calmon@laas.fr, haubert@laas.fr, plana@laas.fr

and dynamic range bandpass filters are typically used. These filters have to match different criteria mainly concerning insertion losses, attenuation, and more important tuning capability. The tuning capability can be achieved using various solutions. One of them is the use of the MEMS switches [1-3]. These switches used in either linear (e.g., varactors) or non-linear (e.g., switches) modes demonstrated superior RF performance compared to their major (and 'classical') competitors such as PIN diodes and field-effect transistor. These superior performances from DC to 100 GHz concern the insertion losses, isolation, cutoff frequency and quality factor.

This paper addresses the tunable MEMS filter design and implementation. An original topology the **T**unable **B**and**P**ass **F**ilter (TBPF) is proposed and analyzed. This topology is based on the use of quarter wavelength stubs in combination with TCSS for achieving the desired behavior. The filters were implemented using **F**inite **G**round **C**o**P**lanar **W**aveguide (FGCPW) technology in order to facilitate the integration with other components and the DC actuation of the TCSS. This topology is basically an extension of the previously proposed Tunable Bandstop Filter (TBSF) that has been already manufactured and characterized [4, 5]. The filters have been designed for 60 GHz applications. This band is not licensed and presents a growing interest because a lot of applications can be envisaged: secure short range communications, wireless sensors systems, or the extension of the RFID (**R**adio**F**requency **ID**entification) systems in the millimeter wave spectrum for developing MMID (**M**illi**M**eter wave **ID**entification) systems.

2. TBPF: Topology and Modeling

One of the most used solutions to achieve a bandstop behavior in the filter design is the use of the short-end or open-end quarter wavelength stubs [6-8]. These stubs can be implemented in various configurations: series or parallel, folded or unfolded in the central line of CPW, or even in the ground plane. In order to facilitate the DC actuation of the TCSS, the stubs are located in the finite ground plane of CPW line. Basically, the tuning of the bandstop filters based on quarter wavelength stubs (short-end or open-end) can be achieved by adjusting the electrical length of the stubs. When TCSSs are used, the electrical length of the stubs can be tuned by switching the TCSS between the OFF (no actuation voltage is applied and the TCSSs are in the up position) and ON state (the actuation voltage is applied and the TCSSs are in the down position). The proposed TBPF used the same principles in order to obtain a tunable bandpass behavior.

Figure 1 and **Figure 2** show the generalized transmission line model of TBPF and the top view of TBPF layout, respectively. In order to achieve bandpass behavior, TBPF uses two quarter wavelength stubs with different geometrical lengths: l_{stubs1} and l_{stubs2}. These stubs introduce two zeros in the

transmission coefficient (at frequencies f_{z1} and f_{z2}), and, consequently, the structure acts as a bandpass filter. Two TCSSs are positioned to the end of these stubs in order to obtain a tunable behavior. A similar topology (but non-tunable) with the structure presented in **Figure 2** has been proposed in [9]. Note that open-end stubs can be also used.
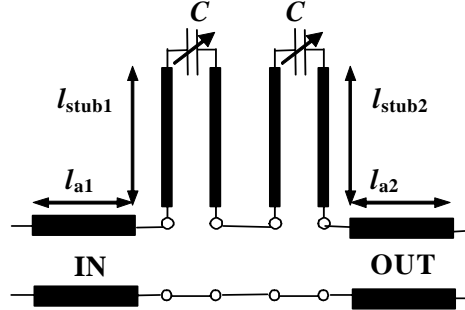
Figure 1. *Generalized transmission line model for the TBPF topology. The CPW access lines have the geometrical lengths l_{a1} and l_{a2}, while l_{stub1} and l_{stub2} represent the geometrical lengths of the stubs*
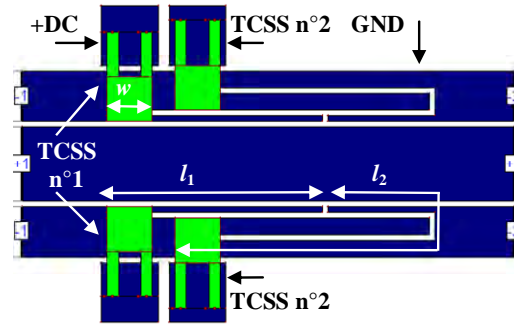
Figure 2. *Top view of the TBPF layout (not to scale)*

As shown in **Figure 1**, the presence of the TCSS can be modeled by using a variable capacitance C. The capacitance C varies between C_{OFF} and C_{ON}. C_{OFF} and C_{ON} represent the capacitance of the TCSS in the OFF (no actuation voltage is applied and the TCSSs are in the up position) and ON state (the actuation voltage is applied and the TCSSs are in the down position). These capacitances can be computed using the following analytical formulas [1]:

$$C_{OFF} = \frac{\varepsilon_0 S}{d - t_d + \dfrac{t_d}{\varepsilon_r}} + C_f, \qquad (1)$$

$$C_{\mathrm{ON}} = \frac{\varepsilon_0 \varepsilon_{\mathrm{r}} S}{t_{\mathrm{d}}}, \qquad\qquad (2)$$

where: t_{d} is the thickness of the dielectric layer, d is the distance between the TCSS and the metallization of the CPW line, ε_{r} is the relative dielectric permittivity of the dielectric layer, $\varepsilon_0 = 8.85 \cdot 10^{-12}$ F/m is the absolute relative permittivity, S is the surface of the parallel plate capacitor (between TCSS and CPW line), C_{f} is the capacitance due to the 'fringing effect' and their value is about $10 \div 40\%$ of parallel plate capacitance.

Normally, the S-parameters of the TBPF can be computed using a circuit approach based on the transmission line model (**Figure 1**). But this approach is not (enough) accurate. Using TCSS, the stubs are charged by impedance $Z_{\mathrm{TCSS}} \neq 0$, that changes when C varies from C_{OFF} to C_{ON}. The value and the position of this 'localized' impedance cannot be accurately estimated. The propagation mode inside the stubs seems to be a typically 'slotline' mode, while the propagation mode between the input and output ports is more or less a 'coplanar' mode. Therefore we have two characteristic impedances: one for the CPW line, which contains the filter, and other one for the stubs. The TBPF has been manufactured on a multilayer substrate and we do not have accurate analytically formulas to compute the characteristic impedance for these stubs. Consequently, the S-parameters computed using a circuit approach do not well agree with the electromagnetic simulation and measurement results. Instead of the use of this circuit approach we propose an original design methodology based on the properties of the quarter wavelength stubs and the use of intensive full-wave electromagnetic simulations.

3. TBPF: Design Methodology

The TBPF was implemented using FGCPW lines and a special designed MEMS switch: TCSS (Two Cantilever Shunt Switch). This switch consists of two cantilever beams positioned above the stubs (as shown in **Figure 2**). The TCSS uses a cantilever structure, usually encountered in series switch. But, despite the case of the series switch, the cantilever is not placed in series with the central conductor of the CPW line. Consequently the TCSS has a typically shunt switch behavior. Because of the use of two cantilevers (for achieving a shunt switch behavior), this switch is named **T**wo **C**antilevers **S**hunt **S**witch (TCSS) [10]. TCSS exploits the low intrinsic spring constant of the cantilever beam. From a theoretical point of view [1], the TCSS spring constant is less than the spring constant of the fixed-fixed beam, which is usually used in the typical shunt switch configuration. Note that the stubs are positioned in the lateral ground plane in order to facilitate the electrostatic actuation of the TCSS. Also,

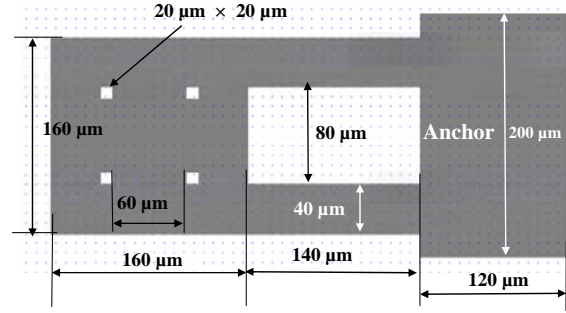the RF and DC signal paths are separated, but the ground (GND) is common for high frequency and DC signals.

Figure 3. *Top view (not to scale) and the major dimensions of the TCSS*

As the transmission line theory states, the bandstop frequency (f_0) and the physical length (l) of the stubs can be related using the following formula:

$$l = \frac{c}{4 f_0 \sqrt{\varepsilon_{\text{reff}}}}, \tag{3}$$

where: $c = 3 \cdot 10^8 \, \text{m/s}$ is the speed of light and $\varepsilon_{\text{reff}}$ is the relative effective permittivity for the CPW lines. This effective permittivity can be obtained by using quasi-static analytic formulas or, more accurately, by using electromagnetic simulations with dedicated software such as Zeland IE3D [11]. Based on Formula (**3**), the bandstop frequency (f_0) for the TBSF and the zeros of the transmission coefficient $(f_{z1}$ and $f_{z2})$ for the TBPF can be computed as follows:

$$f_{z1} = \frac{c}{4 l_{z1} \sqrt{\varepsilon_{\text{reff}}}}, \tag{4}$$

$$f_{z2} = \frac{c}{4 l_{z2} \sqrt{\varepsilon_{\text{reff}}}}, \tag{5}$$

where:
  (i) $l_{z1} = l_1$ (TCSS n°1 OFF) and $l_{z1} = l_1 - w$ (TCSS n°1 ON), w is the width of the cantilever beam (**Figure 2**);
  (ii) $l_{z2} = l_2$ (TCSS n°2 OFF) and $l_{z2} = l_2 - w$ (TCSS n°2 ON) for the TBPF (**Figure 2**).

Note that Formula (**3**) is based on transmission line theory, and represents an approximate relation, which does not take into account discontinuities, coupling or other parasitic effects such as dispersion or higher order modes

propagation. The capacitance of the TCSS is not taken into account in Formula (**3**). Despite of these limitations, Formula (**3**) is a very good start point in the design but, in order to obtain more accurate results, intensive electromagnetic simulations must be used. We also remark that if f_{z1} and f_{z2} are very close the tuning is not possible. The reason in this case is that the difference between l_{OFF} and l_{ON} is limited by the geometrical dimension of the cantilever beam (160 µm in this case) determined from the electromechanical design of TCSS.

Design methodology in the case of TBPF consists of the following steps:

(i) Supposing that the zeros frequencies $\left(f_{z1} \text{ and } f_{z2} \right)$ are imposed from the design requirements, we can compute the l_{1OFF} and l_{2OFF} using Relations (**4**) and (**5**). Note that l_{1OFF} and l_{2OFF} are the lengths of the stubs corresponding to the TCSS OFF (no actuation voltage are applied and the cantilever beam are in the up position);

(ii) Supposing that after the TCSS actuation the zeros are located at f'_{z1} and f'_{z2}, we can derive l_{1ON} and l_{2ON} using Relations (**4**) and (**5**). Note that l_{1ON} and l_{2ON} are the lengths of the stubs corresponding to TCSS ON (the actuation voltage is applied and the cantilever beam is in the down position). We also remark that:

$$l_{1OFF} - l_{1ON} \geq w, \; l_{2OFF} - l_{2ON} \geq w; \qquad (6)$$

(iii) Electromagnetic simulations have to be performed in order to determinate the 'exact' position of the zeros. As expected the 'exact' position of zeros is shifted with respect to the position imposed by the design requirements and computed using analytical formulas. Using electromagnetic simulations, we can obtain the optimized lengths $l_{1OFF}{}^{opt}$ and $l_{2OFF}{}^{opt}$ (by performing electromagnetic simulations with the TCSS OFF) and $l_{1ON}{}^{opt}$ and $l_{2ON}{}^{opt}$ (by performing electromagnetic simulations with the TCSS ON).

4. TBPF: Experimental and Simulation Results

TBPF has been manufactured on a special dielectric membrane [4, 5]. The dielectric membrane presents major advantages in the 60 GHz band, such as low losses and very low dispersion. The relative effective permittivity for this membrane is approximately: $\varepsilon_{reff} = 1.5$. Note that the realization of the TCSS on membrane was an important challenge from a technological point of view and a trade-off between technology and electromagnetic design has been made. Two types of the TBPF have been manufactured:

(i) TBPF-type I: in this structure the dielectric used for the capacitive contact in the TCSS is localized only in the region situated under the TCSS.

This is the most usual solution implemented in the manufacturing of capacitive MEMS switches. **Figure 4** shows a top view of TBPF-type I structure.

(ii) TBPF-type II: in this structure the dielectric used for the capacitive contact is extended in a larger region as indicated in **Figure 5**. This solution is easier to implement from the manufacturing point of view, but we expect a rise of the insertion losses.
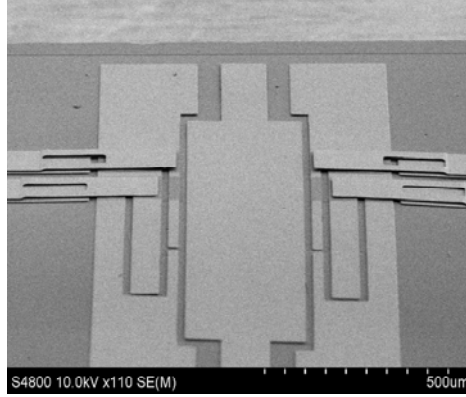
Figure 4. Top view of the TBPF-Type I
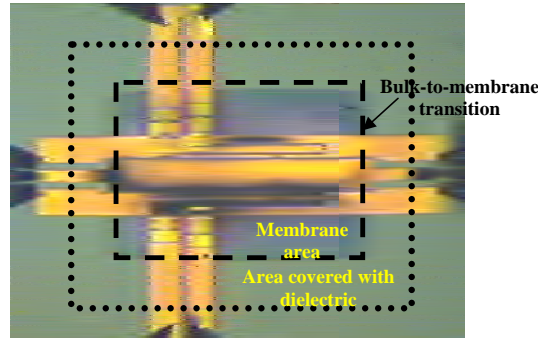
Figure 5. Top view of the TBPF-Type II

Figure 6 shows the simulated transmission coefficient for the TBPF-Type II obtained using IE3D software. These simulations have performed based on the following simplified hypothesis: (i) the dielectric layer used for capacitive contact is extended to infinite in the horizontal cut; (ii) the two bulk-to-membrane transition is neglected; (iii) no losses have been taken into account; (iv) standard values of the electrical permittivity (and not measured values) have been taken into account for the three-layer membrane.

The on-wafer measurements were performed at LAAS Toulouse using an Anritsu ME7808A VNA (Vector Network Analyzer) equipped with an extension module 3742A-EW (65÷110 GHz), a Karl Suss PM5 probe station

and DC bias network. The measurements setup is shown in **Figure 7**. The measured actuation voltage of the TCSS used in TBSF is about 20 V.

Figure 6. *Simulated (IE3D) transmission coefficient for TBPF*

Figure 7. *The experimental setup used for TBPF characterization*

| a) | b) |

Figure 8. *Experimental results for TBPF-Type I (a) and TBPF-Type II filters (b)*

Figure 8 represents the experimental results obtained for TBPF-Type I and TBPF-Type II filters. As shown in this figure the TBPF presents a good tunable behavior. Note that these experimental results include the effects of the two membrane-to-bulk tran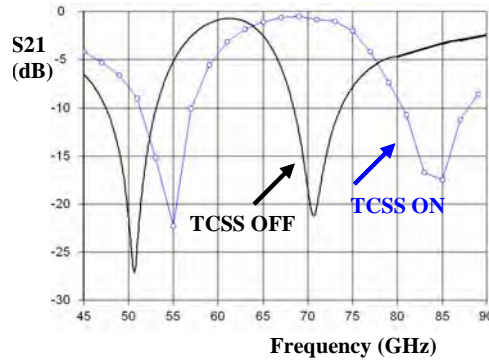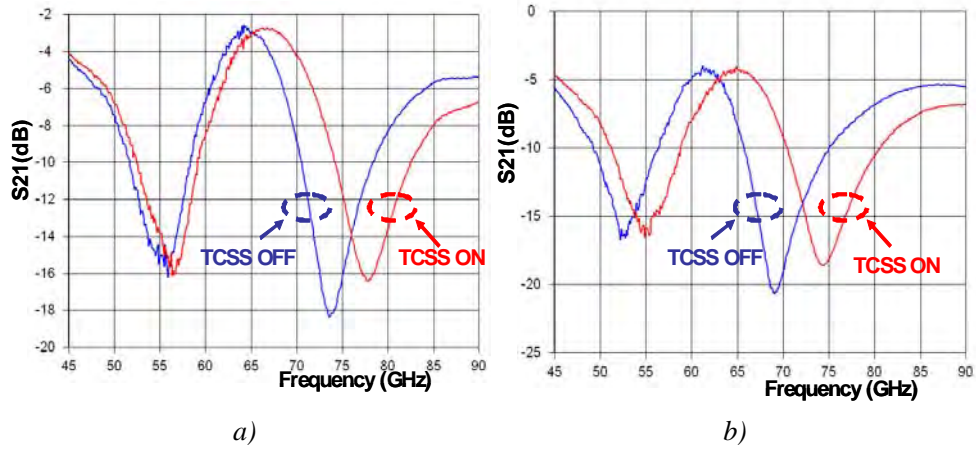sition. Only a standard SOLT (**S**hort **O**pen **L**oad **T**rhu) calibration has been performed before the measurements. As expected the TBPF-Type II presents important insertion losses in the bandpass and it will be not retained for future applications. The TBPF-Type I presents a minimum insertion loss of 2.4 dB at 64.2 GHz with TCSS in OFF state, and 2.5 dB at 67.3 GHz with TCSS in ON state. A good reproducibility on the same wafer has been observed during measurements. Further works (under run) will allow us to improve the analytical model and the agreement between measurements and simulation (especially with the TCSS in the ON state).

5. Conclusion

An original topology for millimeter wave tunable filter has been proposed. The proposed structure combines an original switch (TCSS) with conventional stub-based bandstop filter topology. A simple and ready to use design methodology based on transmission line theory and the use of electromagnetic simulation has been proposed. In order to minimize the insertion losses, the filters, including TCSS, have been manufactured on dielectric membrane. The simulation and the measurement results demonstrated very good results in the 60 GHz band.

Acknowledgments

References

1. G.M. REBEIZ – *RF MEMS: Theory, Design, and Technology*, John Wiley & Sons, Hoboken, NJ, 2003

2. H.J. De Los SANTOS – *RF MEMS Circuit Design for Wireless Communications*, Artech House, Boston, MA, 2002

3. V.K. VARADAN, K.J. VINOY, K.A. JOSE – *RF MEMS and their Applications*, John Wiley & Sons, Hoboken, NJ, 2003

4. A. TAKACS, D. NECULOIU, D. VASILACHE, A. MULLER, P. PONS, L. BARY, P. CALMON, H. AUBERT, R. PLANA – *Tunable Bandstop MEMS Filter for Millimeter-Wave Applications*, Electronics Letters, Vol. 43, No. 12, pp. 675-677, Jun. 2007

5. A. TAKACS, D. NECULOIU, D. VASILACHE, A. MULLER, P. PONS, L. BARY, P. CALMON, R. PLANA, H. AUBERT – *New Topologies of Tunable Bandstop MEMS Filters for Millimeter Wave Applications*, Proc. of the 2007 European Microwave Conference, EUMC '2007, pp. 126-129, Munich, Germany, Oct. 9-12, 2007

6. R.N. SIMONS– *Coplanar Waveguide Circuits, Components, and Systems*, John Wiley & Sons, New York, NY, 2001

7. T.M. WELLER, L.P. KATEHI – *Miniature Stub and Filter Designs Using the Microshield Transmission Line*, IEEE MTT-S International Microwave Symposium Digest, Vol. 2, pp. 675-678, Orlando, FL, May 16-20, 1995

8. A. TAKACS, H. AUBERT, P. PONS, T. PARRA, R. PLANA, J. GRAFFEUIL – *Miniature Coplanar Bandstop Filter for Ka-Band Applications Based on Original Resonant Coupling Irises Topology*, Electronics Letters, Vol. 40, No. 20, pp. 1274-1275, Sep. 2004

9. N. YANG, Z.N. CHEN, Y. ZHANG – *CPW Bandpass Filter with Serially-Connected Series-Stub Resonators*, Proc. of the 2005 European Microwave Conference, EUMC '2005, Vol. 1, Paris, France, Oct. 4-6, 2005

10. A. TAKACS, D. VASILACHE, C. TIBEICA, D. NECULOIU – *A New Topology of RF MEMS Shunt Switch for Reconfigurable Systems Applications*, MEMSWAVE 2005 Workshop, pp. 107-113, Lausanne, Switzerland, Jun. 23-24, 2005

11. *IE3D: MoM-Based EM Simulator*, Zeland Software, http://www.zeland.com/ie3d.htm

Miniaturization of Compact Quadrifilar Helix Antennas for Telemetry, Tracking and Command Applications

Alexandru Takacs[1, 2, *], Hervé Aubert[1, 3], Daniel Belot[4], and Hubert Diez[4]

Abstract—This paper addresses the miniaturization of Quadrifilar Helix Antennas (QHAs) for space applications (VHF Telemetry, Tracking and Command). Several shape miniaturization techniques were presented, and the impact of height reduction is quantified in terms of radiation pattern, gain and phase center. Simulated and experimental results demonstrate that Compact Quadrifilar Helix Antennas (CQHAs) with a height reduced up to 70% reported to the reference QHA can be designed. By using an appropriate optimization method, the impact of the miniaturization on CQHA performances in terms of radiation pattern and polarization purity can be minimized. Moreover, the impact on the gain is quantified, and design rules are reported. Finally a closed-form expression for estimating the gain of CQHAs from the height reduction factor is found.

1. INTRODUCTION

Quadrifilar Helical Antenna (QHA) is formed by four helical antennas wound around the same longitudinal axis [1]. Each helical antenna is rotated 90° with respect to one another. This 60-years old antenna is naturally convenient for radiating circularly-polarized waves with a large variety of radiation patterns and radiation modes. Compared with the (monofilar) helical antenna QHAs are a new class of antennas allowing better performances mainly in terms of maximum gain, (circular) polarization purity and phase center stability. Most of QHA designs require a ground plane perpendicular on the longitudinal axis of the helical antennas. The input ports can be located on the ground side (bottom side of the QHA) or at the opposite ends (top side of the QHA). Open-ended or short-circuited QHA can be designed if the unfed ends are open-ended or short-circuited. The input ports can be fed with equal amplitude, clockwise or counterclockwise, in phase quadrature with a phase progression of +90° (direct) or −90° (reverse) between two consecutive ports. Thus forward or backward wave can be generated by properly controlling the wounding sense of the helical antennas and the phase progression of the input signals.

QHAs are resonant structures, and the length of each constitutive helical antenna is multiple of the quarter wavelength. QHAs can be manufactured using wires or by using printed techniques. The wire is more suitable for low-frequency applications (VHF band) while the printed techniques are widely used for high-frequency applications (UHF or upper bands). The inherent properties of the QHAs (purity of the circular polarization, easy shaping of the radiation pattern and circularly-polarized radiated fields over a wide beamwidth) qualified QHA as an ideal candidate for satellite applications especially for Telemetry, Tracking and Command (TTC) applications. VHF QHAs are quite long antennas and, as other traditional antennas (e.g., parabolic antennas) QHAs face today to accommodation issues in the modern cost-effective satellite launch configuration. Consequently the miniaturization without significant degradation of radiation characteristics is the major challenge for any modern QHA design. QHAs are composed by four monofilar helical antennas.

The compact QHAs reported in this paper are planned to be used for a telemetry link in VHF band on board of the satellite Space-based Multi-band Variable Object Monitor (SVOM), a science satellite project developed in bilateral cooperation between the French Space Agency (CNES) and Chinese Space Agency. Several CQHA designs compatible with TTC requirements are presented here in order to analyze the impact of the miniaturization technique on antenna key parameters such as radiation patterns, antenna gain and phase center stability. Measurement results are reported for experimental validation purposes. The design of standard QHA is summarized in Section 2. The adopted miniaturization technique and CQHA design are presented in Section 3. The obtained experimental and simulated results of CQHAs are discussed in Section 4 with a focus on the impact of the miniaturization technique on the antenna gain.

2. QHA DESIGN

VHF QHAs are mainly used for low data rate telemetry link in the satellite communication systems. The key descriptors of QHA are the radius r of the helix (the radius of the supporting cylindrical structure), pitch angle α (or alternatively the number n of the turns can be used) and height h of the antenna (the height of the supporting cylindrical structure if it is used). The combination between the pitch angle, antenna height and antenna radius determines the antenna radiation characteristics. Fig. 1 shows a 3D simulation model of an open-ended QHA for $n < 1$, the geometrical descriptors and relationship between n, α, r, h and l, where l denotes the total length of a single helical wire and, the simulated 3D radiation patterns (gain) of a short-circuited QHA. The length of the helical wire typically sets the resonant frequencies and is approximately an integer multiple of the quarter wavelength. $\lambda/4$ or $3\lambda/4$ configurations are generally used for the open-ended QHA while $\lambda/2$ or λ configurations are often used for short-circuited QHA. Other key parameters impacting QHA design and performances are the diameter d_g of the ground plane and the wire radius for wire-supported QHA (or the strip width for printed QHA). Wire-supported QHA designs were reported in [2–9] while printed QHA were studied in [10–15].

QHAs are mainly implemented on cylindrical surfaces (helical wires or strip lines are rolled up on cylindrical surfaces). However, QHAs can be conformed on conical [16], spherical [17] or square [18] surfaces.

Compact design is required for space application in order to fit the launch constraints. Thus
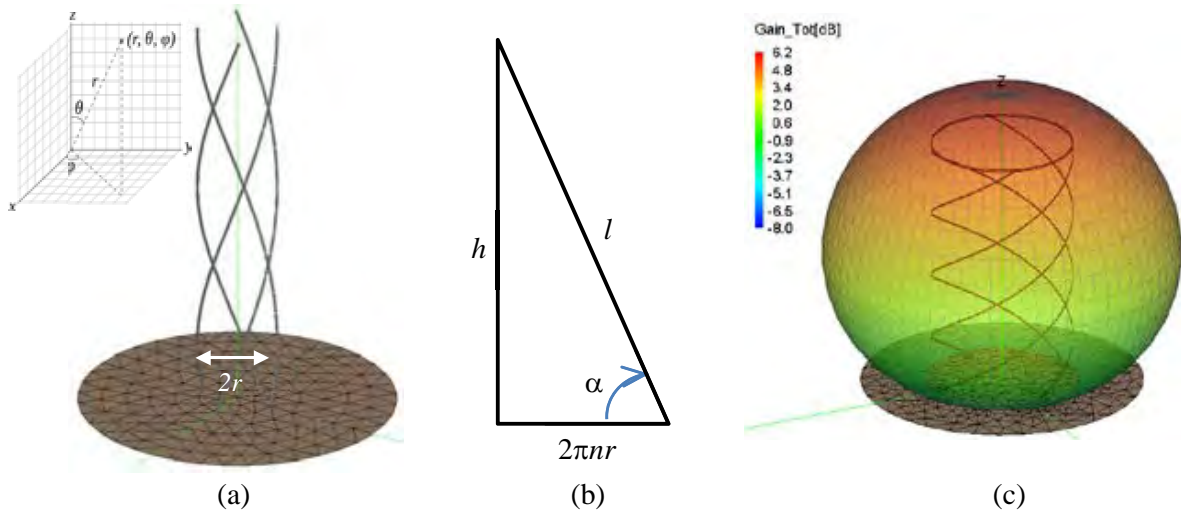

Figure 1. (a) Air-supported simulation model (FEKO) for an open-end QHA including the finite-sized ground plane (the inset illustrates the adopted system of coordinates); (b) the geometrical relationship between the key descriptors of QHAs; (c) simulated (FEKO) 3D radiation pattern (gain, in dB) for a typical short-circuited QHA (axial mode).

quarter/half wavelength configurations are preferred in spite of their well-known poor input matching (especially for the quarter wavelength design). The poor input matching can be compensated by the feeding network that operates, in most of cases, as a matching network. The feeding/matching network is not discussed in this paper.

Two designs for TTC space applications, called here QHA1 and QHA2, were selected as reference QHAs. These antennas are planned to be used for a telemetry link in VHF band on board of the SVOM satellite [19]. QHA1 is an open-ended quarter-wavelength QHA designed for operating at 137 MHz while QHA2 is a short-ended half-wavelength QHA operating at 162 MHz. Both of them radiate circularly-polarized electromagnetic fields in the so-called *axial mode* (the maximum power is radiated along the positive Oz direction). The main descriptors of these two reference QHAs are reported in Table 1.

Table 1. Geometrical descriptors of reference antennas QHA1 and QHA2.

		α	r (mm)	dg (mm)	h (mm)	l (mm)
QHA1	value	70°	50	400	514	547
	normalized to wavelength		0.05	0.18	0.24	0.25
QHA2	value	33°55'	125	500	450	930
	normalized to wavelength		0.07	0.27	0.24	0.50

3. MINIATURIZATION TECHNIQUES AND CQHA DESIGN

3.1. Miniaturization Techniques

Several miniaturization techniques were proposed in order to implement CQHA. Those techniques can be classified as follows:

(i) *shaping-based technique*: the helical wires are shaped in order to reduce the axial height of the helix while keeping the total length of the wires almost unchanged and consequently, the operating frequency;

(ii) *dielectric-loading technique*: a dielectric with medium/high dielectric constant is used as a cylindrical support for the CQHA, and consequently, shorter wires (and smaller axial height) are used to operate at the desired frequency.

These two techniques can obviously be combined. The dielectric-loading technique facilitates the manufacturing process, but the radiation efficiency can be drastically degraded because of the dielectric loss. For this reason, the shaping-based technique is preferred here for miniaturizing the reference antennas QHA1 and QHA2 while keeping the radiation properties unchanged.

3.2. Quadrifilar Helix Antenna with Arbitrary Shape

In the past years, the shapes of constitutive wires in CQHAs were described by sinusoidal [6, 12, 15], periodic triangular [20], periodic trapezoidal [20], rectangular [12, 21], meandered [13, 14], pre-fractal [22], non-linear functions [23] and more recently, by the combination of fractal and sine functions [24] (a review of the patents on CQHAs can be found in [25]). The axial height of the QHA can be also reduced by modifying the geometry/the shape at the center of the helical section [7, 8].

CQHA with an arbitrary wire shape can be modeled by the following system of parametric equations:

$$\begin{cases} x(t_{i+1}) = r\cos(\theta_i) \\ y(t_{i+1}) = r\sin(\theta_i) \qquad\qquad\qquad i \geq 1 \\ z(t_{i+1}) = t_{i+1}\sin(\alpha) + f(t_{i+1})\cos(\alpha) \end{cases}, \qquad (1)$$

$$\begin{cases} \theta_i = \dfrac{\displaystyle\sum_{j=1}^{i-1}[g(t_{j+1}) - g(t_j)]}{R} = \dfrac{g(t_i) - g(t_1)}{R}, & i \geq 1 \\ g(t) = t\cos(\alpha) - f(t)\sin(\alpha), & t \in \Re, \quad t \in [0, t_{\max}] \end{cases} \qquad (2)$$

where t is a positive real number, $t_{\max}$ the solution of the equation $h = z(t_{\max})$, and $f(t)$ designates an arbitrary function called the *shaping function*. Eq. (1) allows numerically computing each point of the CQHA as function of the angular coordinate θ_i. By choosing the real-valued numbers t_i it is possible to adjust the number of points that controls the shape of helical wires of CQHA. A standard Cartesian coordinate system is adopted here with the origin sets at the center of the ground plane. The first point ($\theta_i = 0°$) of the helical wire is positioned at $x(0) = r$, $y(0) = 0$ and $z(0) = 0$. A helical wire for QHA/CQHA is generated by using Eqs. (1) and (2). The three other constitutive helical wires of the QHA or CQHA are derived from a standard rotation over the z-axis with $90°$, $180°$ and $270°$ of the first helical wire. The shaping function of the reference QHA is given by:

$$f(t) = t \tag{3}$$

while CQHAs with a sinusoidal profile (i.e., with wires mathematically described by a linear combination of n sine functions) are such that:

$$f(t) = \sum_{j=0}^{n-1} A_j \sin(\omega_j t) \tag{4}$$

where A_j et ω_j denote the geometrical descriptors of the sinusoidal profile and can be viewed as amplitude and pulsation coefficients, respectively. Fractal shapes are generally not defined from closed-form expressions but are the result of an iterative process which can be further implemented inside most electromagnetic software. In order to obtain smaller structures the so-called *modified fractal profiles* (e.g., modified Von Koch or Peano) may be advantageously used. The procedure for modifying standard fractal shapes is detailed in [24] and [27]. These modified fractal profiles can be combined with a sine function as reported in [24] and [27] in so-called *Sine-Modulated Modified Fractal* (SMMF) profiles.

From a manufacturing point of view it can be convenient to print the shape of the helical wire (antenna) in a 2D plane and then to roll-up the printed 2D shape around a cylindrical supporting structure to form the CQHA. Fig. 2 illustrates 2D printed surfaces using various profiles and the corresponding 3D simulation models (FEKO) for CQHA. A periodicity is added into the design by
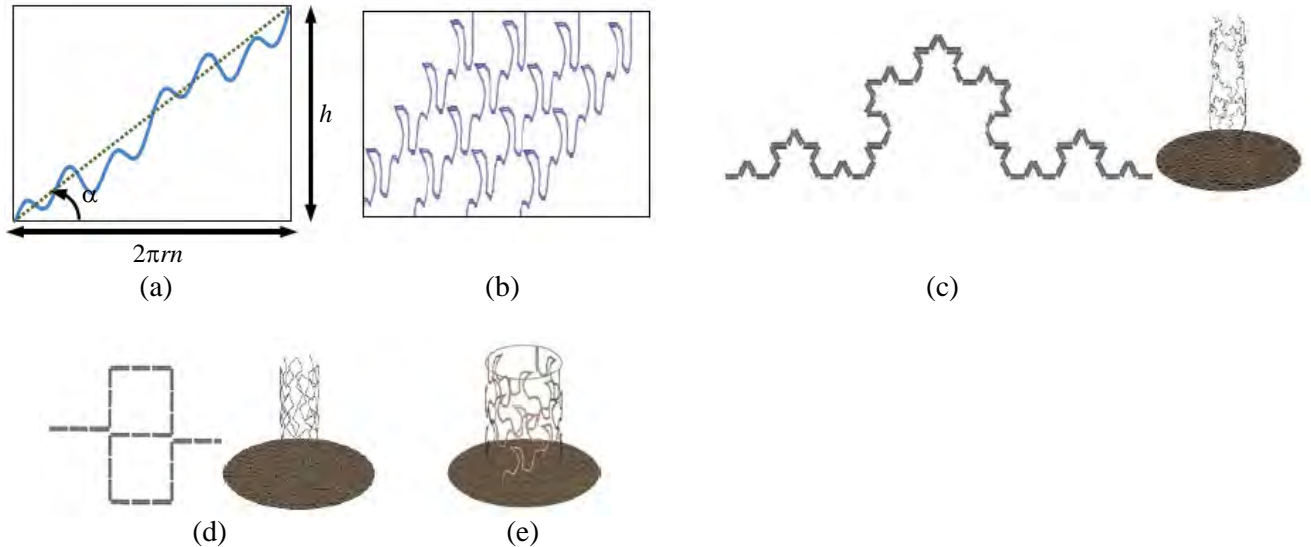
Figure 2. Some CQHA shapes considered in this paper: (a) a 2D shape combining multiple sine functions (continuous line) before rolling it up for generating a compact helical antenna; (b) four metallic strips having a Von Koch SMMF profile printed on a planar surface before rolling it up for generating a CQHA; (c) prefractal Von Koch profile and the resulting CQHA 3D simulation model (FEKO); (d) prefractal Peanoprofile and the resulting CQHA 3D simulation model (FEKO); (e) 3D simulation model (FEKO) for a CQHA with a Von Koch SMMF.

duplicating the elementary cell along each constitutive helical antenna. For example the cell appears twice in Fig. 2(a) while in Fig. 2(b) it is repeated four times. This periodicity (or number of cells) is an additional design parameter and is advantageously used during the optimization process.

3.3. Optimization Methodology

Miniaturizing QHA may impact the intrinsic antenna radiation performances. For TTC space applications it is mandatory to keep unchanged the radiation pattern and polarization purity. As the height of QHA becomes smaller, the antenna gain decreases. Depending on the application and overall power budget link lower gain can be increased by adding power amplifiers. However, the modification of the radiation pattern due to the antenna miniaturization cannot be easily compensated.

A good trade-off among compactness, directivity, input matching, antenna gain and efficiency can be obtained by using an adequate optimization methodology.

In order to find the best fitted CQHA, an optimization process has been implemented using the optimization module of FEKO software. The following objective (goal) function GF has been defined in CADFEKO (OPTFEKO):

$$
\begin{aligned}
&GF = w_1 \cdot GF_1 + w_2 \cdot GF_2 + w_3 \cdot GF_3 + w_4 \cdot GF_4; \\
&GF_1 : S_{11} < 0.3 \\
&GF_2 : LHC(D) > 0\,\text{dB} \quad \text{for} \quad -60° \leq \theta \leq 60°, \quad \forall \\
&GF_3 : RHC(D) < -10\,\text{dB} \quad \text{for} \quad -180° \leq \theta \leq 180°, \quad \forall \\
&GF_4 : G_{\max} > 0\,\text{dB}
\end{aligned}
\tag{5}
$$

where w_1, w_2, w_3 and w_4 are weight coefficients (positive real numbers); LHC and RHC designate respectively the left-handed and right-handed circular components of the directivity; S_{11} denotes the magnitude of the reflection coefficient at each port of the CQHA; $G_{\max}$ is the maximum gain of CQHA. The goal function GF is computed at the desired operating frequency, that is, (i) at 137 MHz for QHA1 and CQHAs derived from QHA1 and, (ii) at 162 MHz for QHA2 and CQHAs derived from QHA2. The TTC technical specifications in VHF band require main polarization (LHC) of the reference QHA to be positive for $-60° \leq \theta \leq 60°$ while the cross-polarization (RHC) level is required to be lower than $-10\,\text{dB}$ for $-180° \leq \theta \leq 180°$. Consequently the goal function GF intends to maintain the impedance matching (*GF1*), radiation pattern and polarization purity (*GF2* and *GF3*) at the same level than the reference antenna. This allows facilitating the comparisons between radiation performances of optimized CQHAs and will force the best-fitted CQHAs to fulfill the typical technical requirements for TTC applications. In Eq. (5) a fourth goal is targeted for classifying the designed CQHA in terms of maximum gain criteria. For TTC application it is not convenient to use antennas with negative gain (in dBi) and consequently, $G_{\max} > 0\,\text{dBi}$ is required as an additional goal *GF4*. The optimization process uses the *Grid Search Method* implemented in FEKO and is based on the methodology described in [6] and [26]. Thousands of CQHAs based on sinusoidal, standard or modified prefractal and, SMMF [24, 27] profiles were chosen for optimization purposes. The obtained results are summarized and discussed in the next section.

4. CQHA: RESULTS AND DISCUSSION

To demonstrate the concept and evaluate the impact of the miniaturization process on the antennas performances, two approaches were applied. On one hand, the wire-supported QHA1 and optimized CQHAs were manufactured using a low-cost technique based on a PVC tube (3 mm thick) for the cylindrical supporting structure [28, 29]. PVC has a relative dielectric permittivity close to 4 and high dielectric losses(dielectric loss tangent is around 0.06 [30]). On the other hand, the printed QHA2 and optimized CQHAs were manufactured using: (i) either a paper substrate (relative dielectric permittivity close to 3 and thickness of 0.15 mm) and a quasi-printed technique [27] or (ii) the Dupont Melinex 339 PET dielectric (relative dielectric permittivity close to 3, loss tangent 0.007 and thickness of 0.1 mm) and the commercially available technology from Inkjetflex [31]. Wire-supported QHA1 and a set of five CQHAs derived from QHA1 are shown in Fig. 3 while printed QHA2 and CQHAs derived from QHA2 are shown in Fig. 4.

Figure 3. Manufactured wire-supported CQHAs derived from QHA1 using as shaping function various combinations of sine functions (CQHA1a, CQHA1b, CQHA1c and CQHA1d) and prefractal (Von Koch) profile combined with a sine function (CQHA1e).
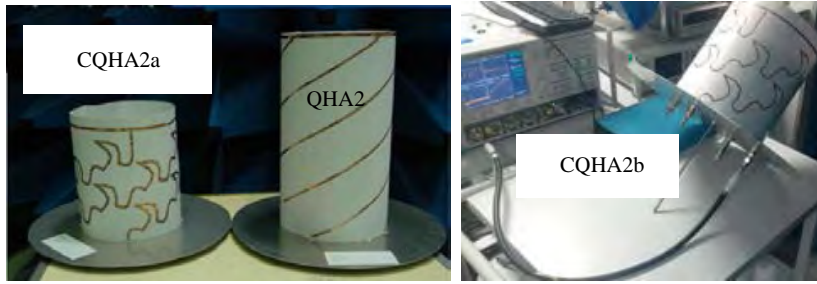

Figure 4. Manufactured printed CQHAs derived from QHA2 using a Von Koch-based SMMF as shaping function. CQHA2a was fabricated using the quasi-printed home-made technique on paper substrate while CQHA2b was manufactured using the commercially available technology from Inkjetflex.

Taking into account the dielectric supporting structure in the simulation model, the computational time increases significantly. For instance, the air-supported CQHA (i.e., without the cylindrical dielectric supporting structure) can be simulated in less than one minute on a PC with quad-core processor Intel Q9300 and 4GB of RAM, while the PVC-supported CQHA requires at least one hour. The computational time is a critical issue in the design/optimization process because thousands of CQHAs need to be computed here for finding the best-fitted CQHAs. In order to minimize the simulation time, the optimization was performed by using air-supported CQHA. Consequently, simulation and optimization results reported in this paper concern antennas without the cylindrical supporting structure. However, in order to predict the eventual impact of such a structure on antenna performances, electromagnetic simulations have been performed by taking into account this structure only for the optimized designs selected for the manufacturing. Adding dielectric (supporting tube or thin film) decreases more or less the operating frequency and degrades the antenna efficiency and gain. This effect is found to be critical for wire-supported CQHA using thick PVC tube and to be not significant for printed CQHA printed on thin dielectric film.

4.1. Measurement Technique

The reflection coefficient at the input ports of the antennas was measured by using an Anritsu 37369C Vector Network Analyzer. When the reflection coefficient at one port is measured, the unfed three other ports are loaded by $50\,\Omega$. The radiation pattern measurement in the VHF band is not an easy task, and near field techniques are required. Radiation patterns have been measured by the French Space Agency using spherical near field measurement technique. In order to evaluate the antenna gain, the reference Lindgren dipole [32] over a ground plane was used.

4.2. Simulation and Experimental Results

As previously explained, the wire-supported antennas (QHA1 and the CQHAs derived from QHA1) have been designed/optimized without taking into account the cylindrical PVC supporting structure. Consequently, the initial operating frequency was down-shifted from 137 MHz to approximately 120 MHz depending on the specific design. Five best-fitted wire-supported CQHAs were manufactured and characterized. Their characteristics are summarized in Table 2.

Table 2. QHA1/CQHA1 measured characteristics.

Antenna name	Height (mm)	Relative height (%)	Measured S_{11} (dB)	Measured directivity (dBi)	Shaping function $f(t)$
QHA1	514	100	−6.2 at 123 MHz	5.9	Straight line
CQHA1a	270	52.5	−8.1 at 120 MHz	5.6	Sinusoidal
CQHA1b	217	42	−8.3 at 118 MHz	5.6	Sinusoidal
CQHA1c	193	37.5	−8.6 at 115 MHz	5.4	Sinusoidal
CQHA1d	135	26.2	−7.6 at 119 MHz	5.6	Sinusoidal
CQHA1e	167	32.5	−9.5 at 125 MHz	5.2	Von Koch SMMF

In order to compare the performances of overall manufactured antennas, the operating frequency of 120 MHz was selected for measuring the radiation patterns. The electromagnetic simulations indicate that the polarization purity and shape of the radiation pattern are not significantly modified compared with the reference antenna in a 10% bandwidth centered at the resonant frequency. Table 2 experimentally demonstrates that CQHAs with a height reduced up to 70% reported to the reference QHA can be designed.

Figure 5 shows the measured and simulated LHC and RHC components of the directivity for the reference QHA1 at 120 MHz. These results demonstrate that TTC requirements given by Eq. (5) regarding the radiation pattern and the polarization purity are fulfilled by QHA1. As expected, the maximum directivity (5.9 dBi) was measured for $\Phi = \theta = 0°$.
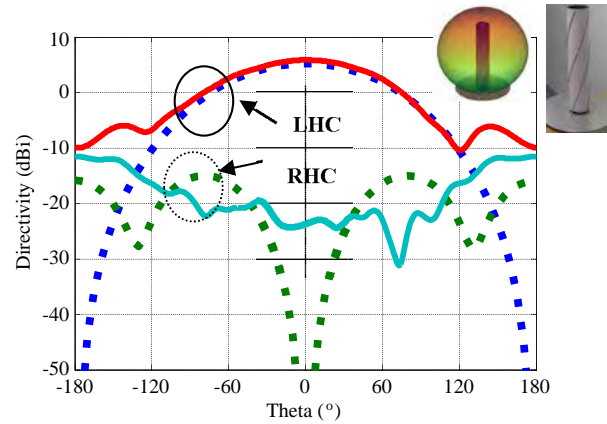
Figure 5. Experimental (continuous line) and simulated using FEKO (dashed line) results for the radiation pattern ($\Phi = 0°$) for the PVC-supported reference QHA1 at 120 MHz. The insets give the 3D simulated radiation pattern (directivity) and the photography of the manufactured QHA1 prototype.

Figure 6 shows the normalized gain (QHA1 is taken as reference results) for CQHA1a, CQHA1b, CQHA1c and CQHA1d. The gain is significantly impacted when the height of the antenna decreases because the helix radius is quite small in this work and consequently, a strong electromagnetic coupling occurs between the constitutive helical antennas. This coupling is also favored by the PVC supporting cylindrical structure.

Figure 6. Measured gain of the CQHA relative to the measured gain of the QHA1 (frequency: 120 MHz).

Figure 7. Gain of best-fitted CQHAs (regarding the goal function defined by Eq. (5)) as a function of the antenna relative height for various wire profiles (simulated results). The dashed curve fits all the data reported in this figure.
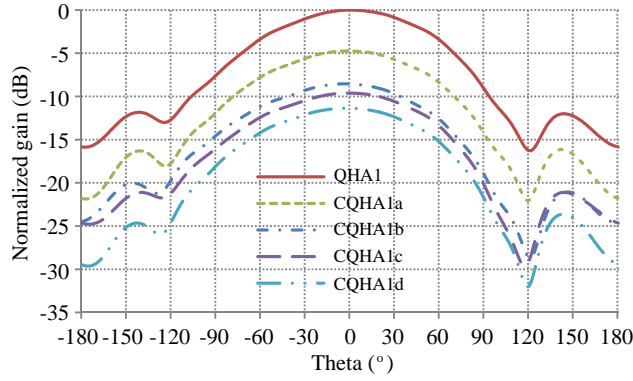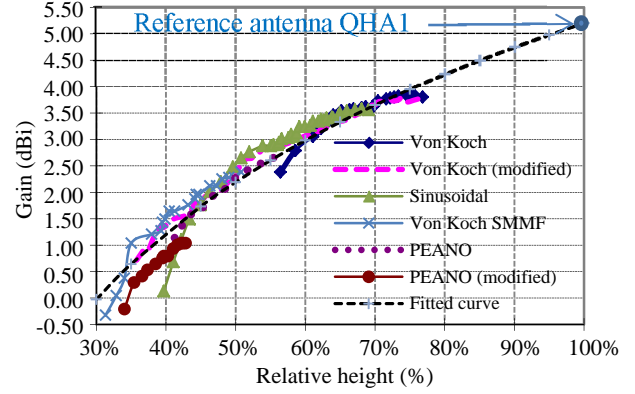
Figure 7 reports the simulated gain of CQHAs as a function of the antenna relative height for various wire profiles. The relative height is denoted R_H and is defined as the ratio between the height of the CQHA and height of the reference QHA. Each point of the curves reported in Fig. 7 corresponds to the best-fitted CQHA obtained by using the optimization methodology described in Section 3.3.

Typically, thousands of candidates were tested in order to derive the best-fitted solution. Moreover, the optimization process based on the goal function described by Eq. (5) may not bring acceptable solutions for a given profile and a given relative height. For example, the Von Koch profile does not provide solution (fitted to the goal function) for $R_H < 55\%$.

The goal function $GF4$ defined in Eq. (5) requires $G_{\max} > 0$ dBi. Thus the best-fitted CQHAs reported in Fig. 7 are such that $G_{\max} > -0.5$ dBi, and consequently, the relative height compared with the reference antenna QHA is higher than 30%. For relative height higher than 60% basically the same gain for all the analyzed profiles was found. Prefractal shapes provide no solution to Eq. (5) for relative height lower than 55% (Von Koch) or 40% (Peano). For obtaining smaller structures, the modified fractal profiles (e.g., modified Von Koch or Peano profiles) may be used. Moreover, sinusoidal profiles can be advantageously used when a relative height ranging from 40% to 90% is required, but the gain is significantly reduced when the relative height is lower than 45%. Modified fractal shape is a better choice in this case as it allows obtaining higher gain. From Fig. 7 it can be observed that the combination of modified fractal profile with a sine function allows maximizing the gain for very compact CQHAs (i.e., for relative height lower than 40%). As shown in Fig. 7, lower limits exist for the relative height. These lower limits depend on the chosen objective goal function (see Eq. (5)). For a given goal function and for a given CGHA profile, these limitations are caused by: (i) the overlapping between close wires (geometrical limitation) and (ii) the increase of the electromagnetic coupling between the constitutive helical wires of the CQHA that increases the amount of the electromagnetic energy stored by the CQHA.

Surprisingly, whatever the chosen profile or shaping function is, all the best-fitted solutions reported in Fig. 7 seem to follow a simple law described by the following closed-form expression:

$$G_{\mathrm{CQHA}}\,(\mathrm{dBi}) = 10 \cdot \log(R_H) + G_{\mathrm{QHA}}\,(\mathrm{dBi}) \qquad (6a)$$

or equivalently:

$$\frac{G_{\mathrm{CQHA}}}{G_{\mathrm{QHA}}} = \frac{h_{\mathrm{CQHA}}}{h_{\mathrm{QHA}}} = R_H \qquad (6b)$$

where G_{QHA} and G_{CQHA} denote respectively the gain of the reference antenna QHA and the gain of the CQHA, and h_{QHA} and h_{CQHA} designate respectively the height of QHA and the height of CQHA. The physical interpretation of Eq. (6) is not obvious. For obtaining the numerical data reported in

Fig. 7, thousands of CQHA based on six different shapes (sinusoidal, Von Koch, Peano, Von Koch modified, Peano modified, and Von Koch SMMF profiles) and with various geometrical descriptors were numerically simulated by using the methodology described in Section 3.3. Hundreds of best fitted CQHAs were selected according to the goal function Eq. (5) and reported in Fig. 7. Eq. (6) can be very useful in practice: for a given antenna height (or R_H), the designer can predict the gain achievable by a CQHA, checking if the resulting compact antenna fulfills the launch system requirement and decide if the proposed CQHA is suitable for the TTC system.

The impact of the miniaturization process on the wire supported CQHA was investigated by the authors in [26] with a focus on the phase center stability. Exact location of the phase center is crucial mainly for high resolution GPS (Global Positioning Systems) application. As expected, the phase center of QHAs/CQHAs is always located on the symmetry axis of CQHAs and positioned below the phase center of the QHA. As a general rule, the phase center approaches the antenna ground plane as the height reduction increases [26]. The position of the phase center is in the range of CQHA height for moderate reduction size factor and can slightly exceed the antenna height for very compact CQHAs.

Printed QHA/CQHA were designed and manufactured. Their characteristics are summarized in Table 3.

Table 3. QHA2/CQHA2 measured characteristics.

	h (mm)	Relative height (%)	f_0 (MHz)	S_{11} (dB)	D_{max} (dBi)	G_{max}^1 (dBi)	G_{max}^2 (dBi)
QHA2	450	-	162	−13	6.4	2.37	6
CQHA2a	265	58.8	161.3	−10	5.4	−1.3	2
CQHA2b	262	58.2	159.4	−14	N/A[3]	N/A	N/A

[1]the insertion loss of the feeding network is included in this gain
[2]the insertion loss of the feeding network is de-embedded
[3]not available before the submission deadline of this paper

The compact structures CQHA2a and CQHA2b are based on a modified Von Koch shape combined with a sine function because this profile leads to higher gain for very compact CQHA (i.e., when the relative height is lower than 50%). As expected, the down-shift of the operating frequency is reduced in this case because a thinner dielectric substrate (0.15 mm instead of 3 mm) with lower dielectric constant (3 instead of 4) was used as a cylindrical supporting structure instead of a PVC tube. The measured operating frequency f_0 is reported in Table 3.

In order to perform one port radiation pattern measurement of the CQHAs, a feeding network based on commercially available couplers and phase shifters was fabricated. The average insertion loss of the feeding network was found to be 3.7 dB with a minimum reflection coefficient at the antenna terminals of −35 dB at 155 MHz. The measured phase progression between two adjacent ports at the output of the feeding network (the input of the QHA2/CQHA2) is 91.6° (port 1 to 2), 90.8° (port 2 to 3) and 89.8° (port 3 to 4), respectively. Fig. 8 shows the simulated co-polarization (LHC) and cross-polarization (RHC) components of the gain for QHA2 and CQHA2 at 162 MHz. As represented in Fig. 8, CQHA2 fulfills the requirements for a TTC application implemented by the goal function (Eq. (5)). The supporting thin dielectric film (paper for CQHA2a and PET for CQHA2b) was not taken into account in the simulation model.

Figure 9 shows the measured directivity (LHC and RHC components) of CQHA2a as a function of angle θ for two cut planes: $\phi = 0°$ and $\phi = 90°$.

The differences observed in these planes are mainly caused by the manufacturing process. They are more important for cross-polarization components (RHC) and negligible for the co-polarization component (LHC) in the targeted beamwidth $−60° \leq \theta \leq 60°$. The CQHA2b should minimize these discrepancies because a symmetrical structure was fabricated using a more reliable fabrication technology. No measurement was performed onCQHA2b before the submission deadline of this paper, but the electromagnetic simulation demonstrates performances similar to ones obtained for CQHA2a.
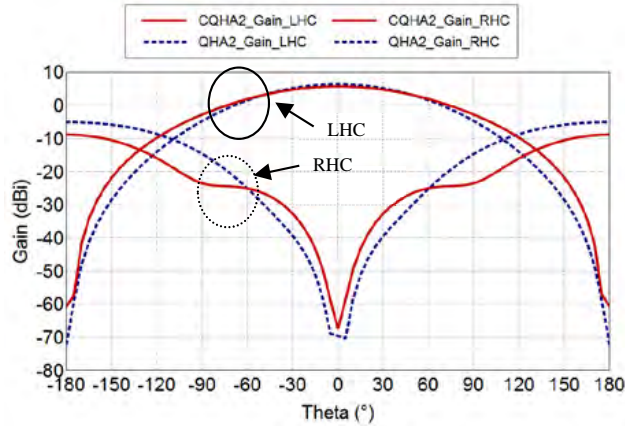
Figure 8. Simulated co-polarization (LHC) and cross-polarization (RHC) components of the gain for the reference antenna QHA2 and the compact antenna CQHA2a.
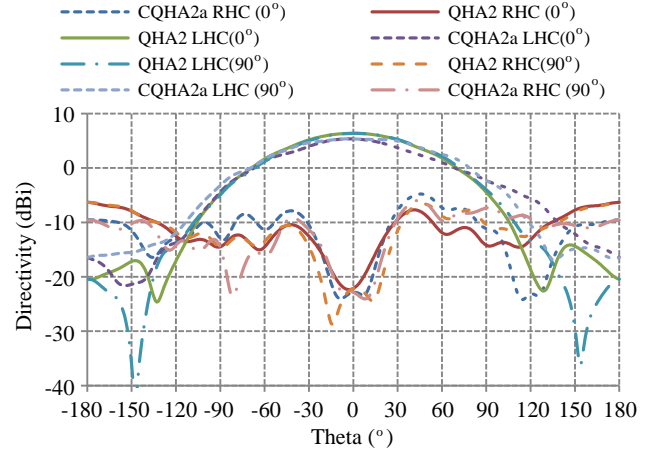

Figure 9. Measured co-polarization (LHC) and cross-polarization (RHC) components of the directivity for the references antenna QHA2 and the compact antenna CQHA2a as function of theta angle (°) for phi = 0° (xOy) and phi = 90°.

5. CONCLUSION

Simulated and experimental results demonstrate that CQHAs with an axial height reduced up to 70% reported to the reference QHA can be obtained by using various shape profiles and an appropriate optimization method. The impact of the miniaturization on CQHA performances in terms of radiation pattern and polarization purity can be controlled and minimized in order to fulfil the technical requirements of a VHF TTC system. It was shown that the choice of the shape profile is not critical when relative height higher than 60% is required. Moreover, standard prefractal profiles such as Peano and Von Koch shapes cannot provide very compact structures. The impact of the shape is critical on the gain for very compact quadrifilar helix antennas (i.e., when relative height lower than 40% is required). In order to estimate the gain achievable by CQHA, a practical closed-form equation, very useful from a system design point of view, was derived from extensive numerical data. It was established that whatever the chosen profile is, the gain of CQHA normalized by the gain of the reference QHA equals the height of the CQHA normalized by the height of the QHA.

REFERENCES

1. Balanis, C. A., *Modern Antenna Handbook*, John Willey & Sons, 455–457, 2008.
2. Kilgus, C. C., "Resonant quadrifilar helix," *IEEE Trans. on Antennas and Propagation*, Vol. 17, No. 3, 349–351, May 1969.
3. Kilgus, C. C., "Multielement, fractional turn helices," *IEEE Trans. on Antennas and Propagation*, Vol. 16, No. 4, 499–500, Jul. 1968.

4. Kilgus, C. C., "Resonant quadrifilar helix design, technical feature," *Microwave Journal*, 49–54, Dec. 1970.

5. Kilgus, C. C., "Shaped-conical radiation pattern performance of the backfire quadrifilar helix," *IEEE Trans. on Antennas and Propagation*, Vol. 23, No. 3, 392–397, May 1975.

6. Takacs, A., N. J. G. Fonseca, and H. Aubert, "Height reduction of the axial-mode open-ended quadrifilar helical antenna," *IEEE Antennas and Wireless Propagation Letters*, Vol. 9, 942–945, 2010.

7. Amin, M. and R. Cahil, "Compact quadrifilar helix antenna," *IET Electronics Letters*, Vol. 41, No. 12, 672–674, Jun. 2005.

8. Amin, M., R. Cahil, and V. F. Fusco, "Mechanically tunable multiband compact quadrifilar helix antenna with dual mode operation," *IEEE Trans. on Antennas and Propagation*, Vol. 56, No. 6, 1528–1532, Jun. 2008.

9. Amin, M. and R. Cahil, "Effect of helix turn angle on the performance of a half wavelength quadrifilar antenna," *IEEE Microwave and Wireless Propagation Letters*, Vol. 16, No. 6, 384–386, Jun. 2006.

10. Auriol, A., "Helix-type antenna and its manufacturing process," European Patent, publication number: 0320404A1, Jun. 14, 1989.

11. Adams, A., R. Greenough, R. Wallenberg, A. Mendelovicz, and C. Lumjiak, "The quadrifilar helix antenna," *IEEE Trans. on Antennas and Propagation*, Vol. 22, No. 2, 173–178, Mar. 1974.

12. Ibambe, M. G., Y. Letestu, and A. Sharaiha, "Compact printed quadrifilar helical antenna," *IET Electronics Letters*, Vol. 43, No. 13, 697–698, Jun. 21, 2007.

13. Chew, D. K. C. and S. R. Saunders, "Meander line technique for size reduction of quadrifilar helix antenna," *IEEE Antennas and Wireless Propagation Letters*, Vol. 1, 109–111, 2002.

14. Bhandari, B., S. Gao, and T. Brown, "Meandered variable pitch angle printed quadrifilar helix antenna," *Proc. of LAPC'2009*, 325–327, Loughborough, UK, Nov. 16–17, 2009.

15. Hanane, L., S. Hebib, H. Aubert, and N. J. G. Fonseca, "Antenna of the helix type having radiating strands with a sinusoidal pattern and associated manufacturing process," Patent International Publication Number WO 2009/034125 A1, Mar. 19, 2009.

16. Back, J., J. Zackrisson, M. Ohgren, and P. Ingvarson, "A new quadrifilar helix antenna family with flexible coverage for space applications," *Proc. of EuCAP 2007*, 1–6, Edinburgh, UK, Nov. 11–16, 2007.

17. Mirkamali, A., L. Akhoondzadeh, K. Keyghobad, and M. Soleimani, "A novel quadrifilar helix antenna for use in LEO satellite communications," *Proc. of International Conf. on Antenna Theory and Techniques*, 509–511, Sevastopol, Ukraine, Sep. 9–12, 2003.

18. Son, W. I., W. G. Lim, M. Q. Lee, S. B. Min, and J. W. Yu, "Printed square quadrifilar helix antenna (QHA) for GPS receiver," *Proc. of EUMC'2008*, 1292–1296, Amsterdam, Netherlands, Oct. 2008.

19. http://smsc.cnes.fr/SVOM/Fr/GP_satellite.htm.

20. Inoue, J., "Helical antenna," International Publication Number WO 01/24315, Apr. 4, 2001.

21. Saunders, S. R. and D. Kwan Chong Chew, "Multifilar helix antennas," US Patent 7,142,170 B2, Nov. 28, 2006.

22. Fonseca, N., S. Hebib, H. Aubert, and L. Hanane, "Helix antenna," Patent International Publication Number WO 2008/142099 A1, Nov. 27, 2008.

23. Ermutlu, M. and K. K.-P. Kiesi, "Multi-filar helix antennae," US Patent 6,232,929 B1, May 15, 2001.

24. Aubert, H., H. Diez, D. Belot, and A. Takacs, "Compact helical antenna with a sinusoidal profile modulating a fractal pattern," Patent International Publication Number WO 2013139935 A1, 2013.

25. Fonseca, N. and H. Aubert, "Compact helical antennas — A review," *Recent Patents Electr. Eng. J.*, Vol. 9, 942–945, 2010.

26. Takacs, A., H. Aubert, H. Diez, and D. Belot, "Miniaturization of quadrifilar helical antenna: Impact on efficiency and phase center position," *IET Microwaves, Antennas & Propagation*, Vol. 7,

No. 3, 202–207, Feb. 19, 2013.

27. Takacs, A., T. Idda, H. Aubert, and H. Diez, "Compact VHF quadrifilar helix antenna," *Proc. of EUMC'2012*, Amsterdam, Netherlands, Oct. 28–Nov. 2, 2012.

28. Fonseca, N. J. G., A. Takacs, and H. Aubert, "Design and experimental validation of a compact quadrifilar helix antenna in VHF band," *Proc. of APMC 2009*, Singapore, Dec. 7–10, 2009.

29. Takacs, A., N. J. G. Fonseca, H. Aubert, and X. Dollat, "Miniaturization of quadrifilar helix antenna for VHF band applications," *Proc. of LAPC'2009*, 597–600, Loughborough, UK, Nov. 16–17, 2009.

30. *Modern Plastics Encyclopaedia*, McGraw Hill, New York, 1981–1982.

31. www.inkjetflex.com.

32. http://www.ets-lindgren.com/3121D.

Microwave Power Harvesting for Satellite Health Monitoring

Alexandru Takacs, *Member, IEEE*, Herve Aubert, *Senior Member, IEEE*, Stephane Fredon, Laurent Despoisse, and Henri Blondeaux

Abstract—This paper addresses the microwave energy harvesting on board of geostationary satellites for health satellite monitoring. To prove the feasibility of such a concept, we investigated the electromagnetic environment existing on antenna panels. Based on established cartographic maps, three designs of rectennas are proposed. Measured dc powers ranging from 0.256 to 1.28 mW can be harvested for electric field levels ranging from 91 to 121 V/m and by using very simple and compact designs. The harvesting structures consist of only one Schottky diode per rectenna and present a total surface of 2.4 cm^2. They are suitable for powering the new generation of ultra-low power transceivers, thus enabling autonomous wireless power networks for satellite health monitoring.

Index Terms—Autonomous wireless sensors, energy harvesting, microwave circuits, rectennas, satellite applications.

I. INTRODUCTION

HEALTH monitoring is a key issue for any satellite application and especially for the implementation of reliable and long-life satellite-based broadcasting links. In order to provide reliable and high bit-rate broadcasting links, high-gain microwave antennas operating in C-, X-, Ku-, K-, or Ka-band are used. These antennas are located on panels positioned on the external surface of the satellite. Surveying the health of these panels involves the use of sensors (e.g., for thermal or for mechanical/structural monitoring) deployed in small networks to cover the targeted surface. A very promising solution is to implement small autonomous wireless sensor networks saving the cost of deploying long wires in harsh environments. In some areas located on antenna panels of broadcasting satellites, the electric field generated by the spill-over loss of microwave antennas can reach the following maximum levels (effective values): 40 V/m in C-band, 49.5 V/m in X-band, 106 V/m in

Ku-band, and 127 V/m in K-band. These high-frequency electromagnetic field levels are unusual for terrestrial applications, but they are available on satellites if data links are functional and can be harvested in order to power autonomous wireless sensors used for monitoring the structural health of the satellite. Moreover, the electromagnetic power radiated by microwave antennas is almost constant and consequently the dc power regulatory circuits should be minimal for harvesting systems.

The electromagnetic environment of the antenna panels is analyzed in Section II. Rectifier antenna (rectenna) topologies [1] and design methodology developed for proving the concept of microwave power harvesting for satellite health monitoring are discussed in Section III. The main goal of this paper is to demonstrate that microwave energy harvesting based on specific rectenna designs is an ideal solution for powering autonomous sensors for satellite health monitoring.

II. ELECTROMAGNETIC ENVIRONMENT

Broadcasting satellite antennas operating in C-, X-, Ku-, and K-band radiate electromagnetic power between 50–100 W with linearly or circularly polarized electromagnetic field. Recently, Thales Alenia Space performed an analysis of the electromagnetic energy illuminating antenna panels. Intensive electromagnetic simulations using GRASP software from TICRA [2] were performed by taking into account the case of a Spacebus class-C satellite. Figs. 1–4 show typical electromagnetic field levels (E-field in V/m, peak values) on panels located on the lateral side or on the Earth side of a broadcasting geostationary satellite. These levels were obtained in C, Ku, and K frequency bands. We observed that large areas of antenna panels are covered with field levels higher than 4 V/m. This electromagnetic field available at the surface of antenna panels can be advantageously harvested by using rectennas [3] for supplying power to autonomous sensors dedicated to satellite health monitoring. As shown in Fig. 3, a maximum E-field level of 180 V/m (peak value) can be reached at 17.7 GHz.

As shown previously (Figs. 1–4) satellite panels can be illuminated with electromagnetic energy at various frequencies. Moreover, the incident waves illuminating satellite panels arrives various directions and have various polarizations (dependently on satellite antennas types and their mounting position). Thus, the antenna of the rectenna has to be engineered to meet these criteria (operating frequency, polarization, and radiation pattern shape/tilt angle) in order to maximize the amount of the RF power injected at the input of the (rectenna) rectifier.
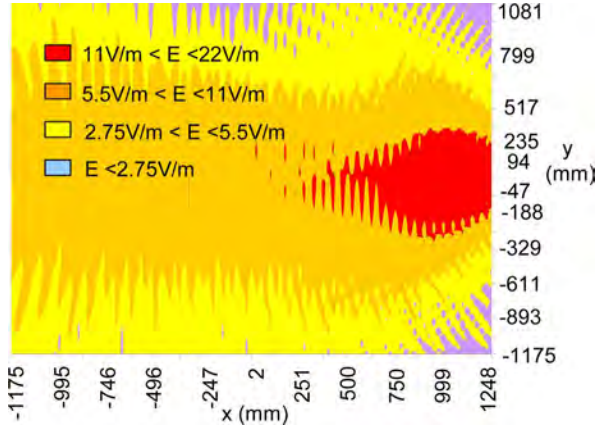
Fig. 1. E-field distribution (peak value) on a lateral panel at 3.5 GHz (C-band). Radiated power: 90 W. The x- and y-coordinates are in millimeters.
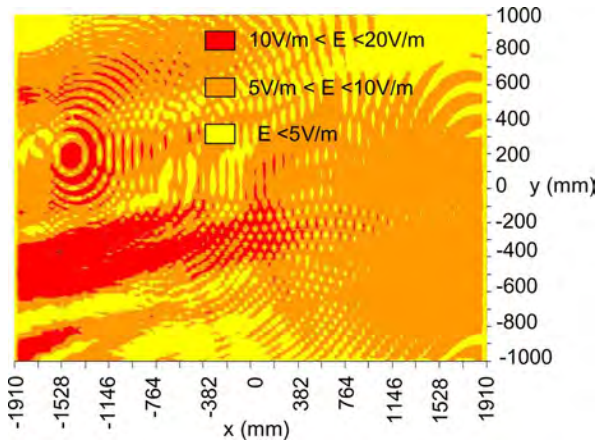

Fig. 2. E-field distribution (peak value) on a lateral panel at 10.7 GHz (Ku-band). Radiated power: 86.5 W. The x- and y-coordinates are in millimeters.
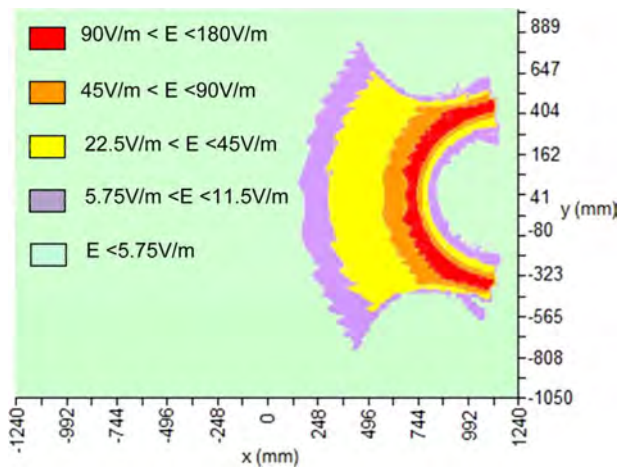

Fig. 3. E-field distribution (peak values) on Earth side of satellite at 17.7 GHz. Radiated power: 70 W. The x- and y-coordinates are in millimeters.

III. MICROWAVE RECTENNAS: DESIGN AND MEASUREMENT RESULTS

Rectennas are intensively used for wireless power transfer or energy-harvesting applications. Many designs and topologies
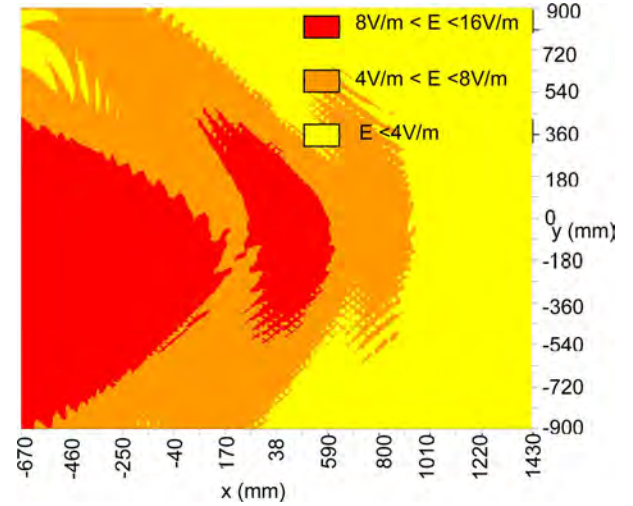
Fig. 4. E-field distribution (peak values) on a lateral side of satellite at 21.4 GHz. Radiated power: 85 W. The x- and y-coordinates are in millimeters.

have been proposed for various applications, such as GSM [4], GPS [5], C-band (industrial–scientific–medical (ISM) 2.45 GHz) [6]–[10], 5.8 GHz [10], and X-band [11], [12] applications. Dual-band [9] or broadband [12] designs have been studied while applications beyond 10 GHz have been addressed in the past mainly for wireless power transfer [13] application [3], [14], [15] but not for power harvesting because of the lack of powerful environmental electromagnetic sources for terrestrial applications. Several research studies have been reported on the rectenna design for energy harvesting at frequencies higher than 10 GHz [16]–[19]. A reconfigurable rectenna device that is capable of adapting itself to the incident power level is described in [20]. In order to evaluate the feasibility of such microwave energy harvesting, several rectennas were designed and the measured dc power was compared with typical power requirements for wireless transceivers. Note that ultra-low power receivers are now available [21] and their power consumption is around 2 mW only (voltage supply of 1.2 V–1.8 V with current below 2 mA).

A. Rectenna Topology

In order to keep the proposed designs compatible with the specific technical requirements for space applications, several design guidelines were adopted, which were: 1) the rectenna topology has to be as simple as possible; 2) all the components in the rectenna (dielectric substrate, diode, capacitors, etc.) must be qualified for space applications, ready to be qualified or at least with performances compatible with space requirements; 3) the operating frequencies must be chosen by taking into account the electromagnetic environment existing on board of satellite antenna panels (typical E-field distributions were presented in Section II); and 4) a nonoptimal dc loading for rectenna could be chosen; in this a worst case scenario, the input impedance/resistance of the sensors and/or the transceiver to be powered may be far from the optimal dc load that maximizes the dc power generated by the rectenna. Keeping in mind these design requirements, the rectenna was designed to power a temperature sensor (load) with a typical resistance

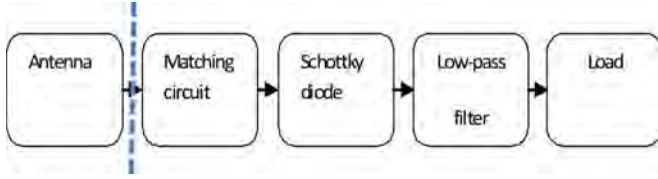Fig. 5. Rectenna topology: the vertical dotted line indicates the position (reference plane) of the 50-Ω test point (end-launch K connector).

Fig. 6. Photographs of the developed rectenna designs: R1 (R1a and R1b), R2 (R2a and R2b), and R3 (R3a and R3b).

in the range of 9–10 kΩ. The rectenna was fabricated on a Rogers 6002 substrate (relative permittivity: 2.94, loss tangent: 0.0012, thickness: 508 μm, metallization thickness: 35 μm) [22]. Two GaAs flip-chip Schottky diodes were selected: an M/A Com MA4E-1317 diode [23] and Aeroflex/Metelics MZBD-9161 diode [24]. These diodes were chosen based on their RF power handling, thermal capabilities, and high operating frequency. An important issue in rectenna design is the antenna that should: 1) match the polarization of the incident electromagnetic field; 2) have a gain as high as possible in order to increase rectenna conversion efficiency; 3) present a high large half-power beamwidth to efficiently operate for various directions of the incident field; and 4) be easily matched to the rectifier at the operating frequency. Reproducing in the laboratory the electromagnetic environment existing on satellite panels is not an easy task. As presented in Section III-C, by using the setup S2, an incident wave illuminating the rectenna under test with a linearly polarized E-field, with various power densities (E-field levels) and at various frequencies can be easily generated in the laboratory. Consequently we selected (for our rectennas designs) linearly polarized antennas with at least 50° half-power beamwidth and a maximum gain of at least 4 dBi.

The proposed rectenna designs are based on the topology shown in Fig. 5. The antenna collects the surrounding electromagnetic power density and transfers it at the input of the rectifier (Schottky diode) through a matching circuit. The matching circuit allows the conjugate impedance matching and maximizes the RF power level flowing from the antenna to the rectifier. Moreover, the matching circuit should stop the reflected power at the operating frequency and harmonics to be radiated by the antenna. The rectifier converts the RF power to a dc power. The dc power is injected into the load through a low-pass filter that blocks any undesirable RF signal at operating frequency or harmonics. In order to facilitate the testing and debugging of such a rectenna, a 50-Ω test point (end-launch K connector) was added between the antenna and the matching circuit. Although it may introduce undesirable losses and impedance mismatch, this 50-Ω test point was very useful in the early stages of the design.

Based on the topology sketched in Fig. 5, three rectennas were designed, fabricated, and measured. These rectennas, called R1 (R1a and R1b), R2 (R2a and R2b), and R3 (R3a and R3b), are shown in Fig. 6. The rectennas R1a (using the MA4E-1317 diode) and R1b (using the MZBD-9161 diode) were the first developed demonstrator. Only the rectifier and its 50-Ω input port are shown in Fig. 6. They used only a single-stub matching circuit and a lumped RC low-pass filter.
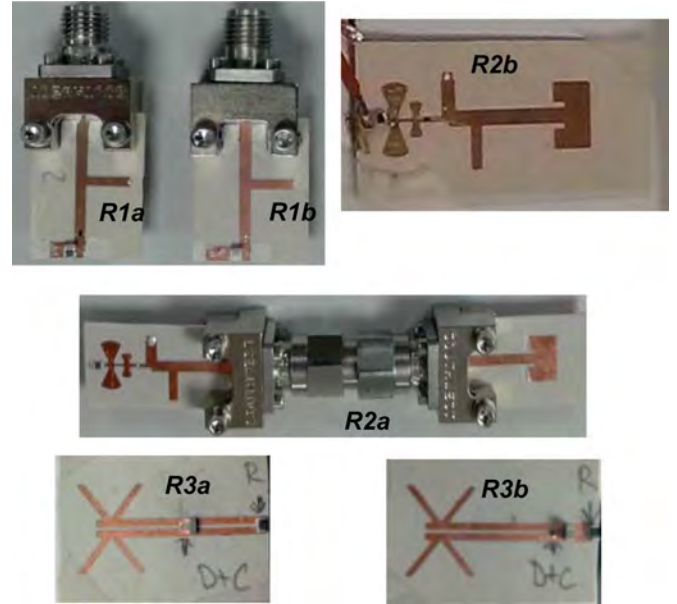
The 10 kΩ load impedance is integrated in the filter structure. The results obtained with these simple topologies were recently reported by the authors [16]. The main drawback of the R1-rectenna is its low efficiency at 17.7 GHz, and consequently, a high-gain (horn) antenna is needed for harvesting a dc power higher than 2 mW. Two new rectenna designs, called R2 and R3, with improved harvesting performances were developed and are now presented.

The rectenna R2 uses the MA4E-1317 diode, a double-stub matching circuit and a distributed low-pass filter containing two radial stubs. The radial stubs were designed for rejecting the operating frequency (17.7 GHz) and the second-order harmonic (35.4 GHz). The rectenna R2a was composed of a rectifier and a patch antenna having a gain around 4 dBi. The rectifier and the antenna are connected using a K-adapter. The 50-Ω test point allows characterizing the rectifier and the antenna performances separately. This test point was eliminated in the rectenna R2b. The rectenna R3 is more compact. A similar topology, based on a dual dipole like (DDL) antenna and operating at 2.45 GHz, was proposed in [9]. The antenna was excited by a coplanar stripline. No matching circuit was necessary, and the maximum power transfer (between antenna and diode/rectifier input) and the suppression of the undesirable reflected power at the second harmonic were achieved by properly controlling the input impedance of the antenna. A capacitance of 1.5 pF was used for shunting the RF signal at the operating frequency and its harmonics. In order to maximize the performances of this design, it is crucial to properly control the diode mounting position.

B. Rectennas Design and Simulation Methodology

One of the major challenges in the effective design of rectennas in the microwave frequency range (Ku-band and higher) is the accurate nonlinear modeling of the diode. The most relevant parameters of the MA4E-1317 diode were derived

Fig. 7. Simulation model (AWR) of the rectenna R2a (without patch antenna) and its dimensions.

Fig. 8. Simulation model (Feko) of the R3-rectenna design (see the text for the dimensions).

Fig. 9. Setup S1.

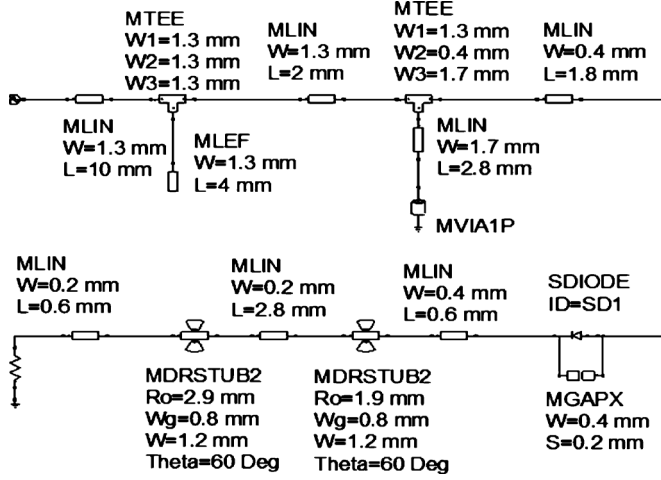from an available datasheet [23] (total capacitance: 0.045 pF, series resistance: $Rs = 4 \Omega$) and from the extrapolation of the I–V measured characteristic (derived ideality factor: $n \approx 1.2$ and saturation current: $Is \approx 0.1$ pA). For the MZBD-9161 diode, the SPICE equivalent model proposed in [24] was used, but with a much lower breakdown voltage (3.5 V instead of the 10 V given in the datasheet). A lower breakdown voltage was needed to accurately model the observed nonlinear power behavior of the diode. The simulation model for the MZBD-9161 diode given in [24] uses two antiparallel diodes (with different parameters) in order to simulate the single Schottky diode used in the rectenna. Fig. 7 shows the complete simulation model in AWR software [25] for the rectenna R2 (without the patch antenna) using closed-form models for the distributed components (transmission lines, stubs, and via-hole).

The harmonic-balance simulation engine was used for performing nonlinear simulations. A generic nonphysical diode model available in AWR software [25] was customized with the MA4E-1317 and MZBD-9161 diode parameters. The rectangular patch antenna was designed, simulated, and optimized using the HFSS antenna design kit [26].

The design procedure for the design of the rectenna R3 was quite different. First the DDL antenna was designed and simulated using FEKO [27] for operation at the desired frequency (17.7 GHz). The antenna radiation pattern, gain, and radiation efficiency were calculated and the distribution of the electric currents on the metallic strips were analyzed. The design requires a low load resistance for working efficiently. A load of 510 Ω was used. For simulation purposes, the diode was replaced by a voltage port while the capacitance (1.5 pF) and the load (510 Ω) were modeled as port loads. Fig. 8 shows a top view of the rectenna R3. The dimensions of the R3 design are $l_x = 20$ mm, $l_y = 14$ mm, $l_d = 5.5$ mm, $l_r = 15$ mm, $l_s = 1.4$ mm, $l_{ax} = 6.3$ mm, and $l_{ay} = 8.3$ mm. The coplanar strip line is characterized by a strip width of $w = 0.8$ mm and a gap size of $g = 0.4$ mm. A metallic plate (dotted line contour in the Fig. 8) was printed below the radiating element ($l_{gx} = 10$ mm and $l_y = 14$ mm). R3 design is very compact with a total surface of 2.4 cm^2.
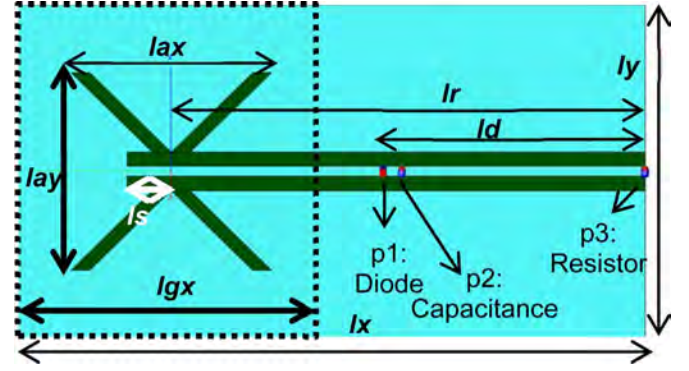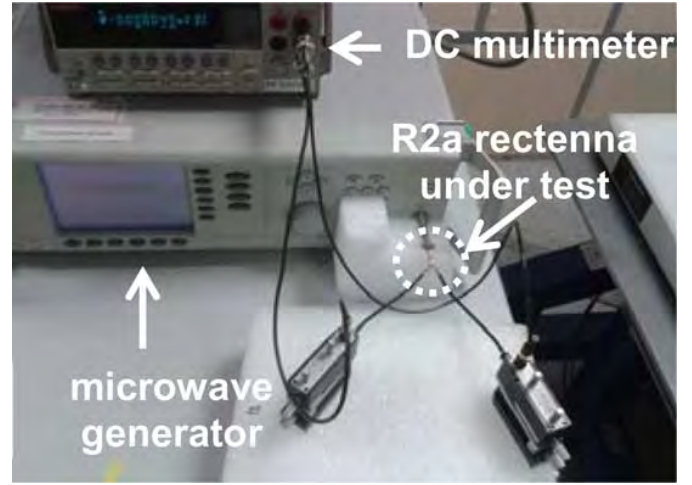
C. Experimental Setup

Two experimental setup configurations, called S1 and S2, were used. In the S1 setup shown in Fig. 9, a continuous millimeter-wave signal generated from an Anritsu MG3694B generator was directly injected at the 50-Ω test point of the manufactured prototypes and the resulting dc voltage was measured at the input port of the load impedance with a Keythley 2000 multimeter.

The setup (S1) is appropriate for testing the rectifier part (e.g., R1a, R1b, R2a) of the rectennas when equipped with a 50-Ω test point (coaxial K connector). In the S2 setup shown in Fig. 10, a microwave signal generated from an Anritsu MG3694B generator was injected at the input of a horn antenna (VT220HA20-SK from Vector Telecom [28]), which illuminated the rectenna under test with a linear polarized E-field. This setup is appropriate for testing the rectennas (R2b, R3) or rectifiers equipped with a 50-Ω test point/coaxial K connector (e.g., R1a, R1b, R2a) connected with an external antenna.

An automatic acquisition routine was implemented in Labview software from National Instruments [29] in order to speed up the acquisition process. The harvested dc voltage was measured with the microwave source OFF (dc noise: V_off V) and with microwave source ON (dc voltage: V_on). The dc voltage of interest (Vout) was then derived from the difference Vout =

Fig. 10.   Setup S2.

Fig. 12.   Measured dc output power (setup S1) for R1a (dotted red line (in online vesion), square marker) and R2a (dotted violet line (in online version), "x" marker design). The simulation results obtained by using AWR simulation model for R2a are represented with a continuous (blue in online version) line (diamond marker).

Fig. 11.   Measured dc output voltages (setup S1) for R1a (dotted red line (in online version), square marker) and R2a (dotted violet line (in online version), "x" marker design). The simulation results obtained by using AWR simulation model for R2a are represented with a continuous (blue in online version) line (diamond marker).
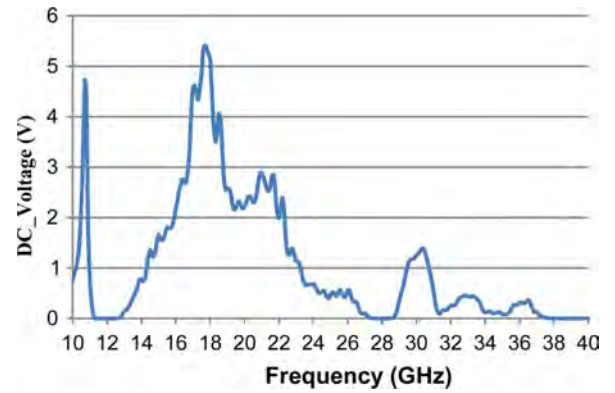
Fig. 13.   Measured dc output voltage (setup S1) for R2a design as a function of the frequency for an RF power of 13 dBm at the input of 50-Ω test point.

$V\_\text{on} - V\_\text{off}$. Digital filters were used for minimizing the noise level. The measurement was performed twice and the average value of V out was registered as the final result.

D. Simulation and Experimental Results

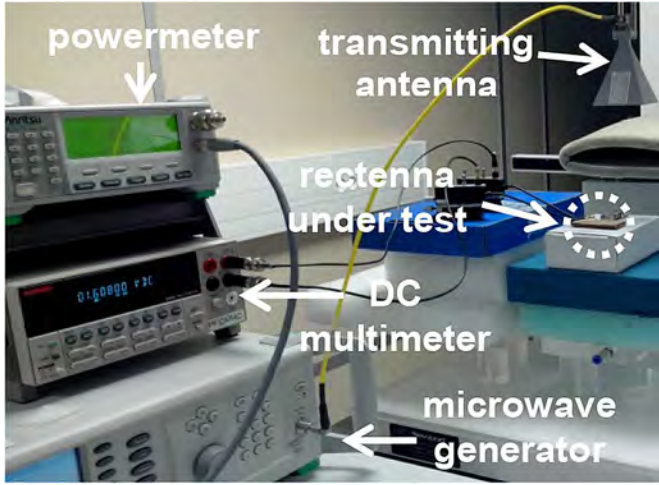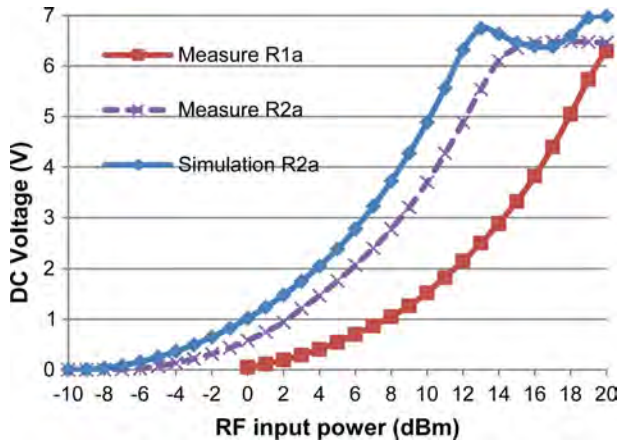The layouts of rectennas were accommodated with the tolerances required by a fabrication in a laboratory equipped for general-purpose printed circuit boards (PCBs). A solid silver-filled epoxy system EPO-TEK H20E was used for soldering the diodes by a low-temperature process (110 °C).

Figs. 11 and 12 show a comparison between the measured performances (by using the setup S1) of the rectifiers R1a and R2a in terms of the harvested dc voltage (Fig. 11) and dc power (Fig. 12) at the input of the load impedance (10 kΩ).

A dc voltage up to 6.4 V and a dc power up to 4 mW can be harvested with the R2a design when an RF power around 15 dBm is injected at the input of the rectifier (Schottky diode). A maximum worst case efficiency of 15.4% was achieved for an RF input power of 13 dBm (experimental results). This worst case efficiency takes into account the losses and the impedance

mismatch introduced by the 50-Ω K-connector and by the male-to-male K-adapter. This low efficiency is mainly due to the nonoptimal load impedance (10 kΩ) chosen as reference.

Precursory of the R1a/R1b structures, reported in [30] and [31], were tested at the French Space Agency (CNES) Laboratory by applying a standard thermal cycling procedure for space applications (30 thermal cycles performed between -65 °C and $+125$ °C). Despite the *soldering-free* homemade fixation system, the prototypes still remained operational after the thermal cycling without a major impact on the RF performances.

The output dc voltage as a function of the operating frequency obtained for an RF input power of 13 dBm is displayed in Fig. 13. The maximum voltage of 5.4 V was obtained at 17.7 GHz, which is the central operating frequency of the single-stub matching circuit.

Fig. 14 shows the measured dc voltage harvested by the R2b-rectenna design when illuminated with the electric field of a horn antenna (gain: 18.6 dBi at 17.7 GHz). A microwave power ranging from 10 to 24 dBm was injected at the input of the horn antenna. The distance between the radiating aperture of the horn antenna and the rectenna R2b is 15 cm. The input port (coaxial K connector) of the transmitting horn antenna is located
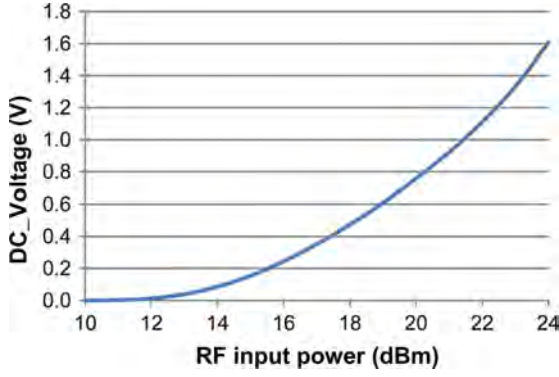
Fig. 14. Measured dc output voltage (setup S2) for the R2b-rectenna design as a function of the RF power injected at the input port of a transmitting (horn) antenna (operating frequency: 17.7 GHz).

at 25 cm above the rectenna R2b under test. A maximum dc voltage of 1.6 V was measured and a low harvested dc power of 0.256 mW was obtained. In order to measure the RF power collected by the patch antenna, a calibrated Anritsu ML2437A powermeter was used. The measured RF power received with the patch antenna alone (gain: 5 dBi at 17.7 GHz) was found to be 4.5 dBm: when this RF power was directly injected at the input port of the rectifier (using the 50-Ω test point of R2a in the setup S1), the harvested dc voltage was found to be 1.63 V. Consequently, the measurement results obtained using setup S2 (Fig. 14) are coherent with the results depicted in Fig. 11.

To obtain a harvested dc power higher than 2 mW, an antenna with a gain of at least 12 dBi should be used instead of the patch antenna. Alternatively, a dc combining circuit could be proposed to combine the dc power harvested from many rectennas [1].

The power P received at a given frequency by an antenna of gain G at a location where an electric field level E exists can be approximated by [32]

$$P = \frac{E^2}{120 \cdot \pi} \cdot \frac{G \cdot \lambda^2}{4 \cdot \pi} \qquad (1)$$

where λ denotes the free-space wavelength. Consequently, the RF power at the output of the receiving antenna (input of the 50-Ω test point) can be estimated for a given incident E-field level (Table I). Equation (1) can be also written as

$$E = \frac{2 \cdot \pi}{\lambda} \cdot \sqrt{\frac{120 \cdot P}{G}}. \qquad (2)$$

When specifying the required RF power at the output of a calibrated antenna (with a known gain), the needed E-field level can then be derived from (2). Three typical antenna gains were considered: 18.6 dBi (e.g., horn antenna), 11 dBi (for comparison purposes), and 5 dBi (e.g., patch antenna).

To design rectenna R3, the variation of the input impedance of the DDL antenna as a function of the diode mounting position was analyzed. The simulated input impedance Z_{in} of the antenna viewed at the distance $l_r - l_d$ along the coplanar stripline is depicted in Fig. 15 as a function of l_d (see Fig. 7). The imaginary part (reactance) was found to be positive. As the estimated input impedance of the MZBD-9161 diode is $8 - j * 80\ \Omega$, the

TABLE I
ESTIMATED RF POWER AT THE INPUT OF THE 50-Ω TEST POINT, MEASURED DC VOLTAGE EXTRACTED FROM FIG. 11 AND THE COMPUTED DC POWER FOR R2a DESIGN ($f = 17.7$ GHz)

E (V/m)	G (dBi)	RF power (dBm)	R2a design (MA4E-1317)	
			DC voltage (V)	DC power (mW)
107	18.6	17	6.48	4.2
67	18.6	13	5.54	3.07
48	18.6	10	3.67	1.37
34	18.6	8	2.78	0.77
27	18.6	5	1.75	0.31
15	18.6	0	0.58	0.033
127	11	10.9	4.27	1.82
91	11	8	2.78	0.77
72	11	6	2.07	0.43
51	11	3	1.21	0.015
36	11	0	0.58	0.033
127	5	4.9	1.75	0.31
121	5	4.5	1.6	0.28
114.5	5	4	1.47	0.21
102	5	3	1.21	0.015
91	5	2	0.94	0.088
72	5	0	0.58	0.033
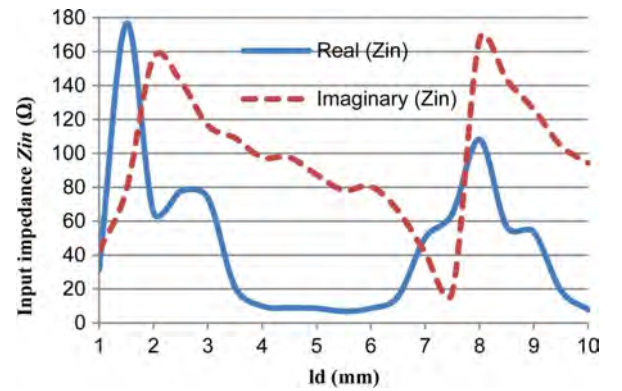
Fig. 15. Simulated input impedance Z_{in} of the antenna (R3 design) viewed at the distance $l_r - l_d$ along the coplanar stripline as a function of l_d.

diode should be located approximately at $l_d = 5.5$ mm to ensure the conjugate impedance-matching condition. Moreover, since the (simulated) impedance Z_{in} at $l_d = 5.5$ mm is $24.5 + j*130\ \Omega$ at 35.4 GHz (i.e., at the first harmonics) and $204 + j * 203\ \Omega$ at 53.1 GHz (i.e., at the second harmonics), the reflected power radiated back by the antenna of the rectenna (R3 design) is expected to be small at the first two higher order harmonics.

The simulated radiation pattern displayed in Fig. 16 shows that the maximum gain of the DDL antenna is approximately 6 dBi.

The measured dc voltage (setup S2, power injected at the input of a horn antenna: 23 dBm, distance between the horn aperture and the R3a rectenna: $d = 15$ cm) as a function of the frequency is depicted in Fig. 17.

A maximum dc voltage of 0.81 V (dc power of 1.28 mW) was recorded at a frequency of 18.8 GHz while a dc voltage of only 0.36 V (dc power of 0.25 mW) is measured at the targeted operating frequency $f = 17.7$ GHz. This can be explained by: 1) the
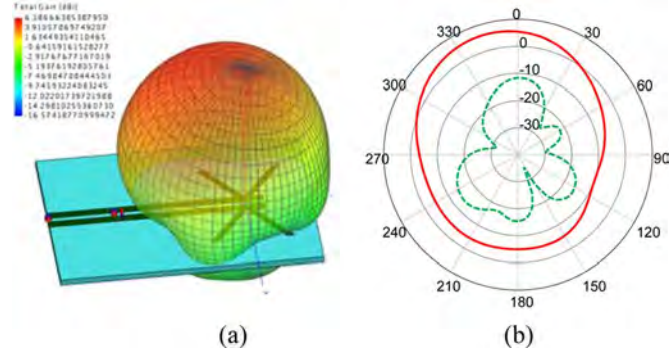
Fig. 16. Simulated radiation pattern (gain) of rectenna R3a. (a) 3-D radiation pattern and (b) E-plane polar cut: main (E_{phi}) and cross (E_{theta}) components of the total gain (values in dB, angles in degrees) are represented with continuous (red in online version) and dotted (green in online version) lines, respectively.
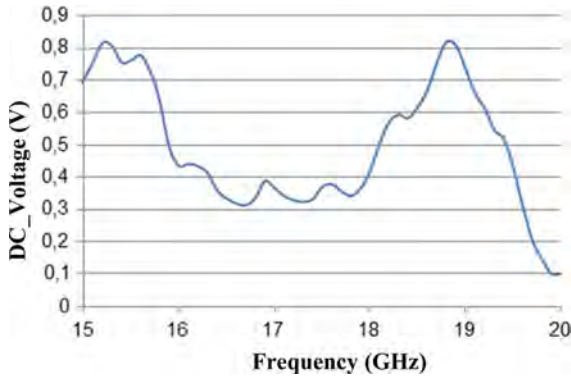
Fig. 17. Measured dc voltage (S2 setup) at the input of the load (510 Ω) as a function of the frequency (R3 design).

inaccuracy of the adopted design methodology (in the electromagnetic model, the antenna is loaded by a voltage electromagnetic port instead of the actual nonlinear loading of the diode); 2) manufacturing tolerances (all the rectennas were fabricated in an university laboratory not equipped for high-frequency PCB manufacturing); and 3) error in the positioning of the diode during its mounting on the PCB. However, the rectenna R3a is very compact (2.8 cm^2) and performs very well in a very wide frequency range (from 15 to 20 GHz). The measured RF power (using a calibrated Anritsu ML2437A powermeter) at the output of the manufactured patch antenna is 2 dBm and is consistent with the E-field level of 91 V/m at 17.7 GHz estimated on the rectenna surface. In order to calculate the efficiency η (in %) of this rectenna, the following worst case definition is used [7], [33]:

$$\eta = \frac{P_{\mathrm{DC}}}{S \cdot A_G} \cdot 100 \qquad (3)$$

where P_{DC} is the measured harvested dc power, S is the incident power density, and A_G denotes the area of the radiating surface. The power density (expressed in μW/cm^2) can be computed as function of the E-field effective value E on the antenna surface as follows:

$$S = \frac{E^2}{120 \cdot \pi} \cdot 100. \qquad (4)$$

TABLE II
COMPARISON OF THE RECTENNAS PERFORMANCES FOR
REPORTED DESIGN (BEYOND 10 GHz)

eff (%)	f (GHz)	Diode	Size (mm^2)	Note
39	35	DMK6606 (Alpha)	>24	[14]: a waveguide array simulation technique [34] was used to measure the overall rectenna efficiency; the reported efficiency defined as the ratio of DC power to the input power into diode was measured for 60 mW of input power into the diode and for an optimum load of 400Ω
35	35	M/A Com MA4E-1317	>110	[15]: the reported efficiency (received RF power/output DC power) was measured using a free space setup for an incident power density of 30 mW/cm^2 and for a load resistance of 50Ω
54.6	24	M/A Com MADS-001317-1320AG	NR*	[16]: the efficiency was measured by illuminating the rectenna with a signal delivered by a waveguide expander positioned in the close vicinity of the rectenna under test. The reported value was obtained for 130 mW of RF input power (supposed to be at the input of the rectifier) and an optimal load of 400 Ω
82	24	M/A Com MA4E-1317	NR*	[17]: the reported efficiency (for 5 mW of RF power at the input of the rectifier) concerns only the microwave rectifier loaded by an optimal resistive load (value NR*)
17	25.7	M/A Com MA4E-2502L	328.5	[19]: only the efficiency of the rectifier part is reported; value obtained for a RF power of 8 dBm at the input of the diode and an optimal load of 1500 Ω
42	18.8	Metelics MZBD-9161	280	This paper: the rectenna efficiency (worst case definition: eq. 3) was measured by using the setup S2, for an incident E-field of 91 V/m (incident power density around of 2.2 mW/cm^2) and for a load of 510 Ω

* NR : Not Reported

In the case of the R3 design, an efficiency of 42% is derived for $A_G = 1.4$ cm^2 and $E = 91$ V/m (we consider here that the geometrical surface of antenna is the surface of the metallic plate printed below the DDL radiating element, i.e., 10 mm × 14 mm). Taking into account the geometrical surface of the patch antenna, which is approximately 1 cm^2 for the rectenna R2b, we obtain a worst case efficiency of 11.4% ($A_G = 1$ cm^2 and $E = 91$ V/m) according to (3). This low efficiency can be explained by: 1) the nonoptimal loading of the MA4E-1317 diode by a 10-kΩ load and 2) the MA4E-1317 diode (forward voltage in the range of 0.7 V) serially connected with the patch antenna requires a high RF input power in order to be properly self-biased and to operate efficiently. This high RF input power cannot be delivered by the patch antenna under the test condition (setup S2, incident E-field: $E = 91$ V/m).

Several rectennas operating at frequencies beyond 10 GHz were reported in the literature [14]–[19]. Table II summarizes the performances (efficiency: **eff** in % as a function of the frequency: **f** in GHz, and size in **mm^2**) of these rectennas compared with our work. We note that only [14] and [15] present measured

values (with a setup and experimental conditions well detailed) for the overall efficiency of the rectennas.

We note that for lower frequencies (e.g., 2.45 GHz or below), higher efficiencies (up to 80%) can be obtained.

IV. CONCLUSION

We have presented the cartography of the electromagnetic environment available on antenna panels of broadcasting geostationary satellites. Large areas of those panels are illuminated with an electromagnetic field ranging from 4 to 127 V/m. This electromagnetic energy can be harvested to supply power to wireless sensor networks for satellite health monitoring. In order to prove the feasibility of the concept, three rectennas, called R1, R2 and R3, were proposed. The rectennas were developed in a worst case scenario, namely, when the rectifier/Schottky diode is not optimally loaded by the dc load impedance. Moreover, constraints concerning the space applications were taken into account in the rectennas design. Measured dc powers ranging from 0.256 mW (R2 design for an incident E-field level around 121 V/m) to 1.28 mW (R3 design for an incident E-field around 91 V/m) were harvested. If a higher antenna gain is used in the R2 design, a dc power higher than 2 mW, (i.e., the typical power consumption of the new generation of ultra-low power transceivers) may be harvested. The very compact rectenna (design R3 with a total surface of 2.8 cm^2) can harvest a dc power around 2 mW if more electromagnetic energy is available (e.g., if the E-field level reaches 127 V/m). Moreover, the well-known stability of the microwave links will reduce the complexity of any dc power management, storage, or regulatory circuits.

REFERENCES

[1] Z. Popović, "Cut the cord low-power far-field wireless powering," *IEEE Microw. Mag.*, vol. 14, pp. 55–62, Mar./Apr. 2013.

[2] TICRA. Copenhagen, Denmark. [Online]. Available: http://www.ticra.com/

[3] W. C. Brown, "The history of power transmission by radio waves," *IEEE Trans. Microw. Theory Techn.*, vol. MTT-32, no. 9, pp. 1230–1242, Sep. 1984.

[4] S. Ladan, N. Ghassemi, A. Ghiotto, and K. Wu, "Highly efficient compact rectenna for wireless energy harvesting application," *IEEE Microw. Mag.*, vol. 14, no. 1, pp. 117–122, 2013.

[5] N. Zhu, R. W. Ziolkowski, and H. Xin, "Electrically small GPS L1 rectennas," *IEEE Antennas Wireless Propag. Lett.*, vol. 10, pp. 935–938, 2011.

[6] Z. Harouni, L. Cirio, L. Osman, A. Gharsallah, and O. Picon, "A dual circularly polarized 2.45-GHz rectenna for wireless power transmission," *IEEE Antennas Wireless Propag. Lett.*, vol. 10, pp. 306–309, 2011.

[7] Z. Popović, E. A. Falkenstein, D. Costinett, and R. Zane, "Low-power far-field wireless powering for wireless sensors," *Proc. IEEE*, vol. 101, no. 6, pp. 1397–1407, Jun. 2013.

[8] H. J. Visser and R. J. M. Vullers, "RF energy harvesting and transport for wireless sensor network applications: Principles and requirements," *Proc. IEEE*, vol. 101, no. 6, pp. 1410–1423, Jun. 2013.

[9] H. Sun, Y.-X. Guo, M. He, and Z. Zhong, "Design of a high-efficiency 2.45-GHz rectenna for low-input-power energy harvesting," *IEEE Antennas Wireless Propag. Lett.*, vol. 11, pp. 929–932, 2012.

[10] Y.-H. Suh and K. Chang, "A high-efficiency dual-frequency rectenna for 2.45- and 5.8-GHz wireless power transmission," *IEEE Trans. Microw. Theory Techn.*, vol. 50, no. 7, pp. 1784–1789, Jul. 2002.

[11] L. W. Epp, A. R. Khan, H. K. Smith, and R. P. Smith, "A compact dual polarized 8.51-GHz rectenna for high-voltage (50 V) actuator applications," *IEEE Trans. Microw. Theory Techn.*, vol. 48, no. 1, pp. 111–119, Jan. 2000.

[12] A. Hagerty, F. B. Helmbrecht, W. H. McCalpin, R. Zane, and Z. B. Popovic, "Recycling ambient microwave energy with broadband rectenna arrays," *IEEE Trans. Microw. Theory Techn.*, vol. 52, no. 3, pp. 1014–1024, Mar. 2004.

[13] B. Strassner and K. Chang, "Microwave power transmission: Historical milestones and system components," *Proc. IEEE*, vol. 101, no. 6, pp. 1379–1395, Jun. 2013.

[14] T.-W. Yoo and K. Chang, "Theoretical and experimental development of 10 and 35 GHz rectennas," *IEEE Trans. Microw. Theory Techn.*, vol. 40, no. 6, pp. 1259–1266, Jun. 1992.

[15] Y.-J. Ren, M.-Y. Li, and K. Chang, "35 GHz rectifying antenna for wireless power transmission," *Electron. Lett.*, vol. 43, no. 11, pp. 602–603, May 2007.

[16] N. Shinohara, K. Nishikawa, T. Seki, and K. Hiraga, "Development of 24 GHz rectennas for fixed wireless access," in *URSI Gen. Assemb. Sci. Symp.*, Aug. 13–20, 2011, pp. 1–4.

[17] S. Ladan and K. Wu, "High efficiency low-power microwave rectifier for wireless energy harvesting," in *IEEE MTT-S Int. Microw. Symp. Dig.*, 2013.

[18] A. Takacs, H. Aubert, L. Despoisse, and S. Fredon, "Microwave energy harvesting for satellite applications," *Electron. Lett.*, vol. 49, no. 11, pp. 722–723, May 23, 2013.

[19] A. Collado and A. Georgiadis, "24 GHz substrate integrated waveguide (SIW) rectenna for energy harvesting and wireless power transmission," in *IEEE MTT-S Int. Microw. Symp. Dig.*, 2013.

[20] V. Marian, B. Allard, C. Vollaire, and J. Verdier, "Strategy for microwave energy harvesting from ambient field or a feeding source," *IEEE IEEE Trans. Power Electron.*, vol. 27, no. 11, pp. 4481–4490, Nov. 2012.

[21] Microsemi. Aliso Viejo, CA, USA. [Online]. Available: http://www.zarlink.com/zarlink/ZL70250_PP_Aug2012.pdf

[22] "RT/duroid®6002 high frequency laminates," Rogers Corporation, Chandler, AZ, USA, 2013. [Online]. Available: http://www.rogerscorp.com/documents/609/acm/RT-duroid-6002-laminate-data-sheet.pdf

[23] "MA4E1317, MA4E1318, MA4E1319-1, MA4E1319-2, MA4E2160: GaAs flip chip Schottky barrier diodes," M/A-COM, Lowell, MA, USA, 2013. [Online]. Available: https://www.macomtech.com/datasheets/MA4E1317_18_19_2160.pdf

[24] "GaAs beam lead detector diodes: Zero bias," Aeroflex Microelectron. Solutions, Sunnyvale, CA, USA, 2013. [Online]. Available: http://www.aeroflex.com/ams/metelics/micro-metelics-prods-GaAs-Beam-lead-ZB.cfm

[25] AWR. El Segundo, CA, USA [Online]. Available: www.awr-corp.com

[26] [Online]. Available: http://www.ansys.com/Products/Simulation+Technology/Electromagnetics/Signal+Integrity/ANSYS+HFSS

[27] FEKO. Stellenbosch, South Africa. [Online]. Available: www.feko.info

[28] Vector Telecom. Melbourne, VIC,, Australia, Horn antenna: VT220HA20+SK. [Online]. Available: http://www.vectortele.com/VT Datasheet/Antennas/Standard Gain Horn Antenna/VT220SGAH20SK.pdf

[29] LabVIEW System Design Software. Nat. Instrum., Austin, TX, USA, 2012. [Online]. Available: http://www.ni.com/labview/

[30] A. Takacs, H. Aubert, M. Bafleur, J. M. Dilhac, F. Courtade, S. Fredon, L. Despoisse, C. Vanhecke, and G. Cluzet, "Energy harvesting for powering wireless sensor networks on-board geostationary broadcasting satellites," in *Proc. IEEE iThinghs 2012*, Besançon, France, Nov. 20–23, 2012, pp. 637–640.

[31] A. Takacs, H. Aubert, L. Despoisse, and S. Fredon, "Design and implementation of a rectenna for satellite application," in *Proc. IEEE WPTC*, Perugia, Italy, May 15–16, 2013, pp. 183–186.

[32] C. Balanis, *Antenna Theory Analysis and Design*, 3rd ed. New York, NY, USA: Wiley, 2005, ch. 2.

[33] E. Falkenstein, M. Roberg, and Z. Popovic, "Low-power wireless power delivery," *IEEE Trans. Microw. Theory Techn.*, vol. 60, no. 7, pp. 2277–2286, Jul. 2012.

[34] P. W. Hannan and M. A. Balfour, "Simulation of phase-array antenna in a waveguide," *IEEE Trans. Antennas Propag.*, vol. AP-13, no. 5, pp. 342–353, May 1965.

Alexandru Takacs (M'12) was born in Simleu Silvaniei, Romania, in March 1975. He received the Engineer diploma in electronic engineering from the Military Technical Academy, Bucharest, Romania, in 1999, and the Master degree and Ph.D. degree in microwave and optical communications from the National Polytechnic Institute of Toulouse, Toulouse, France, in 2000 and 2004, repectively.

From 2004 to 2007, he was a Lecturer with the Military Technical Academy of Bucharest, and an Associate Researcher with the Microtechnology Institute of Bucharest. From 2008 to 2010, he occupied a Postdoctoral position with the Laboratory for Analysis and Architecture of Systems (LAAS), National Center for Scientific Research (CNRS), Toulouse, France. During 2011, he was an R&D RF Engineer with Continental Automotive SAS France, where he was in charge of antenna design and automotive electromagnetic simulation. Since 2012, he has been an Associate Professor with the University (Paul Sabatier), Toulouse, France, where he performs research within LAAS–CNRS. He has authored or coauthored one book, one book chapter, 15 papers in refereed journals, and over 70 communications in international symposium proceedings. His research interests include the design of microwave and RF circuits, energy harvesting and wireless power transfer, microelectromechanical systems (MEMS) circuits and systems, small antenna design, electromagnetic simulation techniques, and optimization methods.

Hervé Aubert (M'94–SM'99) was born in Toulouse, France, in July 1966. He received the Eng. Dipl. degree in electrical engineering and Ph.D. degree (with high honors) in electrical engineering from the Institut National Polytechnique (INPT), Toulouse, France, in 1989 and 1993, respectively.

Since February 2001, he has been a Professor with INPT. In February 2006, he joined the Laboratory for Analysis and Architecture of Systems (LAAS), National Center for Scientific Research (CNRS), Toulouse, France. From April 1997 to March 1998, he was a Visiting Associate Professor with the School of Engineering and Applied Science, University of Pennsylvania, Philadelphia, PA, USA. From July 2001 to January 2005, he was Co-Chairman of the Electronics Laboratory, INPT, and from July 2002 to September 2005, the Head of the Electromagnetics Research Group, Electronics Laboratory, INPT. From September 2004 to September 2011, he was the Director of the Research Master Program in Microwaves, Electromagnetism and Optoelectronics, Toulouse, France. Since January 2012, he has been the Co-Chairman of the Micro- and Nano-systems for Wireless Communications Research Group, LAAS–CNRS. He is a contributor to *Fractals: Theory and Applications in Engineering* (Springer, 1999), *Micromachined Microwave Devices and Circuits* (Romanian Acad. Edition, 2002), and *New Trends and Concepts in Microwave Theory and Techniques* (Res. Signpost, 2003). He has authored or coauthored one book, two book chapters, 71 papers in refereed journals, and over 186 communications in international symposium proceedings. He holds four international patents in the area of antennas. He has performed research on integral-equation and variational methods applied to electromagnetic wave propagation and scattering. His current research activities involve the electromagnetic modeling of complex (multi-scale) structures.

Dr. Aubert is an Expert for the French Research Agency (ANR) since 2009 and an Expert for the European Commission since 2012. From 2009 to 2013, he was the secretary of the IEEE Antennas and Propagation French Chapter, from 2004 to 2009, the vice-chairman of the IEEE Antennas and Propagation French Chapter, and from 2001 to 2004, secretary of the IEEE Antennas and Propagation French Chapter.

Laurent Despoisse received the General Engineer Master's degree (with a command and signal processing specialty) from the Ecole Centrale de Nantes, Nantes, France, in 2004, and the Advanced Master's Degree in space systems engineering from the Institut Supérieur de l'Aéronautique et de l'Espace, Toulouse, France, in 2005.

From 2005 to 2007, he was an Electrical Power Subsystem Engineer with Eutelsat, Paris, France, following the in-orbit telecommunication satellites' health and the new satellites procurement. From 2007 to 2008, he was a Research and Development Systems Engineer with the European Space Agency, Noordwijk, The Netherlands. Since 2008, he has been an Electrical Power Systems Engineer with Thales Alenia Space, Cannes, France, in charge of research and development activities, and of the Observation and Science Satellites' Electrical Power Systems Architecture and Engineering.

Henri Blondeaux received the Ph.D. degrees in microwaves and optic communications from the University of Limoges, Limoges, France, in 2001. His doctoral research concerned radiated filters in Ka-band, supported by Thales Alenia Space.

In 2001, he joined the Satellite Payload Engineering Department, Thales Alenia Space, Cannes, France, where he was in charge of radiated electromagnetic compatibility (EMC) and electromagnetic interference (EMI) aspects from design phase to satellite test phase. Since 2006, he has been with Thales Alenia Space, Toulouse, France, as an EMC/EMI Expert on telecommunications and observations satellites and as an Expert on RF satellite tests in compact antenna test range: antennas, payload, and compatibility performances.

Energy and radiosciences / Énergie et radiosciences

Multiband rectenna for microwave applications

Rectenna multi-bandes pour des applications micro-ondes

Abderrahim Okba, Alexandru Takacs, Hervé Aubert, Samuel Charlot, Pierre-François Calmon

LAAS–CNRS, Université de Toulouse, CNRS, UPS, INPT, 6, allée Émile-Monso, 31400 Toulouse, France

A B S T R A C T

This paper reports a multiband rectenna (rectifier + antenna) suitable for the electromagnetic energy harvesting of the spill-over loss of microwave antennas placed on board of geostationary satellites. Such rectenna is used for powering autonomous wireless sensors for satellite health monitoring. The topology of the rectenna is presented. The experimental results demonstrate that the proposed compact rectenna can harvest efficiently the incident electromagnetic energy at three different frequencies that are close to the resonant frequencies of the cross-dipoles implemented in the antenna array.

© 2016 Published by Elsevier Masson SAS on behalf of Académie des sciences. This is an open access article under the CC BY-NC-ND license (http://creativecommons.org/licenses/by-nc-nd/4.0/).

R É S U M É

Cet article présente une nouvelle rectenna (antenne + redresseur) multi-bandes utilisable pour la récupération d'énergie électromagnétique à bord de satellites géostationnaires. L'objectif est de récupérer l'énergie électromagnétique rayonnée par les antennes placées à bord du satellite. L'énergie ainsi récupérée est alors utilisée pour alimenter des capteurs autonomes sans fil. Les résultats expérimentaux montrent que cette rectenna récupère, avec une bonne efficacité, l'énergie électromagnétique à trois fréquences, qui correspondent aux fréquences de résonance de l'élément rayonnant de la rectenna.

© 2016 Published by Elsevier Masson SAS on behalf of Académie des sciences. This is an open access article under the CC BY-NC-ND license (http://creativecommons.org/licenses/by-nc-nd/4.0/).

1. Introduction

The last decade has known a significant development of a wide range of wireless electronic devices such as RFID systems and wireless sensors networks. For many critical applications (e.g., space, aeronautic, and medical applications), the sensors used to monitor physical and structural quantities should be wireless and energetically autonomous. The energy, under its different forms (kinetic, thermal, solar, radio waves...) can be used to power these sensors. In this work, the use of the radio waves as energy source for autonomous power sensors is addressed. The autonomy of the wireless sensors can
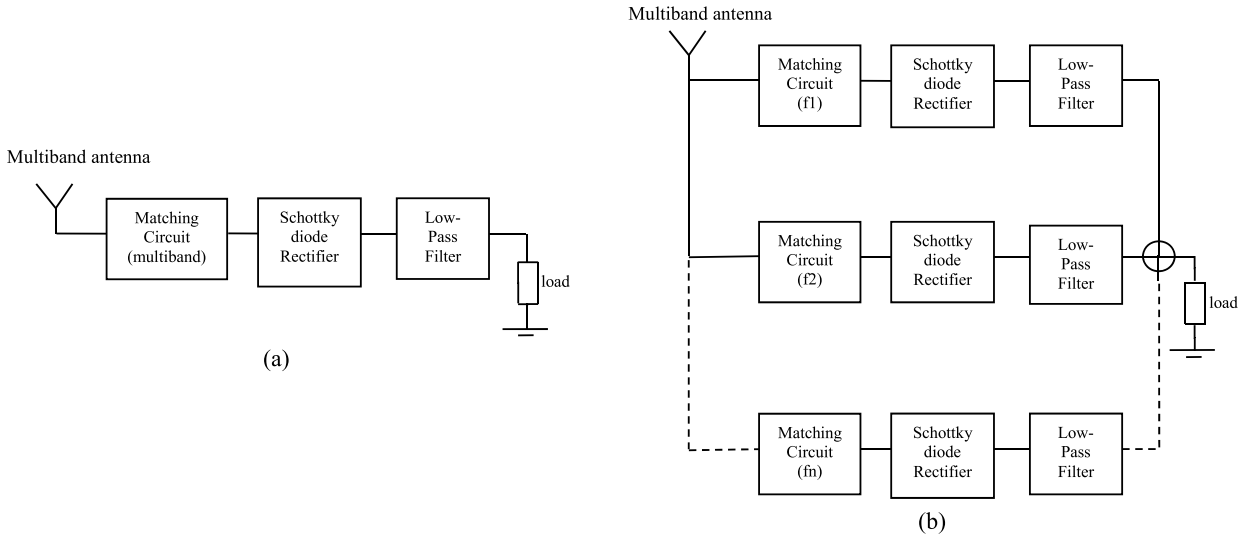
Fig. 1. Topologies for multiband rectennas: (a) rectenna with one RF band-pass filter for a broadband/multiband RF matching, and (b) rectenna combining the harvested DC powers at each frequency.

be achieved mainly by two techniques: (*i*) wireless power transfer and (*ii*) energy harvesting. These are two important concepts of "energy in radiosciences"; the first one consists in transmitting an electromagnetic energy generated by a dedicated/intentional transmitter and converting this energy into DC on the wireless sensor node by using a rectenna (coming from *rect*ifier ant*enna*), and the second one consists in harvesting the energy of the existing/surrounding radio waves by using a rectenna. In geostationary telecommunication satellites, high-gain microwave antennas are mounted on the external panels of the satellite for communication broadcasting. The radiofrequency (RF) power radiated by such antennas is in the range of 100 W. Consequently, an important amount of electromagnetic energy is available around the satellite and illuminates the (antenna) panels. The electric field generated by the spill-over loss of these microwave antennas can reach the following highest levels (effective values): 40 V/m in C-band, 49.5 V/m in X-band, 106 V/m in K_u-band, and 127 V/m in K-band [1]. Thus, electromagnetic energy harvesting was identified as a realistic solution to power autonomous wireless sensors deployed along the surface of the panels for structure health monitoring [1]. The rectenna (antenna + rectifier circuit) plays a crucial role in receiving and converting RF power into DC power. It consists of two main blocks: the first block is the antenna used to capture RF energy and converts it into an RF signal; the second block is the rectifier that converts this RF signal into a DC voltage used to power an autonomous wireless sensor. This paper presents recent results obtained in K_u and K bands through using an innovative rectenna topology reported in [2] and developed in [3] and [4], which is composed of four-printed-cross-dipole antenna arrays and uses a single low-cost Schottky diode [5]. Rectennas using a cross-dipole antenna were also reported in [1,6], while a rectenna using a two-cross-dipole array was reported in [7]. The rectenna topology and the design methodology are presented in Section 2. The experimental results are reported in Section 3 and show that very good performances can be achieved in three frequency bands by using a single rectenna. The proposed compact topology is an extension of the rectenna using two cross dipoles antenna array reported in [7].

2. Rectenna topology and design

In order to implement a multiband rectenna, two topologies can be considered. They are shown in Fig. 1. They consist of a multiband antenna that captures the ambient electromagnetic energy and converts it into a RF signal. This RF signal is then transferred to the rectifier via an impedance matching circuit/band pass filter for maximizing the transfer of power and minimizing the return loss at operating frequencies. The rectifier (e.g., a Schottky diode) is another key element of a rectenna and must be chosen carefully. Its role is to rectify the RF signal and a low-pass filter is then used in order to suppress the fundamental frequency component and its harmonics. The sensing device (typically a resistor) is modeled as a load impedance to be powered. As shown in Fig. 1a, the first possible topology uses only one rectifier for addressing all the targeted frequencies. As a drawback, this topology generally requires a multiband/broadband matching network that can be very challenging to design/implement in practice. A rectenna based on this topology is reported in [8,9]. Another solution is shown in Fig. 1b. A specific rectifier is used with its own impedance matching circuit at each targeted frequency. Then all the obtained DC powers are combined for powering the load (i.e. the sensing device). The rectenna proposed in [10] is based on this topology. For compactness purposes, the topology shown in Fig. 1a is adopted here. Moreover, by adopting this topology, a non-resonant matching technique is used. Matching is carried out by controlling the impedances of the antenna and of the rectifier. From a theoretically point of view, another topology can be proposed: it consists in using a specific rectenna (with a narrow-band/single-band antenna) for each frequency band and then combining the harvested DC powers. Nevertheless, this solution leads to a very large design.
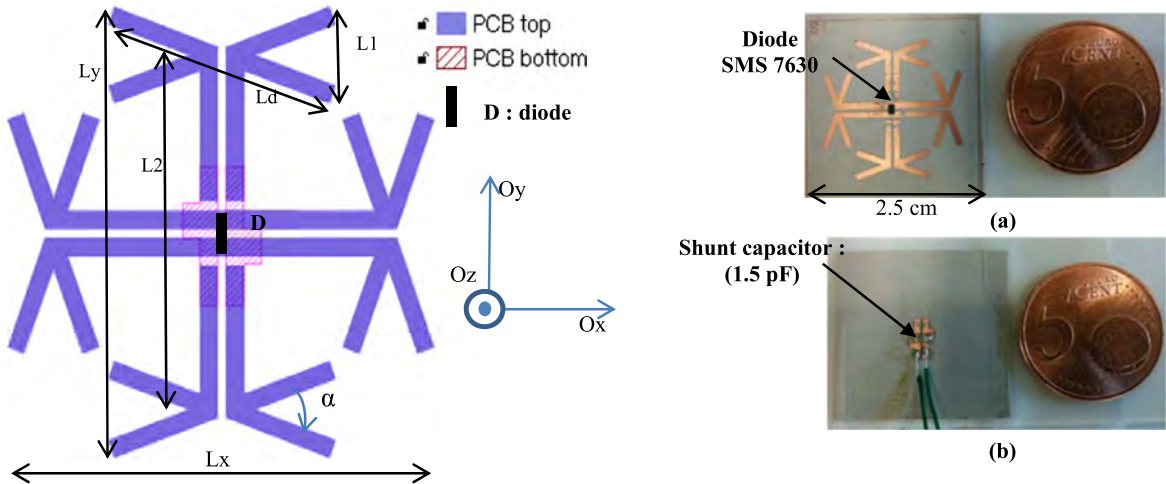
Fig. 2. (a) Top view (not to scale) of the layout of the 4CDAA rectenna, and (b) photos of the top and bottom sides of the manufactured rectenna. The wires shown here were used to connect a variable resistance in order to reach the optimal load impedance.

The proposed topology is composed of a four-cross-dipole antenna array (4CDAA) and of a silicon Schottky diode— Skyworks SMS7630—[5] mounted in shunt configuration. In order to select the topology of our antenna, several requirements were taken into account: (*i*) the rectenna should be as compact as possible (we note that the size of our design is determined mainly from the size of its antenna), (*ii*) the gain should be as high as possible in order to increase the rectenna's efficiency, (*iii*) the antenna should have a multiband behavior. As we will show later, the 4CDAA topology represents a good trade-off between the previously mentioned criteria. The best way to feed the 4CDAA is to use Coplanar Strip Lines (CPS). Thus the use of a single diode in a shunt configuration seems to be the best solution to implement the rectifier. Then the rectifier is comprised of (*i*) a silicon SMS7630 diode mounted in shunt configuration, (*ii*) a shunt capacitor to implement the DC low-pass filter, (*iii*) the CPS lines and via-holes used to interconnect the lumped components (diode and capacitance). From an electrical point of view, the rectifier views the input impedance of the CDAA as shunt impedance.

The PCB layout and a photo of the manufactured rectenna are shown in Fig. 2. The antenna array and the diode are implemented on the top of the PCB, while the RF shunt capacitor is mounted on the bottom side of the PCB. A metallic plate is added on the bottom side in order to enhance the antenna gain. This compact topology (its size is fixed by the size of the antenna array) is an extension of the rectenna using the two-cross-dipole antenna array 2CDAA reported in [7]. Moreover, a non-resonant matching technique is used here. Instead of using a dedicated matching circuit that acts as a (resonant) band-pass filter, we try here to implement directly the (conjugate) matching requirements by properly controlling the input impedances of the 4CDAA and of the rectifier. Then, the matching circuit is virtually suppressed and leads to a more compact structure. The main goal is to achieve the best impedance matching at the resonant frequencies of the 4CDAA.

The rectifier consists of the diode and the low pass RC filter (composed of the shunt capacitor and the load itself). The 4CDAA can be viewed as an array formed by four-cross-dipole arrays printed on the top of the PCB. Each cross dipole is an array with two dipoles in cross configuration, as shown in Fig. 2. The substrate used is the Rogers RT/Duroïd 6002 (substrate thickness: 0.508 mm, relative dielectric permittivity: 2.94 and dielectric loss tangent: 0.0012) [11].

3. Design of the rectenna

Some specific technical requirements for space applications must be fulfilled for designing an efficient rectenna: (i) the rectenna topology has to be as simple as possible; (ii) all the components in the rectenna (dielectric substrate, diode, capacitors, etc.) must be qualified for space applications, ready to be qualified or at least with performances suitable for space requirements; (iii) the operating frequencies must be chosen from the electromagnetic environment existing on board of satellite antenna panels. An analysis of the electromagnetic energy available on the panels at different frequencies is reported in [1].

3.1. Design of the antenna

Intensive full-wave electromagnetic simulations were performed by using Ansys HFSS software in order to design the 4CDAA structure. The diode was replaced by a voltage port, while the shunt capacitor and the load were modeled as lumped RLC boundaries as shown in Fig. 3. The antenna was initially simulated and optimized for 12 GHz, but it also displays a good impedance matching at two other frequencies, which corresponds to the higher resonant modes of the 4CDAA. The simulated return loss shows a multi-band behavior (12 GHz, 17.6 GHz and 20.2 GHz). Fig. 4 displays the simulated results regarding the return loss and the input impedance versus frequency.
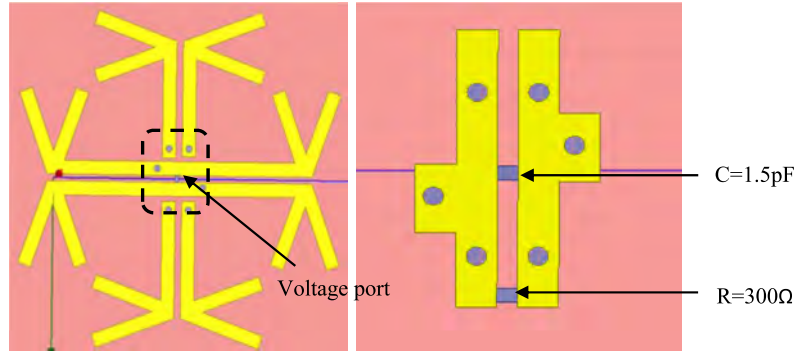
Fig. 3. The antenna with its voltage port and the lumped RLC boundaries.
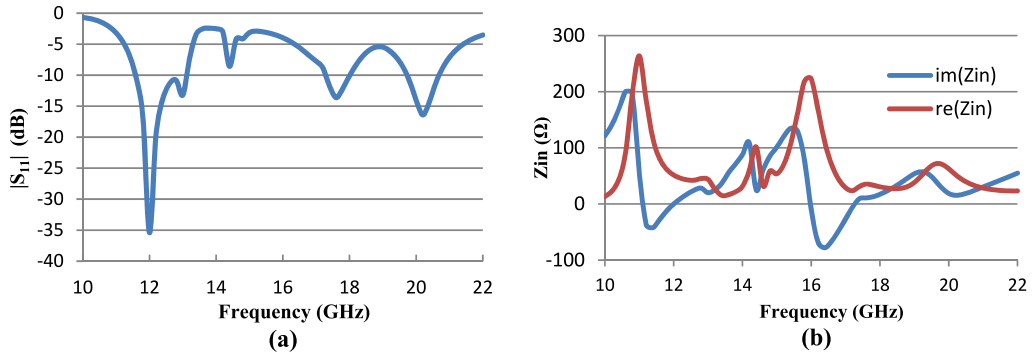

Fig. 4. (a) S11 viewed at the input port of the diode vs. frequency; (b) input impedance viewed at the input port of the diode vs. frequency.

The highest gain of such an array can be estimated by using the following expression:

$$G_{max} = 10 \cdot \log_{10} n + G_d = 11.18 \text{ dBi} \tag{1}$$

where n is the number of dipoles ($n = 8$ in our case) and G_d is the gain of each (lossless) dipole. This gain can be increased when a reflector is properly positioned below the antenna surface. The expected maximum gain is 14.2 dBi when half-wavelength dipoles ($G_d = 2.15$ dBi) are used. This gain should be considered as an upper limit for any practical 4CDAA design.

There are no accurate closed-form expressions for designing such arrays, but some rules and methodology can be applied in order to start the design. The length of each dipole (L_d in Fig. 2) should be approximately half wavelength and the distance between the center of two opposite cross dipoles (L_2 in Fig. 2) should be an integer multiple of half wavelength. The angle between the dipoles (α in Fig. 2) impacts the polarization of the radiated field and the maximum achievable gain. CoPlanar Strip (CPS) lines are used to feed each cross dipole.

We target here a linear polarization, but other polarizations (e.g., circular polarization) can be obtained by controlling the angle α between the crossed dipoles and the relative phase at the input of each cross dipole. Depending on the system requirements, the microwave antennas of the broadcasting satellites may operate using circular or linear polarization [1]. Linear polarization is adopted here because the (in-house) experimental setup used for rectenna characterization has been built up by using a linearly polarized horn antenna. The diode is mounted at the center of the array, as shown in Fig. 2. Six metallic via holes were used to connect the top and the bottom sides of the PCB. A shunt capacitor is mounted on the bottom side of the PCB. The main dimensions of the fabricated (optimized) rectenna are: $L_1 = 4$ mm, $L_2 = 15.3$ mm, $L_d = 10.6$ mm, $L_x = L_y = 19.5$ mm.

At the first operating frequency ($f_0 = 12$ GHz), the length of each dipole (L_d) is close to the half wavelength ($L_d \sim \lambda/2$), and the distance between the center of the opposite dipoles (L_2) is close to the wavelength ($L_2 \sim \lambda$). The second operating/resonant frequency is $f_1 \sim 1.5 f_0$. At this frequency, $L_d \sim 0.7\lambda$ and $L_2 \sim 1.5\lambda$. The third operating/resonant frequency is $f_2 \sim 2 f_0$. At this frequency, $L_d \sim \lambda$ and $L_2 \sim 2\lambda$. Fig. 5 shows the simulated radiation patterns (gain) of 4CDAA at the three resonant (operating) frequencies 12 GHz, 17.6 GHz and 20.2 GHz. Fig. 6 shows the surface current density on the rectenna. From a theoretical point of view, at the third frequency (20.2 GHz), the radiation pattern is expected to be null along the Oz axis. This is not the case because L_d is not exactly equal to λ and also because an electromagnetic coupling exists between the cross dipoles. The designed 4CDAA exhibits the following simulated gain (values obtained for $\theta = \varphi = 0°$): 11.7 dBi at 12 GHz, 11.7 dBi at 17.6 GHz and 12.7 dBi at 20.2 GHz. As expected, the simulated gains for the 4CDAA are much higher than the theoretical gain of a single dipole (2.15 dBi for an ideal half-wavelength dipole).

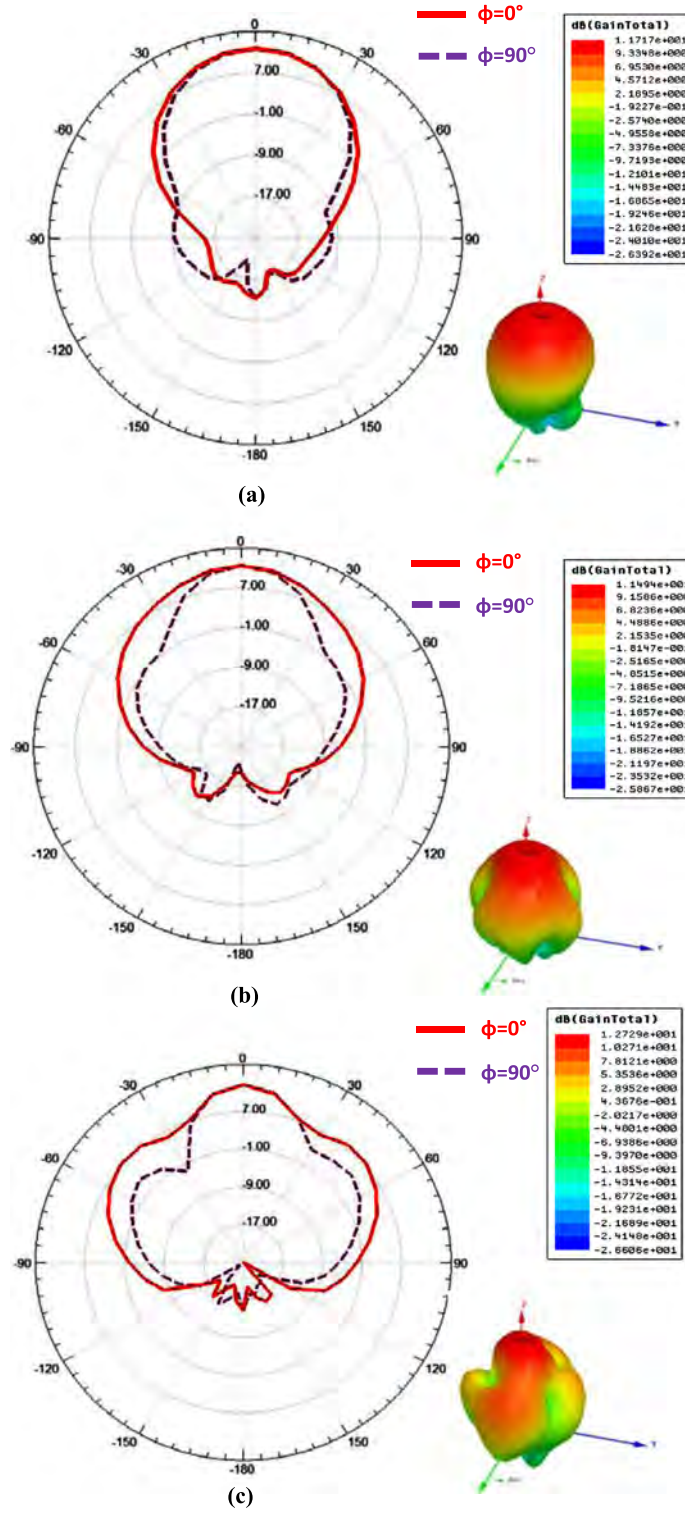**(a)**

(b)

(c)

Fig. 5. Simulated (HFSS) radiation pattern (gain) in the xOz plane ($\varphi = 0°$, continuous line) and in the yOz plane ($\varphi = 90°$, dashed line) of the 4CDAA at the frequencies of (a) 12 GHz, (b) 17.6 GHz, and (c) 20.2 GHz.
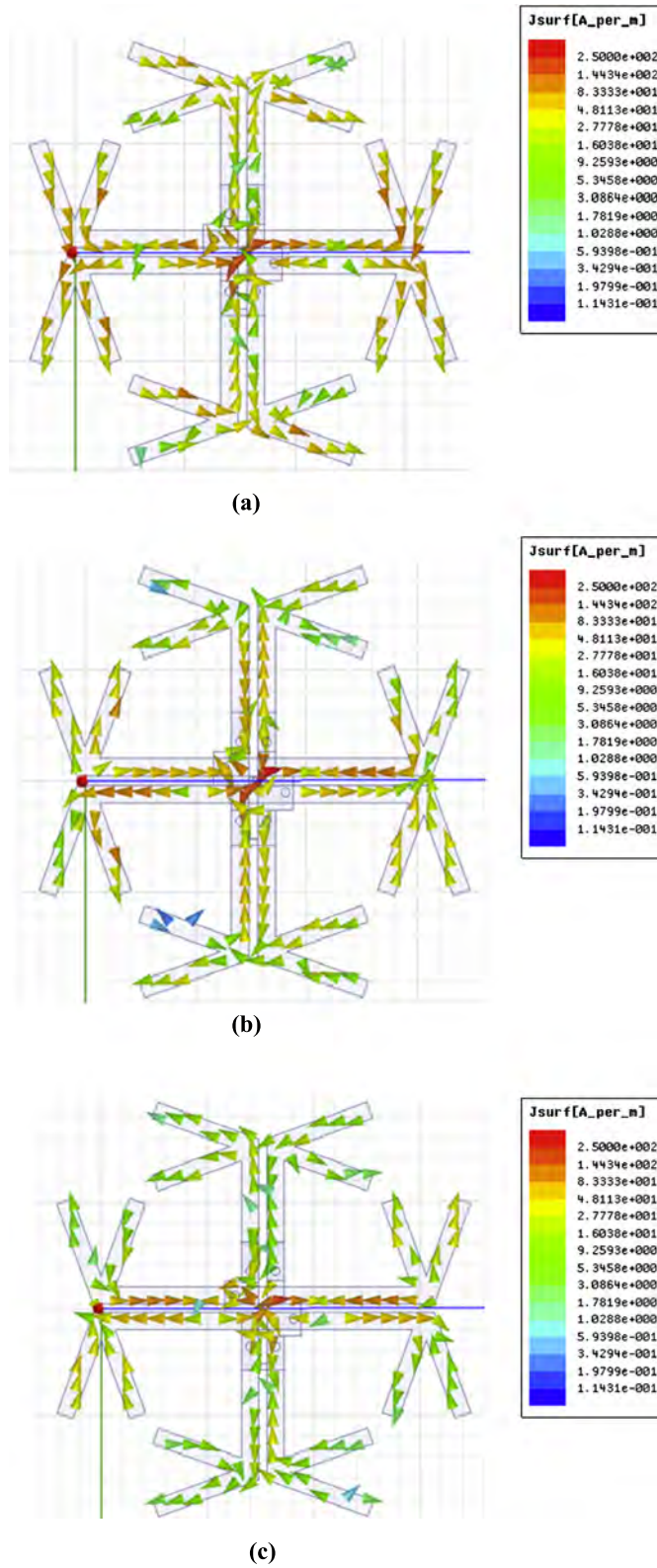
(a)

(b)

(c)

Fig. 6. Surface current density on the 4CDAA at (a) 12 GHz, (b) 17.6 GHz, and (c) 20.2 GHz.

RF shunt capacitor
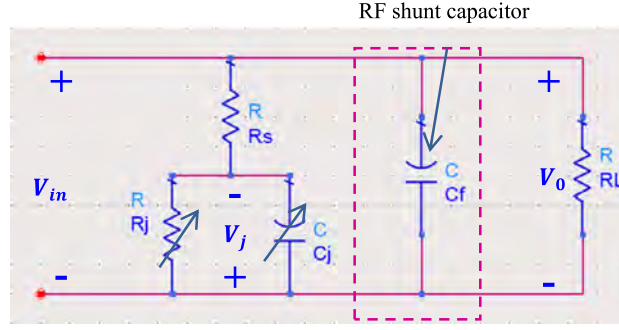
Fig. 7. Equivalent circuit of the diode.

Table 1
Schottky diode parameters.

Parameter	Value
Ohmic resistance (R_s)	20 Ω
Junction capacitance (C_{j0})	0.14 pF
Saturation current (I_s)	5 μA
Forward voltage (V_f)	0.34 V
Reverse breakdown voltage (B_v)	2 V

3.2. Rectifier

The diode is the key element of the rectifier. The choice of an appropriate diode is crucial and must be done carefully in the design of a high-efficient rectifying circuit. This is because the diode is the main source of losses and its performance impacts significantly the performances of rectennas. The equivalent circuit of the diode/rectifier is shown in Fig. 7. It consists of the series resistance (R_S), a nonlinear junction resistance (R_j) derived from the *I–V* characteristic of the diode and a nonlinear junction capacitance (C_j). Due to the self-biasing nature of the shunt connected diode, C_j depends on the bias voltage across the diode as follows [12,13].

$$C_j = C_{j0} \sqrt{\frac{V_f}{V_0 + V_f}} \tag{2}$$

where C_{j0} is the zero-bias junction capacitance of the diode and V_0 denotes the DC output voltage. Following [12], an ideal DC pass-band filter is assumed here. Three key parameters of the diode impact the RF-to-DC conversion efficiency. The series resistance (R_s) limits the efficiency through the dissipation losses, the zero-bias junction capacitance (C_{j0}) affects the harmonic currents through the diode and the breakdown voltage (V_{BR}) limits the power handling capability of the rectifier.

The diode used in this design is the silicon Schottky diode SMS7630 from Skyworks. Its main parameters are reported in Table 1 (see [14,15]).

4. Experimental results and discussion

The experimental setup used in order to characterize the rectenna is shown in Fig. 8. A microwave signal provided by an Anritsu MG3694B generator is injected at the input of a horn antenna using a coaxial cable. During the measurement, the rectenna was aligned in order to match the (linear) polarization of the transmitting horn antenna. The horn antenna is placed at a distance *d* above the rectenna and allows illuminating the rectenna with a linearly polarized electric field. An automatic acquisition routine is implemented in Labview software from National Instruments to speed-up the acquisition process. The harvested DC voltage is measured by using a DC multimeter. The DC power can be derived from the measured DC voltage as long as the load is known. The measured losses due to the coaxial cable and connectors placed between the signal generator and the horn antenna are around 3 dB in the operating frequency band (12 GHz). Two different transmitting horn antennas are used here: the first one covers the 12 GHz–16 GHz frequency band and the second one covers the 16 GHz–22 GHz frequency band.

The efficiency η (in %) of the rectenna can be computed as follows [16]:

$$\eta(\%) = \frac{P_{DC}}{S A_{eff}} \cdot 100 = \frac{4\pi P_{DC}}{S G_R \lambda^2} \cdot 100 \tag{3}$$

where P_{DC} is the harvested DC power, S is the incident electromagnetic power density, A_{eff} is the antenna effective area, G_R is the simulated gain of the (rectenna's) antenna and λ is the free-space wavelength of the illuminating electromagnetic wave at a given frequency.
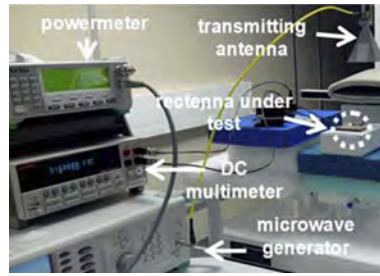
Fig. 8. Experimental setup used to characterize the multiband rectenna.

Table 2
Comparison of the rectennas' performances.

Ref.	Operating frequency	Diode	Incident power density/RF power at the rectifier's input	Dimensions	Maximum conversion efficiency
[12]	35 GHz	Skyworks DMK6606	20.79 dBm, $R_L = 400\ \Omega$ 17 dBm, $R_L = 100\ \Omega$	NC[a]	39%
[17]	2.45 GHz–5.8 GHz	Macom MA4E1317	2.38 mW/cm^2–8.77 mW/cm^2	NC[a]	84.4%–82.7%
[18]	24 GHz	Macom MA4E1317	10 mW/cm^2	Length: 55 mm $1.9\lambda_0$	24%
[19]	35 GHz	Macom MA4E1317	30 mW/cm^2	Length: 23.55 mm $2.7\lambda_0$	35%
[20]	25.7 GHz	Macom MA4E2502L	8 dBm	21.9×15 mm^2 $2.4\lambda_0^2$	16%
[21]	5.8 GHz	Macom MA4E1317	12 mW/cm^2	NC[a]	76%
This work	12 GHz–17 GHz–20 GHz	Skyworks SMS7630	1.8 mW/cm^2	25×25 mm^2 λ_0^2 at 12 GHz	41%

[a] Not communicated.
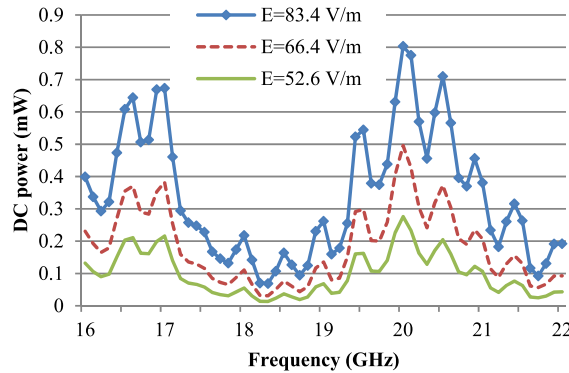
Fig. 9. Measured DC power at the input port of a resistive load ($R_L = 300\ \Omega$) as a function of frequency and for various amplitudes of the electric field.

From equation (3), power density (μW/cm^2) can be computed as a function of the electric field's effective value E (V/m) on the antenna surface or as a function of the RF power P_t injected at the input of the transmitting horn antenna (gain G_t) and positioned at a distance d from the rectenna, as follows:

$$S = \frac{E^2}{120\pi} \cdot 100 = \frac{30 P_t G_t}{d^2 120\pi} \cdot 100 \tag{4}$$

The electric field and the power density illuminating the rectenna can be computed as a function of G_t and d by using Eq. (3). Fig. 9 shows the measured harvested DC power at the input port of a resistive load ($R_L = 300\ \Omega$) in the frequency band 10 GHz–16 GHz for various amplitudes of the electric field (the gain G_t of the first transmitting horn antenna at 12 GHz is 19 dBi). The maximum DC power was measured at 12 GHz, as shown in Fig. 9.

Fig. 10 displays the measured DC power on a load of $R_L = 300\ \Omega$ in the frequency band 16 GHz–22 GHz as a function of the electric field (the gain G_t of the transmitting horn antenna at 12 GHz is 19.5 dBi). The measurement results shown in Fig. 10 demonstrate also a multi-band behavior. The proposed rectenna harvests efficiently the RF power at 17 GHz and 20 GHz. The optimal load was also determined, and Fig. 11 shows the DC power as a function of the load for an electric field of 48 V/m at 12 GHz. A standard potentiometer (0–10 kΩ) was used as a load impedance. The results shows that the
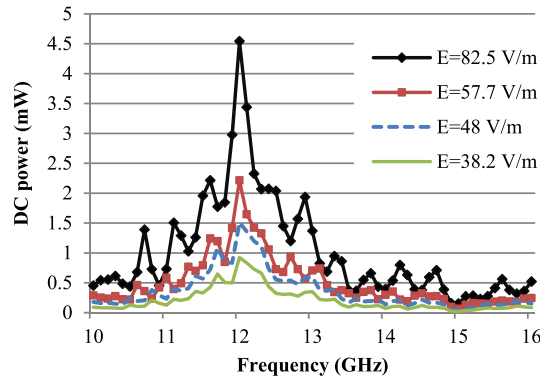
Fig. 10. Measured DC power at the input port of a resistive load ($R_L = 300\ \Omega$) as a function of the frequency for various amplitudes of the electric field.
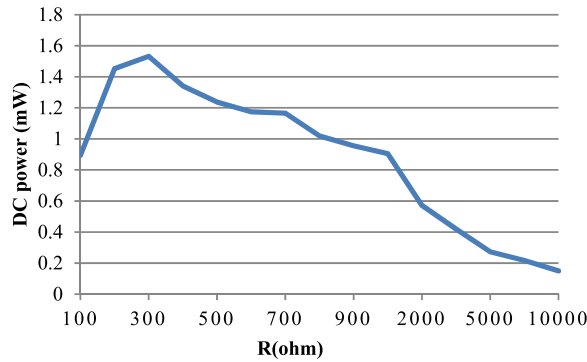
Fig. 11. Measured DC power as a function of the resistance of the load for an electric field of 48 V/m.
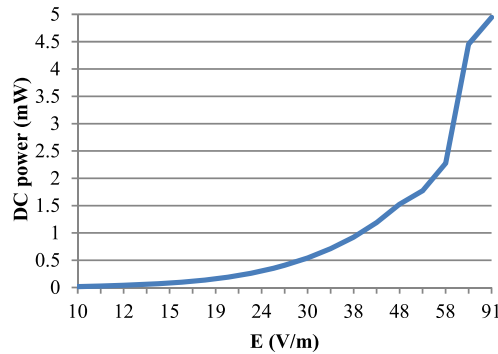
Fig. 12. Measured DC power at the input of a load ($R_L = 300\ \Omega$) as a function of the illuminating electronic field amplitude at 12 GHz.

DC power decreases (i.e. the efficiency decreases) when the load impedance increases. The highest DC power is obtained when $R = 300\ \Omega$.

The harvested DC power for electric field $= 300\ \Omega$ as a function of the electric field illuminating the 4CDAA at the frequency of 12 GHz is reported in Fig. 12. From a practical point a view, at least 1 mW of DC power is required to supply an autonomous wireless sensor for satellite health application. Typically, such a wireless sensor is comprised of a sensor (DC power consumption in the range of few μW), a DC-to-DC converter, a power management unit, and a wireless low-power transceiver (DC power consumption in the range of the mW). However, the electromagnetic energy illuminating the antenna panels is almost constant and the DC circuitry (including the power management unit) should be minimal [1]. As shown in Fig. 12, the rectenna can provide a DC power of 1 mW or higher when it is illuminated by an electric field amplitude higher than 38 V/m. The efficiency of 4CDAA rectenna is computed by using Eq. (2). Fig. 13 represents the RF-to-DC conversion efficiency as a function of the electric field illuminating the rectenna under test.

The highest efficiency is approximately 41% at 12 GHz for an illuminating electric field amplitude ranging between 51 V/m and 83 V/m. Table 2 compares the main performances of this rectenna with other state-of-art multiband rectennas. At the second resonant frequency ($f_1 = 17.6$ GHz), the highest efficiency is approximately 12% while an efficiency of about
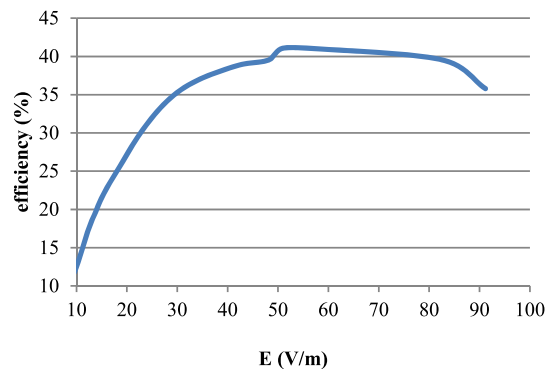
Fig. 13. Rectenna efficiency at 12 GHz as a function of the illuminating electronic field amplitude for $R_L = 300\ \Omega$.

20% is obtained at 20 GHz. The main sources of power loss are: (i) the ohmic resistance of the selected low-cost silicon diode and (ii) the eventual mismatch between the antenna and the rectifier (due to the adopted non-resonant matching technique and to the lack of accurate simulation models of the selected diode). The overall performances of the 4CDAA rectenna can be further improved by optimizing the PCB layout on the bottom side, which has a major impact on the impedance matching between the rectifier and the antenna located on the top side of the PCB. Efficiencies greater than 25% can be obtained at the first resonant frequency by using a low-cost silicon Schottky diode (SMS7630) when the electric field amplitude exceeds 19 V/m. The rectenna is very compact, as shown in Fig. 2. Its size is 2.5 cm × 2.5 cm. Moreover, this rectenna exhibits a tri-band feature, which is obtained from the multiple resonant frequencies of the cross-dipole antenna array.

5. Conclusion

A compact rectenna based on the use of an original four cross dipoles antenna array was designed, manufactured, and measured. The experimental results demonstrate that a DC power greater than 1 mW can be harvested in the K_u band (12 GHz) for an electric field amplitude higher than 38 V/m. This DC power is sufficient to power a wireless sensor (including the sensor, the sensing device, the power management unit and the wireless transceiver) for satellite health monitoring applications. A maximum RF-to-DC conversion efficiency of 41% was obtained for a load of 300 Ω and an incident electric field of 51 V/m., this rectenna exhibits a multi-band behavior at frequencies that correspond to the available multiple resonant frequencies of the cross-dipole antenna array.

Acknowledgements

References

[1] A. Takacs, H. Aubert, S. Fredon, L. Despoisse, H. Blondeaux, Microwave power harvesting for satellite health monitoring, IEEE Trans. Microw. Theory Tech. 62 (4) (2014) 1090–1098.

[2] A. Okba, S. Charlot, P-F. Calmon, A. Takacs, H. Aubert, Cross dipole rectenna for satellite health monitoring, in: URSI Conference, Nantes, France, March 2016.

[3] A. Okba, S. Charlot, P-F. Calmon, A. Takacs, H. Aubert, Multiband rectenna for microwave applications, in: IEEE Wireless Power Transfer Conference, Aveiro, Portugal 5–6 May 2016.

[4] A. Okba, S. Charlot, P-F. Calmon, A. Takacs, H. Aubert, Cross dipoles rectenna for microwave applications, in: European Microwave Conference, London, UK, 3–7 October 2016.

[5] http://www.skyworksinc.com/Product/511/SMS7630_Series.

[6] H. Sun, Y.-X. Guo, M. He, Z. Zhong, Design of a high-efficiency 2.45-GHz rectenna for low-input-power energy harvesting, IEEE Antennas Wirel. Propag. Lett. 11 (2012) 929–932.

[7] A. Takacs, H. Aubert, A. Luca, S. Charlot, S. Fredon, L. Despoisse, Rectenna design for K band application, in: 2014 European Microwave Conference, Rome, Italy, 5–10 October 2014.

[8] V. Kuhn, C. Lahuec, F. Seguin, C. Person, A multi-band stacked RF energy harvester with RF-to-DC efficiency up to 84%, IEEE Trans. Microw. Theory Tech. 63 (5) (2015) 1768–1778.

[9] K. Niotaki, S. Kim, S. Jeong, A. Collado, A. Georgiadis, M.M. Tentzeris, A compact dual-band rectenna using slot-loaded dual band folded dipole antenna, IEEE Antennas Wirel. Propag. Lett. 12 (2013) 1634–1637.

[10] C. Song, Y. Huang, J. Zhou, J. Zhang, S. Yuan, P. Carter, A high-efficiency broadband rectenna for ambient wireless energy harvesting, IEEE Trans. Antennas Propag. 101 (8) (2015) 3486–3495.

[11] RT/duroid® 6002 high frequency laminates, Rogers Corporation, Chandler, AZ, USA, 2013. Online available: http://www.rogerscorp.com/documents/609/acm/RT-duroid-6002-laminate-datasheet.pdf.

[12] T.-W.Y. Chang, K. Chang, Theoretical and experimental development of 10 and 35 GHz rectennas, IEEE Trans. Microw. Theory Tech. 40 (12) (1992) 2359–2366.

[13] J. Guo, X. Zhu, An improved analytical model for RF-DC conversion efficiency in microwave rectifiers, in: IEEE MTT-S International Conference, Montreal, QC, Canada, 17–22 June 2012.

[14] http://www.skyworksinc.com/uploads/documents/Surface_Mount_Schottky_Diodes_200041AB.pdf.

[15] Skyworks application notes 'mixer and detector diodes', http://www.skyworksinc.com/uploads/documents/200826A.pdf.

[16] Z. Popovic, E.A. Falkenstein, D. Costinett, R. Zane, Low-power far-field wireless powering for wireless sensors, Proc. IEEE 101 (6) (2013) 1397–1407.

[17] Y.-H. Suh, K. Chang, High-efficiency dual-frequency rectenna for 2.45- and 5.8-GHz wireless power transmission, IEEE Trans. Microw. Theory Tech. 50 (7) (2002) 1784–1789.

[18] S. Ladan, A.B. Guntupalli, K. Wu, A high-efficiency 24 GHz rectenna development towards millimeter-wave energy harvesting and wireless power transmission, IEEE Trans. Circuits Syst. I, Regul. Pap. 61 (12) (2014) 3358–3366.

[19] Y.-J. Ren, M.-Y. Li, K. Chang, 35 GHz rectifying antenna for wireless power transmission, Electron. Lett. 43 (11) (2007) 602–603.

[20] A. Collado, A. Georgiadis, 24 GHz substrate integrated waveguide (SIW) rectenna for energy harvesting and wireless power transmission, in: IEEE MTT-S International Conference, Seattle, WA, USA, 2–7 June 2013.

[21] Y.-J. Ren, K. Chang, 5.8-GHz circularly polarized dual-diode rectenna and rectenna array for microwave power transmission, IEEE Trans. Microw. Theory Tech. 54 (4) (2006) 1495–1502.

Flexible Substrate Technology for Millimeter Wave Wireless Power Transmission

Zhening Yang[1,2], Alexandru Takacs[1,3], Samuel Charlot[1], Daniela Dragomirescu[1,2]

[1] CNRS, LAAS, 7 Avenue du Colonel Roche, F-31400 Toulouse, France

[2] Univ de Toulouse, INSA, LAAS, F-31400 Toulouse, France

[3] Univ de Toulouse, UPS, LAAS, F-31400 Toulouse, France

In this paper, a technology based on thin flexible polyimide substrate (Kapton) to develop antennas for millimeter wave wireless power transmission is presented. Firstly, we characterize the Kapton polyimide (relative permittivity and loss tangent) by using a ring resonator method up to V band. A 60 GHz patch antenna is designed, fabricated, and measured to validate our technology. Crossed dipoles array antennas at Ku band and K band for energy harvesting are also designed, fabricated and measured. Then a prototype of crossed slot dipole antenna at V band is proposed. Finally, a resistivity characterization of Au bump used in flip chip packaging is done, which leads us one step further towards a heterogeneous integration on flexible substrate of different components for Wireless Sensor Network nodes.

Corresponding author email: daniela.dragomirescu@laas.com; phone: +33 5 61 33 63 79

I. INTRODUCTION

There is an increasing demand of high efficiency antennas and passives for applications where high frequency operation, lightweight, and conforming to a curved surface are required. Flexible electronics have spanned impressively over the past years, and flexible substrate became a strong competitor compared to his rigid counterparts because they are typically lighter, more rugged and portable, and less expensive to manufacture [1].

Table 1. Comparative properties of state-of-art flexible substrates [2].

Material	PET	PEN	Kapton	LCP	Paper
Mechanical properties	Good	Good	Excellent	Good	-
Heat resistance	Low	Very good	Excellent	Good	-
Chemical resistance	Good	Good	Good	Excellent	-
Electrical properties	Good	Good	Good	Good	Good

A) Flexible substrate choice

The choice of flexible substrate for the applications at microwave frequencies is a challenge, because the substrate must exhibits good electrical (e.g. low losses), mechanical and chemical properties. Moreover, the substrate should keep these electrical properties over a wide range of frequencies and under external conditions such as temperature and pressure etc. Finally, substrates used in RF devices should be able to withstand the rigors (e.g. humidity, gasing) of their operating environment and of the fabrication processes used in their packaging [3].

Several flexible substrates used for printed circuit packaging are listed in Table 1, one can see the characterizations of polyethylene teraphthalate (PET) [4], polyethylene naphthalate (PEN) [5], Kapton [6], liquid crystal polymers (LCP) [3] and paper-based substrate [7]. LCP has a nearly constant relative permittivity of 3.1 and low loss (tan δ = 0.002-0.005) up to millimeter wave frequency range, along with a near-hermetic nature (water absorption < 0.04%) which make it suitable for high frequency designs. The paper based substrate is a good candidate thanks to its low cost, but it has limitations issues related to high frequency, absorption, and humidity. Finally, we selected Kapton as substrate for the development of our passive circuits due to its good RF and thermal properties, very good flexibility over a wide temperature range (-73°C to +400°C) and its resistance to many chemical solvents.
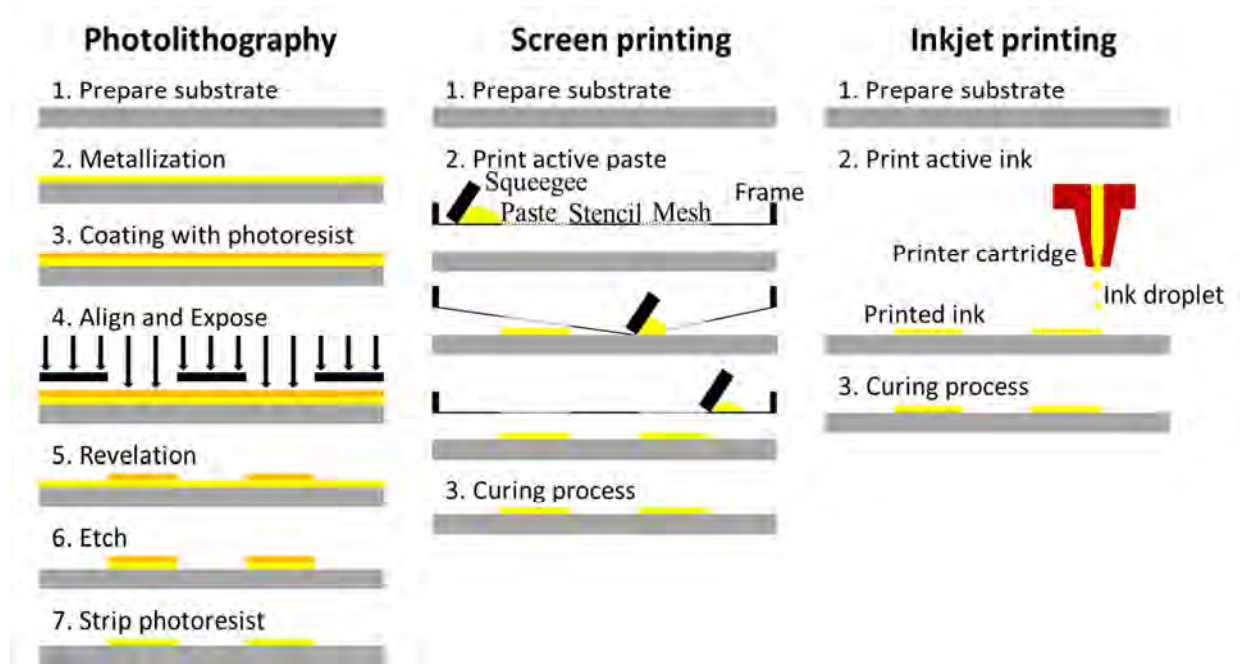
Fig. 1. Comparison of the processing steps involved in subtractive microfabrication, screen printing and inkjet printing [8].

B) Process technology choice

The most widespread technologies used in microfabrication are photolithography, screen printing, and inkjet printing (Fig. 1). Inkjet printing is a direct write technology which presents a low cost advantage because the design pattern is transferred directly to the substrate

and does not require masks. However, the liquid metal nanoparticles used for inkjet printing have much lower conductivity compared to the bulk conductor used for lithography [9][10], which can degrade the printed circuit's performances at RF and millimeter wave frequency. In addition, millimeter wave applications require high accuracy, and both screen printing and inkjet printing can only offer a highest resolution around 20 μm [11]. Antennas fabricated on Kapton at lower frequency have been reported in [12] [13] by using screen printing or inkjet printing, but the traditional photolithography remains the most suitable method for microfabrication at millimeter frequency range.

This paper is organized as follows. The second chapter presents a description of the fabrication process we have developed, followed in the third chapter by a study of Kapton dielectric properties using a ring resonator method. Then, a design of a 60GHz grounded coplanar waveguide feeding patch antenna and two crossed dipoles array antennas at Ku band and K band are described. A prototype of crossed slot dipole antenna at V band is also analysed here. Finally, experimental results concerning the resistivity of Au bump used in flip chip packaging is presented.

II. TECHNOLOGICAL PROCESS FOR FLEXIBLE SUBSTRATE INTEGRATION

To manufacture our circuits onto a flexible substrate, we have chosen the traditional photolithography, the main difficulty during the fabrication process lies on the flexible film handling and its use in micro-technology equipment. In order to overcome this difficulty, a 4-inch silicon wafer is used as a host carrier. One of the critical obstacles consists in finding a way to adhere the polyimide film on the Si support. This adhesion has to be compatible with the various technological stages (vacuum, solvent and temperature) and allows after manufacture a peeling without any physical or chemical constraint.

A matured fabrication process is used where first a PDMS (PolyDiMethylSiloxane) spin coating is performed for the adhesion of the polyimide on the holding wafer. Then the Kapton polyimide is patterned on the PDMS-Si support using a Shipley 360N laminator. A resin spin coating is then realized in a fully automated resist processing tool EVG120, followed by a photolithography process [14].

(a)   (b)
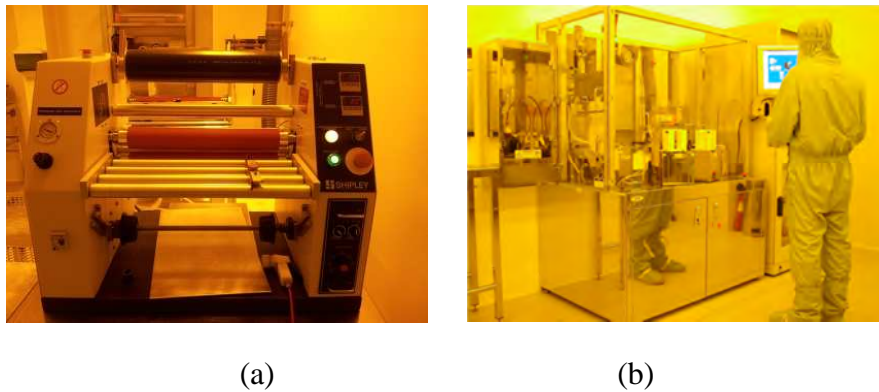
Fig. 2. a) Shipley 360N Laminator; b) EVG120 resist processing system

During the different fabrication processes, Kapton polyimide is metallized with Ti/Au layers (50 nm/ 200 nm) or Ti/Cu layers (50 nm/500 nm) using the Electron Beam Physical Vapor Deposition (EBPVD). In case of Cu coating, the fabrication process will be terminated with a surface finishing (gold immersion deposits) to prevent Cu from oxidizing. Both wet-etching and lift-off methods were carried out during different tests, each of them is able to obtain a sufficient resolution for the metallization tracks.

The skin depths of gold and copper at microwave frequencies are given in Fig. 3. One can see the skin depth decrease with higher frequency. So with the metal thickness mentioned above, selected mainly for V-band applications, high losses at lower frequencies should be expected.
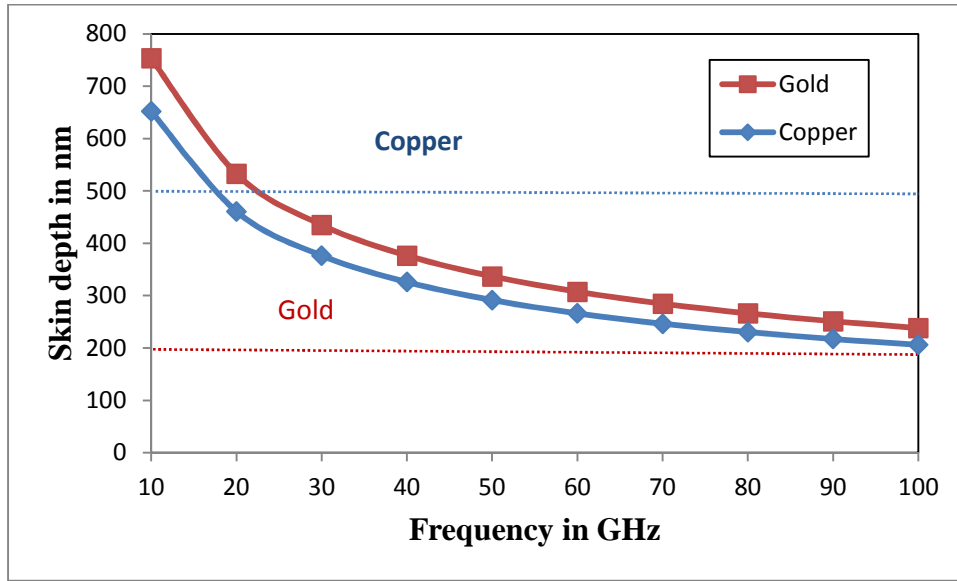
Fig. 3. Skin depth versus frequency, the horizontal lines show the selected metallization thickness

III. CHARACTERIZATION OF KAPTON

A commercially 127-µm Kapton (type 500HN) was chosen as our flexible substrate, which is the thickest product available in the HN series. In fact there is a minimum substrate thickness that must be respected for designing an effective patch antenna in V-band. This antenna is composed by a rectangular patch on the top side of the substrate and a ground plane on the back side. In order to avoid undesired capacitive effect and to ensure a highly-efficient radiation mechanism of a patch antenna, a quick parametric study is done. It shows the influence of substrate thickness versus maximum antenna gain in HFSS simulation [15] (Fig. 4). One can see that the thicker the substrate, the better the antenna gain, regardless its metallization layer: Perfect Electric Conductor (PEC), copper or gold.
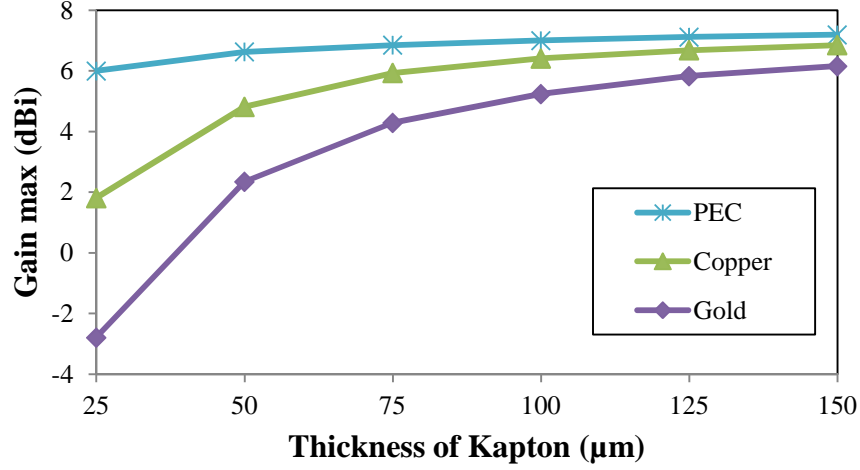
Fig. 4. Maximum simulated antenna gain versus substrate thickness at 60 GHz.

To design properly any high-frequency structure on this 127-μm Kapton by using numerical simulation, the knowledge of dielectric properties of substrate becomes necessary. The dielectric properties of Kapton: the relative permittivity ε_r and the loss tangent tan δ were extracted from S-parameters measurement of a ring resonator [16]. This resonator is composed by a ring with mean radius of 2.95 mm. The width of the microstrip on the Kapton surface is 310 μm to give us a characteristic impedance in the range of 50 Ω. Additionally, a grounded coplanar waveguide (GCPW) to microstrip transition was optimized with the help of HFSS electromagnetic (EM) software to minimize the impedance mismatch. There are two 70 μm gaps at the edges of the ring to couple the resonator with the measurement system, which provides us sufficient coupling to measure the resonator without overload the test equipment (see Fig.5).

The same structures were also modeled using ADS Momentum software [17]. In order to fit measured and simulated data for the entire frequency band, we tuned the dielectric parameters. It is clear that the full 3D Finit Element Method (FEM) used in HFSS software is more accurate than the Method of Moments (MoM) used in ADS Momentum, but in our case, a simulation from 10 to 65 GHz with ADS Momentum is much faster. The correlation between experimental and simulation results is depicted in Fig. 6. Simulated and measured resonant frequencies and quality factors are given in Table 2. The experimental results were obtained by using an Agilent PNA network analyzer and Cascade Microtech GSG probe with a 150 μm pitch. A 2-port on-wafer SOLT calibration method was used. The dielectric properties found for this Kapton polyimide are $\varepsilon_r = 3.2 \pm 0.03$ and tan δ $= 0.012 \pm 0.004$ within the entire frequency band.
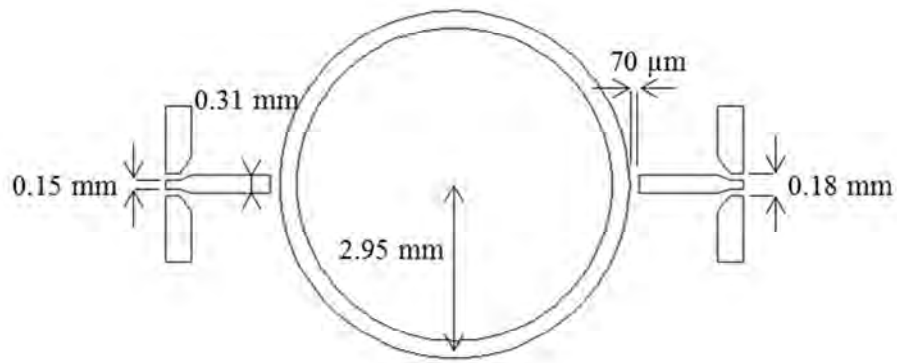
Fig. 5. Ring resonator design
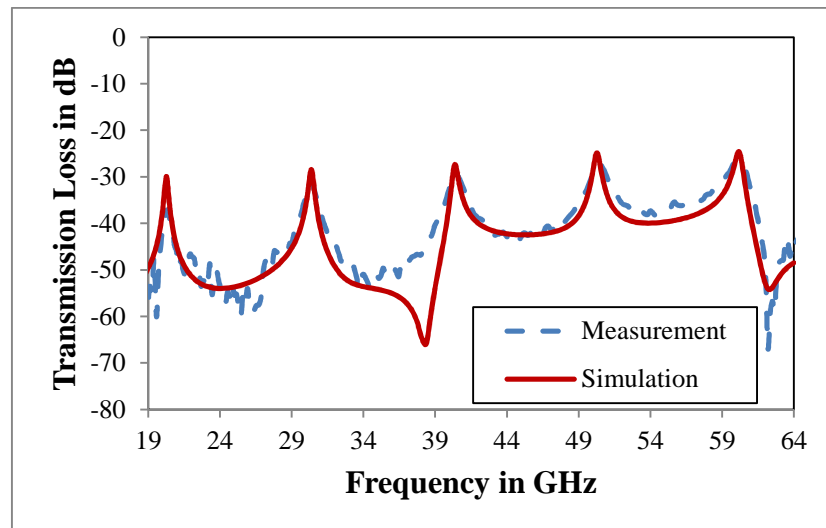
Fig. 6. Simulated and measured insertion loss of the ring resonator.

Table 2. Resonant frequencies & quality factors

Simulation		Measurement	
Resonant Frequency	Q factor	Resonant Frequency	Q factor
20.27	72.4	20.345	36.7
30.36	89.3	30.265	39.1
40.37	98.5	40.34	42
50.28	104.7	50.415	44.4
60.17	114.6	60.18	50.2

IV. DESIGN AND MEASEREMENT OF KAPTON BASED PASSIVE CIRCUITS

A) Patch antenna

A 60 GHz grounded coplanar waveguide (GCPW) feeding rectangular patch antenna (see Fig. 7 a) was designed, fabricated, and measured on a flexible 127-µm-thick polyimide substrate (Kapton). The GCPW-to-microstrip transition was optimized to reduce the impedance mismatch. The antenna was then characterized in terms of return loss, gain, and radiation pattern.
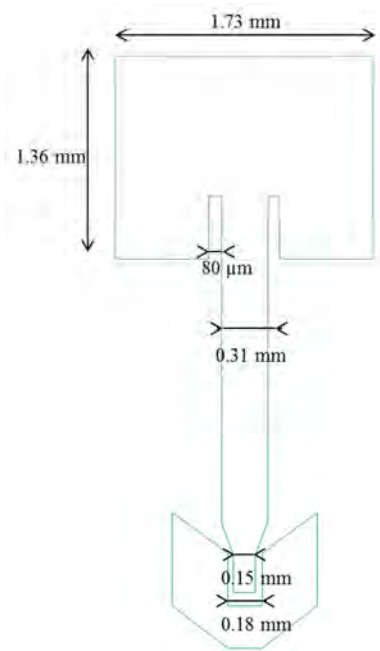
(a)
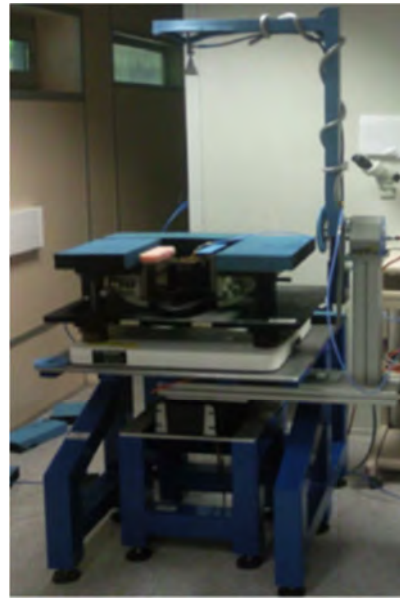
(b)

(c)

Fig. 7. (a) 60GHz GCPW feeding rectangular patch antenna; (b) Measurement setup; (c) Manufactured patch antenna on Kapton
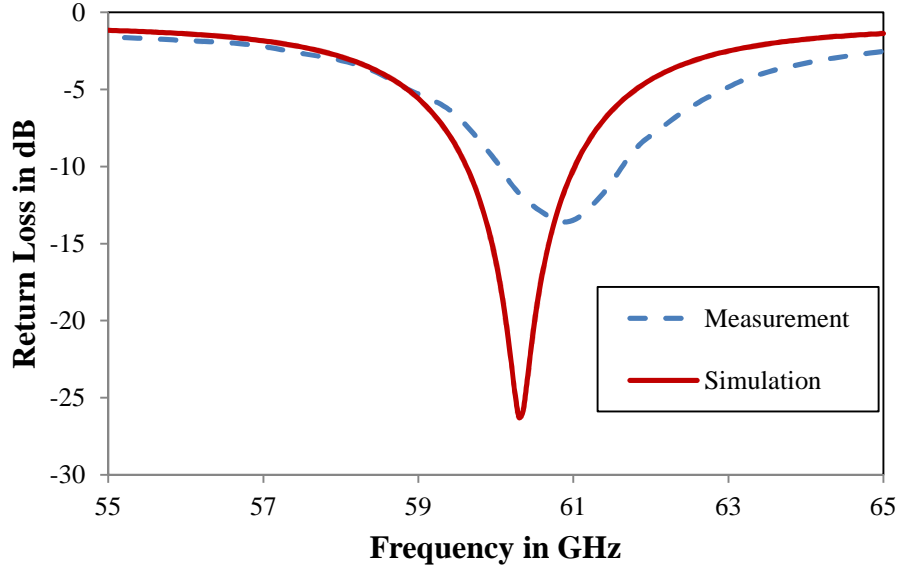
Fig. 8. Simulated and measured return loss of the patch antenna

The simulated and the measured return loss of the patch antenna versus frequency are presented in Fig. 8. The agreement between experiments and simulations is very good: a relative frequency shift of only 0.7% is observed between the simulated (HFSS) and measured results. The difference is due to the uncertainties of the substrate permittivity/permeability value and under/over etching of the conductive patterns. The measured impedance bandwidth, defined by return loss less than -10 dB, is from 60.05 GHz to 61.8 GHz (3% of relative bandwidth).

The far-field radiation pattern and gain measurement were performed with a probe based antenna measurement setup at LAAS (Fig. 7b). The antenna is fed through a 150-µm Ground-Signal-Ground (GSG) probe, and this probe is directly connected to a 65 GHz VNA (Anritsu 37397D) with a flexible V-cable. Dielectric foam from Rohacell was used below the antenna to prevent reflections from the metallic part of the setup. The Antenna Under Test (AUT) was illumined by the field generated by a calibrated VT-15-25-C horn antenna from Vector Telecom.

Under these conditions, a maximum gain of 5 dBi was measured in the perpendicular direction of the antenna at 60.3 GHz. The simulated and measured radiation patterns in the H- and E-plane are given in Fig. 9 and Fig. 10. The difference of gain between simulation and measurement is about 1.7 dB, which may due to insertion loss introduced by the CPW probe and the metallization quality of conductive tracks. The E-plane radiation pattern has a restricted range due to architecture of the measurement setup because the probe was placed in the E-plane. Ripples observed in the E-plane are due to reflection and diffraction effects on the metallic micro-positioner and the probe. The 3dB beamwidth is 56° for the H-plane.

The results demonstrate the quality of fabrication on flexible polyimide substrate and the accuracy of measurement setup for millimeter-wave antenna.
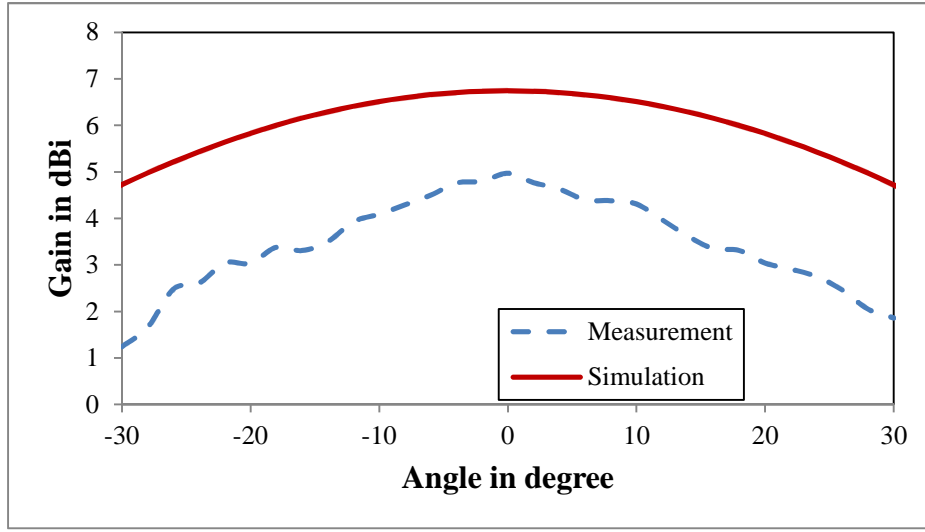
Fig. 9. H-plane radiation patterns of the patch antenna at 60.3 GHz
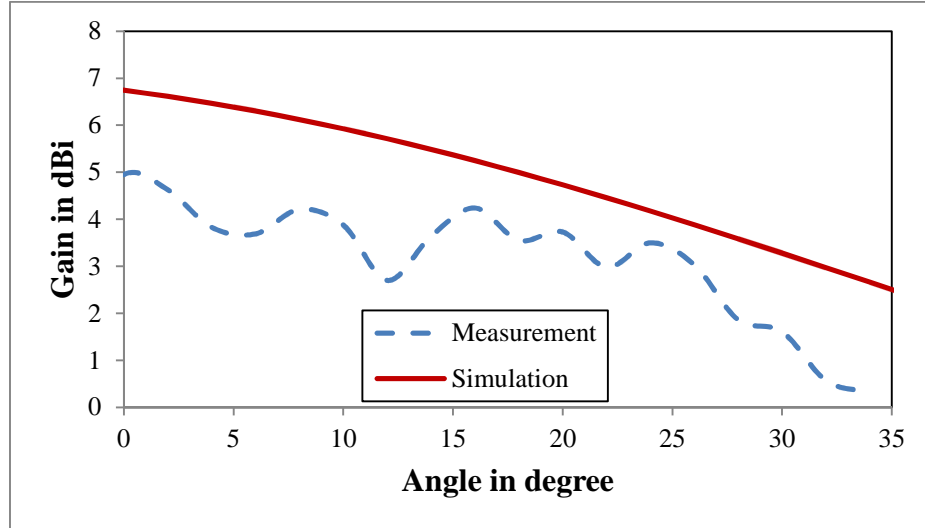
Fig. 10. E-plane radiation patterns of the patch antenna at 60.3 GHz

B)   Cross dipoles array antenna

For the interest of energy harvesting for satellite health monitoring, the cross dipoles array antenna (CDAA) on Kapton polyimide is proposed, which consists of four printed half-wave dipoles arrays on the top side of substrate. As shown in Fig.11, CDAA is a coplanar stripline (CPS) structure. A T-junction CPS-to-microstrip was designed and optimized by using intensive electromagnetic simulations to allow the excitation of the CDAA by a microstrip and the proper connection with a K "end launch" connector from Southwest for measurement purposes [18].

(a)   (b)   (c)
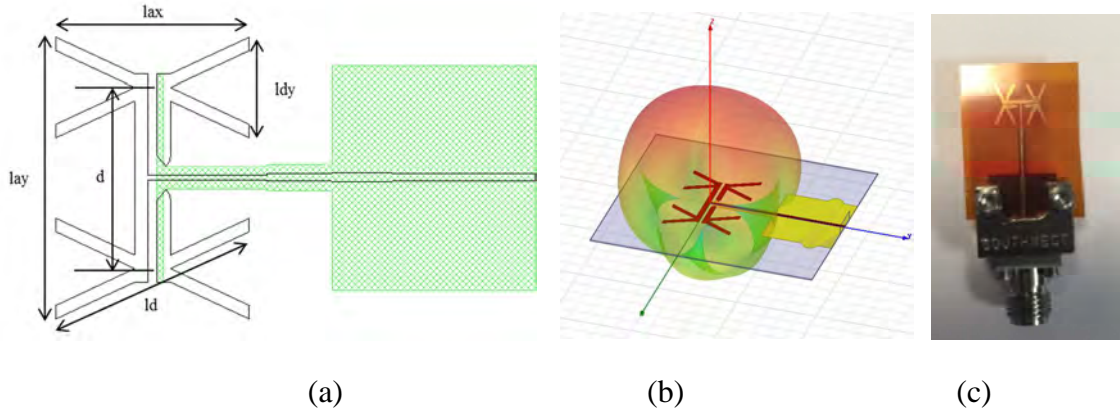
Fig. 11. a) Cross dipoles array antenna: top view of the layout (the bottom layout is represented in filled with green trellis); b) Simulation model; c) manufactured antenna

Table 3. Cross dipoles array antenna dimensions

Band	lax (mm)	lay (mm)	d (mm)	Ld (mm)	Ldy (mm)
Ku	8.5	12.42	8	93.18	4.42
K	5.7	7.5	4.5	6.26	3

Two CDAAs operating in K_u and K band are fabricated and measured respectively, their dimensions are summarized in Table 3. S-parameter measurement and simulation results are reported in Fig. 12 and Fig. 13. One can see a large impedance bandwidth is obtained (measured at S11 = -10 dB) for two proposed antennas, 15.45 GHz to 19.35GHz for the K_u band CDAA (22% of relative bandwidth), and 21.7GHz to 25.7GHz for the K band CDAA (17% of relative bandwidth).

The radiation pattern characterizations were performed in an anechoic chamber. Fig. 14 and Fig. 15 report the measured and simulated radiation patterns in two orthogonal planes at 17 GHz for the K_u band CDAA. Fig. 16 and Fig. 17 report the measured and simulated radiation patterns at 22 GHz for the K band CDAA. We note that the simulation results were obtained in HFSS and the "end-launch" connector was not included in the model. The difference of gain between measurement and simulation is about 2.7 dB may due to (i) the losses introduced by the "end-launch" connector (estimated to be in the range of 1 dB); (ii) the assembling mechanical process for connecting the Kapton structure to the connector that can lead to an imperfect contact; (iii) the skin effect. Metallization layers are composed by: (a) adherent layer of Ti about 50 nm; (b) cooper layer (thickness: 500 nm); (c) gold layer (thickness: a few nanometers). As mentioned in section II, the skin depth of copper at 20 GHz is 460 nm which is comparable with the total metal thickness of 600 nm, thus unexpected RF losses may occur. The ripples observed in the YOZ plane (phi = 90°) are due to reflection and diffraction effects on the connector and the coaxial cable. The 3dB beamwidth is 52° in the XOZ plane and 65° in the YOZ plane for the K_u band CDAA at 17 GHz. For the K band CDAA, The 3dB beamwidth is 58° in the XOZ plane and 62° in the YOZ plane at 22 GHz. As depicted from Fig. 12 to Fig. 17, the proposed CDAAs are wideband antennas (22% of relative bandwidth in Ku band and 17% of relative bandwidth in

K band). The radiation pattern do not change significantly in the relative bandwidth and the measured maximum gain is about 4.3 dBi (included the losses added by the end lunch connector and the associated mounting process and by CPS-to-microstrip T junction). We note that the gain can be increased by 3dB if a metallic plate acting as reflector is properly putted below the CDAA.
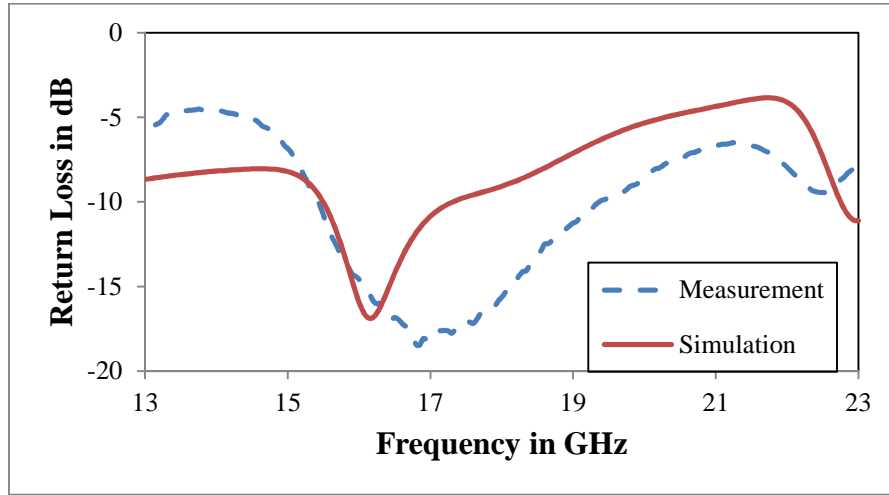
Fig. 12. Simulated and measured return loss of the K_u band CDAA
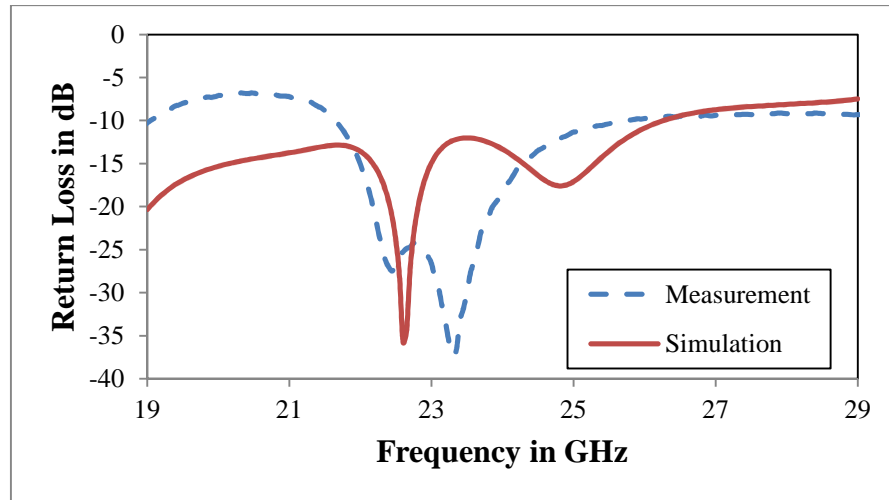
Fig. 13. Simulated and measured return loss of the K band CDAA
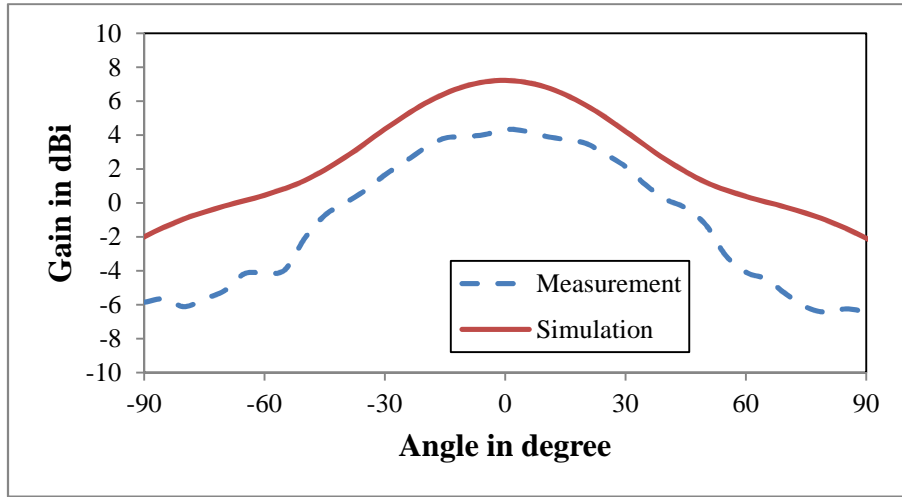
Fig. 14. XOZ plane (phi = 0°) radiation patterns of the K_u band CDAA at 17 GHz
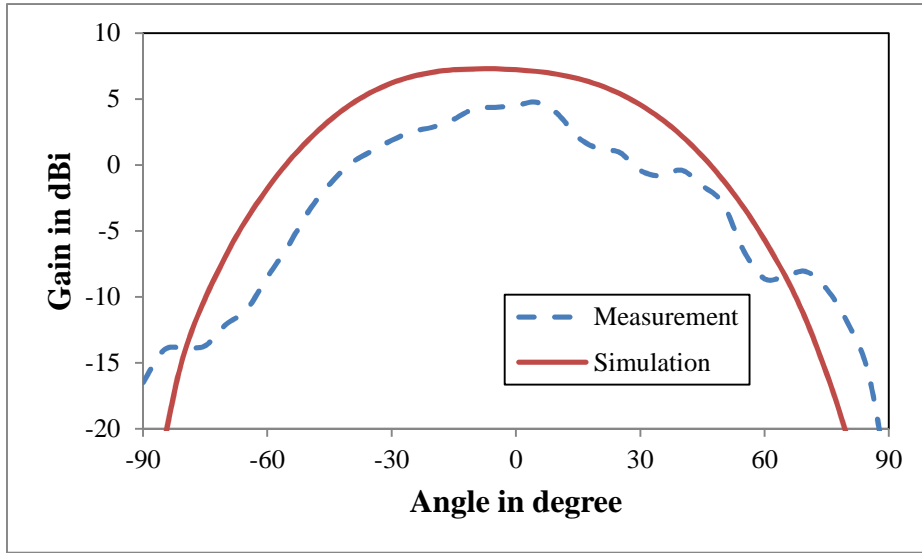
Fig. 15. YOZ plane (phi = 90°) radiation patterns of the K_u band CDAA at 17 GHz
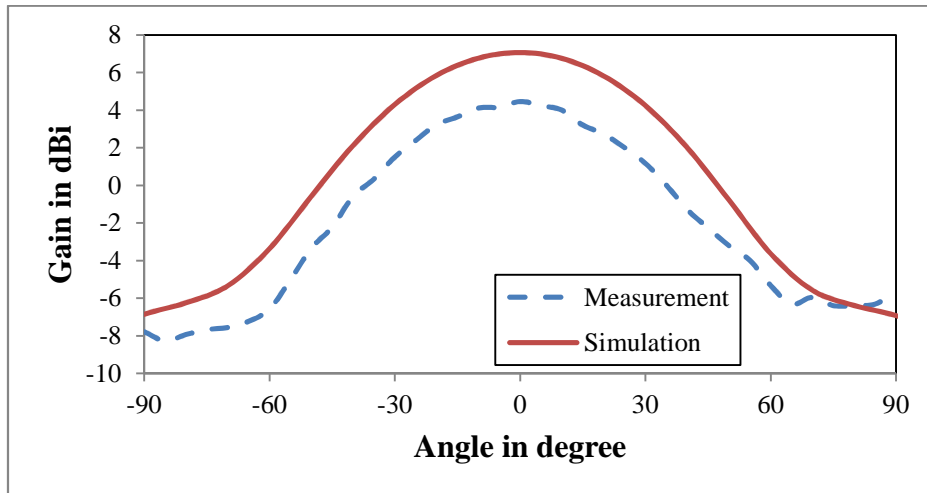
Fig. 16. XOZ plane (phi = 0°) radiation patterns of the K band CDAA at 22 GHz
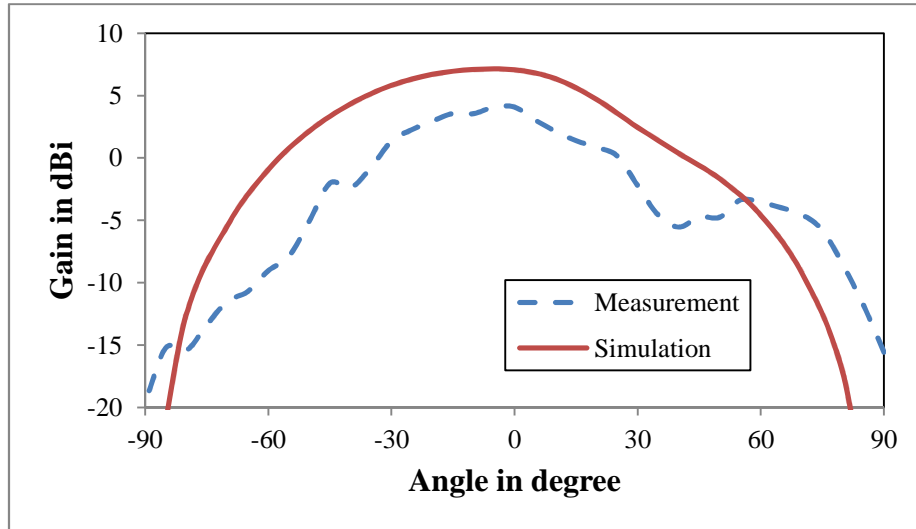
Fig. 17. YOZ plane (phi = 90°) radiation patterns of the K band CDAA at 22 GHz

C) Cross slot dipole antenna

Inspired by the design of CDAAs at K_u band and K band, and the Babinet's principle which relates the radiated field and impedance of a slot antenna to a printed (strip) antenna, a first prototype of Crossed Slot Dipole Antenna (CSDA) in V band is proposed shown in Fig. 18. The antenna is designed on a 127-µm thick Kapton with a dielectric constant 3.2 and a loss tangent 0.006. CPW feed dimensions of S = 170 µm and G = 12 µm were selected corresponding to the 50 Ohm GSG probe. The slot length L is fixed to 1.3 mm (quarter wavelength for 60 GHz) for the simulation, the slot width w, the stub length d and the angle between slots α were set to 40 µm, 0.69 mm and 45° as default respectively.

(a)   (b)
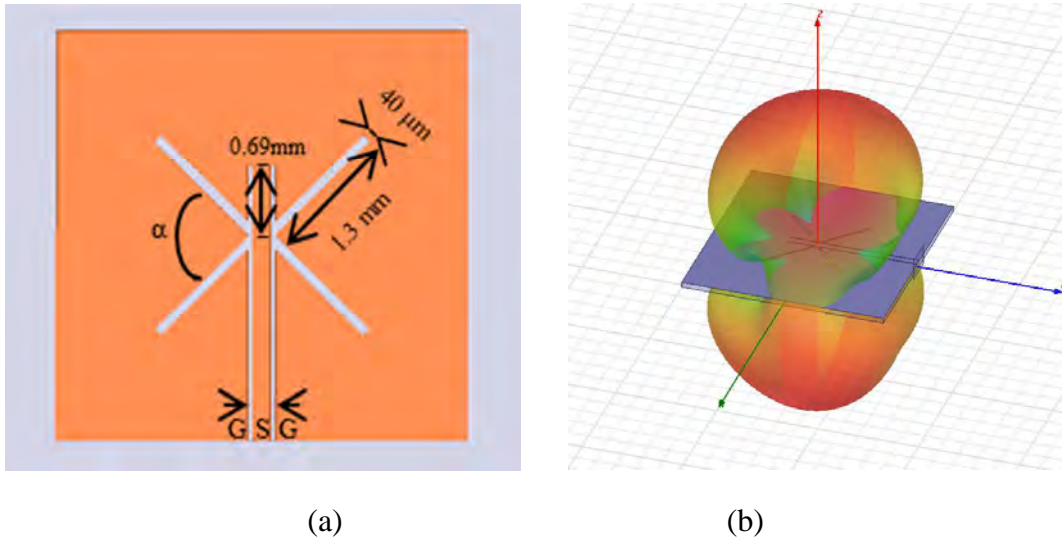
Fig. 18. a) Design of crossed slot dipole antenna; b) Simulation model

Fig. 19 shows the simulated return loss. The center frequency is 60.2 GHz, and the -10 dB bandwidth is from 58.2 GHz to 62.05 GHz (6% of relative bandwidth). The antenna radiation

patterns were also presented in Fig. 20, a peak antenna gain of 4.02 dB is obtained at 60.2 GHz.
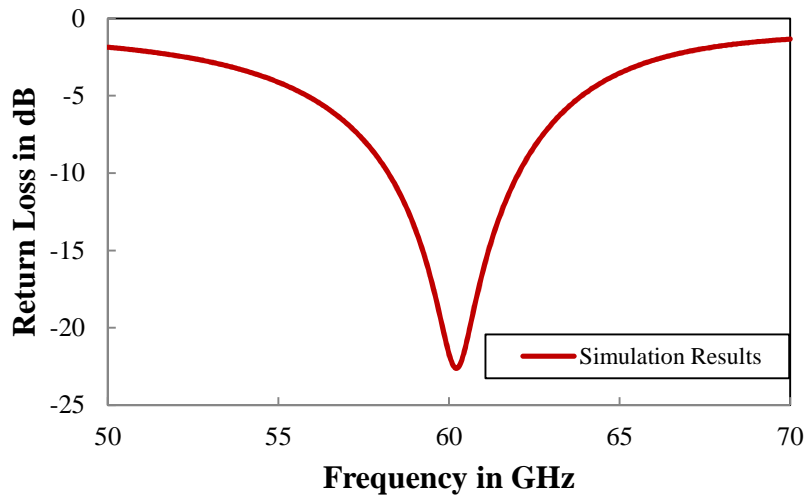
Fig. 19. Simulated return loss of the cross slot dipole antenna
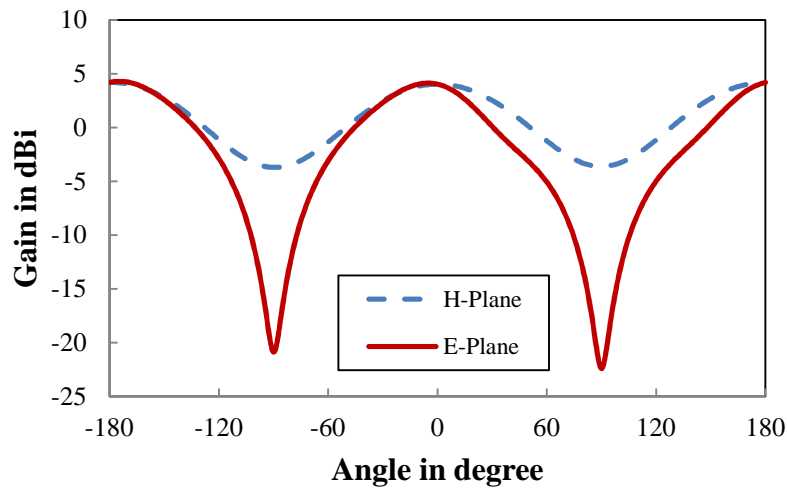
Fig. 20. Simulated (HFSS) radiation patterns in E-Plane and H-Plane at 60.2 GHz

A parametric study for the angle between slots is shown in Table 4. It is seen that when the angle α increase, the peak antenna gain decrease along with a larger half power beamwidth (HPBW) on H-plane. This phenomenon can be explained by the increase of the coupling effect when the slots approach each other.

As demonstrated by the simulation, CSDA has interesting performances in 60 GHz band. This antenna has no ground plane and in V band its performances (input matching and radiation pattern) can be impacted by the surrounding environment placed behind the antenna (the metallic chuck of the probe station used for S-parameters measurement or the dielectric

supporting plate of the antenna setup shown in Fig. 7 b). In order to avoid such issues and obtain a good correlation between simulation and measurements two solutions can be envisaged: (i) redesign this antenna by using a reflector/ground plane properly positioned behind the antenna and (ii) re-simulate the antenna taking into account a representative 3D model of the surrounding environment. Both solutions are time consuming and were not implemented before the submission of this paper.

Table 4. Study of angle α effect on radiation

α (°)	fc (GHz)	Return Loss (dB)	Maximum Gain	HPBW (°)
40	59.7	-21.09	4.14	82
45	60.2	-22.76	4.02	86
50	61.15	-27.48	40.8	90

V.   INTEGRATION ASSEMBLY TEST

For the purpose of integration of different components on Kapton polyimide, different dummy circuits are realised and mounted by using a well matured flip chip technique established in LAAS-CNRS as shown in Fig. 21 [19]. To measure the quality of the contacts, four probe method was used to characterize the bumps resistivity as shown in Fig. 22. A resistance about 10 mΩ was measured for the Au bump, which proves a very good DC contact has been achieved by using this technique.
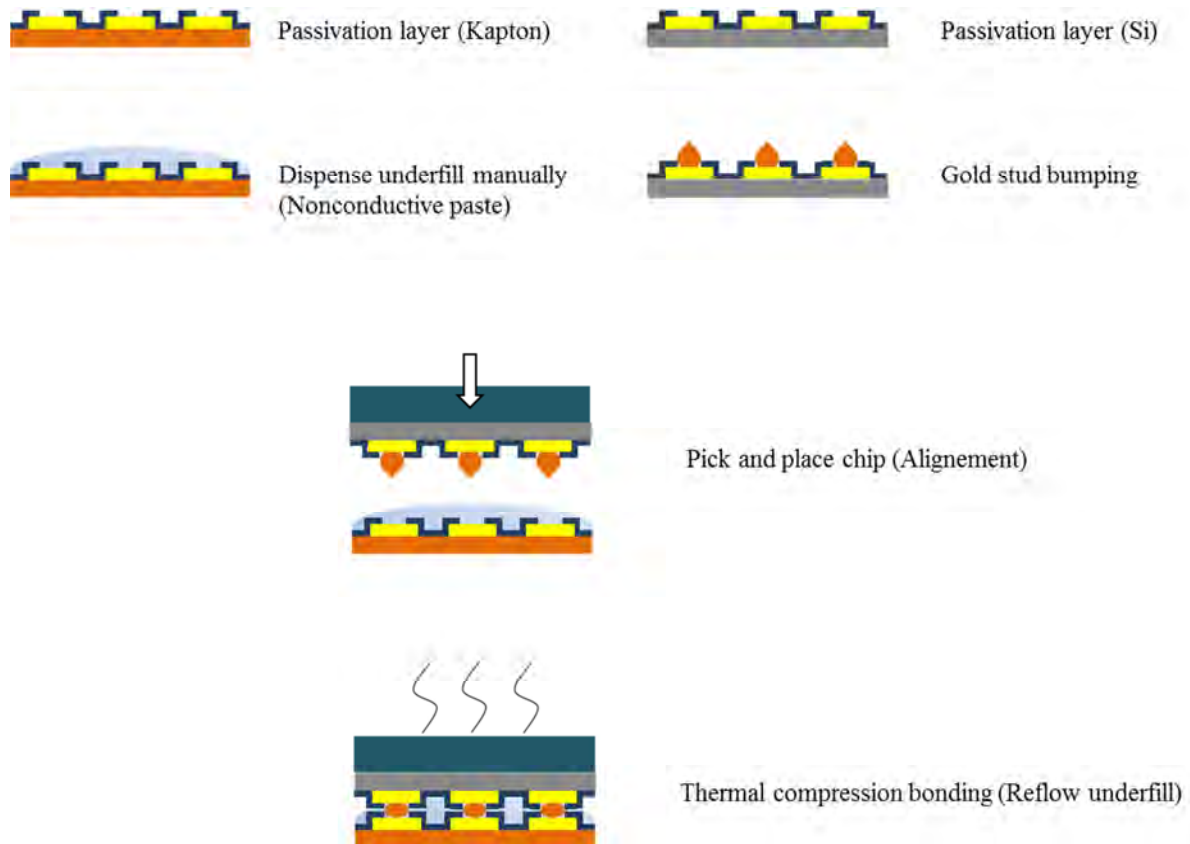
Fig. 21 Description of flip chip process
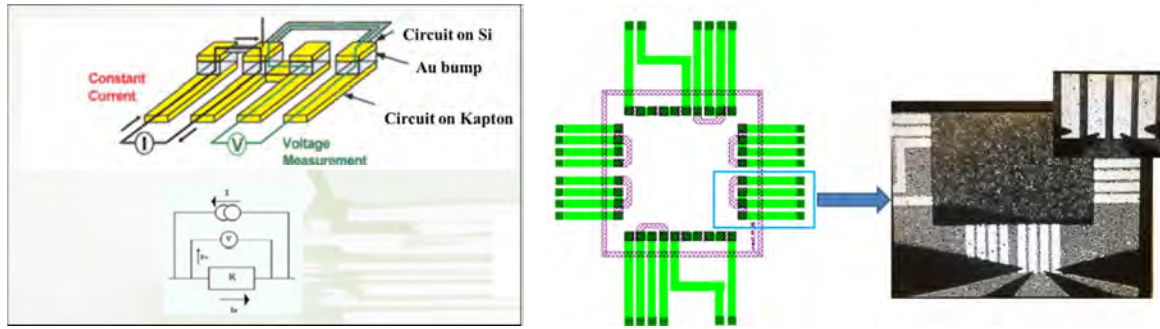
Fig. 22. Four probe method resistivity measurement

The presented Kapton supported technology can be used to develop millimeter wave circuits by heterogeneous integration for the implementation of wireless sensors network (including autonomous wireless sensors by using energy harvesting or wireless power transfer techniques). The RF power used for that application is generally very low and is subject to regulation. For example in V-band, the EIRP limitations for operation in the US limits [20] the EIRP at 40 dBm (conducted power up to 27 dBm). In Europe [21], stipulates a maximum conducted power of less than +10 dBm. To the author best knowledge, these (maximum) authorized power levels are not critical for Kapton technology that has a very good thermal behavior.

VI. Conclusion

In this work, we demonstrate the feasibility of manufacturing microwave passive circuits at high frequency on a commercially available polyimide Kapton substrate through a traditional photolithography process. A 60 GHz patch antenna has been designed, fabricated, and measured to validate our technology. Crossed dipoles array antenna at Ku band and K band for energy harvesting have also been designed, fabricated and measured. Simulation results agree well with the experimental results, only 0.7% of frequency shift is observed for return loss of 60 GHz patch antenna, 6.2% and 3.1% for K_u and K band CDAA respectively. Future measurement for the cross slot dipole antenna will be carry on. The results of flip chip test are one step further towards a heterogeneous integration on flexible substrate of different components for autonomous wireless sensor nodes using wireless power transfer.

REFERENCES

[1] Wong, W.S.; Salleo, A.: Flexible Electronics: Materials and Applications, Springer Publishing Company, Incorporated, 2009.

[2] Vyas, R.; Rida, A.; Bhattacharya, S.; Tentzeris, M.M.: Liquid Crystal Polymer (LCP): The ultimate solution for low-cost RF flexible electronics and antennas, in Antennas and Propagation Society International Symp., 2007, 1729-1732.

[3] Printing Technology for Flexible Substrates, InterLingua Publishing, 2006.

[4] Hettak, K.; Petosa, A.; James, R.: Flexible plastic-based inkjet printed CPW fed dipole antenna for 60 GHz ISM applications, in Antennas and Propagation Society International Symp., 2014, 328-329.

[5] Bisognin, A.; Thielleux, J.; Wei Wei; Titz, D.; Ferrero, F.; Brachat, P.; Jacquemod, G.; Happy, H.; Luxey, C.: Inkjet Coplanar Square Monopole on Flexible Substrate for 60-GHz Applications, Antennas and Wireless Propagation Letters, IEEE, 13(2014), 435-438.

[6] http://www.dupont.com/content/dam/assets/products-and-services/membranes-films/assets/ DEC-Kapton-summary-of-properties.pdf.

[7] Shaker, G.; Safavi-Naeini, Safieddin; Sangary, N.; Tentzeris, M.M.: Inkjet Printing of Ultrawideband (UWB) Antennas on Paper-Based Substrates, Antennas and Wireless Propagation Letters, IEEE , 10(2011), 111-114.

[8] Chauraya, A.; Whittow, W.G.; Vardaxoglou, J.C.; Yi Li; Torah, R.; Kai Yang; Beeby, S.; Tudor, J.: Inkjet printed dipole antennas on textiles for wearable communications, Microwaves, Antennas & Propagation, IET , 7(9)(2013), 760-767.

[9] Swaisaenyakorn, S.; Young, P.R.; Shkunov, M.: Characterization of ink-jet printed CPW on Kapton substrates at 60 GHz, in Antennas and Propagation Conf. LAPC, Loughborough, 2014, 676-678.

[10] Belhaj, M.M.; Wei Wei; Pallecchi, E.; Mismer, C.; Roch-jeune, I.; Happy, H.: Inkjet printed flexible transmission lines for high frequency applications up to 67 GHz, in European Microwave Conf., EuMC 2014, 1528-1531.

[11] Singh, M.; Haverinen, H.M.; Dhagat,P.; Jabbour, G.E.: Inkjet printing—process and its applications, Advanced materials, 22(6)(2010),673-685.

[12] Ahmed, S.; Tahir, F.A.; Shamim, A.; Cheema, H.M.: A Compact Kapton-based Inkjet Printed Multiband Antenna for Flexible Wireless Devices, Antennas and Wireless Propagation Letters, IEEE, 99(2015),1-1.

[13] Aziz, M.A.; Roy, S.; Berge, L.A.; Irfanullah; Nariyal, S.; Braaten, B.D.: A conformal CPW folded slot antenna array printed on a Kapton substrate, Antennas and Propagation EUCAP, 2012, 159-162.

[14] Jatlaoui, M.M.; Dragomirescu, D.; Charlot, S.; Pons, P.; Aubert, H.; Plana, R.: 3D heterogeneous integration of wireless communicating nano-sensors on flexible substrate, Proc. SPIE 7821, Advanced Topics in Optoelectronics, Microelectronics, and Nanotechnologies, 2010.

[15] http://www.ansys.com/Products/Simulation+Technology/Electronics/Signal+Integrity/ ANSYS+HFSS

[16] Thompson, D.; Tantot, O.; Jallageas, Hubert; Ponchak, G.E.; Tentzeris, M.M.; Papapolymerou, J.: Characterization of liquid crystal polymer (LCP) material and transmission lines on LCP substrates from 30 to 110 GHz, Microwave Theory and Techniques, IEEE Trans., 52(4)(2004), 1343-1352.

[17]   http://www.keysight.com/en/pc-1887116/momentum-3d-planar-em-simulator?nid=-33748.0&cc=US&lc=eng.

[18] Takacs, A.; Aubert, H.; Fredon, S.; Despoisse, L.: Design and Characterization of Effective Antennas for K-band Rectennas, in Antennas and Propagation EUCAP, 2015, 1-4.

[19] Jatlaoui, M.M.; Dragomirescu, D.; Ercoli, M.; Krämer, M.; Charlot, S.; Pons, P.; Aubert, H.; Plana, R.: Wireless communicating nodes at 60 GHz integrated on flexible substrate for short-distance instrumentation in aeronautics and space, International Journal of Microwave and Wireless Technologies, 4(2012), 109-117.

[20] https://www.fcc.gov/document/part-15-rules-unlicensed-operation-57-64-ghz-band.

[21] http://www.erodocdb.dk/docs/doc98/official/pdf/Rec0901.pdf.

Microstrip slow-wave line for phase shifting cells

M. Gastaldi✉, D. Dragomirescu, A. Takacs, V. Armengaud and S. Rochette

The design, simulation and measurements of microstrip slow-wave lines implemented in a 0.25 μm SiGe bipolar CMOS (BiCMOS) process is addressed for Ku-band (10–15 GHz) applications. The simulation results and the measurements show better performances for the proposed microstrip slow-wave line compared with the classical microstrip transmission line. These lines present very low insertion losses and a high phase constant.

Introduction: Slow-wave lines (SWLs) are a specific topology of transmission lines that uses the slow-wave phenomenon in order to miniaturise the physical length of a line [1, 2]. Nowadays, CMOS and bipolar CMOS (BiCMOS) technologies are increasingly used for microwave circuits [3] and have become a promising candidate for core-chip circuits used in satellite beamforming antenna control systems (BACS). Mainly for the phase shifter of BACS, the use of microstrip lines requires an important area on the chip. SWL technology can be a valuable candidate for minimising the occupied area on the chip by the microstrip lines used for interconnection or phase shifting [2, 4, 5].

The most common transmission lines implemented using SWL technology are the shielded coplanar waveguide [2]. Nevertheless shielded microstrip lines (S-MSLs) can be designed. This particular type of SWL allows a very compact structure because a large gap is not required. This Letter addresses the design, the simulation and the experimental results of a S-MSL implemented in a 0.25 μm BiCMOS process from IHP.

Results: The stack layers of the used BiCMOS process are represented in Fig. 1. The back end of this technology offers five metal layers: three thin aluminium layers and two thick layers fit for transmission lines and inductors design.
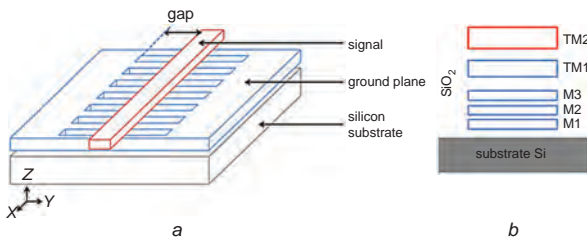
Fig. 1 *Proposed microstrip SWL(S-MSL) in BiCMOS process*
a Simplified structure
b Cross-section of 0.25 μm BiCMOS process
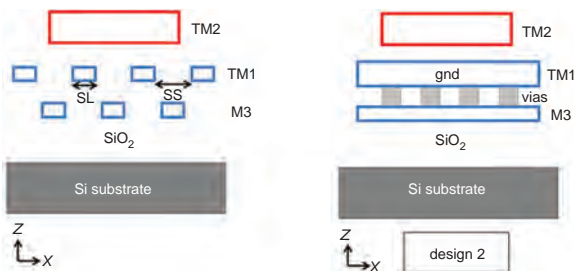
Fig. 2 *Cross-section view of S-MSL structure*

The position of the metal strips forming the ground plane varies for the two structures presented in this Letter. The signal line is always located on the superior metal layer (TM2) while the periodic metal strips are located on the top metal 1 layer (TM1 (design 1)) or on the layer TM1 and M3 (design 2). The two thick metal layers TM2 and TM1 are separated by a 2 μm layer of SiO₂. The capacitance per unit of length (C) is maximised by positioning the metal strips on the layers closest to the signal. However, even in this configuration, the value of the capacitance per unit of length is relatively small conducting to a poor quality factor.

The metal strips in the second design are connected by vias (Fig. 2). This disposition of these strips prevents more effectively the E-field from penetrating inside the substrate and thus improves the quality factor Q.

The metal strips are disposed orthogonally to the direction of propagation so the return currents cannot flow directly under the signal contrary to classical microstrip lines. By making these currents flow far away from the signal line, it is then possible to artificially improve the inductance per unit of length (L). A diminution of the phase velocity for a transmission line can be achieved by controlling C and L

$$V_p = c/\sqrt{\mu_r \varepsilon_r} = 1/\sqrt{LC} \qquad (1)$$

where L is series inductance per unit length and C denotes shunt capacitance per unit length.

The structures (S-MSL and MSL) implemented in 0.25 μm SiGe BiCMOS process were electromagnetically simulated using high-frequency structure simulator software. The manufactured samples were also measured using a vector network analyser (VNA) (Anritsu ME7808A). The S-parameters, attenuation (α) and phase (β) constants were measured/extracted after de-embedding. A special designed Thru, Reflect, Line (TRL) calibration kit was manufactured on the die for de-embed the impact of the microstrip access lines (length: 150 μm) on the S-MSL.

S-parameter measurements were performed with a VNA using a standard SOLT calibration procedure followed by the TRL calibration. A layout view of the structures is shown in Fig. 3. The lines are 500 μm long (a minimum length of 300 μm is required to avoid measurement errors due to the coupling between the probes). The reference MSL is also used as 'line element' in the TRL kit (Fig. 3 bottom left corner). The S-MSLs are preceded by a line length of Thru/2 that will be removed by de-embedding.
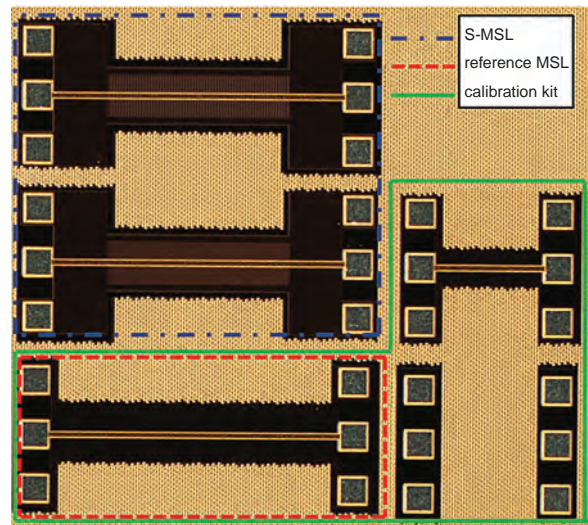
Fig. 3 *Layout photograph of manufactured die including reference microstrip line, S-MSL and TRL calibration kit*

Fig. 4 shows the different measurements and the comparison between S-MSL and MSL. The width of the MSL signal line is $w = 15$ μm conducting to a characteristic impedance of 50 Ω for the reference MSL. The S-MSLs presented here were obtained after the optimisation of three geometrical parameters: SL (the width of the metal strips shown Fig. 2), SS (the strip spacing, Fig. 2) and the gap (the distance between the signal line and the ground plane, cf Fig. 1). The strip spacing was chosen to minimise the eddy currents loss (SS = 6 μm, SL = 2 μm).

The experimental results of the phase constant β show that the structures are working for Ku-band. However, the attenuation of the first S-MSL is 0.42 dB/mm (0.5 dB/mm for design 2) at 12.5 GHz against 0.24 dB/mm for the MSL. The reference MSL has a quality factor inferior to the S-MSL structures. The differences between the MSL and S-MSL appear also in Fig. 4*a*.

The simulation results (not detailed here) demonstrated that the closer the signal is to the ground plane, the more α and β decreases. The gap must be sized as a function of the system specifications (losses and

capacity). According to this work, a reduction of 58% can be expected for the length of the transmission line by using a M-SWL instead of a classical MSL for a targeted phase shift. A 1.78 mm-long conventional MSL is necessary to achieve a 45° phase shift (insertion loss of 0.3–0.4 dB). For the same phase shift a length of only 740 µm is required with the S-MSL (insertion loss of 0.25–0.34 dB). The gap of the fabricated S-MSL is 50 µm which is relatively small compared with other SWLs at 12.5 GHz.
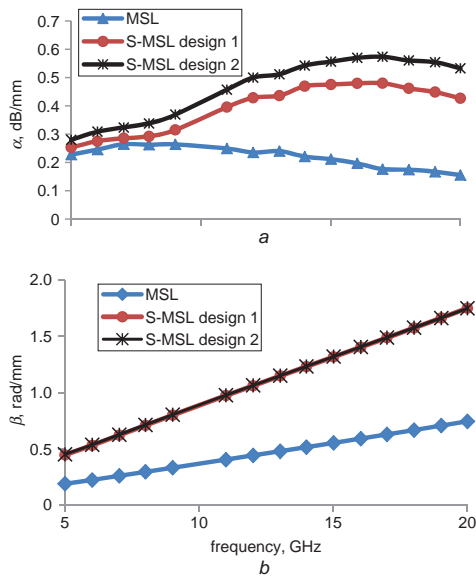
Fig. 4 *Comparison between MSL and S-MSL performances (measurements)*
a Attenuation constant (dB/mm)
b Phase constant (rad/mm)

Conclusion: This Letter has presented two designs of S-MSLs implemented in 0.25 µm SiGe BiCMOS technology. The experimental results show an improvement of the phase constant by a factor 2.4 (β

is improved by 2.4 at 12.5 GHz) compared with the reference MSL while the attenuation constant is not strongly impacted. Thus, the proposed S-MSLs are a very interesting candidates for phase shifting cells.

M. Gastaldi, D. Dragomirescu and A. Takacs (*CNRS, LAAS, 7 Avenue du colonel Roche, F-31400 Toulouse, France*)

✉ E-mail: mgastald@laas.fr

V. Armengaud (*CNES RF/HT, 18 Avenue Edouard Belin, 31400 Toulouse, France*)

S. Rochette (*Thales Alenia Space, 26 Avenue JF. Champollion, BP1187, F-31037 Toulouse Cedex 1, France*)

References

1 Cheung, T.S.D., and Long, J.R.: 'Shielded passive devices for silicon-based monolithic microwave and millimeter-wave integrated circuits', *IEEE J. Solid-State Circuits*, 2006, **41**, (5), pp. 1183–1200, doi: 10.1109/JSSC.2006.872737

2 Tang, X.-L., Franc, A.-L., Pistono, E., Siligaris, A., Vincent, P., Ferrari, P., and Fournier, J.: 'Performance improvement versus CPW and loss distribution analysis of slow-wave CPW in 65 nm HR-SOI CMOS technology', *IEEE Trans. Electron Devices*, 2012, **59**, (5), pp. 1279–1285, doi: 10.1109/TED.2012.2186969

3 Heydari, B., Bohsali, M., Adabi, E., and Niknejad, A.M.: 'Low-power mm-wave components up to 104 GHz in 90 nm CMOS' IEEE ISSCC Dig. Tech. Pap., San Francisco, CA, USA, February 2007, pp. 200–597, doi: 10.1109/ISSCC.2007.373363

4 Lee, J.J., and Park, C.-S.: 'A slow-wave microstrip line with a high-Q and a high dielectric constant for millimeter-wave CMOS application', *IEEE Microw. Wirel. Compon. Lett.*, 2010, **20**, (7), pp. 381–383, doi: 10.1109/LMWC.2010.2049430

5 Dinc, T., Kalyoncu, I., and Gurbuz, Y.: 'An X-band slow-wave T/R switch in 0.25 µm SiGe BiCMOS', *IEEE Trans. Circuits Syst. II, Express Briefs*, 2014, **61**, (2), pp. 65–69, doi: 10.1109/TCSII.2013.2291094

IEEE *Access*

Multidisciplinary : Rapid Review : Open Access Journal

Towards the Design of Wireless Communicating Reinforced Concrete

Gaël Loubet[1], Alexandru Takacs[1, 2], Member, IEEE, and Daniela Dragomirescu[1, 3], Senior Member, IEEE

[1]Laboratory for Analysis and Architecture of Systems (LAAS), National Center for Scientific Research (CNRS), Toulouse, F-31031 France.
[2]University Paul Sabatier (UPS), University of Toulouse, Toulouse, F-31062 France.
[3]National Institute of Applied Sciences (INSA) of Toulouse, Toulouse, F-31077, France.

Corresponding author: Gaël Loubet (e-mail: gael.loubet@laas.fr).

ABSTRACT This paper addresses the concept of a smart-node wireless network designed for structural health monitoring applications. The network architecture is based on a smart mesh composed of sensing nodes and communicating nodes. The sensing nodes are used to implement the so named communicating material/communicating concrete and collect physical data for structural health monitoring purposes. These data are sent to the communicating nodes that interface the smart-node network with the digital world through the Internet. The sensing nodes are batteryless and wirelessly powered by the communicating nodes *via* a wireless power transmission interface. Experimental results have been obtained for a simplified sensing node using a LoRaWAN uplink wireless communication (from the sensing node to the communicating node) proving that the functionality of the sensing nodes can be controlled wirelessly by using only the wireless power transmission downlink.

INDEX TERMS Communicating Materials, Wireless Power Transmission (WPT), Wireless Sensor Network (WSN).

I. INTRODUCTION

The emerging of Internet of Things (IoT) technologies has generated many new possibilities in the field of Structural Health Monitoring (SHM) of buildings and civil and transportation infrastructures (e.g. railway and subway stations, bridges, highways, etc.). Also, the structural health monitoring of buildings, through innovative IoT technologies and approaches, is part of the Smart City concepts and paradigms. Recently, the Building Information Modeling (BIM) concept [1] has provided new tools to more efficiently plan, design, construct, and manage buildings and infrastructures.

An innovative approach to implement the SHM and BIM concepts for construction, civil and transportation engineering is the use of the so named 'communicating material' [2]. The research project McBIM [3] - Communicating Material at the disposal of the Building Information Modeling- aims to provide a practical application of the concept of communicating material in the construction domain, namely communicating precast reinforced concrete. This will be intrinsically able to

generate, process, store and exchange data over several meters or more from its environment and internal physical states to dedicated system(s) -in particular a virtual model: the BIM-, with the ability to function for several decades.

A few works have already provided implementations of communicating materials based on Radio Frequency Identification (RFID) for various materials and aims. Among them can be found the storage and access at short range of some disseminated data in wood [4], textile [5], and concrete [6].

Reinforced concrete is the most common construction material thanks to its scalability, durability and cost [7]. Three particular stages of its life cycle are targeted: the manufacture and storage of precast elements, the construction of a structure, and the exploitation of these construction works, particularly through structural health monitoring. The works [6], [8], [9], and [10] suggest incomplete solutions for the three targeted applications by the project. To implement the 'communicating concrete' concept we propose here a smart wireless micro-nodes network able to sense, store, and communicate data; autonomous in terms

of energy; resilient; and connectable to a digital model. The issues concerning installation and maintenance costs are considered, as well as the need of a system that can reliably function for decades.

In Section II of this paper, we will succinctly introduce the envisaged architecture for the wireless micro-nodes network, as well as describing each of its components, namely the communicating (CN) and sensing nodes (SN). The sensing nodes are intended to be embedded in concrete and operate for decades, without any maintenance. Thus, a batteryless approach by using a Wireless Power Transfer (WPT) interface is proposed in order to increase the lifetime and to avoid the maintenance issue. Preliminary results concerning our first prototype of the sensing node, which communicates through the LoRaWAN protocol, are presented in Section III. SN is wirelessly supplied and an innovative and original concept is proposed in Section IV: to control the periodicity of communication - to control the periodicity of communications -and eventually measurements- by using a well-defined and tailored wireless power transfer system. The inherent constraints of the proposed concept as well as the potential improvements are discussed in Section V.

II. WIRELESS NETWORK ARCHITECTURE FOR COMMUNICATING CONCRETE AND MATERIALS

A. ARCHITECTURE OF THE WIRELESS SMART-NODE NETWORK

In order to implement a communicating concrete, a wireless smart-nodes network is set-up by embedding interconnected SNs and CNs into precast reinforced concrete elements.

Each concrete element hosts one or two communicating nodes -located at the concrete/air interface-, and several sensing ones -randomly located in the concrete-, as presented in Fig. 1. Their number will be a function of the physical properties of the concrete element and of an adopted scenario (defined by the end-user). The communication between the SNs and CNs can be made through the concrete (in the case of neighboring SNs and CNs, i.e. embedded in the same concrete element) or across the air or by all combination of air and concrete as a function of the relative positions of the SNs and CNs. As detailed in the next section, SNs should be low power and batteryless whilst being inaccessible for maintenance whereas CNs will be connected to an energy source (wired electric grid or a high capacitance battery) and accessible for maintenance. The storage of data -in each element and for the entire building- must be redundant, globalized, and secured. For each construction, one or more access points to the digital world -especially to communicate with the BIM- will be available and reprogrammable in order to meet the needs of each stages of the life cycle of the communicating concrete. The term 'real world' is used here to describe the communications and the interactions between SNs and CNs or between various CNs on a physical level (i.e. between the nodes located in neighboring concrete

elements belonging to the same building or civil infrastructure) whereas the term 'digital word' denotes the data exchange performed on the Internet. The proposed wireless smart-node network acts on a 'real word' to collect data and physical measurements and send those data to the digital word where the data are analyzed, stored and used for various (end-user defined) purposes.
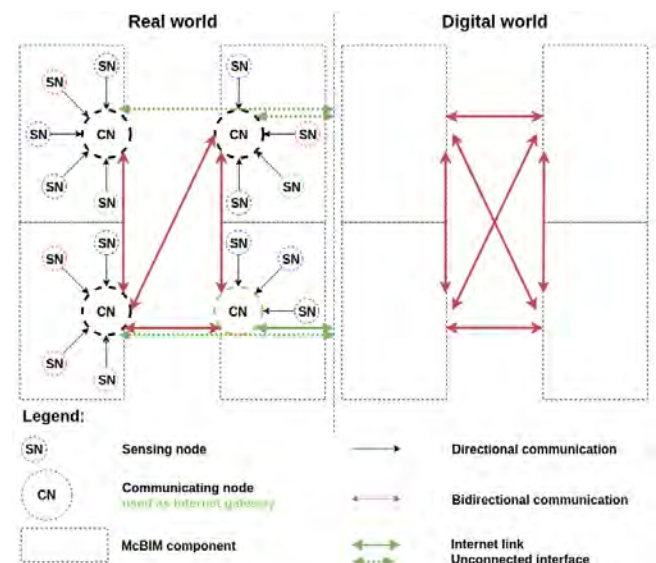
FIGURE 1. Schematic diagram for the envisaged architecture of the smart-nodes network embedded in the precast reinforced concrete.

B. TOPOLOGY OF COMMUNICATING NODES

The topology of communicating nodes is presented in Fig. 2. CNs will securely aggregate, store and share data from sensing nodes, to (and from) other communicating nodes. The data will be collected and shared wirelessly by a radiofrequency transmission across concrete and/or air. In addition, several CNs must implement the communication between *real* and *digital* worlds through a 'n-G' cellular network interface (today the '3G' cellular network standard is supported worldwide, '4G' is available in developed countries mainly in the urban regions, while '5G' is under development or implementation). The minimum communication range between SN and CN is in the range of a few meters whereas the commutation range between CNs is intended to be much larger (10 to 100 meters or even more). Communicating nodes must follow an energy efficient strategy and be reprogrammable in terms of communication interfaces, and software application. These nodes can be supplied with batteries until the exploitation phase of the building, where they can be switched to their main supply source, if available. Moreover, CNs must wirelessly power the SNs by using a wireless power transfer approach.
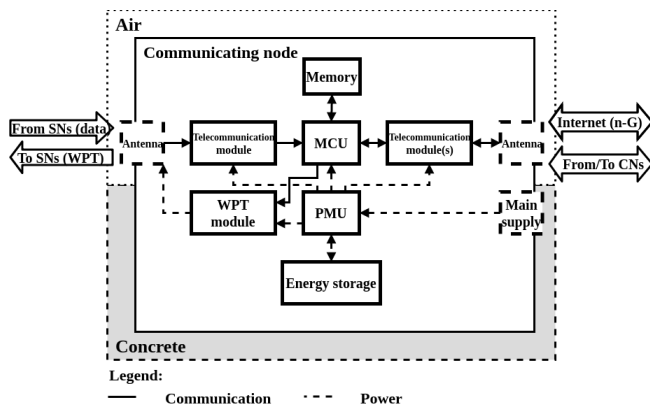
FIGURE 2. Schematic diagram for the envisaged architecture of the communicating nodes.

C. TOPOLOGY OF SENSING NODES

The sensing nodes -presented in Fig. 3- have to generate data by sensing environmental and structural properties of the concrete element (e.g. temperature, humidity, corrosion, cracks detection and location, etc.), and need to transmit these collected data to the associated communicating node(s) through a radiofrequency communication across concrete and/or air. In order to increase the lifetime and to avoid maintenance issues (SNs are embedded in the concrete), the nodes must be autonomous in terms of energy and batteryless. This is feasible by using a wireless power transfer system, managed by the communicating nodes. Moreover, some other restrictions apply for SNs: (i) the overall architecture of a SN needs to be as simple as possible and low power in order to relax the constraints for the WPT interface, (ii) the communication between SNs and CNs is unidirectional (SNs send data to CNs but only receive power via the WPT interface), (iii) the embedded intelligence of SNs is quite limited, their complete functionality must be set before embedding the SNs in the concrete, (iv) no reconfigurability is allowed with only a few exceptions that are detailed in this paper. CNs receive data and send power to SNs by using a WPT approach. By modulating the total amount of power transferred to SNs, the CNs can: (i) wirelessly switch on and switch off the SNs, (ii) manage the periodicity of measurement and transmission of the associated sensing nodes. Ideally, no data are stored in the SNs. In a same way, limited processing capabilities (e.g. a microcontroller unit (MCU) that is represented as optional block in Fig. 3) are embedded into the SNs. We target here a generic platform on which we can associate a specific sensor, and with only a simplified physical interface between the sensor and the transmitter. The sensor itself should be capable of performing measurements in a continuous way as long as the SN is switched on. The measured quantities (data) are sent by the SN to the CN as soon as the transmitter of the SN has enough power to perform a transmission slot. Thus, the overall functionality (and partially the reconfigurability) of the SN can be controlled by CNs via the WPT interface. To the best of the author's knowledge this innovative concept

has not been reported previously and is considered state-of-the-art. We also note that the capabilities of the WPT interface is limited today mainly by regulations (i.e. the maximum Effective Isotropic Radiated Power (EIRP) that can be radiated by CN is regulated for the ISM bands [40]) and not by the technology itself.
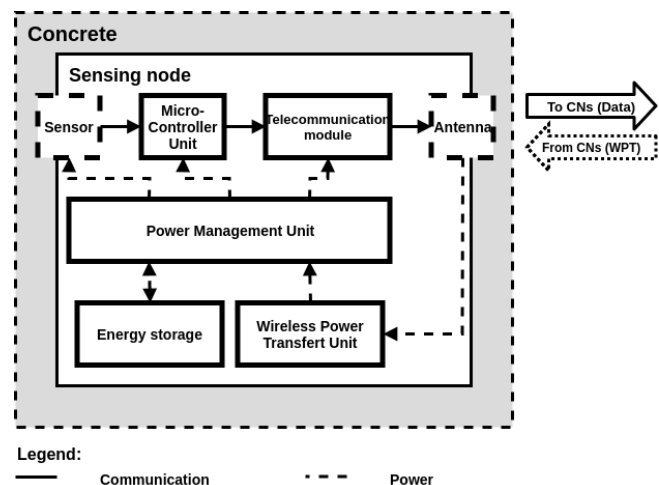
FIGURE 3. Schematic diagram for the envisaged architecture of the sensing nodes.

III. DESIGN OF SENSING NODES

Our first prototype of the sensing node, designed as a proof-of-concept of the adopted architecture, implements several functionalities: (i) the autonomy in terms of energy is assured by the WPT interface, energy storage and power management unit, (ii) a wireless unidirectional communication following LoRaWAN standard was adopted in this work for proof-of-concept purposes, (iii) the periodicity of the communication frames/measurements can be controlled and tuned by CNs via the WPT interface. The measurement functionality was not implemented yet in the SN prototype.

A. WIRELESS POWER INTERFACE

One of the main constraints for implementing the SN concerns its energy autonomy. Some recent works [11] reviewed the available energy in buildings and the best strategy to harvest some of this energy. Nevertheless, the ambient sources of energy seem to be too low, too fluctuating and sometimes unavailable in order to operate efficiently for decades. Neither light, nor temperature gradients are available in concrete and the natural resonant frequency of buildings is less than one Hertz making the harvesting of light, thermic or vibrational energy impractical. In our case, radiofrequency wireless power transfer is a convenient solution when well-adapted [12], [13]. The main advantage of WPT is the control of the whole transmission chain. The user can control the frequency and the amount of transmitted power, therefore the system efficiency can be accurately estimated for a given scenario [12]. Unlike [14], [15], and [16] which work on magnetic WPT, the far-field WPT is

more relevant in our case because of the targeted distance between the sensing and communicating nodes. This distance is in the range of a few to tens of meters, with the possibility of even more if an appropriate frequency band is selected (e.g. ISM 868/915 MHz). The wireless power interface consists of a high-frequency rectifier connected to a WPT receiving antenna, forming a rectenna (acronym from *rec*tifying an*tenna*). The WPT antenna captures the ambient electromagnetic energy and converts it into a RF signal. The rectifier converts the guided RF signal into the DC power for supplying the Power Management Unit (PMU). This PMU contains a DC-to-DC boost convertor that charges a storage energy element (e.g. supercapacitors). The energy stored in the storage element is then used by the PMU to power the SN electronics: the sensor, the low power MCU (if used, the MCU is not mandatory), and the telecommunication module (a low power transmitter in our case). The largest amount of DC power is required by the transmitter (Tx) device during the transmitting of data collected from the sensor(s). Hopefully in most of these scenarios, the measurements will not need to be performed continuously (e.g. the temperature and the humidity should be measured every hour, etc.).

The adopted topology for rectenna design is represented in Fig. 4. The key component of the WPT interface (rectenna) is the non-linear device (e.g., Schottky diode or transistor) used to convert the RF signal into a DC voltage. This device is carefully selected for rectifying low-power signals. Moreover, the rectifying process generates undesirable harmonics at the input and output ports of the non-linear device. At the input port of the non-linear element/rectifier, a matching circuit acting as a band-pass filter is used to prevent these harmonics from being re-radiated by the antenna and to maximize the power conversion efficiency. The harmonics generated at the output port of the non-linear device are filtered by a low-pass filter. The load (that is the PMU of SN) is then supplied with the required DC power to operate.
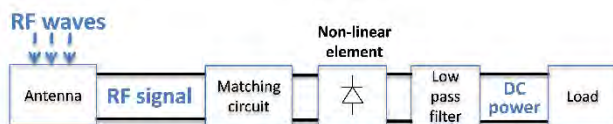
FIGURE 4. Rectenna topology.

We used a rectenna previously developed in our laboratory [17], [18]. It is composed of a compact and broadband flat dipole antenna (enclosed by a rectangular ring) and a single diode rectifier orthogonally connected with the antenna as shown in Fig. 5. The antenna was manufactured on a FR4 substrate (substrate thickness: 0.8 mm, relative electric permittivity: 4.4 and loss tangent: 0.02) whereas the rectifier was manufactured on Rogers RT/Duroid 5870 substrate (substrate thickness: 0.787 mm, relative electric permittivity: 2.3 and loss tangent: 0.0012). The selected Schottky diode (Avago HSMS 2850) is serially connected with the matching circuit and the load. The impedance matching circuit is composed of a bent short-circuited stub and a 30nH inductor

for matching the input impedance of the rectifier around 900 MHz. More details concerning the design and the characterization of the rectenna are reported in [17], [18]. Fig. 5 shows a photo of the manufactured rectenna with its main dimensions. The results depicted in Fig. 6 demonstrate that the manufactured rectenna operates efficiently for low power densities of the incident RF waves: a DC power greater than $20\mu W$ can be harvested as long as the incident power density exceeds $0.4\mu W/cm^2$. Moreover, this rectenna is relatively broadband, covering ISM 868/915MHz frequency band and part of the GSM bands.
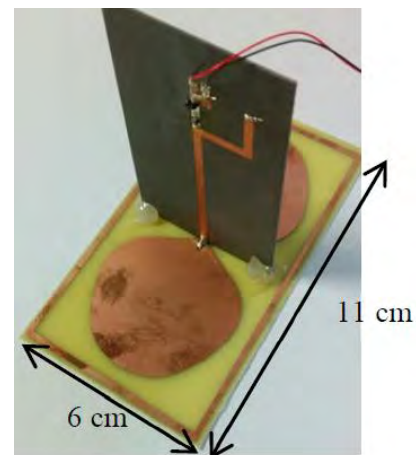
FIGURE 5. Photograph of the manufactured rectenna.
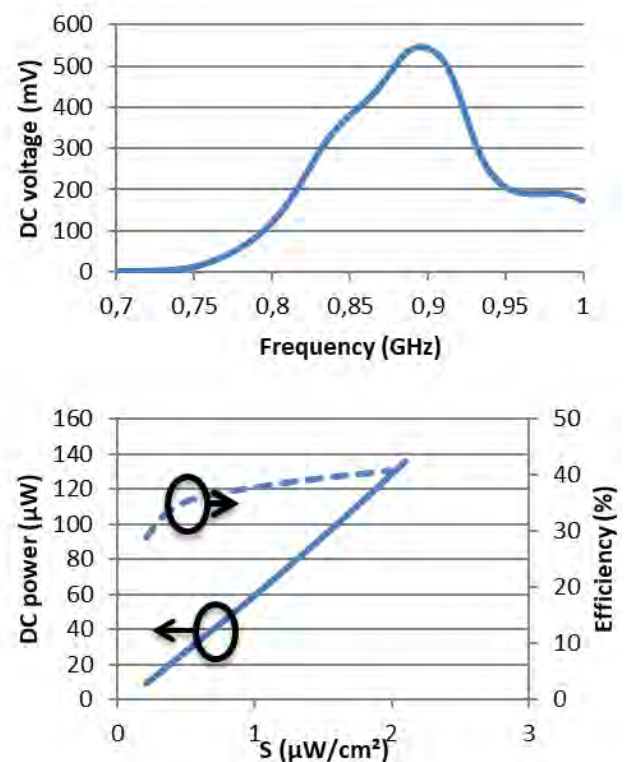
FIGURE 6. Rectenna performances measured on a resistive load of 10 kΩ: a) DC voltage as function of frequency, b) DC power and power conversion efficiency as function of the illuminating/incident power densities (frequency: 900 MHz).

137

B. POWER MANAGEMENT UNIT AND ENERGY STORAGE ELEMENTS

In order to validate our SN topology, we selected a panel of commercially available components (PMUs with DC-to-DC convertors, and capacitors or supercapacitors). An evaluation board containing three PMUs, three different capacitors/supercapacitors and allowing different configurations was developed in our laboratory. This board is shown in Fig. 7.
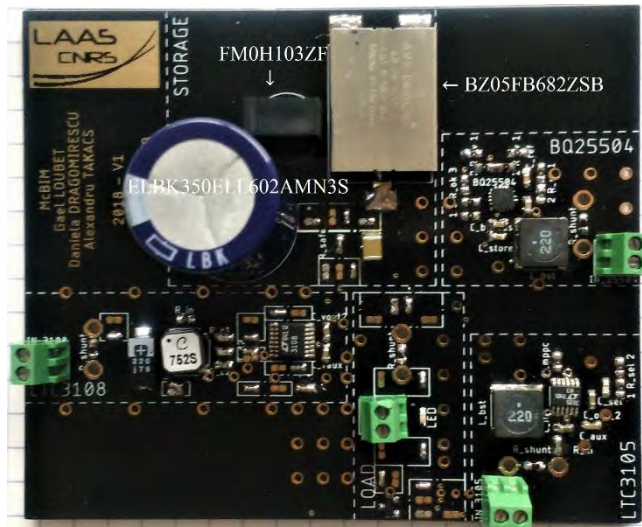
FIGURE 7. Photograph of our evaluation board for PMUs and energy storage elements.

Concerning the PMUs, we tested Analog Devices/Linear Technology LTC3105 [19] and LTC3108 [20], and Texas Instruments bq25504 [21]. The latter requires a lower input power (15μW against 1mW for LTC3108 and 60μW for LTC3105 equipped with a 1:100 step-up transformer) during the cold-start activation and is most suitable for our rectenna in terms of power transfer efficiency. Moreover, its configurability is a non-negligible advantage over others, i.e. we can define minimal and maximal thresholds for controlling the charge and discharge of the energy storage element. For our SN prototype, we chose to use the Texas Instruments bq25504, with the following configured thresholds: (i) the high threshold voltage was set-up at its maximum: 5.15V; when the high threshold is reached the energy stored in the storage element (i.e. supercapacitors) can by transferred to the load (LoRaWAN module), (ii) the low threshold voltage (that was set to 2.8V -then 2.45V-): when this low threshold is reached the load is disconnected in order to prevent the deep discharge of the storage element. The charge process is also restarted once the low threshold voltage is reach.

Concerning the energy storage element, we tested a polarized aluminum electrolytic capacitor -United Chemi-Con ELBK350ELL602AMN3S [22] of 6mF-; and two electric double layer supercapacitors -AVX Corporation BZ05FB682ZSB [23] of 6.8mF, and KEMET FM0H103ZF [24] of 10mF-. The BZ05FB682ZSB is the one with the lowest announced loss current (10μA, against 15μA for the

FM0H103ZF, and 200μA for the ELBK350ELL602AMN3S). The ideal scenario was to choose the most efficient technology, however, despite the BZ05FB682ZSB being the most efficient, we chose the FM0H103ZF due to its package and capacitance value which facilitate the implementation on the prototype board.

A schematic of our prototype, detailing the configuration of the used PMU (that is bq25504), is represented in Fig. 8. The input voltage -provided by the rectenna- is boosted through an inductor of 22μH, after being filtered by a 4.7μF capacitor. Five different resistor dividers allow the configuring of the different thresholds (under- and over-voltage protection, start and stop of the discharge of the storage element, and Maximal Power Point Tracking (MPPT)). A 10nF storage buffer allows for updating the MPPT state every 16 seconds. The charge of the storage element is managed by the PMU, as well as the supply of the load. When the storage element is completely charged at the voltage defined by the maximal threshold (that is 5.15V) the PMU drives an N-MOSFET transistor (through its VBAT_OK signal) which closes the circuit and switches up the load.
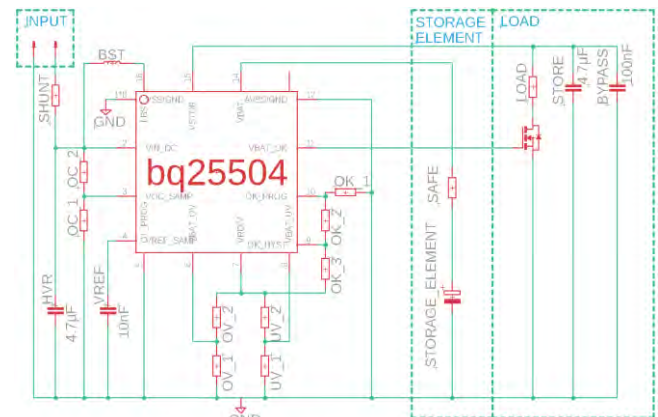
FIGURE 8. Schematic of our PMU and energy storage board.

C. WIRELESS COMMUNICATION

From practical reasons (a LoRaWAN infrastructure is available in our laboratory) we selected the LoRaWAN module (the development board STMicroelectronics B-L072Z-LRWAN1 [25]) as the telecommunication unit for our SN prototype. The B-L072Z-LRWAN1 board contains an all-in-one LoRaWAN communication module Murata CMWX1ZZABZ-091 [26], comprised of (i) a STMicroelectronics STM32L072CZ [27] MCU based on an ARM Cortex M0+, and, (ii) a Semtech LoRa transceiver SX1276 [28]. The transceiver manages the LoRa physical layer protocol, whereas the MCU manages the LoRaWAN protocol stack and the applicative software.

The choice of LoRaWAN was made due to the network infrastructure availability, and the ease of development. It should be noted that this is not the best technology for our application in terms of energy consumption and typical range. A short comparative study of available 'low-power'

wireless communication technologies is displayed in Table I. For the communication between SNs and CNs we only need a unidirectional uplink communication over a few or tens of meters. In the majority of presented standards, bidirectionality is the norm. Nevertheless, LoRaWAN and Bluetooth Low Energy (BLE) can be used only for transmitting data and consequently, control frames (e.g. acknowledgement frames) are not needed. The protocol constraints (e.g. control frames or duration of a transmission) for the selected wireless technology must be considered in order to estimate the energy consumption and thus calibrate the energy storage element. According to Table I, the BLE module is more suitable for our application, in the case of a broadcaster/observer topology, i.e. without connection. Although no module is available, the RuBee standard could be a real opportunity for the McBIM project too. Indeed, reinforced concrete is composed -among others- with multiple materials consisting of different grain sizes, but these sizes are very small when compared with the wavelength at 131 kHz (i.e. 2288 meters in free space). Also, the concrete seems to be transparent for the magnetic field propagation (RuBee operates in near field, with the magnetic field as communication vector) at such a low frequency (131 kHz).

Regarding the prototype, the sent messages are received by a LoRa gateway installed on INSA campus (Toulouse, France, GPS coordinates: 43°34'14.8"N 1°27'58.5"E); at a distance of more than one kilometer from our workspace (LAAS-CNRS Toulouse, France, GPS coordinates: 43°33'45.3"N 1°28'38.4"E). The data are then transmitted to the TheThingsNetwork [29] network, where we can recover and process them.

The communication part is as simplified as possible. We embedded a simple processing system in the sensing node. Thus, a byte of data (hard coded now, but in the future provided by a sensor) is transmitted each time when the system is supplied. The length of the transmitted frame is set at 14 bytes (there are 13 bytes dedicated to the protocol in a LoRaWAN frame and 1 byte of data). The transmission respects LoRaWAN class A standards (the node sends data but it cannot be interrogated), with a +2dBm radio frequency output power at 868MHz (ISM band), an activation by personalization (ABP), and without causing an acknowledgment from the network. This all aids to limit the number of exchanges, and reduce power consumption. The bandwidth is 125kHz, and the spreading factor is 12, allowing a data-rate of 293bps. The transmission time estimated by the LoRa module is 1.156s. Specifically, the software initializes the MCU, the useful peripherals, and the SX1276 module, then makes a LoRaWAN transmission, before being deactivated and shifting to a deep-sleep mode. Fig. 9 provides a consumption profile for the B-L072Z-LRWAN1 board. The treatment lasts approximately 1.4s (0.25s for the initialization and 1.15s for the transmission). The system needs at least 150mJ to work properly, as

detailed later. The software is limited to a low applicative program, the LoRaWAN stack, and several drivers. The recovering, processing and storing of data on the servers has not yet been implemented. We only visually checked on a web-browser for good reception of data as presented in Fig. 10. In this figure, we can validate the good transmission of two frames providing the same data: '5A' in hexadecimal (or '01011010' in binary); with 2h 59min 16s between each one. Other indicators are available as device information (time of reception, frame index, etc.), LoRaWAN parameters (central frequency, kind of physic modulation, data-rate, coding-rate, etc.), and reception indicators (gateway ID, RSSI, SNR, etc.).
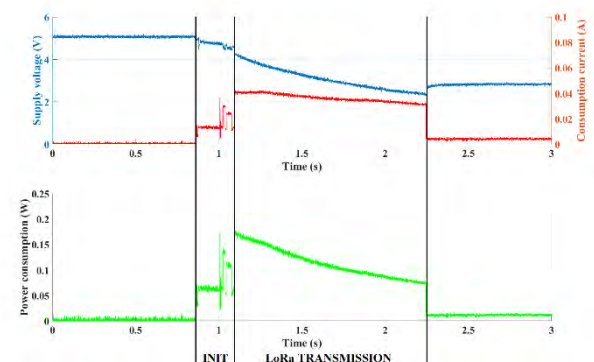
FIGURE 9. Consumption profile of the B-L072Z-LRWAN1 board connected to the PMU and rectenna when a 30mF capacitance charged at 5.15V is used as storage element.
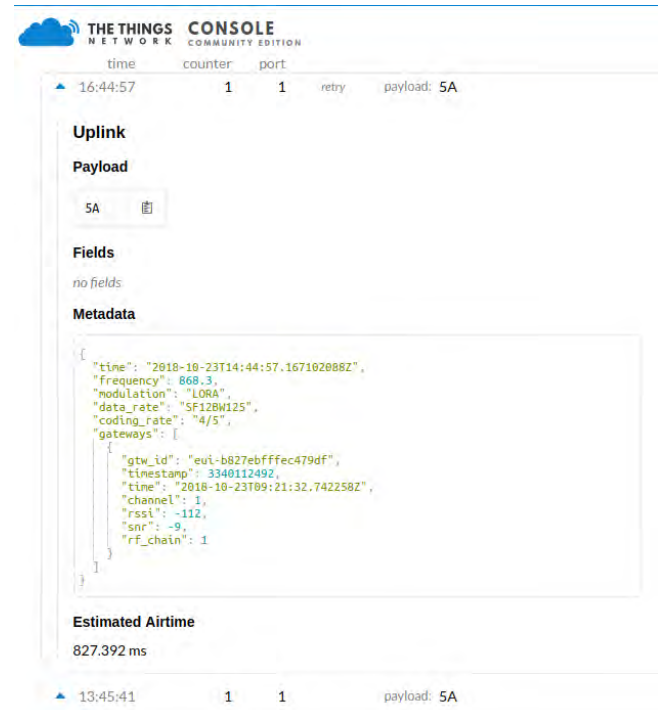
FIGURE 10. Screenshot of TheThingsNetwork interface after receiving checked frames, when the SN was illuminated with a power density of 1.12μW/cm² through the WPT interface.

IV. EXPERIMENTAL RESULTS

Our experiments were carried out in three main steps. Firstly, we characterized our prototype with a controlled input power. Secondly, we tested our system with the rectenna and a RF power transmitter in an anechoic chamber. Finally, we tested our system in a real outdoor environment in order to create easier communication with the LoRaWAN gateway.

A. COMPLETE PROTOTYPE SPECIFICATIONS

Our prototype, developed as a proof of concept in this paper is composed of: (i) a B-L072Z-LRWAN1 board used as a wireless telecommunication unit (ii) a bq25504 used as PMU and connected with KEMET supercapacitors used as storage elements (iii) a rectenna [18] used as WPT interface -this rectenna was designed and optimized for ISM 915 MHz (USA) frequency band but it can be used also in the ISM 868 MHz (EU) frequency band, as presented in Fig. 6-.

The B-L072Z-LRWAN1 board consumes on average 107.3mW, i.e. 32.9mA at 3.36V (average value from 5.15V to 2.45V), during 1.4s, (measured and computed from Fig. 9). Consequently, a minimum energy of 150mJ is needed to execute all the steps required by a complete LoRaWAN transmission. In our tests we used a capacitance of nearly 30mF in order to anticipate the energy consumption for measurement (our prototype does not yet integrate the sensor) and to have a margin for unexpected losses. The energy stored (E) by the storage element can be estimated as:

$$E = \frac{C}{2} \cdot \left(V_{max}^2 - V_{min}^2\right) \qquad (1)$$

where C is the capacitance of the energy storage element, V_{max} and V_{min} the maximal and minimal voltages at the ports of the storage element defined thanks to the bq25504 configuration pins (respectively OK_HYST -pin number 9- and OK_PROG -pin number 10-). Thus, for C=30mF, we obtain:

$$E = \frac{30.10^{-3}}{2} \cdot \left(5.15^2 - 2.45^2\right) = 308mJ \qquad (2)$$

The energy stored (estimated at 308mJ by using theoretical computation) in the storage element (30mF) is sufficiently higher than the needed 150mJ. Although it is not the optimal solution, to approximate this value we used an array of three FM0H103ZF 10mF supercapacitors in parallel.

B. EXPERIMENTATIONS WITH CONTROLLED INPUT POWER

For our first test, we connected directly the RF signal generator (Anritsu MG3694B) with a rectifier (available in our laboratory, this rectifier is a 'precursor' of the rectifier integrated in our 3D rectenna but operates around 985MHz due to its different/not optimized matching circuit). Our system is efficient from -4dBm of RF power at the input of the rectifier, -providing nearly 350mV, enough to start-up (switch-on) the PMU-. Once started, the PMU charges efficiently the energy storage element, and we can decrease the input power to below -7dBm. Fig. 11 shows the voltage at the terminals of the energy storage element (an array of

three FM0H103ZF supercapacitors in parallel) for a particular application, i.e. the transmission of LoRaWAN frames as soon as possible with the lowest input RF power. We observed that every 16 seconds there was an increase in the rectifier output voltage which is due to the MPPT process of the PMU, which opens its input to buffer the input voltage and optimize its performance. Table II displays some characteristics of our system for different input powers and for particular transmission frequencies.

$T_{cold\ start}$ corresponds to the cold start period, after which the PMU works with a nominal behavior. The first charge, which is the worst-case scenario, ends after a time of T_{first}. For each discharge the energy stored is consumed by the communication system during $T_{discharge}$. Experimentally, if $T_{discharge}$ is less than approximatively 1.4 seconds, the LoRaWAN frame is erroneous or not completely sent. In fact, we need nearly 0.25 seconds to initialize the systems, and 1.15 seconds to transmit a frame with one byte of data. If we do not stop the input power, only a period T_{inter} is needed to have a new transmission.

Thus we are able to modulate the frequency of transmission -and in the future, of the measurement-, without the help of the embedded intelligence -i.e. the MCU-, but due to the control of the transmitted power, which we can modulate in terms of power (at least -4dBm at the input of the rectifier is needed for the cold start, and below -7dBm in the nominal mode), or in terms of periods of transmission. During these experiments, we can impose a period of transmission between 1 minute 09 seconds and 26 minutes, for an input power between -7dBm and +10dBm. It should be noted that the auto-discharge is relatively low, so a complete charge is not necessary each time, if the periodicity of transmission is not too large.
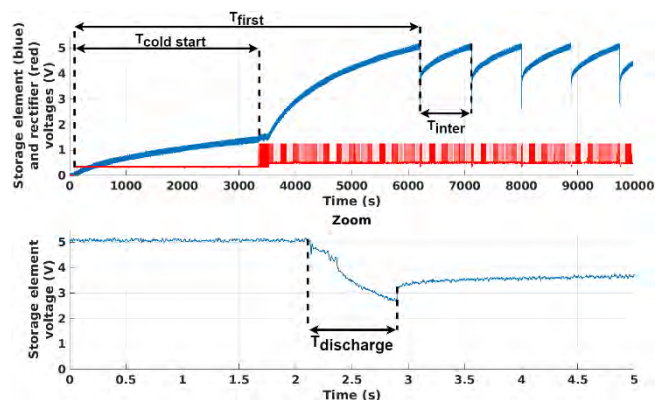
FIGURE 11. a) Evolution of the voltage waveforms at the output ports of the energy storage element (blue) and rectifier output voltage (red) b) Zoom on the voltage at the output ports of the energy storage element during discharge.

C. EXPERIMENTAL RESULTS IN A CONTROLLED ENVIRONMENT: SENSOR NODE POWERED BY A WIRELESS POWER TRANSMISSION TECHNIQUE

The SN prototype was characterized in an anechoic chamber (no multipath or interference effects). As presented in Fig. 12, our system is composed of: (i) a power transmitter (power synthesizer Anritsu MG3694B connected to a patch antenna with a +9.2dBi gain) operating at 868MHz -i.e. in the same ISM band as for the LoRaWAN transmission-, (ii) a 3D rectenna covering booth ISM 868MHz and ISM 915MHz frequency bands, (iii) the PMU (bq25504) and the storage element (30mF -an array of three FM0H103ZF supercapacitors connected in parallel-), (iv) the LoRaWAN board (B-L072Z-LRWAN1), and, (v) an oscilloscope to make voltage waveform measurements (LeCroy WaveRunner 6100). In order to discriminate WPT and communications -which both operate at the same frequency-, and to avoid eventual interferences, we used orthogonal polarizations: the antennas dedicated to the WPT are horizontally polarized, whereas the antenna for the communication is vertically polarized.

We measured some specific cases which are summarized in Table III. The RF power density S (3) is computed as a function of the electric field E (4) (effective value) at the antenna location as:

$$S = \frac{E^2}{120.\pi} \qquad (\text{W/m}^2) \qquad (3)$$

with

$$E = \frac{\sqrt{30.P_T.G_T}}{d} = \frac{\sqrt{30.EIRP}}{d} \qquad (\text{V/m}) \qquad (4)$$

where P_T is the power generated by the RF power synthesizer, G_T the transmission antenna gain, and d the distance between the power transmitter and the rectenna acting as WPT interface for our SN prototype.

The RF power (5) collected by the rectenna can be computed as:

$$P_{RF} = A_{eff}.S \qquad (\text{W}) \qquad (5)$$

where A_{eff} is the equivalent area of the antenna (6) computed as:

$$A_{eff} = G_r.\frac{\lambda^2}{4.\pi} \qquad (\text{m}^2) \qquad (6)$$

where G_R is the rectenna gain and λ the wavelength.

According to (3) and (4), we can generate a power density of 1μW/cm² at 399cm away from a +33dBm EIRP source.

As we test our system in an anechoic chamber, we cannot validate the transmission of the LoRaWAN frame. Nevertheless, the LoRa transmitter was powered for the duration needed to accomplish all the application software and the transmitted frequency spectrum was displayed through a vector analyzer placed in the anechoic chamber.

Previously, we were able to modulate the period of LoRa transmission by controlling the EIRP of the RF source. In our experiments, the period between two consecutive LoRa transmissions was modulated between nearly 20 minutes

(EIRP=30.7dBm, d=150cm, S=4.16μW/cm²) and 1 hour and 32 minutes (EIRP=26.7dBm, d=150cm, S=1.65μW/cm²).
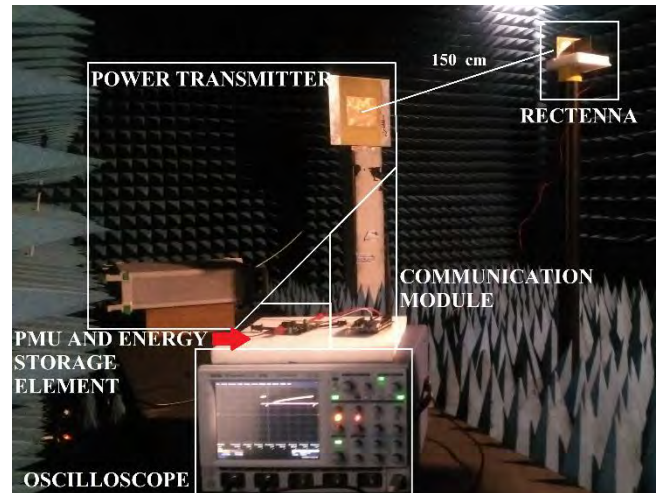
FIGURE 12. Photograph of our experimental setup (SN powered by using a WPT technique) in an anechoic chamber.

D. EXPERIMENTAL RESULTS IN A REAL ENVIRONMENT: SENSOR NODE POWERED BY A WIRELESS POWER TRANSMISSION TECHNIQUE

In order to validate the LoRaWAN transmission, the experimental setup (previously located in anechoic chamber) was installed in a place where we can contact the LoRa gateway more easily (located at the INSA campus, Toulouse, France). The setup is presented in Fig. 13. A power transmitter composed of a signal generator (Anritsu MG3694B), operating at 868MHz, and a patch antenna with +9.2dBi of gain is used as the power source for generating the electromagnetic power density that illuminates the prototype under test. The total losses of the cable and connecters used to interconnect the power generator with patch antenna were approximately -1dB. The measurements were performed on the balcony of our laboratory to ensure the path of least hindrance to the LoRa gateway (located at INSA Toulouse, France) and to be confronted with real environmental conditions (with electromagnetic fields, sun, temperature and humidity variations, wind, etc.) -but not similar to the conditions met inside concrete-. The voltage measurements were performed by using a LeCroy WaveRunner 6100 oscilloscope. The distance between the power transmitter and the rectenna was 150cm or 100cm (in the far field region of the transmitting antenna of the RF source).

In order to discriminate power and communication waves using the same frequency; we chose to use orthogonal polarizations for the WPT and communication (LoRa) links. Thus, the LoRa transmitter and gateway are vertically polarized, whereas the rectenna and power transmitter are horizontally polarized. In this way, no interferences were observed.

As represented in Fig. 14, the energy storage element is charged to 5.15V and discharged to 2.45V. The inter-

discharge time can be modulated by controlling the EIRP of the RF source, as previously demonstrated in the controlled environment (anechoic chamber). We have the possibility to transmit a data frame with a period between 4 minutes and 3 hours. Table IV agglomerates some obtained results for density powers between approximatively 1µW/cm² and 13µW/cm². Concerning the DC voltage measured at the output ports of the rectenna, we observed (each 16 seconds) an increase of the voltage which is due to the MPPT process of the PMU. In fact, the PMU opens the input periodically to buffer the input voltage and optimize its performance.

The discharge lasts several seconds where 0.25 seconds are dedicated to system initialization and 1.16 seconds to LoRaWAN transmission, as represented in Fig. 15. The remaining DC energy (deep sleep mode) could also be used for complementary measurement or a more complex computing process. The receiving of valid frames is validated on TheThingsNetwork, as shown in Fig. 9.

Although the EIRP used in these outdoor experiments were similar to the EIRP used in the anechoic chamber, the voltages at the output of the rectifier are higher and consequently the durations between charges are smaller. We can explain these advantageous results by the real power densities that are more important than the computed/estimated ones, thanks to multipath effects and the use of a wideband rectenna which can harvest energy from GSM communications in contiguous bands.

FIGURE 13. Photograph of our experimental outdoor setup (SN powered by using a WPT technique).
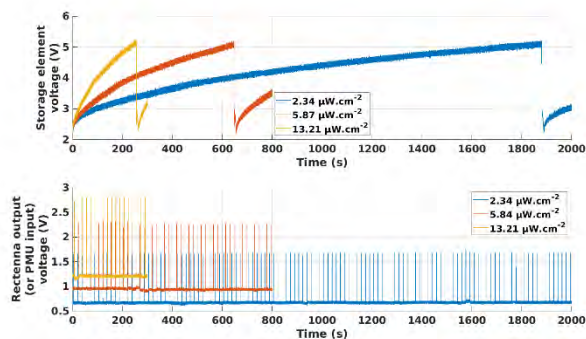
FIGURE 14. a) Voltage waveforms of the charge and discharge graphs measured at the output ports of the energy storage element (30mF) in outdoor experiments for three different generated power densities. b) Rectenna output voltage corresponding of the charge and discharge graphs.
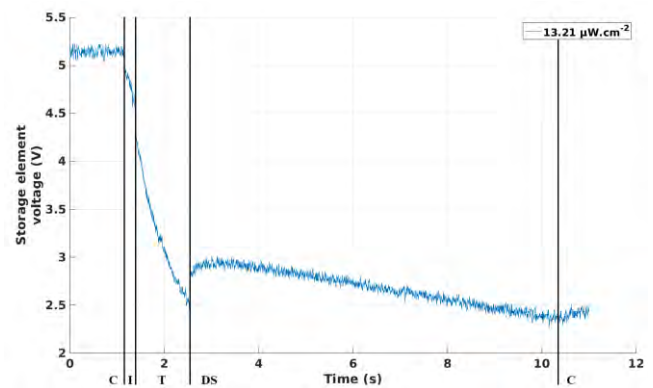
FIGURE 15. Discharge graph of the energy stored in the storage element (30mF) during the outdoor experiments. I: initialization; T: LoRa Transmission; DS: Deep Sleep mode; C: charge.

V. DISCUSSIONS

The prototype of the sensing node has been designed as a proof of the main concepts introduced in this paper: (i) the smart-node wireless network, (ii) the autonomy in energy (of the SNs) obtained by using a wireless power transmission technique, (iii) the control of the functionality of the SNs by a well-tailored wireless power transfer. The prototype of our SN operates in ISM 868 MHz frequency band (EU), receives energy from a dedicated RF source and sends data over the air by using a LoRaWAN standard. We use orthogonal polarization (vertical versus horizontal) between the WPT and data signals/waves and no jamming between WPT and data were experienced during our experiments. As long as the rectenna (used as WPT interface at SN level) is illuminated with an incoming power density higher than 1.12µW/cm² we can perform measurements and send data with a periodicity (defined as the time elapsed between two consecutive LoRaWAN transmission that is equivalent to the inter-discharges duration of storage element) of 3 hours or lower. This periodicity can be controlled by controlling the power density illuminating the SN. Moreover, the proposed SN prototype can be switched on (cold start-up) and switched off by the WPT interface. Supposing that the EIRP of the RF source is limited at +33dBm (as imposed by ETSI regulation for an interrogator in the 868MHz ISM band [40]) we have a maximum theoretical range (free space and line of sight wave propagation) of 4 meters approximately.

Our SN prototype will evolve in order to be more complete, efficient, compact and relevant for the targeted application.

The choice of LoRaWAN technology is not definitive and was justified mainly by the availability of the infrastructure in our laboratory and by its relatively low power consumption in the transmit (Tx) mode. In order to minimize the consumption of the LoRaWAN module more, we could further optimize the software initialization and transmission processes, and eventually change the LoRa configurations (e.g. bandwidth, spreading factor, etc.) according to gateway specifications.

Among the technologies introduced in Table I, BLE is a potential alternative (to be tested in the future), that is more suitable for implementing a unidirectional uplink (Tx only) communication in a low range and low power consumption context. RuBee could also be an applicable alternative (if modules arrive on the market) because the reinforced concrete seems to be transparent at this frequency.

Regarding the energy management aspect, we must implement some improvements in order to optimize efficiency and limit losses. For our application, we have to design a specific rectenna with a well-defined useful frequency band, and a well-adapted matching between the rectifier and the PMU. The use of a unique antenna -both for the WPT and the communications- could allow a high gain of compactness. Also, the design of a specific PMU could be another way to increase the efficiency of the energy management of our system. An accurate estimation of the needed power could allow for decreased energy storage capacitance, allowing a more compact system that needs less input RF power to be completely charged. The choice of a storage element with fewer current losses would allow a gain in terms of efficiency. Another possibility is to add a low-consumption voltage regulator at the PMU output in order to have a constant voltage to supply the load. It could minimize the consumption of the LoRaWAN module because the higher the input voltage, the higher the consumption current. Finally, we must notice that the oscilloscope measurements induce losses. Indeed, the input impedance of the oscilloscope is 1MΩ. That says: for a measured voltage of 5.15V, a power of 26.5μW are lost and 6.0μW for 2.45V.

An optimal solution -compact and low consumption- could be developed using ASIC technology. This would have to combine a PMU, an input ADC for the measurments, an RF output from a communication module, and a logical circuit interface between input and output (to compute the measured data, and encapsulate it in a frame respecting the defined protocol).

The next step in our development is to add a sensor to have a dynamic data to tranmsit. Temperature and humidity are a good starting point due to their relative simplicity and low power consumption. The corrosion, detection and location of cracks is extremely pertinant information for precast reinforced concrete structure. However, corrosion requires a lot of energy and perdiodic calibration and detection necessitates a high quantity of data, all of which involve power hungry signal processing algorithms.

In the future, SNs will have to integrate into precast reinforced concrete elements. There are more than 1200 different methods of creating reinforced concrete, each with specific mechanical and electromagnetic properties. It is very difficult to estimate these electromagnetic properties which are never taken into consideration in the manufacturing process. However, concrete is a heterogenous material with an electrical permittivity and a loss tangent which impacts highly the propagation of the electromagnetic waves within it. On average, the dielectric constant -or relative permittivity- is between 4 and 8, and the delta tangent near 1, but both are highly dependant on the water concentration and the frequency of the electromagnetic wave. Thus it would be relevant to characterize the targeted reinforced concrete (e.g. by using an open-ended coaxial probe [41]). Moreover, the reinforcing elements forming the reinforced concrete could induce different behaviours: they can act as a Faraday cage, or as reflectors, according to their composition (e.g. steel, etc.), geometry, width, or spacing according to the frequency used by the communication technology.

V. CONCLUSION

A wireless network architecture was proposed for SHM applications of buildings and civil engineering structures. It consists of a meshed grid composed of batteryless sensing nodes and communicating nodes. Sensing nodes need to be integrated into concrete for implementing the innovative concept of communicating concrete as a step toward the new generation of structural monitoring systems. The architecture of the sensing node is simplified and tuned in order to minimize its power consumption. The energy autonomy of the sensing node is implemented through a dedicated WPT interface. An innovative concept is proposed here and validated by experiments: the sensing node functionality is controlled through the WPT link. By using this WPT link, the communicating nodes can switch on/switch off the sensing nodes and control wirelessly the periodicity of the measurements and the periodicity of the transmission of data.

REFERENCES

[1]. "What is BIM?", available online at: https://www.autodesk.com/solutions/bim

[2]. S. Kubler, W. Derigent, A. Thomas, and E. Rondeau, "Problem definition methodology for the 'Communicating Material' paradigm", IFAC Proceedings Volumes, vol. 43, no. 4, pp. 198–203, 2010.

[3]. "McBIM research project", available online at http://www.agence-nationale-recherche.fr/en/anr-funded-project/?tx_lwmsuivibilan_pi2%5BCODE%5D=ANR-17-CE10-0014

[4]. J. Jover, "Contribution à la réduction des pertes d'informations dans l'industrie du bois: utilisation de la Résonance Quadrupolaire Nucléaire pour l'identification de marqueurs chimiques et de la virtualisation du processus de production pour la détermination de nomenclatures divergentes", PhD dissertation. Université de Lorraine, 2013.

[5]. S. Kubler, W. Derigent, A. Thomas, and E. Rondeau, "Prototyping of a communicating textile", International Conference on Industrial Engineering and Systems Management, IESM 2011, 2011.

[6]. S. Johann, C. Strangfeld, M. Müller, B. Mieller, and M. Bartholmai, "RFID sensor systems embedded in concrete– requirements for long–term operation", Materials Today: Proceedings, vol. 4, no. 5, pp. 5827-5832, 2016.

[7]. M. L. Wilson, and S. H. Kosmatka, "Design and control of concrete mixtures", High-Performance Concrete, vol. 15, p. 299, 2011.

[8]. N. Barroca, L. M. Borges, F. J. Velez, F. Monteiro, M. Górski, and J. Castro-Gomes, "Wireless sensor networks for temperature and humidity monitoring within concrete structures", Construction and Building Materials, vol. 40, pp. 1156-1166, 2013.

[9]. J. Ikonen, A. Knutas, H. Hämäläinen, M. Ihonen, J. Porras, and T. Kallonen, "Use of embedded RFID tags in concrete element supply chains", Journal of Information Technology in Construction (ITcon), vol. 18, no. 7, pp. 119-147, 2013.

[10]. S. Alahakoon, D. M. Preethichandra, and E. M. Ekanayake, "Sensor network applications in structures–a survey", EJSE Special Issue: Sensor Network on Building Monitoring: From Theory to Real Application, pp. 1-10, 2009.

[11]. J. W. Matiko, N. J. Grabham, S. P. Beeby, and M. J. Tudor, "Review of the application of energy harvesting in buildings", Measurement Science and Technology, vol. 25, no. 1, pp. 012002, 2013.

[12]. A. Costanzo and D. Masotti, "Smart Solutions in Smart Spaces: Getting the Most from Far-Field Wireless Power Transfer", IEEE Microw. Mag., vol. 17, no. 5, pp. 30–45, May 2016

[13]. D. Kim, A. Abu-Siada, and A. Sutinjo, "State-of-the-art literature review of WPT: Current limitations and solutions on IPT", Electric Power Systems Research, vol. 154, pp. 493-502, 2018.

[14]. L. Gallucci, C. Menna, L. Angrisani, D. Asprone, R. S. L. Moriello, F. Bonavolontà, and F. Fabbrocino, "An Embedded Wireless Sensor Network with Wireless Power Transmission Capability for the Structural Health Monitoring of Reinforced Concrete Structures", Sensors, vol. 17, no. 11, pp. 2566, 2017.

[15]. Y. Jang, J. K. Han, J. I. Baek, G. W. Moon, J. M. Kim, and H. Sohn, Jang, Yujin, et al. "Novel multi-coil resonator design for wireless power transfer through reinforced concrete structure with rebar array", Future Energy Electronics Conference and ECCE Asia (IFEEC 2017-ECCE Asia), 2017 IEEE 3rd International. IEEE, pp. 2238-2243, 2017.

[16]. O. Jonah, end S. V. Georgakopoulos, "Wireless power transfer in concrete via strongly coupled magnetic resonance", IEEE Transactions on Antennas and Propagation, vol. 61, no. 3, pp. 1378-1384, 2013.

[17]. A. Okba, A. Takacs, H. Aubert, "900MHz Miniaturized rectenna", IEEE MTT-S Wireless Power Transfer Conference, Montreal, Canada, 3-7 June 2018.

[18]. A. Okba, A. Takacs, and H. Aubert, "Compact Flat Dipole Rectenna for IoT Applications," Progress In Electromagnetics Research C, Vol. 87, 39-49, 2018.

[19]. "Linear Technology - LTC3105 - 400mA Step-Up DC/DC Converter with Maximum Power Point Control and 250mV Start-Up", available online at: https://www.analog.com/media/en/technical-documentation/data-sheets/3105fb.pdf

[20]. "Linear Technology - LTC3108 - Ultralow Voltage Step-Up Converter and Power Manager", available online at: https://www.analog.com/media/en/technical-documentation/data-sheets/3108fc.pdf

[21]. "Texas Instruments - bq25504 Ultra Low-Power Boost Converter With Battery Management for Energy Harvester Applications", available online at: http://www.ti.com/lit/ds/symlink/bq25504.pdf

[22]. Nippon Chemi-Con - Miniature Aluminum Electrolytic capacitors - LBK Series", available online at: http://www.chemi-con.co.jp/cgi-bin/CAT_DB/SEARCH/cat_db_al.cgi?e=e&j=p&pdfname=lbk

[23]. "AVX BestCap® Ultra-low ESR High Power Pulse Supercapacitors", available online at: http://datasheets.avx.com/BestCap.pdf

[24]. "Kemet - Supercapacitors - FM Series", available online at: https://content.kemet.com/datasheets/KEM_S6012_FM.pdf

[25]. "ST Microelectronics - B-L072Z-LRWAN1", available online at: https://www.st.com/en/evaluation-tools/b-l072z-lrwan1.html

[26]. "Murata: LoRa Module Data Sheet", available online at: https://wireless.murata.com/RFM/data/type_abz.pdf

[27]. "ST Microelectronics - STM32L072x8 STM32L072xB STM32L072xZ", available online at: https://www.st.com/resource/en/datasheet/stm32l072v8.pdf

[28]. "Semtech - LoRa - SX1276/77/78/79", available online at: https://www.semtech.com/products/wireless-rf/lora-transceivers/SX1276

[29]. "The Things Network", available online at: https://www.thethingsnetwork.org/

[30]. LoRa Alliance Technical Committee, "LoRaWAN 1.1 specification", 2017.

[31]. IEEE 802.15.1 Working Group, "IEEE Standard for information technology - Telecommunications and information exchange between systems - Local and metropolitan area networks - Specific requirements - Part 15.1: Wireless Medium Access Control (MAC) and Physical layer (PHY) specifications for Wireless Personal Area Networks (WPANs)", IEEE Std 802.15.1, 2005.

[32]. IEEE 802.15.3 Working Group, "IEEE Standard for high data rate wireless multi-media networks", IEEE Std 802.15.3, 2016.

[33]. IEEE 802.15.4 Working Group, "IEEE Standard for local and metropolitan area networks - Part 15.4: Low-rate Wireless Personal Area Networks (LR-WPANs)", IEEE Std 802.15.4, 2011.

[34]. IEEE 802.11 Working Group, "IEEE Standard for information technology - Telecommunications and information exchange between systems - Local and metropolitan area networks - Specific requirements - Part 11: Wireless LAN Medium Access Control (MAC) and Physical layer (PHY) specifications", IEEE Std 802.11, 2007.

[35]. IEEE 1902.1 Working Group, "IEEE Standard for long wavelength wireless network protocol", IEEE Std 1902.1, 2009.

[36]. "NXP: QN908x: Ultra low power Bluetooth 5 system-on-chip solution", available online at: https://www.nxp.com/docs/en/nxp/data-sheets/QN908x.pdf

[37]. "decaWave: DWM1000", available online at: https://www.decawave.com/sites/default/files/resources/DWM1000-Datasheet-V1.6.pdf

[38]. "Atmel: ZIGBIT 900MHZ WIRELESS MODULES", available online at: http://ww1.microchip.com/downloads/en/DeviceDoc/atmel-42269-wireless-zigbit-atzb-rf-212b-0-cn_datasheet.pdf

[39]. "Silicon Labs: Zentri AMW036/AMW136", available online at: https://www.silabs.com/documents/login/data-sheets/ADS-MWx36-ZentriOS-101R.pdf

[40]. ETSI, "Electromagnetic compatibility and Radio spectrum Matters (ERM); Short Range Devices (SRD) intended for operation in the bands 865 MHz to 868 MHz and 915 MHz to 921 MHz; Guidelines for the installation and commissioning of Radio Frequency Identification (RFID) equipment at UHF", ETSI TR 102 436, V2.1.1", 2014.

[41]. B. Filali, F. Boone, J. Rhazi, nd G. Ballivy, "Design and calibration of a large open-ended coaxial probe for the measurement of the dielectric properties of concrete", IEEE Transactions on Microwave Theory and Techniques, vol. 56, no. 10, pp. 2322-2328, 2008.

Gaël Loubet was born in Toulouse, France, in February 1994. He received the Engineering diploma in electronics and automation engineering from the *National Institute of Applied Sciences* (INSA), Toulouse, France, in July 2017. He is currently pursuing a Ph.D. degree in micro- and nano-systems for communications at the *National Institute of Applied Sciences* (INSA), Toulouse, France. His research interests include communicating materials paradigm, electromagnetic wireless power transfer, wireless communication for internet of things applications and wireless sensor networks for structural health monitoring applications.

Alexandru Takacs (M'12) was born in Simleu Silvaniei, Romania, in March 1975. He received the Engineer diploma in electronic engineering from the Military Technical Academy, Bucharest, Romania, in 1999, and the Master degree and Ph.D. degree in microwave and optical communications from the National Polytechnic Institute of Toulouse (INPT), Toulouse, France, in 2000 and 2004, respectively. From 2004 to 2007, he was a Lecturer with the Military Technical Academy of Bucharest, and an Associate Researcher with the Microtechnology Institute of Bucharest. From 2008 to 2010, he occupied a Postdoctoral position with the Laboratory for Analysis and Architecture of Systems (LAAS), National Center for Scientific Research (CNRS), Toulouse, France. During 2011, he was an R&D RF Engineer with Continental Automotive SAS France, where he was in charge of antenna design and automotive electromagnetic simulation. Since 2012, he has been an Associate Professor with the University (Paul Sabatier), Toulouse, France, where he performs research within LAAS–CNRS. He has authored or coauthored one book, one book chapter, 15 papers in refereed journals, and over 70 communications in international symposium proceedings. His research interests include the design of microwave and RF circuits, energy harvesting and wireless power transfer, microelectromechanical systems (MEMS) circuits and systems, small antenna design, electromagnetic simulation techniques, and optimization methods.

Daniela Dragomirescu (M'96-SM'15) Daniela Dragomirescu is Professor at the University of Toulouse (INSA Toulouse) and LAAS-CNRS laboratory. She received the engineering degree with Magna Cum Laude from the Polytechnic University of Bucarest, Romania in 1996, the MSc in circuits design from the University Paul Sabatier, France, in 1997 and the Ph.D. degree with Magna Cum Laude in 2001 from the University of Toulouse, France. Prof. Dragomirescu is the Head of Microwave and Photonics Systems Department, in LAAS-CNRS laboratory since January 2015. She is the IEEE Solid States Circuits French Chapter Chair. Prof. Daniela Dragomirescu was French Government Fellow of Churchill College, Univeristy of Cambridge from February to September 2014. Daniela Dragomirescu is the Dean of Electrical and Computer Engineering Department at INSA Toulouse since June 2017. Prof. Dragomirescu is conducting research in the area of wireless communications with a special focus on Wireless Sensor Networks. Daniela Dragomirescu received in 2005 the French National Research Agency grant for Young Investigator which supported her in setting up the team in the Wireless Sensor Network area. She was also involved in many national and European research projects in the area of wireless communication. Daniela Dragomirescu was the coordinator of one of the nine French NanoInnov project, called Nanocomm on Reconfigurable wireless nano-sensors networks. She published more than 80 papers in journals and conferences proceedings, 2 patents and she authored 7 academic courses.

TABLE I
COMPARATIVE STUDY OF WIRELESS COMMUNICATION TECHNOLOGIES

Technology	Standard	Directionality	Frequency	Theoretical range	Minimal frame size (byte)	Module	Manufacturer	Transmission / Reception power consumption (mW)
LoRa	LoRaWAN [30]	'Transmission only' possible	433/868/915MHz (ISM)	Several kilometers	14	CMWX1ZZABZ-091 [26]	Murata	119 at +10dBm (typ) / Not necessary
Bluetooth Low Energy (BLE)	IEEE 802.15.1 [31]	'Transmission only' possible / Essentially bidirectional	2.4GHz (ISM)	Thousands meters	11	QN908x [36]	NXP	12 at 0dBm (typ) / 12 at 1Mbps (typ)
Ultra-Wide Band (UWB)	IEEE 802.15.3 [32]	Essentially bidirectional	3.1-10.6GHz	Tens meters	N/A	DWM1000 [37]	DecaWave	462 at +9.3dBm (max) / 528 (max)
ZigBee	IEEE 802.15.4 [33]	Bidirectional	868/915MHz 2.4GHz (ISM)	Thousand meters	16	ATZB-RF-212B-0-CN [38]	Atmel	17 at +9dBm (typ) / 31 (typ)
Wi-Fi	IEEE 802.11 [34]	Bidirectional	900MHz 2.4GHz 5GHz (ISM)	Tens meters	33	Zentri AMWx36 [39]	Silicon Labs	19 at 1Mbps (typ)
RuBee	IEEE 1902.1 [35]	Essentially bidirectional	131kHz	30 meters	5	N/A	N/A	N/A / N/A

The power is computed for a 3.3V supply (except for Bluetooth Low Energy and ZigBee modules and their 3V supply). We have to take into consideration the duration of a transmission and reception, and the quantity of needed control frames to estimate precisely the consumption for each standard and module.

IEEE *Access*
Multidisciplinary : Rapid Review : Open Access Journal

TABLE II
CHARACTERISTICS OF THE SN PROTOTYPE FOR DIFFERENT USE CASES

Energy storage element	Rectifier input power (dBm)	Rectifier open-load output voltage (V)	Nominal rectifier output voltage (mV)	Maximal / Minimal voltage at the output port of the storage element (V)	Energy stored (mJ)	Cold start duration	First charge duration	Inter-discharges duration	Discharge duration (s)
ELBK350ELL602AMN3S 6mF	-4	N/A	N/A	3.40 / 2.80	11.2	N/A	~42min	~2min29s	N/A
BZ05FB682ZSB 6.8mF	-7	N/A	N/A	3.40 / 2.80	12.6	N/A	~2h03min	~5min14s	N/A
BZ05FB682ZSB 6.8mF	-4	N/A	N/A	3.40 / 2.80	12.6	N/A	~43min	~2min20s	N/A
FM0H103ZF 10mF	-4	N/A	N/A	3.40 / 2.80	18.6	N/A	~49min	~2min23s	N/A
20mF (two FM0H103ZF of 10mF on parallel)	-4	1.25	510	5.15 / 2.80	186.8	~58min	~1h23min	~16min	~0.750
30mF (three FM0H103ZF of 10mF on parallel)	-4	1.28	500	5.15 / 2.80	280.2	~1h18min	~2h31min	~26min	~1.21
30mF (three FM0H103ZF of 10mF on parallel)	-2	1.38	575	5.15 / 2.80	280.2	~1h	~1h21min	~16min	~1.20
30mF (three FM0H103ZF of 10mF on parallel)	0	1.53	630	5.15 / 2.80	280.2	~42min	~1h08min	~11min	~1.25
30mF (three FM0H103ZF of 10mF on parallel)	2	1.76	740	5.15 / 2.80	280.2	~32min	~48min	~7min	~1.20
30mF (three FM0H103ZF of 10mF on parallel)	4	1.99	760	5.15 / 2.80	280.2	~18min	~28min	~5min	~1.36
30mF (three FM0H103ZF of 10mF on parallel)	6	2.06	860	5.15 / 2.80	280.2	~10min	~16min	~3min	~1.42
30mF (three FM0H103ZF of 10mF on parallel)	8	2.20	900	5.15 / 2.80	280.2	~4min35s	~9min20s	~2min	~1.49
30mF (three FM0H103ZF of 10mF on parallel)	10	2.34	1000	5.15 / 2.80	280.2	~1min45s	~5min22s	~1min09s	~1.48

A rectifier is connected directly to an Anritsu MG3694B power synthesizer. The PMU (bq25504, Texas Instruments) is connected as load for the rectifier. PMU charges various combinations of supercapacitors. The energy stored in these supercapacitors is used to power a LoRaWAN module. The voltage measurements are performed by using a LeCroy WaveRunner 6100 oscilloscope. The cold start voltage (provided by the rectifier) required to switch on the PMU is around 350mV.

147

TABLE III
CHARACTERISTICS OF THE SN PROTOTYPE FOR A COMPLETE WPT IN AN ANECHOIC CHAMBER

EIRP (dBm)	Power density (µW/cm²) [computation]	Rectenna input power (dBm) [computation]	Nominal rectifier output voltage (mV)	Inter-discharges duration	Discharge duration (s)
26.7	1.65	-5.8	514	~1h32min	~9.0
27.7	2.08	-4.8	557	~1h00min	~8.9
28.7	2.62	-3.8	626	~42min22s	~8.9
29.7	3.30	-2.8	705	~29min12s	~8.9
30.7	4.16	-1.8	791	~19min41s	~8.9

A power transmitter composed of a power synthesizer (Anritsu MG3694B, operating at 868MHz) and a patch antenna with +9.2dBi of gain is used as power source for generating the electromagnetic power density that illuminates the prototype under test. The total losses of the cable and connecters used to interconnect the power generator with patch antenna are approximately -2.5dB. The measurements were performed in an anechoic chamber to avoid any interference or multipath effect. The prototype is composed of: a 3D rectenna (the rectenna's antenna gain is around +2.2dBi at 868MHz), the PMU bq25504 connected to a supercapacitors array of 30mF, as well as the LoRaWAN module B-L072Z-LRWAN1. The distance between the power transmitter and the rectenna is 150cm. The voltage measurements are performed by using a LeCroy WaveRunner 6100 oscilloscope. The cold start voltage (provided by the rectenna) required to switch on the PMU is around 350mV. Start and stop thresholds for the discharge are configured at 5.15V and 2.45V respectively. The duration of our processing in the SN is around 1.4s.

TABLE IV
CHARACTERISTICS OF THE PROTOTYPE FOR A COMPLETE WPT OUTDOORS

EIRP (dBm) / Distance (cm))	Power density (µW/cm²) [computation]	Rectenna input power (dBm) [computation]	Nominal rectifier output voltage (mV)	Inter-discharges duration	Discharge duration (s)
25.0 / 150	1.12	-7.4	490	~2h59min	8.8
28.2 / 150	2.34	-4.3	688	~31min28s	8.8
30.2 / 150	3.70	-2.3	816	~18min26s	9.2
32.2 / 150	5.87	-0.3	964	~10min56s	9.5
31.2 / 100	10.49	+2.2	1179	~5min13s	8.9
32.2 / 100	13.21	+3.2	1231	~4min24s	9.3

A power transmitter composed of a power synthesizer (Anritsu MG3694B, operating at 868MHz) and a patch antenna with +9.2dBi of gain is used as power source for generating the electromagnetic power density that illuminates the prototype under test. The total losses of the cable and connecters used to interconnect the power generator with patch antenna are approximately -1dB. The measurements were performed in a balcony of our laboratory in order to make easier the LoRaWAN communication. The prototype is composed of: a 3D rectenna (the rectenna's antenna gain is around +2.2dBi at 868MHz), the PMU bq25504 connected to a supercapacitors array of 30mF, as well as the LoRaWAN module B-L072Z-LRWAN1. The voltage measurements are performed by using a LeCroy WaveRunner 6100 oscilloscope. The cold start voltage (provided by the rectenna) required to switch on the PMU is around 350mV. Start and stop thresholds for the discharge are configured at 5.15V and 2.45V respectively. The LoRaWAN transmission lasts nearly 1.16s, and the initialization of the system 0.24s, that says a 1.4s period for our processing. The polarization of the power transmission and LoRaWAN communication are orthogonal in order to avoid eventual interferences.

using the mothership as a relay station. We note that this concept requires a multistandard system (WPT&COM) as a whole, thus requiring the integration of some basic building blocks that are already available or under development by the scientific community. Fund-raising for research concerning 'Shared Space Laboratory' is one of my priorities.

Let's end this '*prospective*' section of my manuscript by my philosophical view on Research and the Researcher:

The researcher's life is a continuous seeking of innovation. He had dreams and ideas, but his professional life is also a continuous search and fight for funding. His idealist creativity faces the pragmatism of the reality, but the beauty of the Research is that we can keep on dreaming.

CURRICULUM VITAE

ECOLE DOCTORALE DE RATTACHEMENT : ED GEET

Nom :   TAKACS   **Prénom :** Alexandru

Né(e) le : 24/03/1975

Nationalité : Roumaine et Française

Fonctions : MCF, section 63

Doctorat obtenu le …11 juin 2004**..à…**Toulouse

Autre(s) diplôme(s) :

Diplôme d'ingénieur obtenu en 1999 en Roumanie

Diplôme de Master (DEA) obtenu à Toulouse en juillet 2000

I – PARCOURS UNIVERSITAIRE

2004   Doctorat avec mention Très Honorable. La thèse intitulée "Contribution à la conception de circuits passifs à faibles pertes d'insertion en ondes millimétriques" a été proposée au prix de thèse de l'Institut National Polytechnique de Toulouse (INPT)

2000   Master (DEA) à l'INPT, spécialisation Micro-ondes et Télécommunications Optiques, mention: Bien

1999   Diplôme d'ingénieur de l'Académie Technique Militaire (ATM) de Bucarest, Roumanie, Génie Electronique, troisième de la promotion

Maître de conférences à l'Université Paul Sabatier depuis octobre 2011

II – PARCOURS PROFESSIONNEL (après le doctorat)

depuis oct'2011	Maître de Conférences à l'UNIVERSITE PAUL SABATIER Toulouse
2011	Ingénieur R&D à CONTINENTAL AUTOMOTIVE Toulouse en charge avec la conception des systèmes RF et la simulation électromagnétique
2009-2010	Post-doc/Ingénieur de recherche dans le groupe MINC au CNRS-LAAS, Toulouse, France. Travaux dans le cadre des contrats suivants: Antenne hélice VHF/UHF miniaturisée' (étude CNES, 2008-2009), ANR-PNANO-NANOTERRA : Nanodétecteurs de radiation micro-ondes et terahertz bases sur l' effet ratchet (2009-2010), 'Générateur Thermoélectrique sans fil en technologie MEMS' (étude Rockwell-Collins, 2010), 'MEMS Based Millimeterwave Imaging System' – MEMIS (projet européen MNT-ERA.net, 2010), Smart Harness Technologies (projet ELECTRA - financé par la Région Midi-Pyrénées, 2010)
2008	Post-doc à CONTINENTAL AUTOMOTIVE Toulouse, contrat de collaboration

	recherche CONTINENTAL-LAAS-RENAULT
2004-2007	Chercheur associé à l'Institut de Microtechnologie de Bucarest, Roumanie. Travaux de recherche portés sur la conception, la modélisation et la caractérisation fonctionnelle des circuits RF-MEMS (**R**adio-**F**requency **M**icro**E**lectro**M**echanical**S**ystems) en ondes millimétriques dans le cadre de plusieurs projets nationaux (roumains) et du projet FP7-AMICOM.

III – ACTIVITES D'ENSEIGNEMENT (nature et niveaux des enseignements)

Enseignements en Electronique dans le cadre de la FSI/EEA, niveaux L2, L3, M1 et M2 depuis oct 2011, service complet en léger dépassement depuis 2014

Enseignements en Electronique à INSA Toulouse (vacations, environ 25 heures eq. TD par année) depuis 2014, Niveaux IVème année et Vème année. Depuis 2016 j'interviens dans le cadre du master international ISS dans un cours orienté systèmes IoT pendant mon intervention intitulée 'ENERGY for IoT SYSTEMS'(2 séances de cours magistraux) je présente les aspects liés à l'autonomie énergétique de systèmes IoT avec un focus sur les techniques de transfert d'énergie sans fil et de collecte d'énergie.

Enseignements en Electronique à ENSEEIHT Toulouse (vacations, 9h cours magistral sur les systèmes IoT) en 2018, niveaux MASTER

A l'Université Paul Sabatier j'ai mis au point plusieurs travaux pratiques et bureaux d'études sur de sujets connexes à ma thématique de recherche principale (les techniques de transfert d'énergie sans fil et de collecte d'énergie), notamment :
- TP et BE pour la L3 EEA REL de l'Université Paul Sabatier dans le cadre du cours 'Physique du composant ondes'
- BE et mini-projets orientés '*conception rectenna'* pour le master M1 ESET de l'Université Paul Sabatier
- Mini-projets orientés '*conception capteur sans fil et sans batterie*' et 'conception des antennes pour application cubesat/nanosat' dans le cadre d'un bureau d'études hyperfréquence pour le master M2 ESET de l'Université Paul Sabatier
-

IV – ACTIVITES DE RECHERCHE

Nombre de publications internationales et nationales, nombre de proceedings, de brevets, de chapitres d'ouvrages et d'ouvrages

Articles revues et brevets	Total	Premier auteur
Articles publiés dans des revues internationales à comité de lecture et facteur d'impact ISI	**14**	**9**
Articles publiés dans d'autres revues internationales à comité de lecture	**9**	**5**
Brevets d'invention	**4**	

Voir *List of publications*

Citer les cinq publications les plus significatives (titres et noms de tous les autres)

[ISI1]. **A. Takacs**, H. Aubert, H. Diez, D. Belot, "Miniaturization of Quadrifilar Helical Antenna: Impact on Efficiency and Phase Center Position", *IET Microwaves, Antennas & Propagation*, Volume 7, Issue 3, 19 February 2013, pp. 202 – 207.

[ISI2]. **A. Takacs**, H. Aubert, L. Despoisse, S. Fredon, "Microwave energy harvesting for satellite applications", *IET Electronics Letters*, Issue 11, Vol. 49, pp. 722-723, 23 May 2013.

[ISI3]. A. Takacs, H. Aubert, S. Fredon, L. Despoisse, H. Blondeaux, "Microwave power harvesting for satellite health monitoring," *IEEE Trans. on Microwave Theory Tech*, Vol.: 62, Issue: 4 , pp. 1090 - 1098, April 2014.

[ISI4]. M. Gastaldi, D. Dragomirescu, **A. Takacs**, V. Armengaud, S. Rochette, "Micro-strip slow wave line for phase shifting cells", *IET Electronics Letters*, Vol. 51, No. 20, pp. 1589–1591, 1st October 2015.

[ISI5]. A. Okba, **A. Takacs**, H. Aubert, S. Charlot, P-F. Calmon, "Multiband rectenna for microwave applications", *Comptes Rendus Physique*, *ELSEVIER*, Vol. 18, Issue 2, pp 107-117, Feb. 2017

Nombre de conférences, séminaires et communications orales

Scientific papers	Total	Premier auteur
Articles présentés dans des conférences IEEE (avec actes et comité de lecture) et indexés dans la base de données IEEExplore	**55**	**21**
Articles présentés dans d'autres conférences internationales avec actes et comité de lecture, aux workshops et aux symposiums	**27**	**12**

Voir *List of publications*

V – ACTIVITES D'ENCADREMENT : liste nominative des personnes encadrées ou co-encadrées (la part d'encadrement, la durée de l'encadrement et la nature du diplôme préparé par l'étudiant)

Encadrement doctoral

Doctorant	Encadrement et %	Démarrage	Soutenance	Financement	Devenant du docteur	Prix
Dina	H. Aubert : 50%	Octobre	Octobre 2012	Projet ANR	Enseignan	

Medhat Mohamed Abdel Maksoud	A. Takacs : 50%	2009		NANOTERA	te en Egypte	
Guillaume Vigneau	A. Takacs : 100% (avec dérogation de l'Ecole Doctorale GEET)	Février 2013	Juillet 2016	CIFRE Continental Automotive SAS	Ingénieur chez Davidson consulting	Prix de l'école doctorale GEET en 2016
Matthieu Gastaldi	D. Dragomirescu : 50% A. Takacs : 50%	Octobre 2013	Décembre 2016	Bourse CNES et Thales Alenia Space	Ingénieur au CNES Toulouse	
Zhening Yang	D. Dragomirescu : 50% A. Takacs : 50%	Octobre 2013	Décembre 2016	Bourse de l'école GEET	Ingénieur	
Abderrahim Okba	H. Aubert : 50% A. Takacs : 50%	Octobre 2014	Décembre 2017	Bourse de l'école GEET	Chercheur contractuel au LAAS-	Proposition pour le prix de l'école doctorale GEET 2017
Gael Loubet	D. Dragomirescu : 50% A. Takacs : 50%	Janvier 2018	En cours	Projet ANR McBIM		

Encadrement scientifique (étudiants de master M2 en stage)

Etudiant	Titre de stage	Période	Notes
Dina MEDHAT MOHAMED ABDEL MAKSOUD	Etude et simulation électromagnétique d'un banc pour expérimentation physique	Mars'2009-sept'2009	Co-encadrement avec Prof. Aubert, Master ESET
Mohamed Fodil	Miniaturisation d'antennes hélice quadrifilaire dans la bande VHF	Juin'2009-sept'2009	Co-encadrement avec Prof. Aubert Master INP
Mingtian WANG	Optimisation électromagnétique de l'antenne hélice	mars'2010-sept-2010	Encadrement: 50% avec Prof. H. Aubert (INP Toulouse) Master (M2) Recherche Micro-ondes, Electromagnétisme et Optoélectronique (MEMO)
Ayoub RIFAI	Techniques d'optimisation des performances des antennes petites devant la longueur d'onde	Avril'2011-Sept'2011	Encadrement : 100% Master (M2) MEMO
Abdessamad ZAIR	Conception, simulation et modélisation de circuits	Avril'2012-Sept'2012	Encadrement :100% Master M2 ESET/MEMO

	hyperfréquences pour systèmes d'imagerie en ondes millimétriques		
Alex Luca	Conception d'antennes et rectennas compactes pour applications spatiales	Mars'2014-sept'2014	Encadrement : 100% , Master MITAT, Université Paul Sabatier

Encadrement d'un Ingénieur de Recherche (*David Jugieu*) en mission à Continental Automotive SAS (du 01.04.2012 au 31.03.2013) dans le cadre du contrat industriel: '*Etude et modélisation électromagnétique du transfert d'énergie pour le chargeur inductif*' dont j'ai été responsable scientifique.

Publications avec les doctorants encadrés/co-encadrés

Avec Dina MEDHAT MOHAMED ABDEL MAKSOUD

Articles dans des revues internationales avec comité de lecture

[Rev1]. D. Medhat, **A. Takacs**, H. Aubert, "A methodology to study the electromagnetic behavior of a cryogenic metallic system used to control the ratchet effect", *Progress In Electromagnetics Research M*, Vol. 23, 123-137, 2012.

Articles présentés dans des Conférences IEEE (avec actes et comité de lecture) et indexés dans la base de données IEEExplore

[C_IEEE_1]. D. Medhat, **A. Takacs**, H. Aubert, J.C. Portal, "Comparative Analysis of Different Techniques for Controlling Ratchet Effect in a Periodic Array of Asymmetric Antidots", in **Proc. of Asia-Pacific Microwave Conference (APMC'2009),** Singapore, 7-10 Dec 2009, pp. 1711 - 1714.
[C_IEEE_2]. **A. Takacs**, D. Medhat, H. Aubert, J.C. Portal, "Electromagnetic Analysis of the Experimental Setup Used to Investigate the Ratchet Effect in Two-Dimensional Electron System Under Microwave Radiation", in *Proc. of International Semiconductor Conference (CAS'2009)*, Sinaia, Romania, 12-14 Oct. 2009, Vol. I, pp. 337-340.
[C_IEEE_3]. **A. Takacs**, D. Medhat, H. Aubert, J.C. Portal, "A Method for Estimating the Electromagnetic Power Delivered by the Front-End Module used to Investigate the Ratchet Effect in Two-Dimensional Electron Gas System under Microwave Radiation", in *Proc. of 2010 European Microwave Conference (EuMC'2010)*, Paris, France, 28-30 Sept. 2010, pp. 1560 – 1563.
[C_IEEE_4]. D. Medhat, **A.Takacs**, H.Aubert, "Optimum position of the two-dimensional electron gas sample in the cryogenic metallic cavity system used in studying Ratchet Effect", in *Proc. of European Microwave Conference (EUMC'2011)*, Manchester, UK, Oct. 2011, pp. 964-967.

Articles présentés dans des conférences internationales avec actes et comité de lecture, aux workshops et aux symposiums

[C_1]. D. Medhat, **A. Takacs**, H. Aubert, J.-C. Portal, "Investigation of the metallic cavity influence on the electromagnetic behavior of the setup used in studying the Ratchet Effect", in *Proc. of Progress In Electromagnetics Research Symposium (Piers'2011)*, Marrakech, Morocco, 20-23 March 2011.

Avec Guillaume Vigneau (thèse CIFRE partiellement confidentielle) :

Articles dans de revues internationales avec comité de lecture

[Rev1]. **G. Vigneau**, M. Cheikh, R. Benbouhout, **A. Takacs**, "Design and Modeling of PCB Coils for Inductive Power Charging", Wireless Power Transfer, (Cambridge University Press), Vol. 2, Special Issue 02, Sept. 2015, pp 143 – 152. (https://doi.org/10.1017/wpt.2015.17)

Articles présentés dans de Conférences IEEE (avec actes et comité de lecture) et indexés dans la base de données IEEExplore

[C_IEEE_1].   **G. Vigneau**, M. Cheikh, **A. Takacs**, R. Benbouhout, S Bouguern, "Power Source Evaluation of a Wireless Power Transfer System", in Proc. of Wireless Power Transfer Conference (IEEE WPTC'2014), Jeju, Korea, 8-9 May'2014, pp. 9-12.

[C_IEEE_2].   D. Jugieu, **G. Vigneau**, M. Cheikh, S. Kessler, R. Benbouhout, **A. Takacs**, "Design and simulation of printed winding inductors for inductive wireless power charging applications", in Proc. of IEEE WPTC'2015, Boulder, USA, May 2015.

Avec Matthieu Gastaldi :

Articles dans de revues internationales à comité de lecture et avec cotation ISI/facteur d'impact

[ISI2]. **M. Gastaldi**, D. Dragomirescu, **A. Takacs**, V. Armengaud, S. Rochette, "Micro-strip slow wave line for phase shifting cells", IET Electronics Letters, Vol. 51, No. 20, pp. 1589–1591, 1st October 2015 (ISSN: 0013-5194).

Brevets d'invention

[B1].   Une demande de brevet concernant le travail de Matthieu Gastaldi a été déposée en décembre 2016 par Thales Alenia Space :

V/Réf. :	**TAS-TL 1611, Bex1612**
N/Réf. :	**070575 FR CVI/BQT**
Demande de brevet :	*France N° 1601809*
Déposée le :	*20 décembre 2016*
Titre Officiel	*LIGNE DE TRANSMISSION A ONDES LENTES A MEANDRES*
Titulaires :	*CENTRE NATIONAL DE LA RECHERCHE SCIENTIFIQUE / CENTRE NATIONAL D'ETUDES SPATIALES / THALES*
Inventeurs :	*Matthieu GASTALDI, Daniela DRAGOMIRESCU, Alexandru TAKACS,*

Articles présentés dans de Conférences IEEE (avec actes et comité de lecture) et indexés dans la base de données IEEExplore

[C_IEEE_1].   **M. Gastaldi**, D. Dragomirescu, **A. Takacs**, V. Armengaud, "Compact Phase Shifting Cell Based on Micro-Strip Slow Wave Lines", 17th edition of the International Symposium on RF-MEMS and RF-MICROSYSTEMS (MEMSWAVE 2016), July 2016, Bucarest, Roumanie

Avec Zhening Yang :

Articles dans de revues internationales avec comité de lecture

[Rev1]. **Z. Yang, A. Takacs**, S. Charlot, D. Dragomirescu, "Flexible Substrate Technology for Millimeter Wave Wireless Power Transmission", Wireless Power Transfer (Cambridge University Press), Vol.3, N°1, pp.24-33, March 2016. (https://doi.org/10.1017/wpt.2015.21)

Articles présentés dans de Conférences IEEE (avec actes et comité de lecture) et indexés dans la base de données IEEExplore

[C_IEEE_1].   **Z. Yang, A. Takacs**, S. Charlot, D. Dragomirescu, "Design of Kapton based passive circuits at microwave frequencies", in Proc. of 2015 European Microwave Conference (EuMC'2015), Paris, France, 6-11 Sept. 2015.

Articles présentés dans des conférences internationales avec actes et comité de lecture, aux workshops et aux symposiums

[C_1]. **Z. Yang**, **A. Takacs**, S. Charlot, A. Rumeau, D. Dragomirescu, "Technologie pour intégration sur substrat souple dans le domaine millimétrique", in Proc of JNM'2015, Bordeaux, France, 1-5 June 2015.

Avec Abderrahim Okba

Articles dans de revues internationales à comité de lecture et avec cotation ISI/facteur d'impact

[ISI1]. **A. Okba, A. Takacs**, H. Aubert, S. Charlot, P-F. Calmon, "Multiband rectenna for microwave

applications", Comptes Rendus Physique, Vol. 18, Issue 2, pp 107-117, Feb. 2017 (https://doi.org/10.1016/j.crhy.2016.12.002)

Articles présentés dans de Conférences IEEE (avec actes et comité de lecture) et indexés dans la base de données IEEExplore

[C_IEEE_1].   **A. Okba**, S. Charlot, P-F Calmon, **A. Takacs**, H. Aubert, "Cross dipoles rectenna for microwave applications", in Proc. of IEEE WPTC'2016, Aveiro, Portugal, May 2016.

[C_IEEE_1].   **A. Okba**, S. Charlot, P-F Calmon, **A. Takacs**, H. Aubert, "Multiband Rectenna for microwave applications", in Proc. of 2016 European Microwave Conference (EuMC'2016), London, UK, Oct. 2016.

[C_IEEE_3].   **A. Takacs; A. Okba**; H. Aubert; S. Charlot; P-F Calmon, "Recent advances in electromagnetic energy harvesting and Wireless Power Transfer for IoT and SHM applications", in Proc. of 2017 IEEE ECMSM, May 2017

[C_IEEE_4].   **A. Okba, A. Takacs**, H. Aubert, A. Bellion, D. Granena, "A Wideband and Compact Circularly-Polarized Rectenna for Low Power Application", in Proc. of 2017 IEEE Mediterranean Microwave Symposium (MMS'2017), Nov. 2017.

Articles présentés dans des conférences internationales avec actes et comité de lecture, aux workshops et aux symposiums

[C_1]. **A. Okba, A. Takacs**, H. Aubert, S. Fredon, L. Despoisse, 'Récupération de l'énergie micro-onde pour l'alimentation de capteurs sans fil à bord des satellites', in Proc of JNM'2015, Bordeaux, France, 1-5 June 2015.

[C_2]. **A. Okba, A. Takacs**, H. Aubert, "Rectenna à 2.45 GHz utilisant une antenne à dipôle arrondi", Journées Nationales Micro-ondes (JNM'2017), Saint Malo, France, Mai 2017.

J'ai encadré dans la période 2009-2017 6 stagiaires niveaux master M2 et une dizaine de stagiaires niveaux L3/M1.

Research projects and responsibilities:

Contrats	Période	Type contrats/financement	Responsabilités*
AMICOM - Advanced MEMS for RF and MIllimeterwave COMmunications	2014-2017	Européen (FP7)	P
MEMS Based Millimeterwave Imaging System (MEMIS)	2011-2014	Européen (mnt-era.net)	R, PM
ANR-PNANO-NANOTERRA	2009-2011	ANR	P
Générateur Thermoélectrique sans fil en technologie MEMS'	2010	Industriel : Rockwell-Collins	P, PM
Smartharness	2010	Région Midi-Pyrénées	P
Antenne hélice compacte	2011	étude R&T CNES	P
R&T n° 115052 « Evaluation de diverses micro-sources de génération et stockage d'énergie »,	2011-2012	étude R&T CNES	P
Etude et modélisation électromagnétique du transfert d'énergie pour le chargeur inductif	2012 - 2013	Industriel : Continental Automotive	R, M
Evaluation µsources de génération et stockage d'énergie	2013	étude R&T CNES	R, M
Carbon Based Smart Systems for wireless applications (NANO-RF)	2012-2017	Européen (FP7-ICT, STREP)	P
ICT COST Action IC1301 Wireless Power Transmission for Sustainable Electronics (WiPE)	2013-2017	Européen (COST)	R, M représentant de la France dans le Management Committee et leader du SWG 4.1 'Space Application'
Projet Optenloc	2018-en cours	Région Occitanie (en cours)	R,M
Projet ANR McBIM	2017-en cours	ANR	P, PM

*R : coordonnateur et responsable scientifique ; les projets dont j'ai été responsable scientifique sont soulignés en 'gris'
*P : participation au projet (membre dans l'équipe projet)
*PM : participation au montage du projet
*M : montage intégral du projet ou du WP concernant LAAS

List of publications

Papers published in peer-reviewed international journals with ISI impact factor

[ISI1]. **A. Takacs**, H. Aubert, P. Pons, T. Parra, R. Plana, "Miniature coplanar bandstop filters for Ka-band applications based on an original Resonant Coupling Irises topology", *IET Electronics Letters (IET- former IEE periodical)*, Issue 20, Vol. 40, pp. 1274–1275, 30 Sept. 2004. (ISSN: 0013-5194)

[ISI2]. **A. Takacs**, D. Lillonga, H. Aubert, J.W. Tao, P. Pons, R. Crampagne, R. Plana, J.Ch. Cayrou, "Design of a Broadband WR-to-CPWG Millimeterwave Transition", *Microwave and Optical Technology Letters (John Wiley&Sons periodical)*, vol 43, pp: 11-14, 5 Oct. 2004. (ISSN: 0895-2477)

[ISI3]. D. Dubuc, M. Saadaoui, S. Melle, F. Flourens, L. Rabbia, B. Ducarouge, K. Grenier, P. Pons, A. Boukabache, L. Bary, **A. Takacs**, H. Aubert, O. Vendier, J.L. Roux, R. Plana, "Smart MEMS concept for high secure RF and millimeterwave communications", *Microelectronics Reliability (Elsevier journal)*, Issue 6, Vol.44, pp.899-907, June 2004. (ISSN: 0026-2714)

[ISI4]. M. Dragoman, **A. Takacs**, A. A. Muller, H. Hartnagel, R. Plana, K. Grenier, D. Dubuc, "Nanoelectromechanical switches based on carbon nanotubes for microwave and millimeter waves", *Applied Physics Letters (American Institute of Physics periodical)*, vol. 90, 113102 / 2007. (ISSN 0003-6951)

[ISI5]. **A.Takacs**, D. Neculoiu, D. Vasilache, A. Muller, P. Pons, L. Bary, P. Calmon, H. Aubert, R. Plana, "Tunable bandstop MEMS filter for millimeter wave applications", *IET Electronics Letters*, Issue 12, Vol. 43, pp. 676-677, 7 June 2007. (ISSN: 0013-5194)

[ISI6]. **A. Takacs**, M. Huard, S. Kessler, G.A. Chakam, E. Lardjane, "Estimation of low frequency coverage inside car for passive access system entry", *IET Electronics Letters*, Issue 12, Vol. 45, No. 12, pp. 596-597, 4 June 2009. (ISSN: 0013-5194).

[ISI7]. **A. Takacs**, N. J.G. Fonseca, H. Aubert, "Height Reduction of the Axial-Mode Open-Ended Quadrifilar Helical Antenna", *IEEE Antenna and Wireless Propagation Letters,* vol. 9, pp. 942-945, 2010.

[ISI8]. **A. Takacs**, H. Aubert, H. Diez, D. Belot, "Miniaturization of Quadrifilar Helical Antenna: Impact on Efficiency and Phase Center Position", *IET Microwaves, Antennas & Propagation*, Volume 7, Issue 3, 19 February 2013, pp. 202 – 207.

[ISI9]. **A. Takacs**, H. Aubert, L. Despoisse, S. Fredon, "Microwave energy harvesting for satellite applications", *IET Electronics Letters*, Issue 11, Vol. 49, pp. 722-723, 23 May 2013.

[ISI10]. **A. Takacs**, H. Aubert, L. Despoisse, S. Fredon, "Broadcast energy", *IET Electronics Letters*, Issue 11, Vol. 49, 23 May 2013, p. 682.

[ISI11]. **A. Takacs**, H. Aubert, S. Fredon, L. Despoisse, H. Blondeaux, "Microwave power harvesting for satellite health monitoring," *IEEE Trans. on Microwave Theory Tech*, Vol.: 62, Issue: 4 , pp. 1090 - 1098, April 2014.

[ISI12]. M. Gastaldi, D. Dragomirescu, **A. Takacs**, V. Armengaud, S. Rochette, "Micro-strip slow wave line for phase shifting cells", *IET Electronics Letters*, Vol. 51, No. 20, pp. 1589–1591, 1st October 2015.

[ISI13]. A. Okba, **A. Takacs**, H. Aubert, S. Charlot, P-F. Calmon, "Multiband rectenna for microwave applications", *Comptes Rendus Physique*, *Elsevier*, Vol. 18, Issue 2, pp 107-117, Feb. 2017.

[ISI14]. COST Action IC1301 Team (including A. Takacs), "Europe and the future for the WPT", *IEEE Microwave Magazine*, Vol. 18, Issue: 4, pp: 56 - 87, June 2017 (ISSN: 1527-3342).

Papers published in (peer-reviewed) international journals

[Rev1]. **A. Takacs**, A. Serbanescu, G. Leu, H. Aubert, P. Pons, T. Parra, R. Plana, *"Microwave Passive Circuits Optimization Using Genetic Algorithms"*, *Romanian Journal of Information Science and Technology*, vol. 7, Number 3-4, pp: 309-316, 2004. (ISSN 1453-8245)

[Rev2]. **A. Takacs**, D.Neculoiu, D. Vasilache, A. Muller, P. Pons, L. Bary, R. Plana, *"A New Topology of Tunable MEMS Filters for Millimeter Wave Systems"*, *MTA review*, no. 1/2006, pp: 55-61, 2006. (ISSN 1453-259x).

[Rev3]. **A.Takacs**, D. Neculoiu, D. Vasilache, A. Muller, P. Pons, L. Bary, R. Plana, "Design of tunable bandpass MEMS filter for millimeter wave systems", *Revue Roumaine des Sciences Techniques*, tome 51, 4, pp: 471-477, 2006. (ISSN: 0035-4066)

[Rev4]. **A. Takacs,** D.Neculoiu, D. Vasilache, A. Muller, P. Pons, L. Bary, P.F. Calmon, H. Aubert, R. Plana "Tunable bandpass MEMS filter for millimeter wave application: design and results", *MTA review,* Vol. XIX, No. 4, pp. 409-418, Dec. 2009. (ISSN: 1843-3391)

[Rev5]. D. Medhat, **A. Takacs**, H. Aubert, "A methodology to study the electromagnetic behavior of a cryogenic metallic system used to control the ratchet effect", *Progress In Electromagnetics Research M*, Vol. 23, 123-137, 2012.

[Rev6]. G. Vigneau, M. Cheikh, R. Benbouhout, **A. Takacs**, "Design and Modeling of PCB Coils for Inductive Power Charging", *Wireless Power Transfer, (Cambridge University Press),* Vol. 2, Special Issue 02, Sept. 2015, pp 143 – 152.

[Rev7]. **A. Takacs**, H. Aubert, D. Belot, H. Diez, "Miniaturization of Compact Quadrifilar Helix Antennas for Telemetry, Tracking and Command Applications", *Progress In Electromagnetics Research C*, Vol. 60, 125-136, 2015.

[Rev8]. Z. Yang, **A. Takacs**, S. Charlot, D. Dragomirescu, "Flexible Substrate Technology for Millimeter Wave Wireless Power Transmission", *Wireless Power Transfer (Cambridge University Press)*, Vol.3, N°1, pp.24-33, March 2016.

[Rev9]. A. Okba, **A. Takacs**, and H. Aubert, "Compact Flat Dipole Rectenna for IoT Applications," *Progress In Electromagnetics Research C*, Vol. 87, 39-49, 2018.

Papers published in the proceedings of IEEE conferences and symposium (indexed in IEEExplore)

[C_IEEE_1]. **A. Takacs**, P. Pons, H. Aubert, R. Plana, T. Parra, J. Graffeuil, H. Baudrand, J.L. Cazaux 'An original micromachined planar Ka Band filter based on a Resonant Coupling Irises topology', in *Proc of International Semiconductor Conference (CAS'2001)*, Sinaia, Romania, 9-13 Oct. 2001, vol. I, pp. 147-150, (ISBN: 0-7803-6666-2, IEEE catalog number: 01TH8547).

[C_IEEE_2]. K.Grenier, L.Rabbia, **A.Takacs**, P.Pons, T.Parra, P.Caudrillier, O.Pascal, H.Aubert, J.Graffeuil, R.Plana 'MEMS technology as a contender for the future wireless applications', in *Proc. of International Semiconductor Conference (CAS'2001)*, Sinaia, Romania, 9-13 Oct. 2001, vol. I, pp. 101-110, (ISBN: 0-7803-6666-2, IEEE catalog number: 01TH8547).

[C_IEEE_3]. **A. Takacs,** H. Aubert, P. Pons, T. Parra, R. Plana, J. Graffeuil, H. Baudrand, J.L. Cazaux, 'Resonant Coupling Irises for the Design of New Planar Bandstop Filters', *in Proc of European Microwave Conference (EUMC 2002)*, 24-26 Sept. 2002, Milan, Italy, pp. 1-4 (IEEE Digital Object Identifier 10.1109/EUMA.2002.339371)**.**

[C_IEEE_4]. P. Caudrillier, **A. Takacs**, O. Pascal, H. Aubert, P. Pons, R. Plana 'Compact Circularly Polarized Radiating Element for Ka-band Satellite Communications', in *Proc of IEEE AP-S International Symposium*, San Antonio, USA, 16-21 June 2002, vol. I, pp. 18-21. (ISBN: 0-7803-7330-8, IEEE catalog number: 02CH37313)

[C_IEEE_5]. K.Grenier, D.Dubuc, L.Rabbia, **A.Takacs**, P.Pons, T.Parra, P.Caudrillier, H.Aubert, J.Graffeuil, O.Pascal, P.Combes, H.Baudrand, R.Plana, 'MEMS devices for the future wireless applications' in *Proc. of 4th IEEE International Caracas Conference on Devices, Circuits and Systems (ICCDCS'2002)*, Oranjestad (Aruba), 17-19 Avril 2002, pp. D031.1-D031.8 (IEEE Digital Object Identifier 10.1109/ICCDCS.2002.1004045)

[C_IEEE_6]. D.Dubuc, K.Grenier, L.Rabbia, **A.Takacs**, M.Saadaoui, P.Pons, P.Caudrillier, O.Pascal, H.Aubert, H.Baudrand, J.Tao, P.Combes, J.Graffeuil, R.Plana, 'MEMS and MEMS technologies for wireless communications', in Proc. of *23rd International Conference on Microelectronics (MIEL 2002),* Nis, Yugoslavia, 12-15 May 2002, pp.91-98. (IEEE Digital Object Identifier 10.1109/MIEL.2002.1003153)

[C_IEEE_7]. **A. Takacs**, D. Lillonga , H. Aubert ,J.W. Tao , R. Crampagne ,R. Plana , P. Pons , J.Ch. Cayrou, 'Design of a Novel Broadband CPWG-to-WR Transition for Ka-band Satellite Communications', in *Proc. of International Semiconductor Conference (CAS'2003)*, Sinaia, Romania, Sept. 2003, vol I, pp. 69-72. (ISBN 0-7803-7821-0, IEEE catalog number: 03TH8676)

[C_IEEE_8]. J. Kuchenbecker, L. Bary, X. Lafontan, F. Flourens, **A. Takacs**, P. Pons, K. Grenier, D. Dubuc, H. Aubert, F. Pressecq, R. Plana, 'Microwave and physical behavior of micro-machined structures on membrane for space applications', in *Proc. of International Semiconductor Conference (CAS'2003)*, Sinaia, Romania, Sept. 2003, vol I, pp. 105-112 (ISBN: 0-7803-7821-0, IEEE catalog number: 03TH8676).

[C_IEEE_9]. **A. Takacs**, A. Serbanescu, G. Leu, H. Aubert, P. Pons, T. Parra, R. Plana "On Layout Optimisation of the Microwave Diplexer Filter using Genetic Algorithms", in *Proc. of International Semiconductor Conference (CAS'2004)*, Sinaia, Romania, 4-6 Oct. 2004, , vol. I, pp. 133-136. (ISBN: 0-7803-8499-7, IEEE catalog number: 04TH8748)

[C_IEEE_10]. D. Neculoiu, G. Konstantinidis, K. Mutamba, **A. Takacs**, D. Vasilache, C. Sydlo, T. Kostopoulos, A. Stavrinidis, A. Muller, "Electromagnetic modeling of micromachined GaN thin films for FBAR applications", in *Proc. of International Semiconductor Conference (CAS'2005)*, Sinaia, Romania, 3-5 Oct. 2005, vol. 1, pp:119 – 122. (ISBN 0-7803-9214-0)

[C_IEEE_11]. **A. Takacs**, D. Neculoiu, D. Vasilache, A. Muller, P. Pons, L. Bary, R. Plana, "Design of Tunable MEMS Filters for Millimeter Wave Systems", in *Proc. of 13th IEEE Mediterranean Electrotechnical Conference (MELECON'2006),* Malaga, Spain, 16-19 May 2006, vol. I, p. 301-30., (ISBN: 1-4244-0087-2, IEEE catalog number: 06CH37756)

[C_IEEE_12]. A.A. Muller, D. Neculoiu, **A. Takacs**, D. Vasilache, F. Giacomozzi, A. Cismaru, "Lumped element bandpass micromachined filter design for DCS1800(GSM)", in *Proc. of 13th IEEE Mediterranean Electrotechnical Conference (MELECON'2006),* Malaga, Spain, 16-19 May 2006, vol II, p. 643-646. (ISBN: 1-4244-0087-2, IEEE catalog number: 06CH37756)

[C_IEEE_13]. **A. Takacs**, D. Neculoiu. D. Vasilache, A. Muller. P. Pons, H. Aubert, R. Plana, *"Tunable MEMS filters for millimeter wave applications"*, International Semiconductor Conference Proceedings, CAS'2006, pp. 115-118, Sinaia, Romania, 27-30 Sept. 2006 (ISBN: 1-4244-0109-7/06, IEEE catalog number: 06TH8867).

[C_IEEE_14]. M. Dragoman, **A. Takacs**, H. Hartnagel, R. Plana, "RF NEMS switch based on vertical carbonanotube", in *Proc. of International Semiconductor Conference (CAS'2006)*, Sinaia, Romania, 27-30 Sept. 2006, pp. 111-114. (ISBN: 1-4244-0109-7/06, IEEE catalog number: 06TH8867).

[C_IEEE_15]. Andrei A. Muller, D. Neculoiu, D. Vasilache, **A. Takacs**, A. Cismaru, P. Pons, R. Plana, "Micromachined bandpass filter with a new controlled resonance for WLAN 5200 filter applications", in *Proc. of International Semiconductor Conference (CAS'2006)*, Sinaia, Romania, 27-30 Sept. 2006, pp. 451-454. (ISBN: 1-4244-0109-7/06, IEEE catalog number: 06TH8867).

[C_IEEE_16]. D. Neculoiu, F. Giacomozzi. L. Bary, D. Vasilache, Andrei A. Muller, B. Margesin, I. Petrini, C. Buiculescu. **A. Takacs**, R. Plana, A. Muller, "Compact lumped elements micro-machined band-pass filters with discrete switching for 1.8/5.2 GHz applications", in *Proc. of International Semiconductor Conference (CAS'2006)*, Sinaia, Romania, 27-30 Sept. 2006, pp. 107-110. (ISBN 1-4244-0109-7/06, IEEE catalog number: 06TH8867).

[C_IEEE_17]. **A. Takacs**, D. Neculoiu, D. Vasilache, A. Muller, P. Pons, L. Bary, P. Calmon, R.Plana, H.Aubert, "New Topologies of Tunable Bandstop MEMS Filters for Millimeter Wave Applications", in *Proc of European Microwave Conference (EUMC'2007)*, Munich, Germany, 8-12 Oct. 2007, pp.126 - 129.

[C_IEEE_18]. **A. Takacs**, D. Neculoiu, D. Vasilache, A. Muller, P. Pons, H.Aubert, R.Plana, "An innovative and versatile topology for tunable bandpass filter", in *Proc. of International Semiconductor Conference (CAS'2007)*, Sinaia, Romania, 15-17 Oct. 2007, vol. I, pp. 297-300. (ISBN: 978-1-4244-0847-4)

[C_IEEE_19].   **A.Takacs**, D. Neculoiu, D. Vasilache, A. Muller, P. Pons, L. Bary, P. Calmon, H.Aubert, R.Plana, "Tunable Bandstop and Bandpass MEMS Filters for Millimeter Wave Applications", *In Proc. of European Microwave Conference (EUMC'2008)*, Amsterdam, Netherlands, 27-31 Oct. 2008, pp. 591-594. (ISBN 978-2-87487-005-7).

[C_IEEE_20].   **A. Takacs**, D. Medhat, H. Aubert, J.C. Portal, "Electromagnetic Analysis of the Experimental Setup Used to Investigate the Ratchet Effect in Two-Dimensional Electron System Under Microwave Radiation", in *Proc. of International Semiconductor Conference (CAS'2009)*, Sinaia, Romania, 12-14 Oct. 2009, Vol. I, pp. 337-340. (ISBN 978-1-4244-4413-7, IEEE catalog number: CFP09CAS-PRT)

[C_IEEE_21].   **A. Takacs**, M. Huard, S. Kessler, G.A. Chakam, E. Lardjane, "Estimation of magnetic field coverage inside the car for passive access system entry", in *Proc. of 2009 European Microwave Conference (EuMC'2009)*, Rome, Italy, 29 Sept – 1 Oct. 2009, pp. 998 – 1001 (ISBN: 978-1-4244-4748-0).

[C_IEEE_22].   **A. Takacs**, N.J.G. Fonseca, H. Aubert, X. Dollat, "Miniaturization of Quadrifilar Helix Antenna for VHF Band Applications," in *Proc. of LAPC'2009*, Loughborough, UK, Nov. 16-17, 2009, pp. 597-600. (ISBN: 978-1-4244-2721-5)

[C_IEEE_23].   D. Medhat, **A. Takacs**, H. Aubert, J.C. Portal, "Comparative Analysis of Different Techniques for Controlling Ratchet Effect in a Periodic Array of Asymmetric Antidots", in *Proc. of Asia-Pacific Microwave Conference (APMC'2009)*, Singapore, 7-10 Dec 2009, pp. 1711 - 1714. (ISBN: 978-1-4244-2802-1, IEEE Catalog Number: CFP09APM-CDR)

[C_IEEE_24].   N. J. Fonseca, **A. Takacs**, H. Aubert, X. Dollat, "Design and Experimental Validation of a Compact Quadrifilar Helix Antenna in VHF Band", in *Proc. of Asia-Pacific Microwave Conference (APMC'2009)*, Singapore, 7-10 Dec 2009. (ISBN: 978-1-4244-2802-1, IEEE Catalog Number: CFP09APM-CDR)

[C_IEEE_25].   **A. Takacs**, D. Medhat, H. Aubert, J.C. Portal, "A Method for Estimating the Electromagnetic Power Delivered by the Front-End Module used to Investigate the Ratchet Effect in Two-Dimensional Electron Gas System under Microwave Radiation", in *Proc. of 2010 European Microwave Conference (EuMC'2010)*, Paris, France, 28-30 Sept. 2010, pp. 1560 – 1563 (ISBN: 978-1-4244-7232-1)

[C_IEEE_26].   D. Medhat, **A.Takacs**, H.Aubert, "Optimum position of the two-dimensional electron gas sample in the cryogenic metallic cavity system used in studying Ratchet Effect", *In Proc. of European Microwave Conference (EUMC'2011)*, Manchester, UK, Oct. 2011, pp. 964-967.

[C_IEEE_27].   **A. Takacs**, T. Idda, H. Aubert, H. Diez, "Miniaturization of Quadrifilar Helix Antennas for Space Applications", in *Proc Of 15th International Symposium on Antenna Technology and Applied Electromagnetics* (ANTEM), pp. 1-3, Toulouse, France, 25-28 June 2012.

[C_IEEE_28].   **A. Takacs**, T. Idda, H. Aubert, H. Diez, "Miniaturization technique for quadrifilar helix antenna", in *Proc. of IEEE AP-S International Symposium*, Chicago, USA, 8-14 June 2012.

[C_IEEE_29].   **A. Takacs**, T. Idda, H. Aubert, H. Diez, "Compact VHF Quadrifilar Helix Antenna", in *Proc. of European Microwave Conference (EUMC'2012)*, Amsterdam, Netherlands, 28 Oct – 2 Nov. 2012.

[C_IEEE_30].   D. Neculoiu, A. Bunea, P. Calmon, **A. Takacs**, "140 GHz Wide-Band Micromachined Double Folded Slot Antenna", in *Proc. of IEEE APCAP 2012*, Singapore, 27-29 august 2012.

[C_IEEE_31].   **A. Takacs**, A. Bunea, A. Zair, D. Neculoiu, H. Aubert, "Diode Modeling for Millimeter Wave Applications based on Co-Simulation Technique", in *Proc. of IEEE International Semiconductor Conference (CAS'2012)*, Sinaia, Romania, Oct. 2012, pp. 201-204. (ISBN: 978-1-4673-0736-9)

[C_IEEE_32].   A. Bunea, D. Neculoiu, P. Calmon, **A. Takacs**, "Micromachined front-end for 60 GHz Applications', in *Proc. of International Semiconductor Conference (CAS'2012)*, Sinaia, Romania, Oct. 2012, pp. 197-200. (ISBN: 978-1-4673-0736-9)

[C_IEEE_33].   A. Bunea, D. Neculoiu, A. Avram, T. Kiuru, T. Vaha-Heikkila, **A. Takacs**, P. Calmon, "160 GHz Silicon Micromachined Folded Slot Antenna Array", in *Proc. of IEEE APMC 2012*, Taiwan, Dec. 2012.

[C_IEEE_34].   **A. Takacs**, H. Aubert, M. Bafleur, J.M. Dilhac, F. Courtade, S. Fredon, L. Despoisse, C.Vanhecke, G. Cluzet, "Energy harvesting for powering wireless sensor networks on-board geostationary broadcasting satellites", in *Proc. of IEEE international conference on Green Computing and Communications (GreenCom'2012)*, 20-23 Nov. 2012, Besançon, France, pp. 637 - 640.

[C_IEEE_35].   **A. Takacs**, H. Aubert, L. Despoisse, S. Fredon, "Design and implementation of a rectenna for satellite application", in Proc. of *IEEE Wireless Power Transfer Conference (WPTC'2013)*, 15-16 May'2013, pp.183 – 186.

[C_IEEE_36].   **A. Takacs**, H. Aubert, L. Despoisse, S. Fredon, "K-band energy harvesting for satellite application", in *Proc. of IEEE IMS'2013,* Seattle, USA, 2-7 June' 2013.

[C_IEEE_37].   **A. Takacs**, H. Aubert, S. Fredon, L. Despoisse, "K-band energy harvesting circuits for satellite application", *In Proc. of European Microwave Conference (EUMC'2013)*, Nuremberg, Germany, Oct. 2013, pp. 991-994.

[C_IEEE_38].   G. Vigneau, M. Cheikh, **A. Takacs**, R. Benbouhout, S Bouguern, "Power Source Evaluation of a Wireless Power Transfer System", in *Proc. of Wireless Power Transfer Conference (IEEE WPTC'2014)*, Jeju, Korea, 8-9 May'2014, pp. 9-12.

[C_IEEE_39].   **A. Takacs**, H. Aubert, S. Charlot, S. Fredon, L. Despoisse, "Compact Rectenna for Space Application", in *Proc. of IEEE IMS'2014,* Tampa, USA, 1-6 June, 2014.

[C_IEEE_40].   **A. Takacs**, H. Aubert, A. Luca, S. Charlot, S. Fredon, L. Despoisse, "Rectenna Design for K Band Application", in *Proc. of IEEE European Microwave Conference (EUMC'2014)***,** Rome, Italy, Oct'2014**.**

[C_IEEE_41].   A. Bunea, D. Neculoiu, P. Calmon, **A. Takacs**, "Design and Characterization of a Micromachined Receiver for W Band Applications", in *Proc. of IEEE European Microwave Conference (EUMC'2014)***,** Rome, Italy, Oct'2014.

[C_IEEE_42].   **A. Takacs**, H. Aubert, S. Fredon, L. Despoisse, "Design and Characterization of Effective Antennas for K-band Rectennas", in *Proc. of IEEE EUCAP'2015*, Lisbon, Portugal, April'2015.

[C_IEEE_43].   **A. Takacs**, H. Aubert, S. Charlot, "Ultra-Compact Ku band Rectenna", in *Proc. of IEEE IMS'2015,* Phoenix, USA, 17-22 May, 2015.

[C_IEEE_44].   D. Jugieu, G. Vigneau, M. Cheikh, S. Kessler, R. Benbouhout, **A. Takacs**, "Design and simulation of printed winding inductors for inductive wireless power charging applications", in *Proc. of IEEE WPTC'2015*, Boulder, USA, May 2015.

[C_IEEE_45].   Z. Yang, **A. Takacs**, S. Charlot, D. Dragomirescu, "Design of Kapton based passive circuits at microwave frequencies", in *Proc. of 2015 European Microwave Conference (EuMC'2015),* Paris, France, 6-11 Sept. 2015.

[C_IEEE_46].   A. Okba, S. Charlot, P-F Calmon, **A. Takacs**, H. Aubert, "Cross dipoles rectenna for microwave applications", in *Proc. of IEEE WPTC'2016*, Aveiro, Portugal, May 2016.

[C_IEEE_47].   A. Okba, S. Charlot, P-F Calmon, **A. Takacs**, H. Aubert, "Multiband Rectenna for microwave applications", in *Proc. of 2016 European Microwave Conference (EuMC'2016)*, London, UK, Oct. 2016.

[C_IEEE_48].   **A. Takacs**; D. Dragomirescu; S. Charlot; P-F Calmon, "Flexible technology for millimeter-wave wireless sensors applications", in *Proc. of 2017 IEEE ECMSM, May 2017*

[C_IEEE_49].   **A. Takacs**; A. Okba; H. Aubert; S. Charlot; P-F Calmon, "Recent advances in electromagnetic energy harvesting and Wireless Power Transfer for IoT and SHM applications", in *Proc. of 2017 IEEE ECMSM, May 2017*

[C_IEEE_50].   A. Okba, **A. Takacs**, H. Aubert, A. Bellion, D. Granena, "A Wideband and Compact Circularly-Polarized Rectenna for Low Power Application", in *Proc. of 2017 IEEE Mediterranean Microwave Symposium (MMS'2017)*, Nov. 2017.

[C_IEEE_51].   **A. Takacs**, S. Charlot, P. Calmon, D. Dragomirescu, "VHF/UHF Kapton supported antenna for cubesat applications", in *Proc. of IEEE APS (Antennas and Propagation Symposium)*, 9-14 July 2017, San Diego, USA.

[C_IEEE_52].   A.Okba, **A.Takacs**, H.Aubert, **"**900MHz Miniaturized rectenna", in *Proc. of IEEE WPTC'2018*, Montreal, Canada, 3-7 june 2018.

[C_IEEE_53].   **A. Takacs**, A. Okba, H. Aubert, D. Granena, M. Romier, A. Bellion, "Compact C-band Rectenna for Satellite Applications"in *Proc. of IEEE WPTC'2018*, Montreal, Canada, 3-7 june 2018.

[C_IEEE_54].   A.Okba, **A.Takacs**, H.Aubert, 'Compact Flat Dipole Rectenna for Energy Harvesting or Wireless Power Transmission Applications', in *Proc. of IEEE APS (Antennas and Propagation Symposium)*, Boston, Massachusetts, USA, July 2018

[C_IEEE_55].   A. Okba, **A. Takacs**, H. Aubert, 'Compact Planar Integrated Rectenna for Batteryless IoT Applications', in *Proc. of EUMC*'2018, Madrid, Spain, Sept. 2018

Paper presented at international conferences (with reviewing committee)

[C_1].   K. Grenier, R. Plana, T. Parra, P. Pons, L. Rabbia, J. Graffeuil, **A. Takacs**, H. Aubert, P. Caudrillier, O. Pascal, P. Combes, "MEMs and Silicon Micromachined Components for Communications systems", in *Proc. of 8th International Conference on Mixed Design of Integrated Circuits and Systems (MIXDES'2001)*, Zakopane Poland, 21-23 June 2001, pp.23-29.

[C_2].   K. Grenier, L. Rabbia, P. Pons, **A. Takacs**, T. Parra, J. Graffeuil, H. Aubert, R. Plana, *'Advanced analysis and design methods for RF and millimeter wave MEMS'*, in *Proc. of 15th European Conference on Circuit Theory and Design (ECCTD'01)*, Helsinki, Finland, 28-31 Août 2001.

[C_3].   P.Pons, K.Grenier, L.Rabbia, T.Parra, R.Plana, P.Caudrillier, P.Combes, O.Pascal, H.Aubert, **A.Takacs**, M.Salez, G.Gol'tsman, "Membrane supported circuits for millimetric and sub-millimetric waves-length", in *Proc. of 26th International Conference on Infrared and Millimeter Waves (IRMMW'2001)*, Toulouse, France, 10-14 Sept. 2001.

[C_4].   **A. Takacs**, K. Grenier, P. Pons, H. Aubert, R. Plana, T. Parra, J. Graffeuil, H. Baudrand " Nouvelle Topologie de Filtre Micro-usiné Coplanaire pour les Communications en bande Ka" in *Proc. of 12$^{-èmes}$ Journées Nationales Microondes*, Poitiers, France, 16-18 mai 2001.

[C_5].   **A. Takacs**, P. Caudrillier, L. Rabbia, P. Pons, H. Aubert, H. Baudrand, P. Combes, O. Pascal, A. Sarremejean, T. Parra, J. Graffeuil, J. C. Cayrou, R. Plana, *'Module de Réception Multimédia Microusiné'*, 4$^{-ème}$ Journée d'Electromagnétisme et Micro-ondes de Toulouse (JMET'01), 30 janvier 2001, Toulouse, France.

[C_6].   H. Baudrand, H. Aubert, P. Caudrillier , J. C. Cayrou, P. Combes, J. Graffeuil, K. Grenier, O. Pascal, T. Parra, P. Pons, L. Rabbia, A. Sarremejean, **A. Takacs**, "Module de Réception Multimédia Microusiné sur Silicium", presented at " Journées d'Electronique 2001: 'Electronique Aéronautique et Spatiale' ", 15-16 mars 2001, Toulouse, France.

[C_7].   **A. Takacs**, H. Aubert, T. Parra, P. Pons, R. Plana,J. Graffeuil, H. Baudrand, J.-L. Cazaux, " Filtres planaires à « iris de couplage résonants » pour les télécommunications par satellite", presented at 5$^{-ème}$ *Journée d'Electromagnétisme et Micro-ondes de Toulouse (JMET'02)*, Toulouse, France, Feb. 2002.

[C_8].   **A. Takacs,** H. Aubert, P. Pons, T. Parra, R. Plana, J. Graffeuil, H. Baudrand, J.L. Cazaux**, "**New Planar Bandstop Filters with Resonant Coupling Irises for Satellite Communications Systems", presented at *International Workshop on Microwave Filters*, 24-26 June 2002, Toulouse, France.

[C_9].   **A. Takacs**, D. Lilonga, J.W. Tao, R. Crampagne, H. Aubert, R. Plana, P. Pons, J.Ch. Cayrou "Transition WR 28/CPW à faibles pertes d'insertion en bande Ka", invited paper at *JMET 2003*, Toulouse, France, 29 Jan 2003.

[C_10]. M. Saadoui, P. Pons, K. Grenier, D. Dubuc, R. Plana, X. Lafontan, H. Aubert, J.W. Tao, **A. Takacs**, O. Pascal, P. Caudrillier, 'Low losses Microsystems Technology for mm wave applications', in *Proc. of 4th Workshop on MEMS for Millimeterwave Communications (MEMSWAVE'2003)*, Toulouse, France, 2-4 July 2003, pp.F.29-F.32. (ISBN 2-907801-03-8)

[C_11]. J. Kuchenbecker, L. Bary, X. Lafontan, F. Flourens, **A. Takacs**, P. Pons, K. Grenier, D. Dubuc, H. Aubert, F. Pressecq, R. Plana, *'Reliability of Micro-machined Structures on Membrane for Space Applications'*, in *Proc. of 4th Workshop on MEMS for Millimeterwave Communications (MEMSWAVE'2003)*, Toulouse, France, 2-4 July 2003. (ISBN 2-907801-03-8)

[C_12]. P.Pons, D.Dubuc, F.Flourens, M.Saadaoui, S.Melle, **A.Takacs,** J.Tao, H.Aubert, A.Boukabache, T.Paillot, P.Blondy, O.Vendier, K.Grenier, R.Plana, "MEMS-based redundancy ring for low noise millimeter-wave front-end", in *Proc. of SPIE Photonics Europe*, Strasbourg (France), 26-30 Avril 2004, Vol.5455, MEMS, MOEMS, and Micromachining, 2004, pp.181-192. (ISBN 0-8194-5378-1)

[C_13]. **A. Takacs**, H. Aubert, P. Pons, T. Parra, R. Plana, J. Graffeuil, "A reducing size technique for the planar diplexer filter design based on resonant irises topology", presented at *International Workshop on Microwave Filters*, CNES-ESA, Toulouse, France, 13-15 Sept. 2004.

[C_14]. **A. Takacs**, A. Serbanescu, D. Neculoiu, A. Muller,*"Electromagnetic Modeling of the Microwave Switches for Communications Systems"***,** the 36th *Int. Symp. of Military Equipment and Technologies Research Agency*, , Romania, 26-27 May 2005, pp. 681-685. (ISBN 973-0-03923-2)

[C_15]. **A. Takacs**, D. Vasilache, C. Tibeica, D. Neculoiu, *"A New Topology of RF MEMS Shunt Switch for Reconfigurable Systems Applications"*, in *Proc of MEMSWAVE'2005 Workshop*, Lausanne, Switzerland, 22-24 June 2005.

[C_16]. D. Neculoiu, G Konstantinidis, K. Mutamba, **A. Takacs**, D.Vasilache, C. Sydlo, T. Kostopoulos, A. Stavrinidis, A.Muller, "Electromagnetic Modeling of GaN FBAR structures", in *Proc. of MEMSWAVE'2005 Workshop*, Lausanne, Switzerland, 22-24 June 2005.

[C_17]. **A. Takacs**, F. Giacomozzi, G. Konstantinidis, A. A. Muller, I. Petrini, L. Barry, B. Margesin, D. Vasilache, C. Buiculescu, A.Muller, D. Neculoiu, "Design and Realization of Lumped Components for Micromachined Filter Applications", in *Proc. of the 16th Workshop on Micromachining, Micromechanics and Microsystems(MME'2005),* Göteborg, Sweden 04-06, Sept. 2005,.

[C_18]. **A. Takacs,** D.Neculoiu, D. Vasilache, A. Muller, P. Pons, L. Bary, R. Plana, "A New Topology of Tunable MEMS Filters for Millimeter Wave Systems", in *Proc of 6th IEEE Communications International Conference (COMMUNICATIONS'2006),* , Romania, 8-10 June 2006, pp. 291-294. (ISBN 978-973-718-479-5).

[C_19]. **A. Takacs**, D. Neculoiu, D. Vasilache, A. Muller, P. Pons, L. Bary, P. Calmon, R. Plana, H. Aubert "Tunable Bandstop MEMS Filters for Ka and V-band Applications", in *Proc. of 8th International Symposium on RF MEMS and RF Microsystems (MEMSWAVE'2007)*, 26-29 June 2007, Barcelona, Spain. (ISBN 974-84-96736-22-1)

[C_20]. **A. Takacs**, P. Calmon, A. Rumeau, H. Aubert, P. Pons, A. Muller, D. Neculoiu, D. Vasilache, R. Plana, "Design and manufacturing of tunable bandpass filter for millimeter wave applications", in *Proc. of 20th Micromechanics Europe Workshop (MME'2009)*, Toulouse, France, 20-22 Sept. 2009, pp. B03_1-B03_4. (ISBN 2-907801-08-2)

[C_21]. **A. Takacs**, T. Idda, S. Aouba, H.Aubert, P. Pons, E. Girard "RF modeling and characterization of RF-MEMS switches for reconfigurable reflectarray applications", in *Proc. of 11th International Symposium on RF MEMS and RF Microsystems (MEMSWAVE'2010)*, Otranto, Italy, June 28-July 1, 2010.

[C_22]. **A. Takacs,** A. Coustou, H. Aubert, M. Tentzeris, "Electromagnetic Analysis of the Near Field Coupling between a RFID Tag and Harness for Aeronautic Applications", in *Proc. of Progress In Electromagnetics Research Symposium PIERS'2011*, Marrakech, Morocco, 20-23 March 2011.

[C_23]. D. Medhat, **A. Takacs**, H. Aubert, J.-C. Portal, "Investigation of the metallic cavity influence on the electromagnetic behavior of the setup used in studying the Ratchet Effect", in *Proc. of Progress In Electromagnetics Research Symposium (Piers'2011)*, Marrakech, Morocco, 20-23 March 2011.

[C_24]. D. Jugieu, **A. Takacs**, M. Cheikh, S. Kessler, R. Benbouhout, "Design and simulation of printed winding inductors for inductive wireless power charging platforms", présentée aux *3èmes Journées Nationales sur la Récupération et le Stockage d'Energie (JNRSE'2013),* Toulouse, France, 27-28 Mars 2013.

[C_25]. **A. Takacs**, H. Aubert, S. Fredon, L. Despoisse, "Conception et Réalisation d'une Rectenna en Bande K pour la Récupération d'Energie Micro-onde à bord des Satellites de Télécommunication Géostationnaires", in *Proc of JNM'2013*, Paris, France, 14-17 Mai 2013.

[C_26]. Z. Yang, **A. Takacs**, S. Charlot, A. Rumeau, D. Dragomirescu, "Technologie pour intégration sur substrat souple dans le domaine millimétrique", in *Proc of JNM'2015*, Bordeaux, France, 1-5 June 2015.

[C_27]. A. Okba, **A. Takacs**, H. Aubert, "Rectenna à 2.45 GHz utilisant une antenne à dipôle arrondi", *Journées Nationales Micro-ondes (JNM'2017)*, Saint Malo, France, Mai 2017.

ANNEX